THE ELECTRON OPTICAL LIMITS OF PERFORMANCE OF SINGLE-POLEPIECE MAGNETIC ELECTRON LENSES

A Thesis submitted for the degree

of

DOCTOR OF PHILOSOPHY

in

The University of Aston in Birmingham

by

Muna Abdul Kareem Al-Khashab

DEPARTMENT OF PHYSICS

February, 1983

DEDICATION

I dedicate this work to my Mother, to the spirit of my Father and to my Brother Samir Al-Khashab, without whose support this research would never have been possible.

THE ELECTRON OPTICAL LIMITS OF PERFORMANCE OF SINGLE-POLEPIECE MAGNETIC ELECTRON LENSES

A THESIS FOR THE DEGREE OF DOCTOR OF PHILOSOPHY

BY

Muna Abdul Kareem Al-Khashab

ABSTRACT

The thesis is concerned with the electron properties of single-polepiece magnetic electron lenses especially under conditions of extreme polepiece saturation. The electron optical properties are first analysed under conditions of high polepiece permeability. From this analysis, a general idea can be obtained of the important parameters that affect ultimate lens performance. In addition, useful information is obtained concerning the design of improved lenses operating under conditions of extreme polepiece saturation, for example at flux densities of the order of 10 Tesla. It is shown that in a single-polepiece lens, the position and shape of the lens exciting coil plays an important role. In particular, the maximum permissible current density in the windings, rather than the properties of the iron, can set a limit to lens performance. This factor was therefore investigated in some detail. The axial field distribution of a single-polepeice lens, unlike that of a conventional lens, is highly asymmetrical. There are therefore two possible physical arrangements of the lens with respect to the incoming electron beam. In general these two orientations will result in different aberration coefficients. This feature has also been investigated in some detail. Single-polepiece lenses are thus considerably more complicated electron-optically than conventional double polepiece lenses. In particular, the absence of the usual second polepiece causes most of the axial magnetic flux density distribution to lie outside the body of the lens. This can have many advantages in electron microscopy but it creates problems in calculating the magnetic field distribution. In particular, presently available computer programs are liable to be considerably in error when applied to such structures. It was therefore necessary to find independent ways of checking the field calculations. Furthermore, if the polepiece is allowed to saturate, much more calculation is involved since the field distribution becomes a non-linear function of the lens excitation. In searching for optimum lens designs, care was therefore taken to ensure that the coil was placed in the optimum position. If this condition is satisfied there seems to be no theoretical limit to the maximum flux density that can be attained at the polepiece tip. However, under iron saturation condition, some broadening of the axial field distribution will take place, thereby changing the lens aberrations. Extensive calculations were therefore made to find the minimum spherical and chromatic aberration coefficients. The focal properties of such lens designs are presented and compared with the best conventional double-polepiece lenses presently available.

KEYWORDS

Magnetic electron lenses, finite element method, unsaturated lenses, saturated lenses, high flux density lenses, lens of least aberration, ideal lens, high voltage electron microscopes.

CONTENTS

ACKNOWLEDGEMENTS

I am grateful to my Supervisor, Professor T Mulvey for his constant help and encouragement in the compilation of this work.

I also acknowledge the Head of the Physics Department, Professor S E Hunt, for his advice and encouragement, also all the staff in the Physics Department, particularly Mrs J Penny, the Departmental Secretary, and all the staff in the Computer Centre, who gave me invaluable help at various stages in my research.

I also wish to thank my colleague Dr S Christofides, for his discussions, throughout this project.

I would especially like to express my deepest thanks to Miss J J Sharef, for all her help, of which I am most grateful.

I also wish to thank Mrs D James and Miss D Stretton for their help in typing my thesis, and Miss M Broadbent and Miss R Davis for checking the final manuscript before submission.

Lastly, I remain grateful to my Mother and my Brother, Samir, for their patience and encouragement, throughout my work. Had it not been for my Brother's financial assistance, this work would not have been possible.

LIST OF SYMBOLS

(SI units used throughout unless otherwise stated)

A	Winding area
a	Radius of sphere
B	Magnetic flux density
B_{coil}	Magnetic flux denisty at any point due to the coil of a lens
B_{Fe}	Magnetic flux density at any point due to the magnetisation of the iron
B_{max}	Peak value of the axial magnetic flux density distribution
B_0	Maximum axial magnetic flux density at the surface of a sphere
B_{pf}	Poleface magnetic flux density
B_{Total}	Total magnetic flux density at any point ($B_{Total} = B_{coil} + B_{Fe}$)
B_Z	Axial magnetic flux density
C_c	Chromatic aberration coefficient
C_c^*	Scaled chromatic aberration coefficient [$C_c^* = nC_c$]
C_s	Spherical aberration coefficient
C_s^*	Scaled spherical aberration coefficient [$C_s^* = nC_s$]
D_{in}	Inner diameter of the lens bore
D_m	Mean diameter of the coil winding [$D_m = (D_1 + D_2)/2$]
D_{out}	Outer diameter of the lens
D_1	Inner diameter of the coil
D_2	Outer diameter of the coil
D_{rad}	Radial distortion coefficient
D_{sp}	Spiral distortion coefficient
d_{coil}	The half-width of the coil
d_h	Half-width of the axial magnetic flux density distribution

f	Focal length
f_{obj}	Objective focal length
$f_{obj}*$	Scaled objective focal length
f_{proj}	Projector focal length
h	Particular solution to the paraxial ray equation
H	Magnetic field strength ($H = B/\mu_o \mu_r$)
I	Current in a lens coil
J	Bessel function
L'	Lens size (external diameter of the lens)
$L*$	Scaled lens size (external diameter of the lens)
L	Projection distance
NI	Lens excitation
NI_{OR}	Lens excitation giving a poleface flux density B_{pf}
n	Geometrical scaling factor.
Q_{rad}	Image quality factor Q_{rad} (radial) $$Q_{rad} = f_{proj}(D_{rad})^{\frac{1}{2}}$$
Q_{sp}	Image quality factor Q_{sp} (spiral) $$Q_{sp} = f_{proj}(D_{sp})^{\frac{1}{2}}$$
r	Height of the beam from the axis
S'	Thickness of the coil
S	Gap width of the double-polepiece lens
V_{acc}	Electron accelerating voltage
V_r	Relativistically corrected electron accelerating voltage
Y	Particular solution to the paraxial ray equation with the condition $Y_0 = 1$ and $Y'_0 = 0$
Z	Axial distance from pole face
Z_f	Objective focal distance
Z_f*	Scaled objective focal distance
Z_i	Position of the image plane
Z_0	Position of the object

δ	Spatial resolution [$\delta = 0.707\ (C_s\ \lambda^3)^{\frac{1}{4}}$ Å]
μ	Permeability of the magnetic material
μ_o	Absolute permeability of free space ($4\ \pi \times 10^{-7}$ henry/m)
μ_r	Relative permeability ($\mu_r = B/\ \mu_o$ henry/m)
ξ	Paraxial ray parameter for the exponential field distribution [$\xi = K/\ln 2,\ \exp\ (-\ \ln 2/d)Z$]
ρ	Radial height of Gaussian ray in the image
$\Delta\rho$	Distortion in the image
σ	Current density in the lens coil
σ^*	Scaled current density in the lens coil
Δ	Distance from the centre of the coil to the tip of the lens poleface
α_p	Projection semi-angle ($\alpha_p = \rho\ /L'$)

LIST OF FIGURES

LIST OF TABLES

CHAPTER ONE

1. INTRODUCTION

The birth of electron optics may be said to have occurred in 1926, when H. Busch (1926) showed that the action of a short axially symmetrical magnetic field on electron rays was similar to that of a glass lens on light rays. The use of electron lenses for the production of magnified electron images was developed first by Ruska (1931), who worked mainly with magnetic lenses.

Recent years have seen a renewed interest in all aspects of electron optics in both the theoretical and experimental areas within a whole field of science and technology such as the high resolution electron microscope (HREM) (Cosslett, 1946), the scanning electron microscope (SEM) (Von Ardenne, 1938), and the scanning transmission electron microscope (STEM) (Crewe, 1970). The most important element in all these electron optical instruments is the magnetic electron lens itself.

1.1 MAGNETIC ELECTRON LENSES

1.1.1 DOUBLE-POLEPIECE LENSES

Conventional double-polepiece lenses are the most commonly found form of magnetic electron lenses .

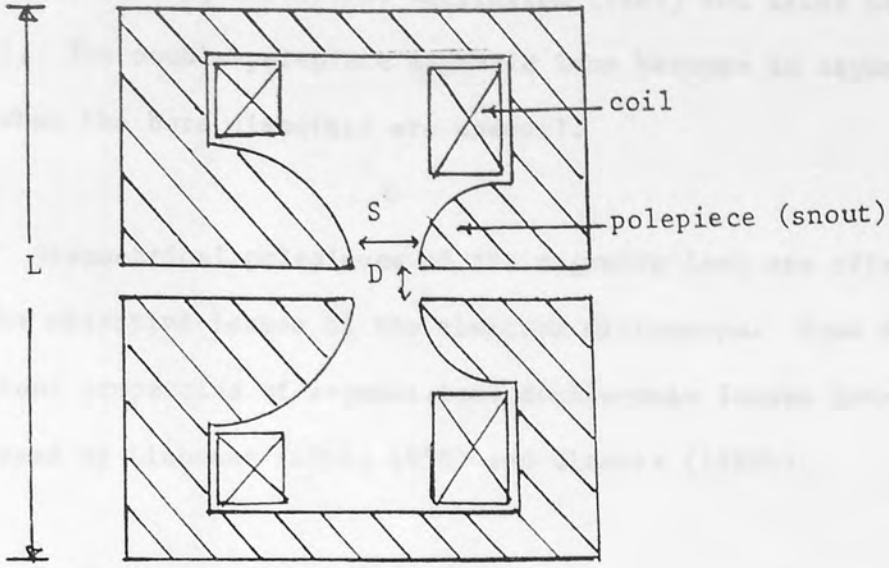

Fig 1.1 Cross section of asymmetrical double-polepiece magnetic lens

Figure 1.1 shows a typical design consisting of a pair of polepieces forming a gap in a magnetic circuit. An exciting coil creates a magnetic field along the axis of the lens.

The iron core of the lens is bored to a diameter D to allow the electron beam to pass through the gap, of width S, between the two iron polepieces. The otherwise uniform axial magnetic field in the gap S is disturbed near the axial bore; this gives rise to a lens action, the properties of which can be expressed in terms of the ratio (S/D) that is, the ratio of gap width to inner diameter. When the bores of the polepieces are of identical diameter D, the lens is considered to be a symmetrical magnetic lens characterised by its S/D ratio.

Many authors have published results of systematic studies concerning these lenses. Amongst these were the papers by

Liebmann and Grad, (1951), Durandeau and Fert (1957), Fert and Durandeau, (1967), Mulvey and Wallington (1969) and later Cleaver (1978). The double-polepiece magnetic lens becomes an asymmetrical lens when the bore diameters are unequal.

Asymmetrical polepieces of the magnetic lens are often used for the objective lenses of the electron microscope. Some of the important properties of asymmetrical double-pole lenses have been discussed by Liebmann (1951, 1955) and Cleaver (1980b).

1.1.2 SINGLE-POLEPIECE LENSES

If the double-polepiece lens in Figure 1.1 is cut in half and one of the halves is removed, the half which is left is a single-polepiece lens such as that in Figure 1.2. This form of lens was first suggested by Mulvey (1972a).

The shape of its axial magnetic field distribution, differs from that of a symmetrical double-polepiece lens. In particular, the maximum of the axial field distribution falls outside the lens structure (Mulvey, 1976).

The advantages of the single-polepiece magnetic lens arise from its essentially different axial flux density distribution as compared to that of the double-polepiece lens (Marai and Mulvey, 1976). For this reason its electron-optical properties cannot be predicted from the data of conventional lenses.

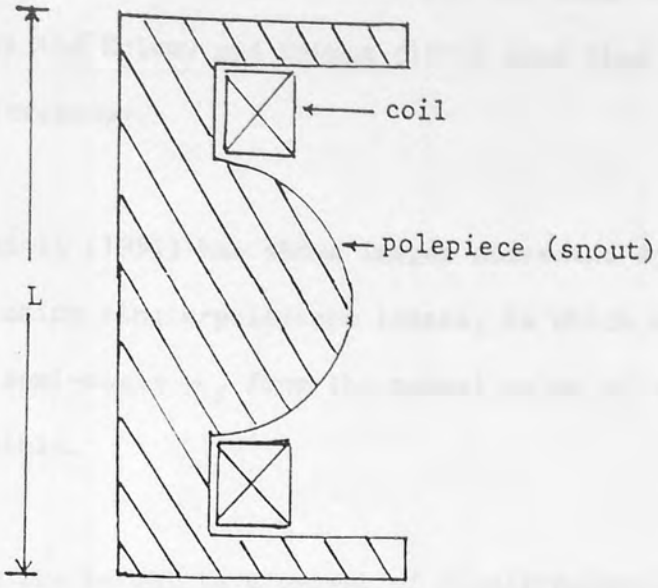

Fig 1.2 Schematic diagram of a single-polepiece lens

Figure 1.2 shows a schematic representation of a single-polepiece lens. The polepiece snout which is surrounded by the coil must be of a suitable shape. If a small hole is bored along the axis of the snout to allow an electron beam to enter, the lens can be used in any branch of microscopy, for example in transmission electron microscopy (TEM) and in scanning transmission electron microscopy (STEM). In scanning electron microscopy (SEM), a lens bore is not always necessary (Mulvey 1974). The single-polepiece lens was used by Mulvey and Newman (1972), as one of the class of miniature lenses. Several papers have been published giving an account of the development of this lens, such as those of Mulvey (1974) and Marai and Mulvey (1974). A single-polepiece lens may be used as an objective lens in TEM and STEM (Mulvey 1974) or otherwise as a projector and objective lens (Mulvey and Newman 1974), (Juma and Mulvey 1975), or as a condenser lens for use with a field-emission electron gun (Cleaver 1980a). Mulvey and Newman (1972)

and Juma and Mulvey (1974), have carried out basic experiments on these lenses and Mulvey and Newman (1974) used them in high voltage electron microscopy.

Elkamali (1981) has shown images corrected for spiral distortion using single-polepiece lenses, in which an increase in projection semi-angle α_p from the normal value of $\alpha_p = 8°$ to 30° is possible.

With the recent development of single-polepiece lenses for micro-x-ray sources (Christofides and Mulvey, 1980), it is now also possible to use these lenses as objective lenses (Christofides, 1982), in high resolution electron microscopy.

1.2 THE AXIAL FLUX DENSITY DISTRIBUTION OF THE SINGLE-POLEPIECE LENS

The axial flux density distribution of the single-polepiece magnetic electron lens (Juma and Mulvey, 1980a) is asymmetrical, rising slowly to a peak and falling off rapidly within the body of the polepiece itself.

The properties of the axial magnetic flux density distribution of the single-polepiece lenses were studied experimentally by Juma and Mulvey (1980a) and later by Juma and Faisal (1981). They studied the lenses under non-saturation conditions (μ_r large), but were unable to determine the flux density distribution in the iron circuit and especially in the polepiece itself.

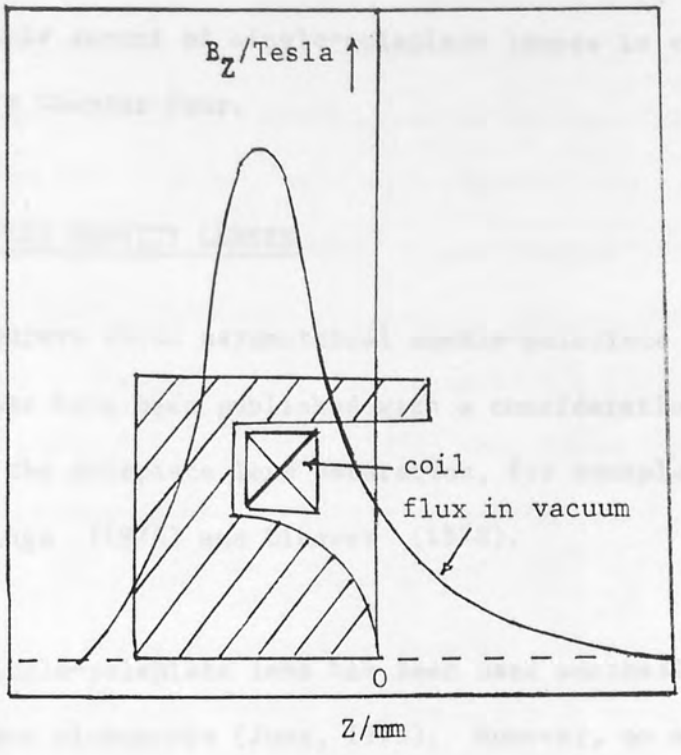

Fig 1.3 Schematic diagram of the axial magnetic flux density in the single-polepiece lens of zero bore diameter

If the magnetic flux density of the single-polepiece lens reaches a maximum other than at the snout tip, as shown in Figure 1.3, such a lens, when operated under saturation conditions, will exhibit saturation effects within the polepiece before the tip reaches saturation. Christofides (1982) observed that some irregularities occur in the magnetic flux density inside the magnetic material of the lens polepiece. These irregularities occur when the polepiece is approaching saturation and are present at the positions where changes occur in the shape of the polepiece. He also explained that the source of the irregularities could be due to inherent defects in Munro's finite element program for calculating the magnetic field in the lens. It is, however, possible

that these effects are associated with the position of the exciting coil. The effect of the coil shape and position on the axial flux density distribution in single-polepiece lenses has been largely ignored, but this aspect of single-polepiece lenses is vitally important, as is shown in Chapter Four.

1.3 HIGH FLUX DENSITY LENSES

Many papers about asymmetrical double-polepiece magnetic electron lenses have been published with a consideration of the influence of the polepiece lens saturation, for example, by Riecke (1972), Kamminga (1976) and Cleaver (1978).

The single-polepiece lens has been used successfully in the 100 kV electron microscope (Juma, 1975). However, no one has published results with single-polepiece lenses using high flux density distribution (5 Tesla).

1.4 IRON-FREE COILS

The iron-free solenoid is the simplest form of a magnetic electron lens. It consists of either a wire or tape wound round a non-magnetic core. Such lenses are of great theoretical and practical interest since they have an unusually low spherical aberration coefficient (Bassett and Mulvey, 1969). An investigation of the properties and aberration has been carried out by Marai (1977) on a wide range of these lenses.

It is therefore of interest to study whether the favourable properties of such a coil can be combined with those of a single iron polepiece.

1.4.1 OPTIMISATION OF MAGNETIC ELECTRON LENSES

Spherical and chromatic aberration are the principal aberrations that affect the performance of objective lenses. The minimum spherical aberration coefficient of an iron-free lens can be achieved by the use of a very thin coil (Bassett and Mulvey, 1969) but there are practical difficulties in the realisation of such a lens. Marai, (1977) found that there is an optimum geometry for iron-free lenses, where the coil thickness is one-tenth of the mean diameter i.e., $S/D_m = 0.1$. Marai (1977) also found that the spherical aberration parameter decreases as the ratio D_2/D_1 increases.

Figure 1.4 shows the absolute spherical aberration parameter $C_s\ B_{max}/V_r^{\frac{1}{2}}$ for different lenses as a function of absolute focal length parameter $f_{obj}\ B_{max}/V_r^{\frac{1}{2}}$. With the coil dimension, D_2/D_1 equal to 19 as plotted by Mulvey and Wallington (1973), the parameter $C_s\ B_{max}/V_r^{\frac{1}{2}} = 3 \times 10^{-6}$ m.T.$V^{-\frac{1}{2}}$. Also, the theoretical limit of the spherical aberration parameter $C_s\ B_{max}/V_r^{\frac{1}{2}}$ calculated by Tretner (1959) and Moses (1972) is equal to 2.338×10^{-6} m.T.$V^{-\frac{1}{2}}$ Any lens with a value of $C_s\ B_{max}/V_r^{\frac{1}{2}}$ close to this limit can be regarded as an ideal lens, and hence will be suitable as an objective lens. This point is discussed further in Chapter Four.

1.4.2 COMPARISON OF OBJECTIVE LENSES

To compare the performance of different objective lenses a standard method is needed. This should take into consideration the limiting technological factors affecting the aberration coefficient, such as the saturation magnetic flux density in iron. Another such

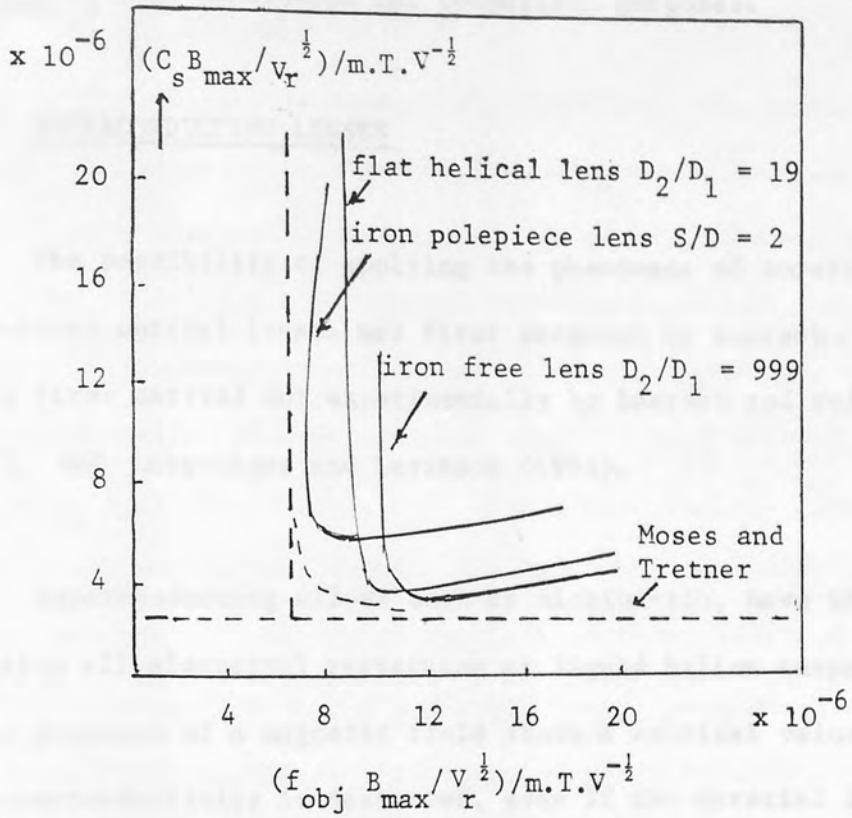

Fig. 1.4 Absolute spherical aberration parameter $C_s B_{max}/V_r^{\frac{1}{2}}$ as a function of absolute focal length parameter $f_{obj} B_{max}/V_r^{\frac{1}{2}}$

factor is the maximum current density permissible in the coil winding (NI).

Mulvey and Wallington (1973) made use of the relevant parameter ($C_s B_{max}/V_r^{\frac{1}{2}}$) for the spherical aberration coefficient and compared the values obtained from different lenses using the corresponding absolute parameters $C_c B_{max}/V_r^{\frac{1}{2}}$, $f_{proj} B_{max}/V_r^{\frac{1}{2}}$, $f_{obj} B_{max}/V_r^{\frac{1}{2}}$ and $Z_f B_{max}/V_r^{\frac{1}{2}}$. It is also possible to compare the values of chromatic aberration coefficient, projector focal length, objective focal length and objective focal distance respectively for the different lenses.

In Chapter Four only the spherical aberration parameter, $(C_s B_{max}/V_r^{\frac{1}{2}})$ is considered for comparison purposes.

1.5 SUPERCONDUCTING LENSES

The possibility of applying the phenomena of superconductivity to electron optical lenses was first proposed by Boersch. It was first carried out experimentally by Boersch and colleagues, (1964), and Laberrigue and Levinson (1964).

Superconducting alloys such as niobium-tin, have the property of losing all electrical resistance at liquid helium temperatures. In the presence of a magnetic field above a critical value, however, the superconductivity is destroyed, even if the material is maintained below the critical temperature.

In the high voltage electron microscope, where one needs high lens excitation (NI), in order to achieve high flux density without dissipating energy in the windings, superconducting lenses can be usefully employed.

The maximum current density that can be achieved in superconducting windings depends on the manufacturing methods, (Dietrich, 1976). For example a typical current density of Nb-Sn sinter material with Cu additions is nearly 3×10^5 A-t/cm^2. Up to now, no one has used superconducting windings in single-polepiece lenses.

1.6 THE FINITE ELEMENT METHOD

The finite element method provides a powerful numerical technique for solving magnetic field problems. The partial differential equation of the boundary-value field problem is first replaced by a corresponding function, whose minimisation is equivalent to solving the original differential equation. The internal region inside the boundary is then divided into many small sub-regions called finite elements. These finite elements may be triangles, quadrilaterals or more complicated shapes. The potential distribution within each element is then approximated by the same simple function of position, e.g., a first order polynomial (first order elements), or a second order polynomial (second order elements), or a high order polynomial if extreme accuracy is required. Using this approximation, the potential distribution within each element is then expressed as a function of the potential at mesh points associated with the element. In this way, the contribution from each element to the overall value of the functional is expressed in terms of the mesh point potentials.

The requirement that the functional is to be minimised is then used to determine a set of algebraic equations, interrelating the potentials at adjacent mesh points.

1.7 MODELS OF THE AXIAL FIELD DISTRIBUTION OF SINGLE-POLEPIECE LENSES

Many different mathematical models have been proposed to represent the axial field distribution B(Z). Such a model is useful

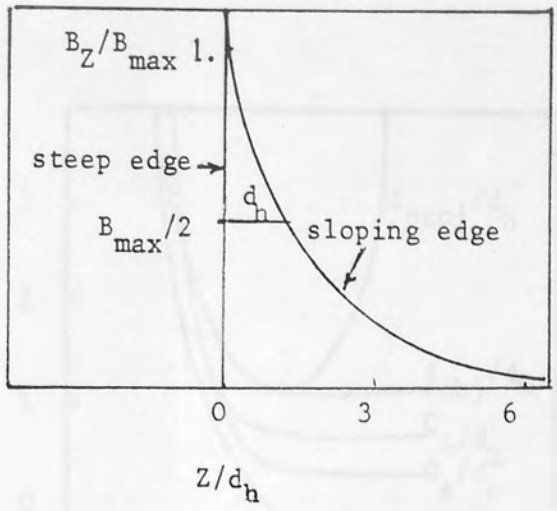

Fig 1.5 The exponential field model

since it can give a design basis for a lens, especially if the model is capable of being realised physically.

At present, there are two types of models for single-polepiece lenses, the exponential field model used by Marai and Mulvey (1974) and the spherical field model used by Al-Shwaikh and Mulvey (1977).

1.7.1 THE EXPONENTIAL FIELD MODEL

The axial field distribution of the exponential field model (Glaser, 1952) takes the form:

$$B_Z = B_{max} \exp(-\ln 2/d_h)Z \quad \ldots\ldots\ldots\ldots\ldots\ldots\ldots\ldots \quad 1.1$$

where d_h is the half width defined as the axial distance from the position of maximum field B_{max} to the point where the field has fallen to half this value Figure 1.5.

The resulting focal properties as given by Marai (1977) are shown in Figure 1.6.

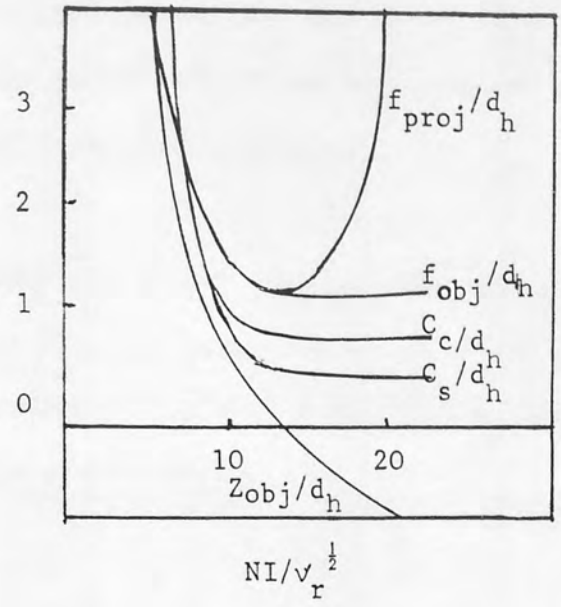

Fig 1.6 Focal properties and aberration coefficients of the exponential field model

The aberration coefficients are constant for excitation parameters $NI/V_r^{\frac{1}{2}} \geqslant 13$. The objective focal length is also constant over this region. This is a consequence of the fact that, for an exponential curve, the shape of the trajectory does not vary with excitation.

Although the exponential field (Marai, 1977) is extremely useful in predicting the general form of the properties of single-polepiece magnetic lenses, it nevertheless suffers from certain defects. The most serious is that the field distribution cannot be related directly to polepiece structure, nor can it explain certain curious features of single polepiece lenses, such as the slight, but measurable, increase in objective focal length at high lens excitations. The spherical field model seems more realistic since it is based on the magnetic properties of a magnetised sphere.

1.7.2 THE SPHERICAL FIELD MODEL

The uniformly magnetised iron sphere is a special case of a uniformly magnetised solid. The analytical solution for the magnetic potential due to such a sphere has already been calculated (Kelvin, 1872; see also Al-Shwaikh and Mulvey, 1977).

If a sphere is placed inside a uniform magnetic field, a uniform field will arise in the sphere as shown in Figure 1.7. In addition an external field will be created, which is symmetrical about the Z axis of the sphere.

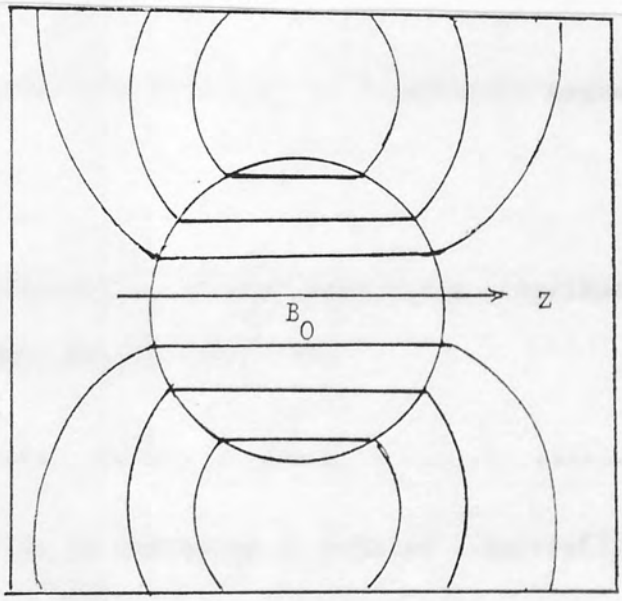

Fig 1.7 The uniformly magnetised sphere (Kelvin, 1872)

If the permeability μ_r is high, the axial flux density distribution (see Figure 1.8) is given by:

$$B(Z) = B_0 \, (a/Z)^3 \quad \ldots\ldots\ldots\ldots\ldots\ldots\ldots\ldots \quad 1.2$$

This axial field distribution is known as the spherical field model for $Z \geq a$ (where a is the radius of the sphere and Z is measured from the centre of the sphere).

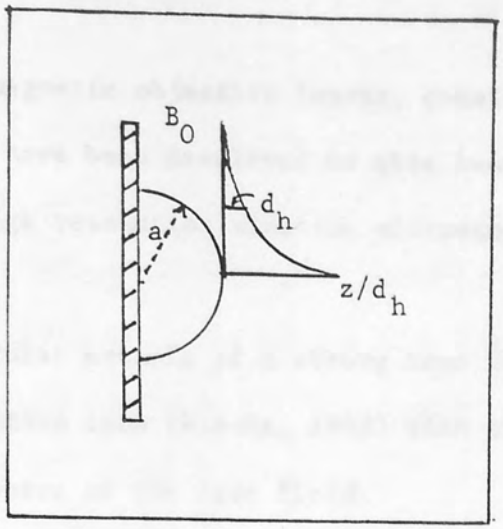

Fig 1.8 The spherical field due to a uniformly magnetised hemisphere

The half-width d_h of the above field distribution found by Al-Shwaikh and Mulvey (1977) is:

$$d_h = 0.26a \quad \ldots\ldots\ldots\ldots\ldots\ldots\ldots\ldots\ldots\ldots \quad 1.3$$

The half-width d_h is therefore determined essentially by the radius of the spherical polepiece.

The focal properties of this field distribution have been calculated by the above authors. In general they are similar to those of the experimental field. Minimum objective and projector focal lengths coincide at an excitation parameter $NI/V_r^{\frac{1}{2}} = 14$. For larger excitations the objective focal length does not remain constant as in the experimental field, but slowly increases.

1.8 THE EFFECT OF POLEPIECE SHAPE AND COIL POSITION ON SINGLE-POLEPIECE LENSES

Strong magnetic objective lenses, considered initially by Glaser (1941), have been developed to give lens forms of particular relevance to high resolution electron microscopy.

A particular example of a strong lens is the symmetrical condenser-objective lens (Riecke, 1962) with the specimen situated close to the centre of the lens field.

Condenser objective lenses have been used recently, in a high-resolution 600 KV microscope (Cleaver, 1977). Their electron optical properties have been described by Riecke (1972), Mulvey and Wallington (1973) and, with consideration of unsaturated polepieces by Kamminga (1968/69), and with the influences of the polepiece saturation by Kamminga (1976) and Cleaver (1978, 1980b). There has been no publication, to date, of the properties of high flux density of single-polepiece lenses (in the region of 5 Tesla).

The main aim of this thesis therefore, is to investigate the electron optical limits of performance of single-polepiece objective lenses, with the aid of computer calculation based on the finite element method.

A suitable set of computer programs was available in the department. In designing the objective and the projector lenses, three of Munro's programs (Munro, 1975), were used, namely the programs M12, M13 and M21. Also, one of Marai's (1977) programs

was used, namely the program PROJECTOR and two of Nasr's programs (Nasr, 1981), were used, namely the programs AREA and BIOT. These are detailed in Chapter Two.

Before considering the properties of such lenses under conditions of saturation, it is useful to consider lenses whose iron circuits have a high permeability. This part of the study included the systematic calculation of the electron optical properties of a range of lens geometries for the two modes of lens operation under a wide range of excitation parameters $NI/V_r^{\frac{1}{2}}$. Since there is a linear relation between flux density and excitation, it is therefore possible to represent the focal properties of such lenses in the form of universal curves as set out in Chapter Three.

Chapter Four describes the results of calculations of axial flux density distribution in saturated single-polepiece lenses.

It was therefore decided to carry out a systematic investigation of the electron optical properties of a series of well-defined lenses under different degrees of polepiece saturation.

The spherical aberration coefficients obtained with ideally-designed single-polepiece lenses have been compared (Chapter Four) with those of iron-free lenses.

The calculations of single-polepiece lenses were extended to the case of projector lenses with single-polepieces of rectangular cross section. This study takes into account some important

aberrations of projector lenses such as spiral distortion for different polepiece sizes. These results are discussed in Chapter Five. Finally, the thesis concludes with an initial design study of two kinds of single-polepiece lenses proposed by Dr Venables of Sussex University, intended for use with a field emission source. These results are given in Chapter Six.

CHAPTER TWO

2. COMPUTER PROGRAMS

The lens calculations described in this thesis were mainly carried out with the aid of the ICL 1904S computer at Aston University and the University of Manchester Regional Computer Centre (UMRCC) using the SWAN system.

The SWAN system enables jobs to be submitted to, and files to be transferred to Birmingham or Manchester. The main system runs on the Aston ICL 1904S. The latter is linked by G.P.O. lines to Birmingham University's ICL 1906A, which in turn is linked to the ICL 1904S at the University of Manchester UMRCC. The ICL 1904S at UMRCC gives access to the CDC 7600 joint system. The SWAN system is accessible from the Aston ICL 1904S and Harris 4500.

A mesh size which is used in the design of the lenses, has a maximum mesh size of JM = 70 mesh-points in the axial direction and of IM = 32 mesh-points in the radial direction using the Manchester computer UMRCC because the core size in the Aston computer (25 x 50) is not large enough to calculate the field distribution of saturated and non-saturated lenses.

The finite element method developed by Munro (1971, 1975) formed the basis of the computation of the magnetic field. The advantages of the method are that:

(1) A polepiece of any shape can be dealt with easily, because the shape of the finite element mesh can be varied to fit different shapes of the polepieces.

(2) Magnetic saturation of the polepieces can be handled easily, because the finite element equations can take account of local changes in permeability by an iterative calculation.

(3) The flux density distribution throughout the magnetic circuit for different sizes and positions of the coil windings can readily be computed.

(4) Complete magnetic circuits can be analysed, because the finite element equations can be formulated in terms of the vector potential, which allows coil windings with various positions and dimensions to be included in the analysis.

In designing the objective and the projector lenses, three of Munro's programs (Munro, 1975) were used, namely the programs M12, M13 and M21. Also one of Marai's programs, (Marai, 1977) was used, namely the program PROJECTOR and two of Nasr's programs (Nasr, 1981) were used, namely the programs AREA and BIOT. A brief description of these programs is given for reference purposes.

2.1 PROGRAM M12 - PROGRAM FOR COMPUTING VECTOR POTENTIAL DISTRIBUTIONS AND FLUX DENSITY DISTRIBUTIONS THROUGHOUT THE MAGNETIC CIRCUIT AND COIL WINDINGS OF UNSATURATED MAGNETIC LENSES

Program M12 computes the vector potential distribution and hence the flux density distribution throughout the entire magnetic circuit and coil windings of any unsaturated, rotationally symmetric magnetic lens. The magnetic circuit is assumed to have a constant finite permeability. The flux density is computed at

points throughout the magnetic circuit; the results can be used to check that the magnetic circuit will not saturate in undesirable places under practical conditions.

2.2 PROGRAM M13 - PROGRAM FOR COMPUTING VECTOR POTENTIAL DISTRIBUTIONS AND FLUX DENSITY DISTRIBUTIONS THROUGHOUT THE MAGNETIC CIRCUITS AND COIL WINDINGS OF SATURATED MAGNETIC LENSES

Program M13 computes the vector potential distribution and flux density distribution throughout the magnetic circuit and coil windings of any saturated, rotationally symmetric lens.

In addition, program M13 performs the same function as progam M12, except that this version deals with saturated magnetic lenses, in which the lens excitation is so high that the non-linear magnetisation curves of the magnetic materials must be taken into account. The program can handle composite magnetic circuits, i.e. circuits constructed from up to five different magnetic materials. Any desired magnetisation curve can be specified for each magnetic material.

As in the case of program M12, the axial flux density distribution, and the flux density values throughout the magnetic circuit and the vector potential throughout the two-dimensional mesh system within the boundary conditions are computed. The magnetisation curve used in conjunction with this program is illustrated in Table 2.1, which is that of soft iron. The

Table 2.1 The Values of H, B and μ_r of soft iron.

B_{Tesla}	μ_r	$H_{(A-t/m)}$
.400	6366.2	50.0
.680	5411.3	100.0
.880	4668.5	150.0
1.020	4058.0	200.0
1.224	2831.4	344.0
1.325	1735.0	807.7
1.351	1033.6	1040.1
1.377	815.3	1344.1
1.442	521.9	2720.0
1.500	253.1	4716.6
1.589	142.4	8880.8
1.623	116.1	11124.9
1.679	85.6	15613.1
1.790	51.8	27509.4
1.840	33.2	44157.6
1.866	24.4	60940.5
1.898	19.5	77421.0
1.919	16.5	92464.1
1.937	14.4	106713.4
2.000	10.1	156847.3
2.100	7.1	236424.8
2.300	4.6	395597.8
2.600	3.3	634312.3
2.900	2.6	888045.1
3.100	2.4	1028397.0

corresponding permeability μ_r of the iron is also shown in Table 2.1. The table shows that in soft iron even at a flux density of 3 Tesla the permeability $\mu_r \simeq 3$.

2.3 PROGRAM M21 - PROGRAM FOR COMPUTING THE OBJECTIVE PROPERTIES OF ANY MAGNETIC LENS

Program M21 computes the objective focal length, spherical and chromatic aberration coefficients of any given axial flux density distribution , for example an axial field distribution previously computed by program M12 or M13. The program can handle "zero magnification" or "probe-forming" conditions as illustrated in Figure 2.1.

For a specified range of beam voltages, the program computes the excitation parameter, the object and/or image plane, the objective principal plane, the objective focal length, the object magnification, the spherical aberration coefficient, the chromatic aberration coefficient, and the magnetic flux density at the object or image plane as appropriate.

There are some difficulties in Munro's program. Program M21 can be used to calculate the electron trajectory for Ray II beam orientation only as shown in Figure 2.1.

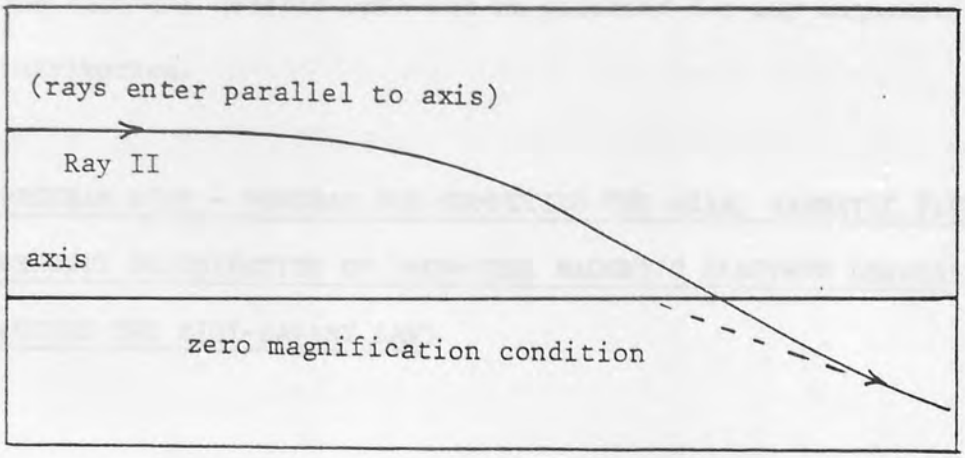

Fig 2.1 Ray diagram defining the zero magnification conditions, for which program M21 can compute the electron optical properties of a magnetic lens.

To find the trajectory from the other side, the field distribution should be reversed. After reversing the field, the aberration and focal properties of Ray I beam orientation can be calculated.

2.4 PROGRAM PROJECTOR - PROGRAM FOR COMPUTING THE PROJECTOR PROPERTIES OF ANY MAGNETIC LENS

The PROJECTOR program employed by the present author was originally written by Marai (1977) and was used to compute the projector properties of any magnetic lens whose axial flux density distribution has been computed previously using program M12 or M13. For a specified range of beam voltages, the program computed the excitation parameter, the projector focal length, the radial distortion coefficient, the spiral distortion coefficient, the image quality factor (radial) and the image quality factor (spiral).

Here (D_{rad}, D_{sp}) are radial and spiral distortion coefficients, (Q_{rad}, Q_{sp}) are the image quality factor (radial and spiral), and f_{proj} is the projector focal length.

The relevant coefficients can be obtained for any magnetic field distribution.

2.5 PROGRAM BIOT - PROGRAM FOR COMPUTING THE AXIAL MAGNETIC FLUX DENSITY DISTRIBUTION OF IRON-FREE MAGNETIC ELECTRON LENSES (USING THE BIOT-SAVART LAW)

The BIOT program (short for BIOT SAVART LAW) computes the axial magnetic flux density distribution of any rotationally symmetric iron-free magnetic electron lens, using the Biot-Savart law.

This program can be used to compute the axial magnetic flux density B_{coil} produced by an iron-free coil. For example it is convenient to be able to calculate the direct contribution of the coil of a saturated single-polepiece lens to the axial field distribution. The axial magnetic field B_{Total} in such a lens may be regarded as the sum of the contribution B_{coil} from the coil and the contribtion B_{Fe} from the magnetised iron. The Munro programs M12 and M13 in fact calculate the total field B_{Total}. Therefore, the contribution B_{coil} is subtracted from the total field B_{Total} and so we obtain the contribution to the field from the iron, i.e.

$$B_{Fe} = B_{Total} - B_{coil} \quad \ldots\ldots\ldots\ldots\ldots\ldots\ldots\ldots\ldots\ldots \quad 2.1$$

This simple additional calculation provides useful information about the state of magnetisation of the polepiece tip in a saturated lens. In a well designed lens the polepiece tip should reach its saturation flux density. It will be shown later that this condition is not easy to satisfy unless care is taken with the positioning and shape of the coil.

In addition, the variation of B_{Fe} with axial distance Z can also be used as a check on the accuracy of the finite element calculation. Since the iron circuit does not contribute additional ampere turns to the magnetic circuit, the integral

$$\int_{-\infty}^{+\infty} Bz_{(Fe)}\, dZ = 0 \qquad \text{2.2}$$

This means that the total area under the B_{Fe}, Z distribution must be zero. In general this is not the case with the finite element method with a finite boundary, since it tends to underestimate the magnetisation of the iron in the "open" part of the lens magnetic circuit (Mulvey and Nasr, 1981).

If the total axial magnetic flux density distribution of the lens B_{Total}, which is equal to the summation of $(B_{coil} + B_{Fe})$, has been previously computed by program M12 (or M13), the difference between the total axial magnetic flux density distributions of the lens and the coil winding gives the contribution to the axial flux density distribution due to the iron itself (B_{Fe}).

This simple calculation can be used to obtain useful information about the magnetisation of the iron circuit, in particular whether or not the polepiece tip has reached saturation magnetisation.

2.6 PROGRAM AREA - PROGRAM FOR COMPUTING THE AREA UNDER THE AXIAL MAGNETIC FLUX DENSITY DISTRIBUTION (USING THE TRAPEZOIDAL RULE)

Munro's programs M12 and M13, were originally developed to

compute the axial magnetic flux density distribution of conventional lenses in which the axial magnetic flux density distribution is completely immersed in the body of the lens. These programs require the vector potential to be zero at the mesh boundary. For conventional lenses this condition is usually satisfied since the axial magnetic flux density distribution is surrounded by a magnetic circuit of high permeability.

For a single polepiece lens this condition is satisfied only in the region which is surrounded by the magnetic circuit. This leaves one side of the lens open. This means that in this area the vector potential is zero only at infinity. To satisfy the above conditions the boundary on this side of the single polepiece lens must be set at a large distance from the lens.

The magnetic circuit of the lens and the area around it, inside the boundary, are divided into meshes as required by the finite element method. The distance between the meshes should be as equal as possible along the entire boundary. The number of meshes one is able to use is restricted by the size of the computer memory store available and hence an equal distance between the meshes may not be possible. Generally a high concentration of meshes is distributed around the polepiece which is the most important part of the single-polepiece lens. These meshes then deviate from this high concentration as one approaches the boundaries. When an abrupt change of the mesh size occurs, a discontinuity appears in the axial magnetic flux density distribution. These discontinuities have a harmful effect on the calculation of the aberrations of the lens and they should be smoothed out before the electron optical properties of the lens are calculated. When the axial magnetic flux density dis-

tribution has been smoothed, the area under it may change. This area should of course correspond to the lens excitation, which was used by the program during the computation.

In order to ensure that the smoothing of the axial magnetic flux density distribution has been carried out correctly, the area under the smoothed distribution may be computed by program AREA; this program determines the area by means of the trapezoidal rule. The area under the axial magnetic flux density distribution is given by:

$$\int_{-\infty}^{+\infty} B_z dz = \mu_o NI \qquad \text{2.3}$$

where,

μ_o is the permeability of free space

NI is the lens excitation

The smoothed axial magnetic flux density distribution can then be used as the data for programs M21, or PROJECTOR.

CHAPTER THREE

3. OPTIMUM DESIGN OF NON-SATURATED SINGLE-POLEPIECE OBJECTIVE LENSES

3.1 NON-SATURATED LENSES

An objective lens should have a low spherical aberration coefficient C_s and also a low chromatic aberration coefficient C_c. In addition, it is desirable that the maximum free space should be provided around the specimen, to allow for specimen tilting and the placing of x-ray and other detectors.

The single-polepiece objective lens has many advantages, amongst which are short focal length and low spherical aberration constants compared with its polepiece dimensions in both the STEM and TEM mode (Mulvey, 1974).

The electron optical properties of such lens designs have been studied extensively in the present investigation in order to discover the principal factors controlling the electron optical performance. Since one may imagine that both polepiece shape and relative size of bore (D_{in}/D_{out}) are involved, it is convenient to discuss such lenses initially under linear excitation (non-saturation) conditions, i.e., where the flux density everywhere in the lens is linearly related to the lens excitation. Under such conditions the focal properties can be scaled linearly with respect to lens geometry and excitation. Once optimum design conditions have been discovered, further calculations can be made in the saturation region.

3.1.1 DESIGN CONSIDERATIONS FOR LENSES OF HIGH PERMEABILITY

The properties of a single-polepiece magnetic electron lens, in common with all other lenses, depend on the shape of the axial magnetic flux density distribution. The shape of this distribution might be expected to depend on the shape of the polepiece and the relative size of the polepiece bore, and possibly on the size and position of the coil. These factors can be investigated readily by direct calculations with the finite element method, by making certain assumptions about the permeability μ_r of the iron circuit.

3.1.2 THE MAGNETIC PERMEABILITY (μr) OF THE IRON CIRCUIT

In order to classify the concept of a "non-saturated" magnetic lens, the curves of Figure 3.1 show how the relative permeability (μ_r) of heat treated soft iron (solid line) and non heat-treated iron (dashed line) varies as a function of the magnetic flux density (B) in the iron. At low flux densities (less than 1T), the effect of heat treatment is to cause an appreciable improvement in relative permeability, typically to a value of $\mu_r \simeq 5000$. In the saturation region, however, (flux density greater than 2T), the heat treatment has a negligible effect on permeability. In this region the relative permeability is comparatively low.

For example, at a flux density 2 (T) the relative permeability of the soft iron is about ten; this therefore represents an upper limit for the linear region of flux density and lens

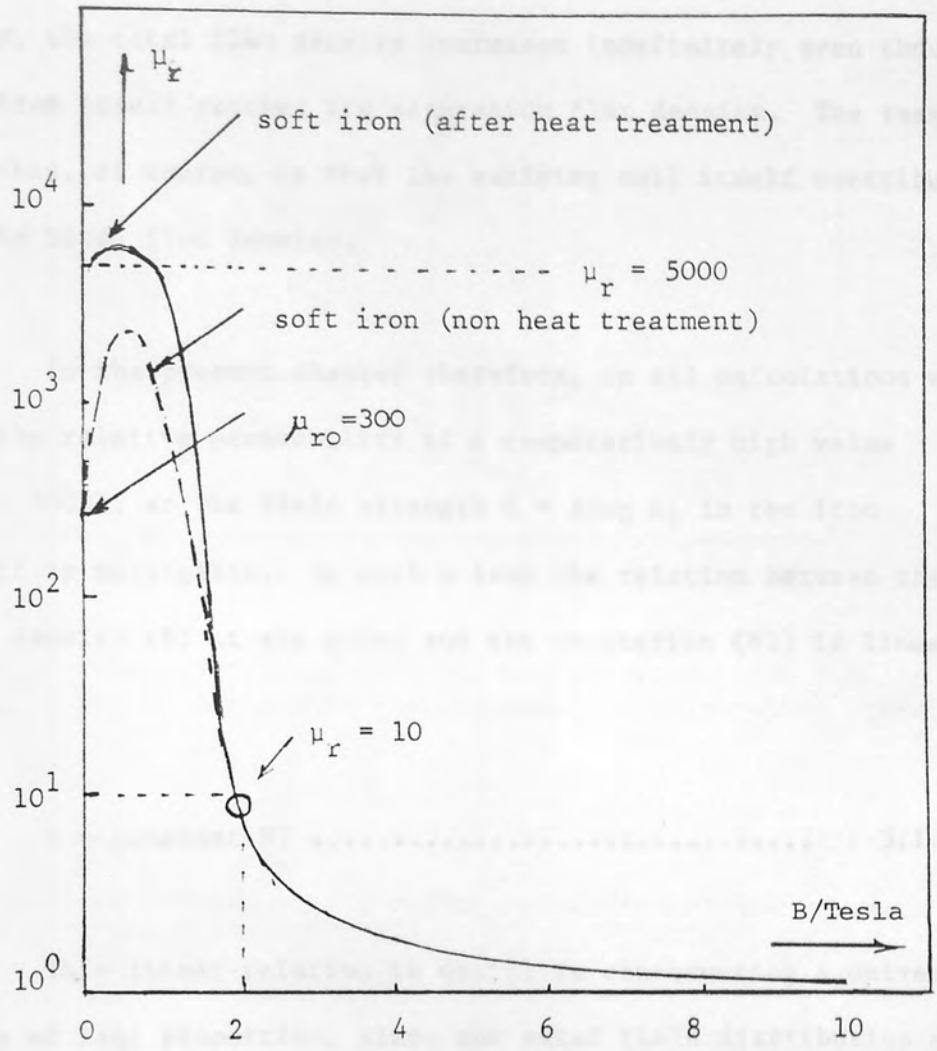

Fig 3.1 Schematic variation of relative permeability μ_r with magnetic inducution B for soft iron

excitation in a well-designed lens i.e., one in which saturation effects are restricted to a small region at the polepiece. Under these conditions we may refer to this region as the "unsaturated" region. Note, however, that badly-designed lenses may experience so-called "saturation" effects at much lower poleface flux densities.

In general therefore, true saturation effects should only begin to appear at flux densities appreciably higher than 2 Tesla. It should perhaps be pointed out that at these high iron flux

densities, although the permeability falls to a value approaching unity, the total flux density increases indefinitely even though the iron itself reaches its saturation flux density. The reason for this, of course, is that the exciting coil itself contributes to the total flux density.

In the present chapter therefore, in all calculations we set the relative permeability at a comparatively high value (μ_r = 5000), so the field strength H = $B/\mu_0 \mu_r$ in the iron itself is negligible. In such a lens the relation between the flux density (B) at any point and the excitation (NI) is linear i.e.,

$$B = \text{constant } NI \quad \ldots\ldots\ldots\ldots\ldots\ldots\ldots\ldots \quad 3.1$$

This linear relation is useful in constructing a universal curve of lens properties, since the axial field distribution of a given lens structure may be scaled linearly both in respect of lens excitation and also of its linear dimensions, as explained below.

3.1.3 PROPERTIES OF THE AXIAL FIELD DISTRIBUTION

The axial magnetic flux density distribution of a single-polepiece magnetic electron lens is inherently asymmetrical. As the polepiece is approached the axial flux density rises slowly to a peak value near the polepiece and then rapidly falls within the polepiece itself as indicated in Figure 3.2.

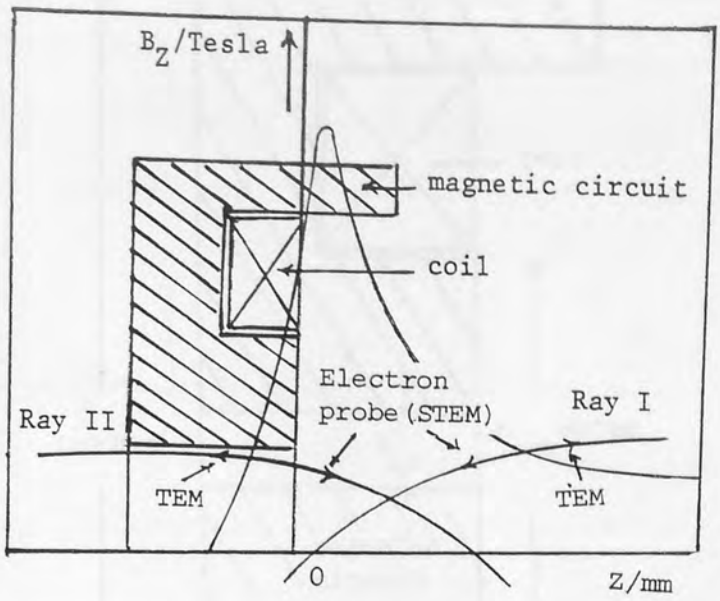

Fig 3.2 Schematic diagram of a single-polepiece lens showing the two possible beam orientations for an electron beam.

This highly asymmetric field distribution has different electron optical properties depending on its orientation with respect to the electron beam. There are two modes of operation in a single-polepiece lens - the electrons either enter or leave the lens from the open side of the magnetic circuit (Ray I) or from the closed side of the lens (Ray II); Figure 3.2 shows these two types of ray. The electron beam entering the axial magnetic flux density distribution of a lens will experience a different field gradient dB/dZ and strength (B_Z) of magnetic flux, depending on the orientation of the beam with respect to the lens. This gives rise to different electron optical properties for each orientation.

It is possible to design a given electron optical instrument using either Ray I or II. Perhaps it should be pointed out that commercially available high resolution microscopes make use of Ray II, especially when an asymmetric objective lens is employed. On

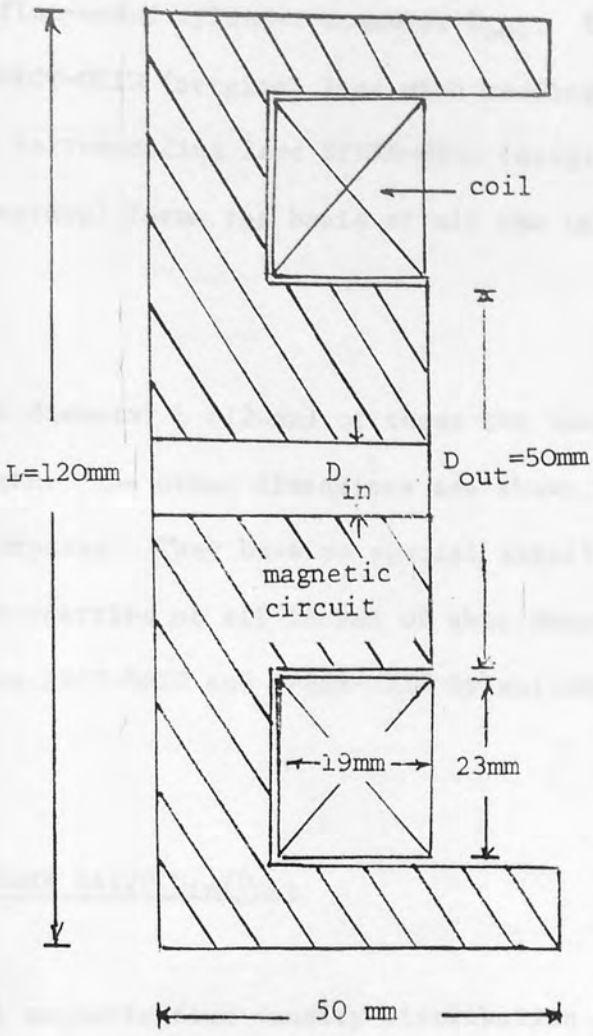

Fig 3.3 Rectangular (cross-section) polepiece lens (RECT-ORIG) of variable bore for the investigation of focal properties and aberration coefficients of single-polepiece lenses with rectangular section polepieces. (Coil area = 437 mm^2)

the other hand, a microfabrication equipment may use Ray I since this allows an electron probe to be formed on a large specimen surface.

3.2 THE RECTANGULAR (CROSS-SECTION) POLEPIECE LENS

3.2.1 THE EFFECT OF RELATIVE BORE DIAMETER ON THE AXIAL FLUX DENSITY DISTRIBUTION OF THE RECTANGULAR POLEPIECE LENS

In order to establish the terminology and methods of calculation, consider the single-polepiece lens shown in cross-section in Figure 3.3. It has a simple geometrical shape; the

polepiece is a flat-ended cylinder diameter D_{out}. This lens, referred to as RECT-ORIG (original lens with rectangular polepiece), together with a corresponding lens SPHER-ORIG (original lens with a spherical polepiece) forms the basis of all the calculations in this Chapter.

The outer diameter L (120mm) of these two lenses is used as a reference length. The other dimensions are shown in Figure 3.3 for reference purposes. They have no special significance except that the focal properties of all lenses of this shape have been deduced from lens RECT-ORIG and SPHER-ORIG by suitable scaling operations.

3.2.2 OPTIMUM BORE RATIO D_{in}/D_{out}

The axial magnetic flux density distribution of RECT-ORIG was computed by PROGRAM M12 (See Chapter 2) for different bore ratios D_{in}/D_{out}, and for a constant (arbitrary) excitation value NI_{OR} of 7000 ampere-turns. A family of five different lenses was thus obtained, whose axial magnetic flux density distributions are shown in Figure 3.4. In a magnetic circuit energised with an excitation NI, the integral

$$\int_{-\infty}^{+\infty} (B_z / \mu_r)\, dZ = \mu_0 NI \qquad \text{..... 3.2}$$

As a check on the accuracy of the calculations shown in Figure 3.4, this integral was computed by program AREA (cf Chapter Two) and found to be in satisfactory agreement with the NI value used in the axial field calculation.

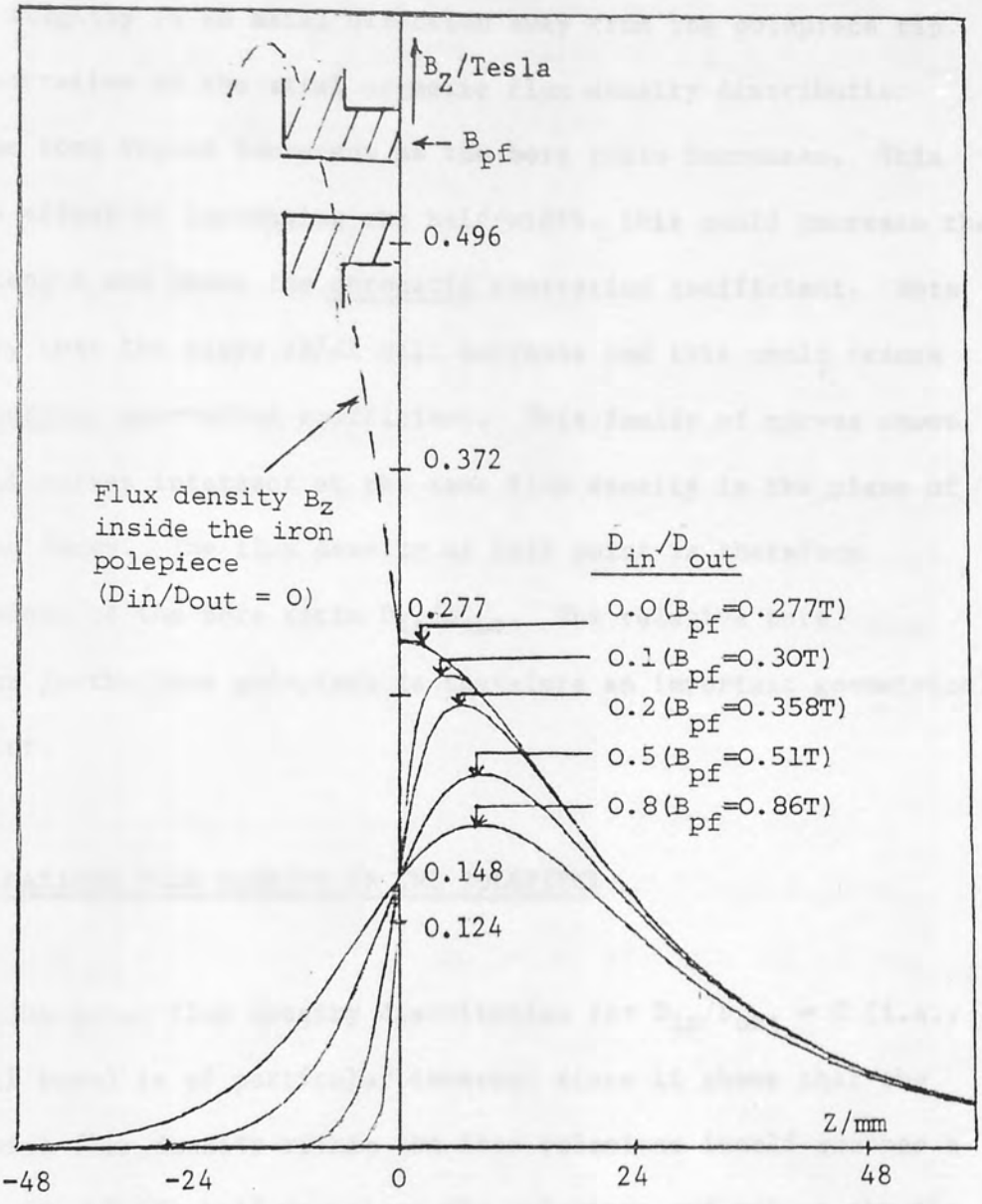

Fig 3.4 Calculated axial flux density distribution of rectangular (cross-section) polepiece lens of Fig 3.3 for different bore ratios D_{in}/D_{out} and for a constant excitation NI_{OR} = 7000 A-t, μ_r = 5000. Origin represents poleface. Poleface flux densities B_{pf} for different values of D_{in}/D_{out} are indicated on the figure.

The axial field distributions of Figure 3.4 exhibit the characteristic appearance mentioned previously, namely, a slowly rising flux density as the polepiece is approached and a rapid fall inside the polepiece bore.

The peak of the axial magnetic flux density distribution decreases, as would be expected, with increasing bore ratio and also shifts slightly in an axial direction away from the polepiece tip. The penetration of the axial magnetic flux density distribution into the bore region increases as the bore ratio increases. This has the effect of increasing the half-width; this could increase the focal length and hence the chromatic aberration coefficient. Note however, that the slope dB/dZ will decrease and this could reduce the spherical aberration coefficient. This family of curves shows that all curves intersect at the same flux density in the plane of the pole faces. The flux density at this point is therefore independent of the bore ratio D_{in}/D_{out}. The relative bore diameter in the lens polepiece is therefore an important geometrical parameter.

3.2.3 MAXIMUM FLUX DENSITY IN THE POLEPIECE

The axial flux density distribution for $D_{in}/D_{out} = 0$ (i.e., no axial bore) is of particular interest since it shows that the peak axial flux density within the iron polepiece itself reaches a maximum ($B_z \simeq 0.6T$) half way along the polepiece and not at the tip of the polepiece itself ($B_{pf} = 0.277T$). This is not of great importance when the permeability is high but would become of critical importance if the lens is to be operated at high axial flux density. In such a case unwanted saturation effects will take place within the polepiece body, preventing high flux densities from being realised in the polepiece tip.

The data of the field distribution curves shown in Figure 3.4 were used to calculate the electron optical properties of these

lenses by means of the Munro program M21 for both Ray I and Ray II. As explained in Chapter Two, this program calculates the focal properties of a given lens, such as RECT-ORIG, for which L = 120 mm , as a function of the excitation parameter $NI/V_r^{\frac{1}{2}}$.

Figures 3.5 a-e show the complete set of focal properties f_{obj}, f_{proj}, Z_f, and the aberration coefficients C_c and C_s for lens RECT-ORIG with different bore ratios (D_{in}/D_{out}), for both Ray I and Ray II. The ordinates of these graphs show immediately the computed values for the original lens with an outside diameter L = 120 mm. In fact the same figures show the value of the quantity f_{obj} (L/120), C_s (L/120), C_c (L/120) etc., for a lens of the same shape but different outside diameter.

From these ten curves, therefore, the principal electron optical characteristics of any lens of the form RECT-ORIG of any size L and at any relativistically corrected accelerating voltage V_r can be deduced.

Before discussing the optimum form that this lens can take, some general remarks should be made concerning the computed results in Figures 3.5 a-e.

The focal properties for Ray II mode are set out on the left hand side of the figures. These focal properties are quite similar to those for double-polepiece lenses. For example, at high excitation the objective focal length can be very small compared with the minimum projector focal length, but only by the use of high excitation parameters ($NI/V_r^{\frac{1}{2}} \simeq 50$). It should be noted that for the lens of

zero (or infinitely small) bore, the spherical aberration coefficient (C_s) is infinite. This arises from the fact that at the poleface ($Z = 0$) the flux gradient $dB/dZ = \infty$. Nevertheless, such a lens has an extremely low chromatic aberration coefficient, as discussed below.

In Ray I mode, on the other hand, for an excitation parameter $NI/V_r^{\frac{1}{2}} \gtrsim 13$, the focal length, chromatic and spherical aberration coefficients do not vary appreciably with the excitation parameter $NI/V_r^{\frac{1}{2}}$. Consequently such lenses may be operated at modest excitations compared with those operating in the Ray II mode.

It should also be pointed out here that the focal properties of the rectangular polepiece lenses differ appreciably from those predicted by the exponential field model and the spherical field model especially in the region of minimum objective and projector focal length. This will be referred to after the results for spherical polepieces have been discussed.

From this brief survey of the results shown in Figures 3.5 a-e it is clear that Ray II lenses of a given polepiece flux density will tend to be large, have large excitations and low chromatic aberration, while Ray I lenses will tend to be small, have comparatively low excitations and have low spherical aberration.

In view of these facts, in order to compare these two modes of operation, it would be sensible to compare lenses of comparable poleface flux density.

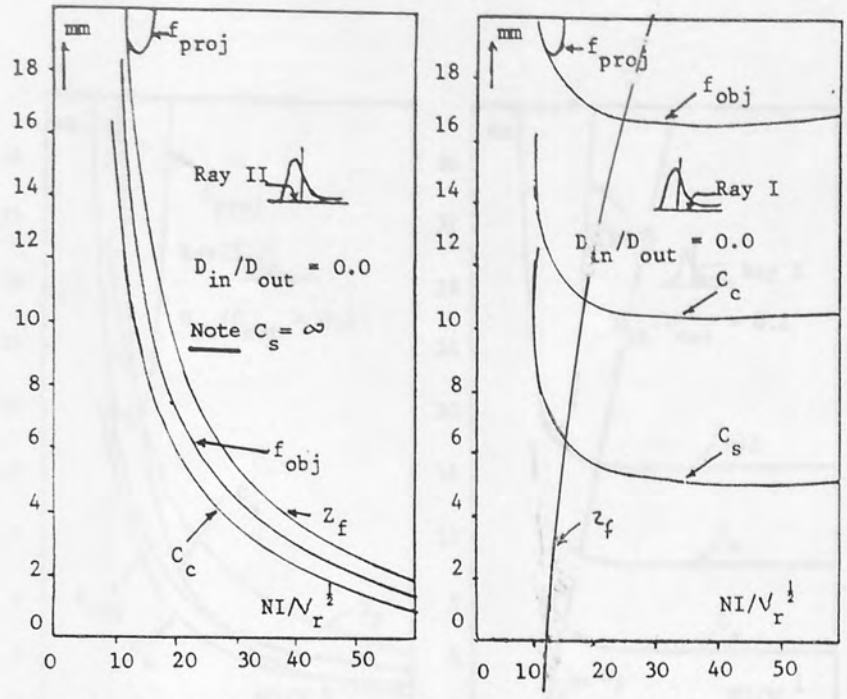

Fig 3.5a Focal properties of the single-polepiece shown in Fig 3.3 as a function of excitation parameter for Ray I and Ray II. (D_{in}/D_{out} = 0.0; B_{pf} = 0.277T)

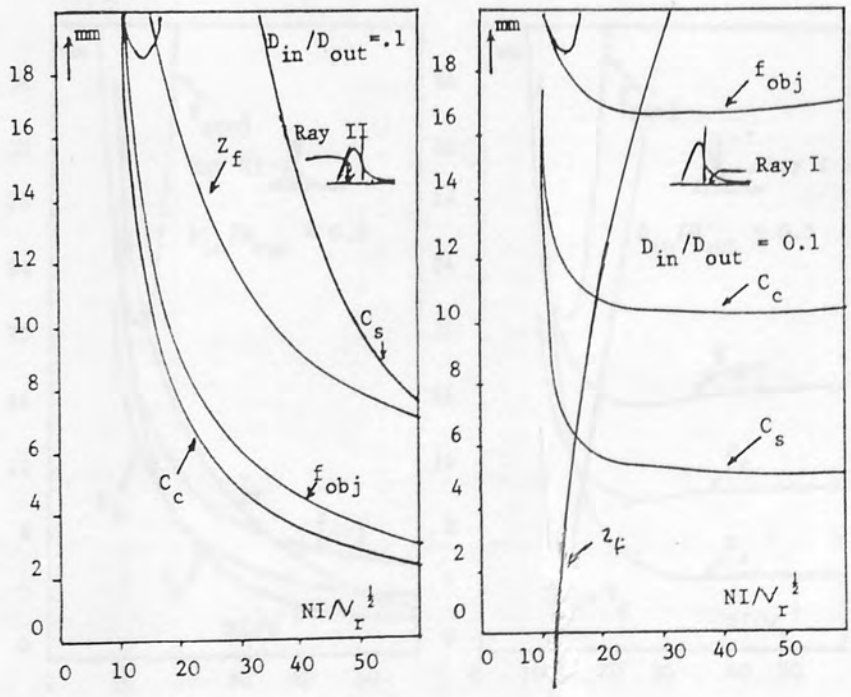

Fig 3.5b Focal properties of the single-polepiece shown in Fig 3.3 as a function of excitation parameter for Ray I and Ray II. (D_{in}/D_{out} = 0.1; B_{pf} = 0.30T)

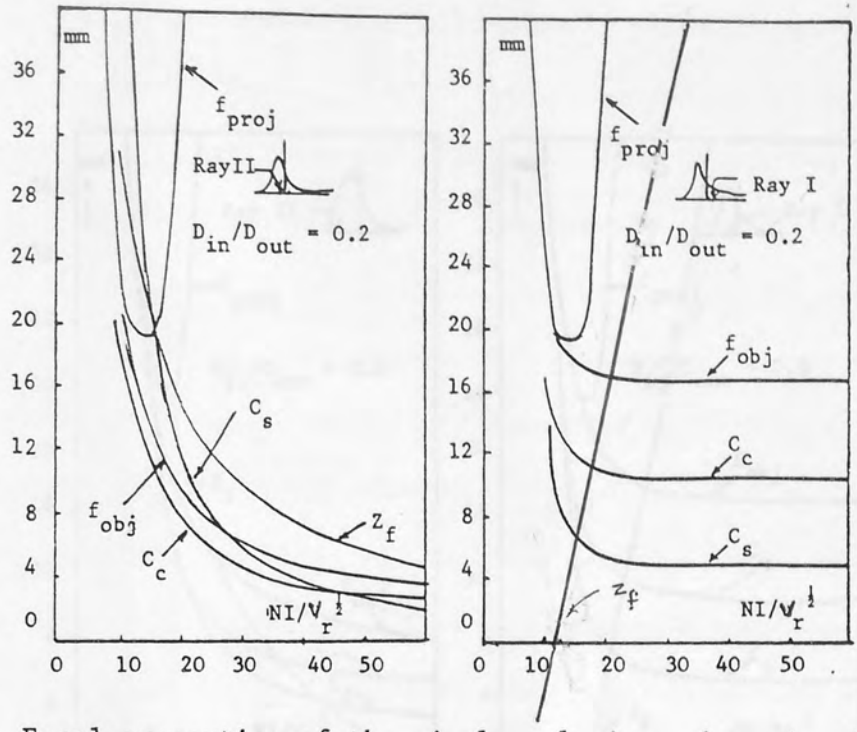

Fig 3.5c Focal properties of the single-polepiece shown in Fig 3.3 as a function of excitation parameter for Ray I and Ray II. (D_{in}/D_{out} = 0.2; B_{pf} = 0.358T)

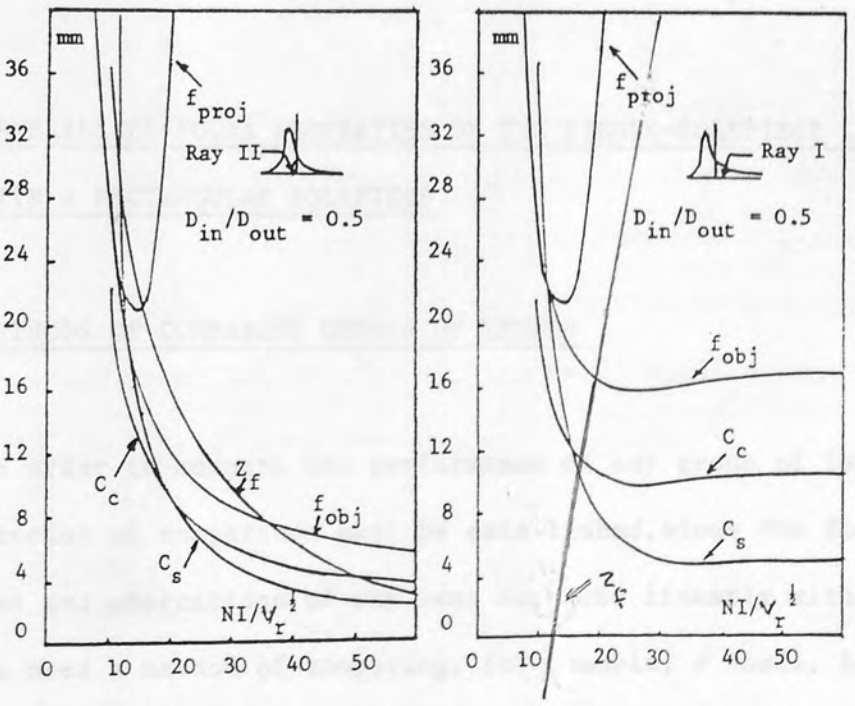

Fig 3.5d Focal properties of the single-polepiece shown in Fig 3.3 as a function of excitation parameter for Ray I and Ray II. (D_{in}/D_{out} = 0.5; B_{pf} = 0.51T)

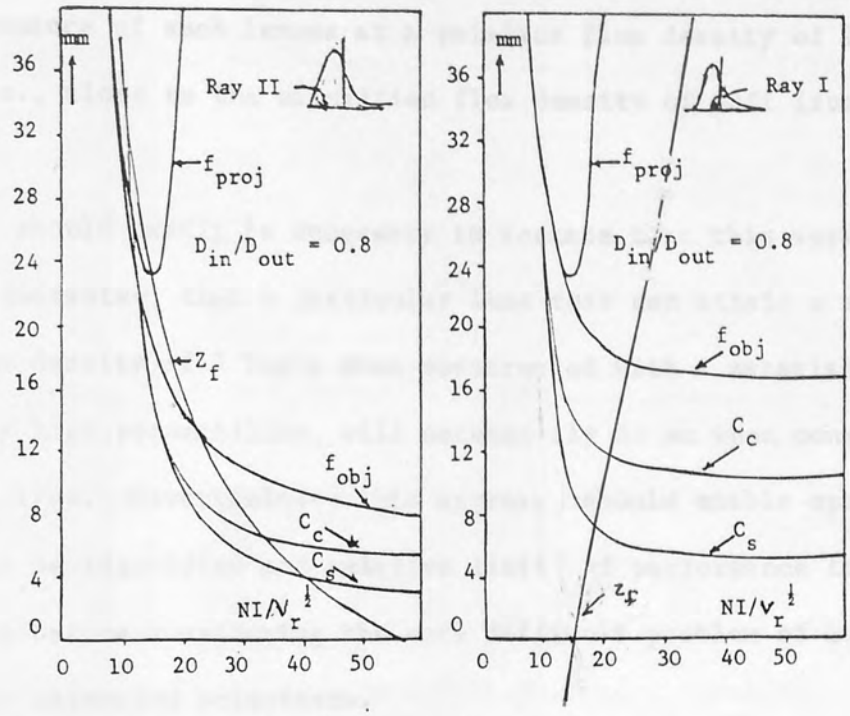

Fig 3.5e Focal properties of the single-polepiece shown in Fig 3.3 as a function of excitation parameter for Ray I and Ray II. (D_{in}/D_{out} = 0.8; B_{pf} = 0.86T)

3.3 GENERALISED FOCAL PROPERTIES OF THE SINGLE-POLEPIECE LENS WITH A RECTANGULAR POLEPIECE

3.3.1 METHODS OF COMPARING GROUPS OF LENSES

In order to compare the performance of any group of lenses, some criterion of comparison must be established, since the focal properties and aberrations of any lens decrease linearly with lens size. We need a method of comparing, for example, a small, bad lens with a large, good lens. Since in practice the poleface flux density of a lens controls its performance, it seems reasonable to

compare lenses of the same poleface flux density. Since the maximum flux density at which lenses can be considered to be in the linear B/H region is about 2 Tesla, it also seems reasonable to compare the performance of such lenses at a poleface flux density of 2 Tesla, i.e., close to the saturation flux density of soft iron.

It should hardly be necessary to restate that this approach does not guarantee that a particular lens that can attain a maximum axial flux density of 2 Tesla when constructed with a material of infinitely high permeability, will necessarily do so when constructed with real iron. Nevertheless, this approach should enable optimum designs to be identified and relative limits of performance to be calculated before considering the more difficult problem of lenses with truly saturated polepieces.

3.3.2 SCALING LAWS

In the linear region of the B/H curve, the magnetic flux density is proportional to the lens excitation. Thus, if the excitation NI_{OR} of an original lens (e.g., RECT-ORIG) with a given pole shape and poleface flux density B_{pf} is scaled by a factor of $(2/B_{pf})$, its poleface flux density B_{pf} becomes 2 Tesla. The excitation NI of the lens is thus given by

$$NI = (2/B_{pf})\, NI_{OR} \quad \ldots\ldots\ldots\ldots\ldots\ldots\ldots \quad 3.3$$

If the dimensions L of the lens are scaled by a factor n, and the lens excitation is also scaled by the same factor, the poleface

flux density in the original and scaled lens will have the same value, namely 2 Tesla. This is expressed in the following relationships

$$NI = n.(2/B_{pf})\ NI_{OR} \quad \ldots\ldots\ldots\ldots\ldots\ldots\ldots \quad 3.3a$$

$$\text{and} \quad L^* = n\ L \quad \ldots\ldots\ldots\ldots\ldots\ldots\ldots\ldots\ldots \quad 3.3b$$

where L* denotes the outer diameter of the scaled lens. The corresponding focal properties f_{obj}*, C_s*, C_c* etc., of the scaled lens will also be scaled by the same factor n so that

$$f_{obj}^* = nf_{obj},\ C_s^* = nC_s \text{ etc.} \quad \ldots\ldots\ldots\ldots\ldots \quad 3.4$$

Equations 3.3 enable us to transform the curves of Figures 3.5 a-e, in which the actual poleface flux density varies with the excitation parameter $NI/V_r^{\frac{1}{2}}$ but the lens size L = 120 mm is constant, into a set of curves in which the poleface flux density is constant at 2 Tesla but the lens size L* varies (linearly) with the excitation parameter $NI/V_r^{\frac{1}{2}}$.

This is carried out as follows dividing both sides of equation 3.3a by $V_r^{\frac{1}{2}}$

$$NI/V_r^{\frac{1}{2}} = n\ (2/B_{pf})\ NI_{OR}/V_r^{\frac{1}{2}} \quad \ldots\ldots\ldots\ldots\ldots \quad 3.5$$

$$\text{ie} \quad n/V_r^{\frac{1}{2}} = (NI/V_r^{\frac{1}{2}})(B_{pf}/2)/NI_{OR} \quad \ldots\ldots\ldots\ldots\ldots \quad 3.6$$

This may be written

$$n/V_r^{\frac{1}{2}} = K\ (NI/V_r^{\frac{1}{2}}) \quad \ldots\ldots\ldots\ldots\ldots\ldots\ldots \quad 3.6a$$

where $K = (B_{pf}/2\ NI_{OR})$.

Equation 3.6a shows that for a given original lens of lens excitation NI_{OR}, the scaling factor n is linearly proportional to $NI/V_r^{\frac{1}{2}}$ and to the square root of V_r. This means that for a given value of V_r

the scaled lens size L* and the corresponding aberration coefficients f_{obj}*, C_s*, C_c* are also proportional to $NI/V_r^{\frac{1}{2}}$.

As an example, Table 3.1 shows how the C_s and L values for Ray I and D_{in}/D_{out} = 0 of Figure 3.3 are transformed to a poleface flux density of 2 Tesla. The figures are calculated for V_r = 100kV.

TABLE 3.1

Scaled focal properties for Ray I mode and D_{in}/D_{out} = 0.0 .

Data: B_{pf} = 0.277T; NI_{OR} = 7000 A-t; V_r = 100 kV.

$NI/V_r^{\frac{1}{2}}$	C_s	n = according to Eq 3.6	C_s* = nCs	L* = nL	σ* = NI/A*
	mm		mm	mm	A-t/mm^2
9.88	11.78	0.067	0.79	8.04	1592.67
12.33	7.25	0.083	0.60	9.96	1295.16
31.00	5.19	0.210	1.09	25.20	502.72
46.24	5.09	0.313	1.59	37.56	341.53
60.10	5.05	0.407	2.05	48.84	262.54

3.3.3 COMPARISON OF THE ELECTRON OPTICAL PROPERTIES FOR RAY I AND RAY II BEAM ORIENTATION OF THE RECTANGULAR POLEPIECE LENS

The focal properties and aberrations in Figures 3.5 a-e, but converted for a poleface flux density of 2 Tesla, are shown in Figures 3.6 - 3.9 as before, as a function of the excitation parameter $NI/V_r^{\frac{1}{2}}$. As the scaled coefficients f_{obj}*, Z_f*, C_s*, C_c* and L* are linearly related to $V_r^{\frac{1}{2}}$, the ordinate of the curve is plotted as $Z_f^*(10^5/V_r)^{\frac{1}{2}}$, $f_{obj}^*(10^5/V_r)^{\frac{1}{2}}$ etc. This has the advantage that the numerical value of the ordinate gives directly

(in mm) the value of Z_f^*, f_{obj}^* for V_r = 100kV.

The variation of the objective focal distance $Z_f^*(10^5/V_r)^{\frac{1}{2}}$ with the excitation parameter $(NI/V_r^{\frac{1}{2}})$ is shown in Figure 3.6. This focal distance $Z_f^*(10^5/V_r)^{\frac{1}{2}}$, is the distance between the apex of the polepiece taken as origin (Z = 0), and the specimen position Z. It can be seen that, for Ray II beam orientation, $Z_f^*(10^5/V_r)^{\frac{1}{2}}$ is in general, positive even at high excitations. The focal distance increases with increasing bore ratio. The lens with a ratio D_{in}/D_{out} = 0, gives the focal distance closest to the polepeice. For Ray I beam orientation, at low excitations the focal distance moves towards the poleface with increasing lens excitation until it reaches a zero value at a lens excitation parameter $NI/V_r^{\frac{1}{2}} \simeq 12$. The negative values indicate that the focal distance is inside the polepiece. The lens with a bore ratio D_{in}/D_{out} tending to zero, gives the shortest working distance.

3.3.4 OBJECTIVE FOCAL LENGTH OF THE NORMALISED LENSES

Figure 3.7 a and b shows the scaled objective focal length $f_{obj}^* (10^5/V_r)^{\frac{1}{2}}$, as a function of excitation parameter $(NI/V_r^{\frac{1}{2}})$, for Ray II and Ray I. The curves of Figure 3.7a show that in Ray II the objective focal length does not vary significantly as the excitation parameter $NI/V_r^{\frac{1}{2}}$ is altered over wide limits. Under Ray I conditions (Figure 3.7b) there is an optimum excitation $NI/V_r^{\frac{1}{2}} \simeq 12$ so that lenses operating in this mode will necessarily be smaller than those operating in Ray II mode, so there is less flexibility in choosing the value of L*.

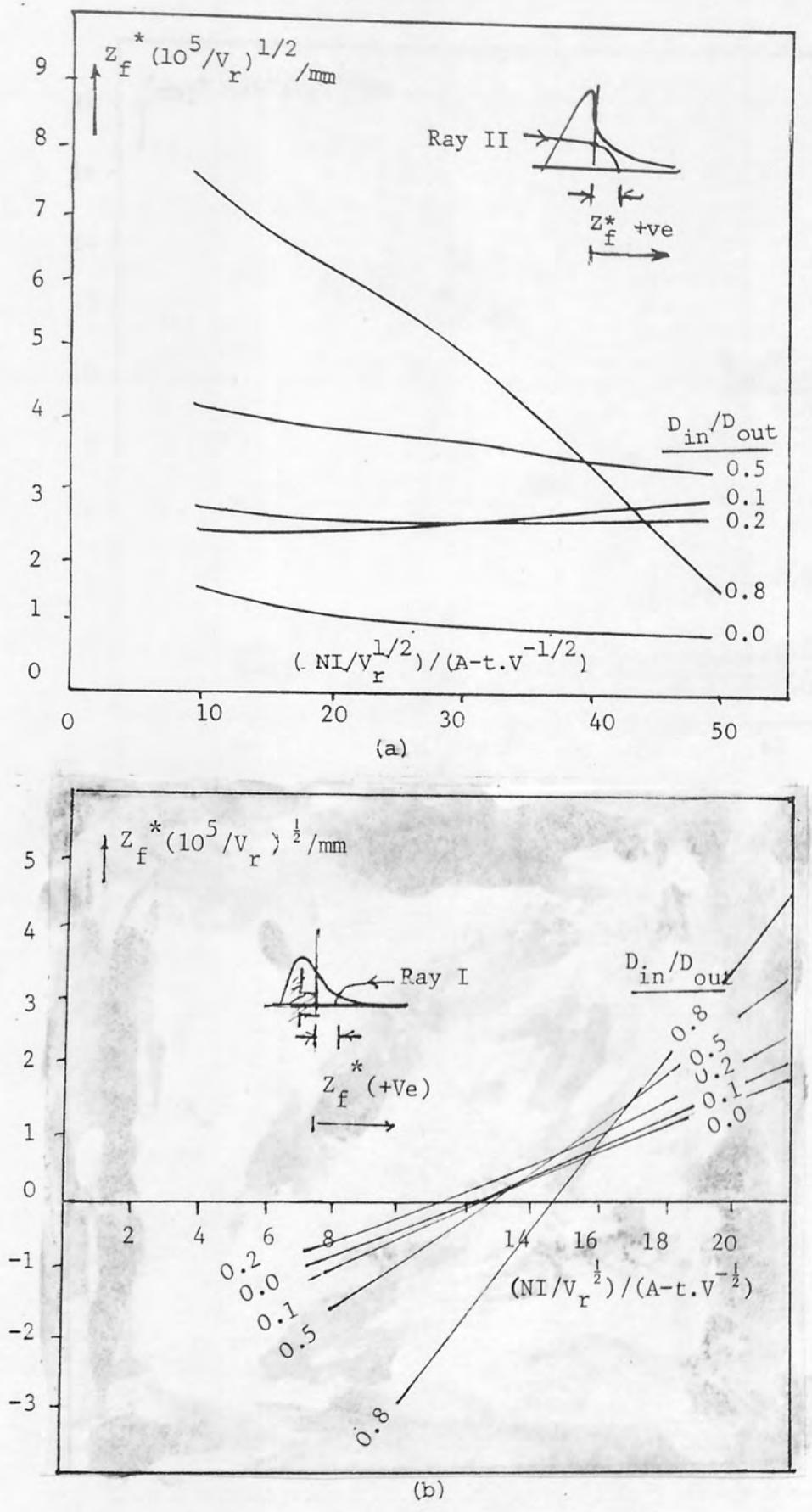

Fig 3.6 Variation of normalised objective focal distance $Z_f^*(10^5/V_r)^{\frac{1}{2}}$ for different bore ratios D_{in}/D_{out} of the lens (RECT-ORIG) as a function of excitation parameter $NI/V_r^{\frac{1}{2}}$ (a) Ray II, (b) Ray I. (B_{pf} = 2T)

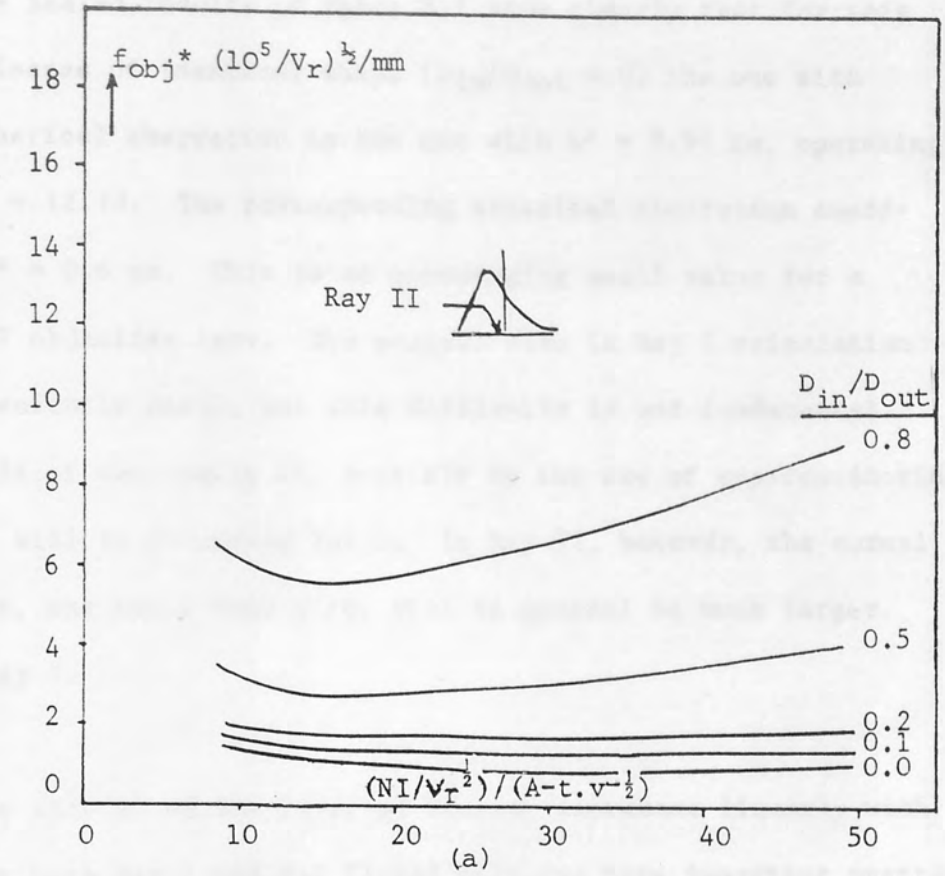

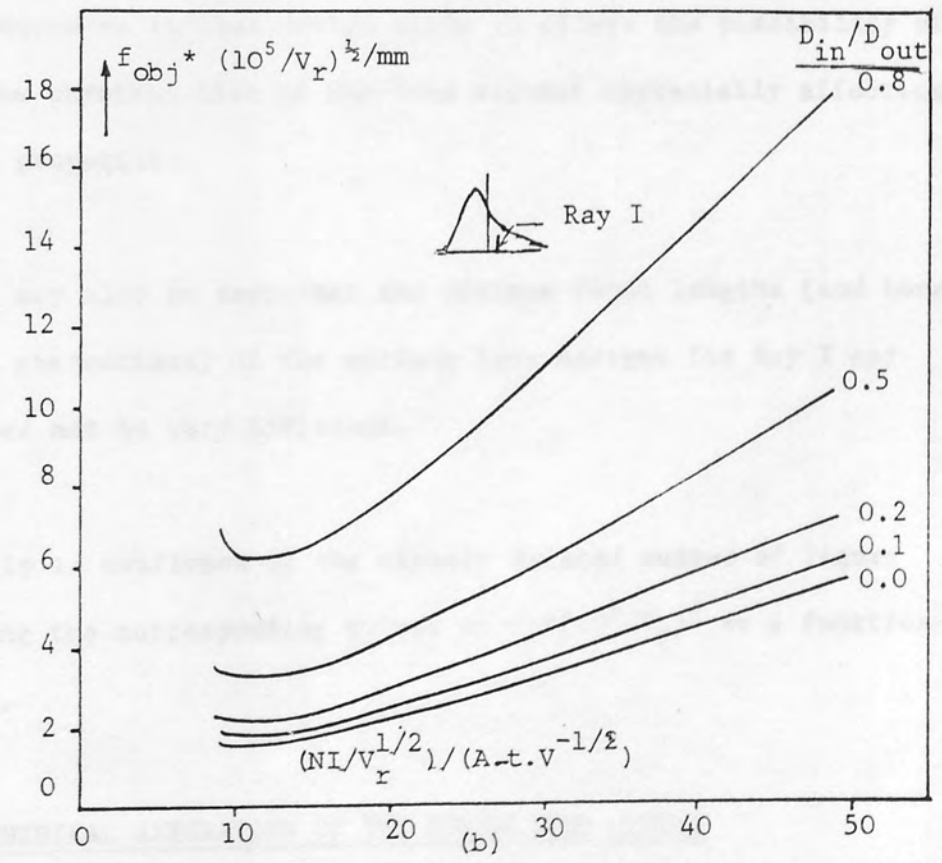

Fig 3.7 Variation of normalised objective focal length f_{obj}*$(10^5/V_r)^{\frac{1}{2}}$ for different bore ratios D_{in}/D_{out} of the lens (RECT-ORIG) as a function of excitation parameter $NI/V_r^{\frac{1}{2}}$ (a) Ray II, (b) Ray I. (B_{pf} = 2T)

The scaled results of Table 3.1 show clearly that for this group of lenses of identical shape (D_{in}/D_{out} = 0) the one with lowest spherical aberration is the one with L* = 9.96 mm, operating at $NI/V_r^{\frac{1}{2}}$ = 12.33. The corresponding spherical aberration coefficient C_s* = 0.6 mm. This is an encouraging small value for a V_r = 100kV objective lens. The overall size in Ray I orientation is inconveniently small, but this difficulty is not fundamental and methods of overcoming it, possibly by the use of superconducting windings, will be discussed later. In Ray II, however, the normal excitation, and hence lens size, will in general be much larger than in Ray I.

The size L* of the lens, of course, increases linearly with $NI/V_r^{\frac{1}{2}}$ for both Ray I and Ray II and this can have important practical consequences in lens design since it offers the possibility of varying the physical size of the lens without appreciably affecting the focal properties.

It may also be seen that the minimum focal lengths (and hence chromatic aberrations) of the optimum lens designs for Ray I and Ray II need not be very different.

This is confirmed by the closely related curves of Figure 3.8 showing the corresponding values of $C_c*(10^5/V_r)^{\frac{1}{2}}$ as a function of $NI/V_r^{\frac{1}{2}}$.

3.3.5 SPHERICAL ABERRATION OF THE NORMALISED LENSES

Figure 3.9 shows the variation of the normalised spherical aberration coefficient $C_s*(10^5/V_r)^{\frac{1}{2}}$, as a function of excitation

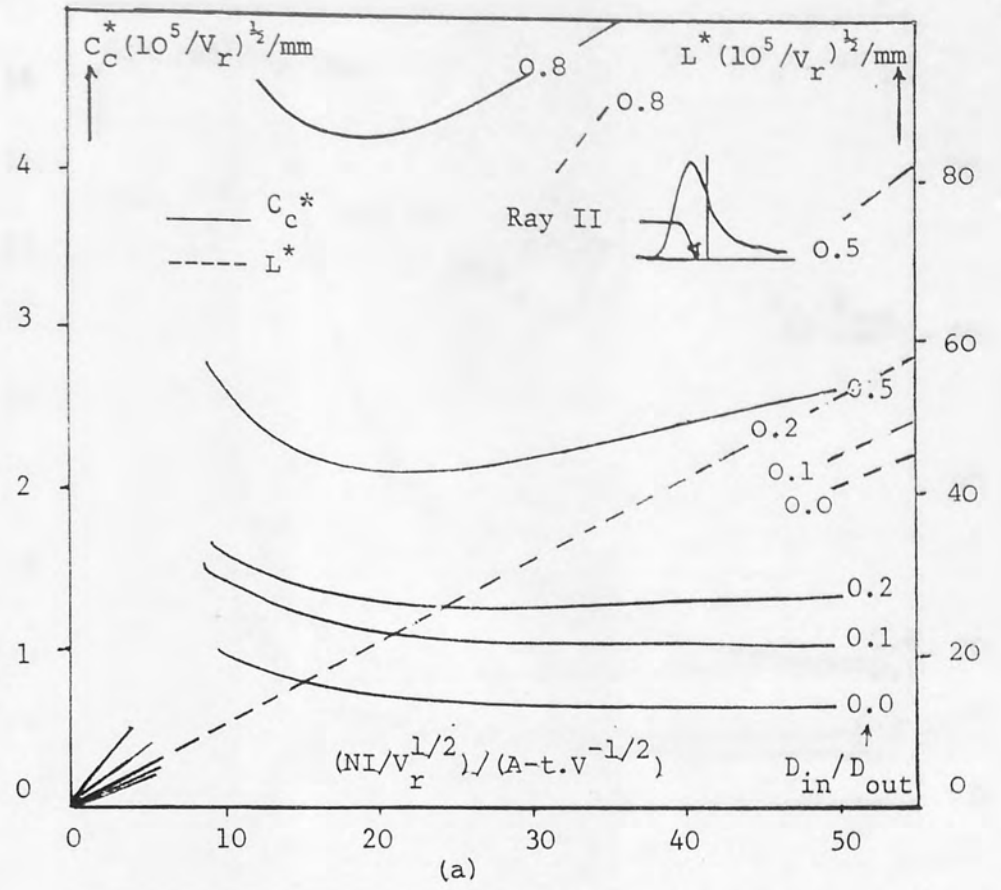

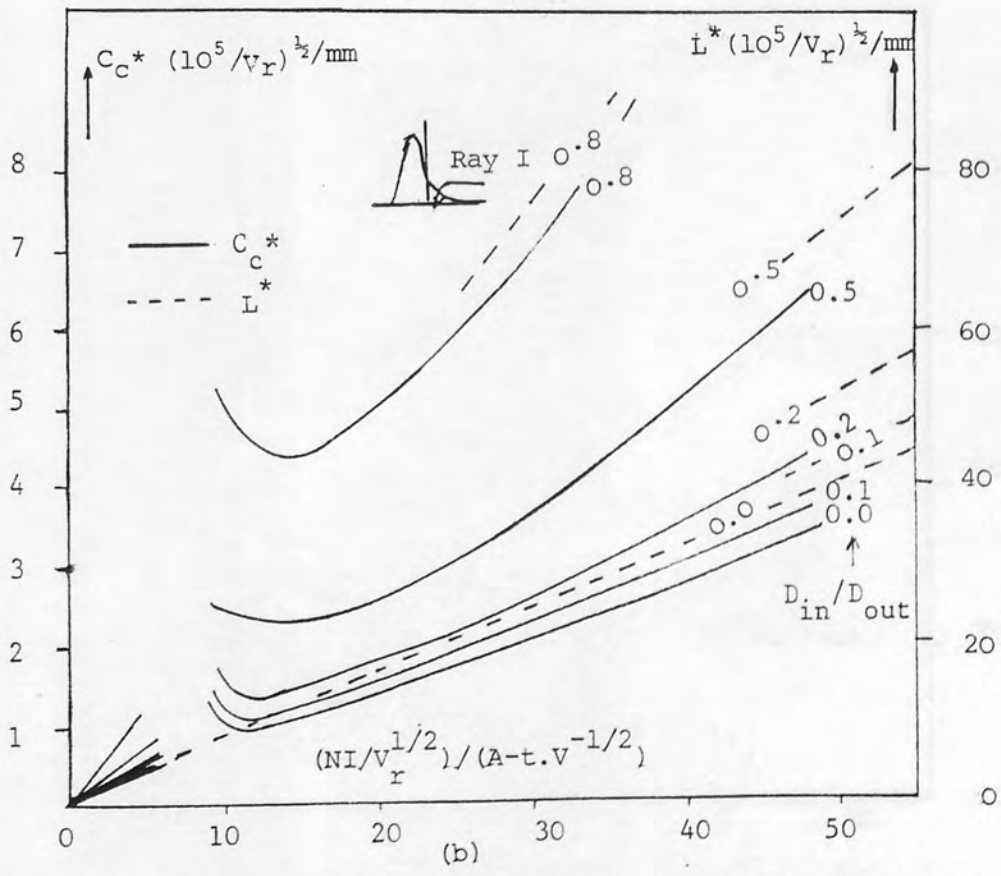

Fig 3.8 Variation of normalised chromatic aberration coefficient $C_c^*(10^5/V_r)^{\frac{1}{2}}$ for different bore ratios D_{in}/D_{out} of the lens (RECT-ORIG) as a function of excitation parameter $NI/V_r^{\frac{1}{2}}$ (a) Ray II, (b) Ray I, (B_{pf} = 2T). The dashed lines indicate lens size.

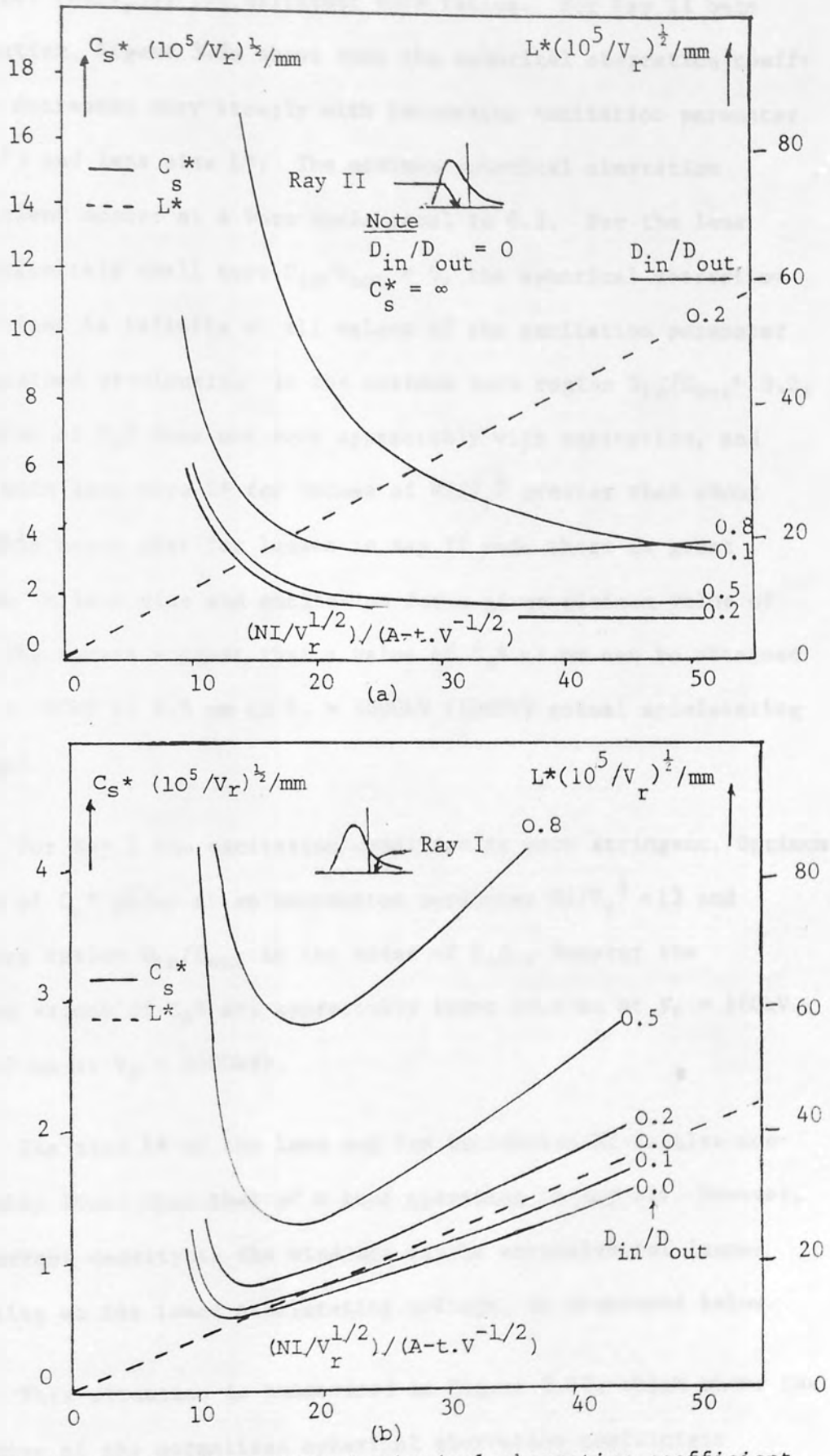

Fig 3.9 Variation of normalised spherical aberration coefficient $C_s^*(10^5/V_r)^{\frac{1}{2}}$ for different bore ratios D_{in}/D_{out} of the lens (RECT-ORIG) as a function of excitation parameter (a) Ray II, (b) Ray I, (B_{pf} = 2T). The dashed lines indicate lens size.

parameter ($NI/V_r^{\frac{1}{2}}$), for different bore ratios. For Ray II beam orientation, Figure 3.9a shows that the spherical aberration coefficient decreases very steeply with increasing excitation parameter ($NI/V_r^{\frac{1}{2}}$) and lens size L*. The minimum spherical aberration coefficient occurs at a bore ratio equal to 0.2. For the lens with infinitely small bore $D_{in}/D_{out} = 0$, the spherical aberration coefficient is infinite at all values of the excitation parameter as explained previously. In the optimum bore region $D_{in}/D_{out} \simeq 0.2$, the value of C_s* does not vary appreciably with excitation, and hence with lens size L* for values of $NI/V_r^{\frac{1}{2}}$ greater than about 30. This means that for lenses in Ray II mode there is great freedom in lens size and excitation for a given minimum value of C_s*. The curves suggest that a value of $C_s^* \simeq 1$ mm can be obtained at V_r = 100kV or 4.5 mm at V_r = 2000kV (1000kV actual accelerating voltage).

For Ray I the excitation condition is more stringent. Optimum values of C_s* occur at an excitation parameter $NI/V_r^{\frac{1}{2}} \simeq 13$ and for bore ratios D_{in}/D_{out} in the order of 0.0 . However the minimum values of C_s* are appreciably lower (0.6 mm at V_r = 100kV and 2.7 mm at V_r = 2000kV).

The size L* of the lens and its excitation NI is also considerably lower than that of a lens operating in Ray II. However, the current density in the windings may be excessive for lenses operating at the lower accelerating voltage, as discussed below.

This situation is summarised in Figure 3.10, which shows the variation of the normalised spherical aberration coefficient $C_s^*(105/V_r)^{\frac{1}{2}}$ as a function of bore ratio D_{in}/D_{out} for different values of $NI/V_r^{\frac{1}{2}}$. For Ray I beam orientation, the spherical

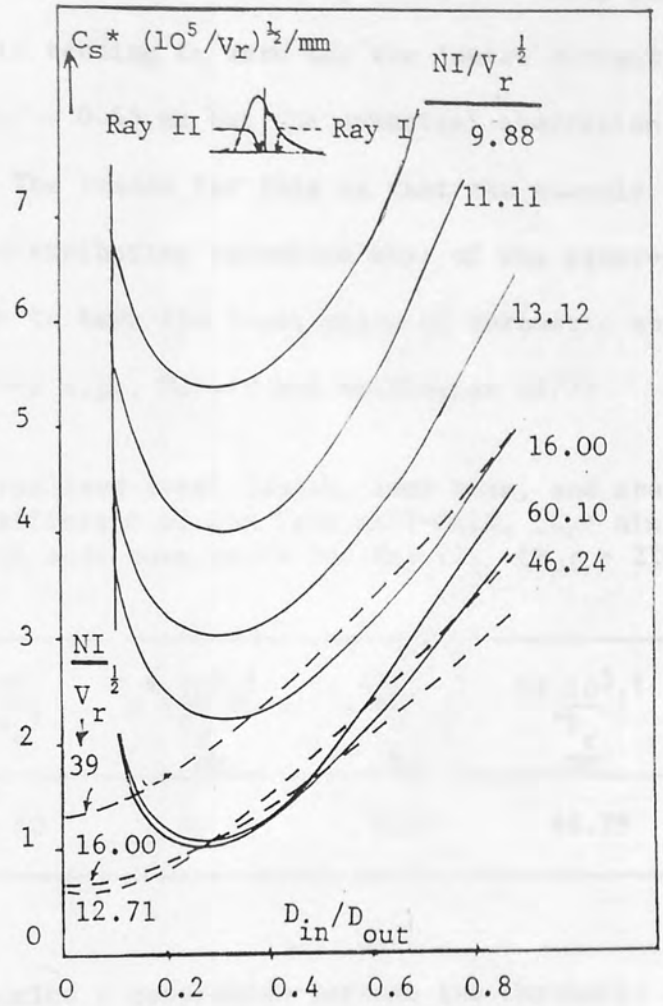

Fig 3.10 Variation of normalised spherical aberration coefficient $C_s^*(10^5/V_r)^{\frac{1}{2}}$ for different bore ratios D_{in}/D_{out} of the lens (RECT-ORIG) at different excitation parameters for Ray I and Ray II. (B_{pf} = 2T)

aberration coefficient decreases steadily with decreasing bore ratio. The minimum value of spherical aberration C_s^* = 0.6mm at V_r = 100kV occurs at an excitation parameter equal to 12.7 and at a bore ratio tending to zero. For Ray II beam orientation, fairly low values of spherical aberration coefficients C_s^* = 1mm at V_r = 100kV occur at high values of excitation parameter (40-50), and a bore ratio $D_{in}/D_{out} \simeq 0.33$. For Ray I beam orientation, the spherical aberration coefficient increases gradually with increasing bore ratio.

3.3.6 OPTIMUM ELECTRON OPTICAL PROPERTIES FOR RAY I AND RAY II

For Ray II beam orientation, Table 3.2 shows that the lens with bore ratio tending to zero has the lowest chromatic aberration coefficient $C_c^* = 0.65$ mm but the spherical aberration coefficient is infinite. The reason for this is that the steeply rising edge of the field distribution resembles that of the square-topped field which is known to have the least value of chromatic aberration coefficient (see e.g., Mulvey and Wallington 1973)

Table 3.2 Normalised focal length, lens size, and aberration coefficient of the lens RECT-ORIG, (C_c^* minimised) with zero bore ratio for Ray II. (B_{pf} = 2T)

Coefficient Minimised	$\frac{NI}{V_r^{\frac{1}{2}}}$	$C_s^*[\frac{10^5}{V_r}]^{\frac{1}{2}}$ mm	$C_c^*[\frac{10^5}{V_r}]^{\frac{1}{2}}$ mm	$L^*[\frac{10^5}{V_r}]^{\frac{1}{2}}$ mm	D_{in}/D_{out}
C_c^*	60	∞	0.65	48.79	0.0

In practice a compromise between low chromatic aberration (lens b) and spherical aberration (lens a) must be sought. A bore ratio $D_{in}/D_{out} = 0.3$ seems to offer such a compromise. Table 3.3, shows the electron optical properties of the above lenses with this bore ratio.

Table 3.3 Normalised focal lengths, lens size, and aberration coefficient of lens RECT-ORIG a, (C_s^* minimised) and lens b (C_c^* minimised) of bore ratio $D_{in}/D_{out} = 0.3$ for Ray II. (B_{pf} = 2T)

Lens	$\frac{NI}{V_r^{\frac{1}{2}}}$	$C_s^*[\frac{10^5}{V_r}]^{\frac{1}{2}}$ mm	$C_c^*[\frac{10^5}{V_r}]^{\frac{1}{2}}$ mm	$L^*[\frac{10^5}{V_r}]^{\frac{1}{2}}$ mm
(a)	60.1	1.0	1.8	72.24
(b)	16.0	2.25	1.55	19.2

For Ray I beam orientation, Table 3.4 shows two extreme cases of the electron optical properties of the best lens with bore ratio tending to zero. One has a very low spherical aberration coefficient (lens a), and the other has a very low chromatic aberration coefficient (lens b).

Table 3.4 Normalised focal lengths, lens size, and aberration coefficient of lens RECT-ORIG a, (C_s* minimised) and lens b (C_c* minimised) of bore ratio D_{in}/D_{out} = 0.0 for Ray I (B_{pf} = 2T)

Lens	$\frac{NI}{V_r^{\frac{1}{2}}}$	$C_s^*[\frac{10^5}{V_r}]^{\frac{1}{2}}$ mm	$C_c^*[\frac{10^5}{V_r}]^{\frac{1}{2}}$ mm	$f_{obj}^*[\frac{10^5}{V_r}]^{\frac{1}{2}}$ mm	$Z_f^*[\frac{10^5}{V_r}]^{\frac{1}{2}}$ mm	$L^*[\frac{10^5}{V_r}]^{\frac{1}{2}}$ mm
(a)	12.33	0.60	1.0	1.50	0.0	9.96
(b)	10.86	0.65	1.0	1.47	0.22	8.76

The lens with low spherical aberration coefficient has also a relatively low chromatic aberration coefficient and it can be regarded as a very good compromise if a lens is required with both low spherical and chromatic aberration, (practical compromise lenses (a) and (b)). Both lenses have identical values of D_{in}/D_{out} = 0.1, and operate at a poleface flux density of 2T. Lens (a) has been optimised for minimum spherical aberration (C_s^* $(10^5/V_r)^{\frac{1}{2}}$ = 0.68mm). Lens (b) has been optimised for minimum chromatic aberration (C_c^* $(10^5/V_r)^{\frac{1}{2}}$ = 1.13 mm), and is slightly smaller than lens (a). Table 3.5 shows the associated focal length f_{obj}, focal distance Z_f^* and lens size L* together with the aberration coefficient C_c^* or C_s^* that was not minimised.

Table 3.5 Normalised focal lengths, lens size, and aberration coefficients of lens RECT-ORIG a, (C_s* minimised) and lens b (C_c* minimised), of bore ratio D_{in}/D_{out} = 0.1 for Ray I (B_{pf} = 2T)

Lens	$\frac{NI}{V_r^{\frac{1}{2}}}$	$C_s^*[\frac{10^5}{V_r}]^{\frac{1}{2}}$ mm	$C_c^*[\frac{10^5}{V_r}]^{\frac{1}{2}}$ mm	$f_{obj}^*[\frac{10^5}{V_r}]^{\frac{1}{2}}$ mm	$Z_f^*[\frac{10^5}{V_r}]^{\frac{1}{2}}$ mm	$L^*[\frac{10^5}{V_r}]^{\frac{1}{2}}$ mm
(a)	13.57	0.68	1.18	1.82	0.26	11.88
(b)	11.11	0.77	1.13	1.65	0.20	9.72

3.4 SINGLE-POLEPIECE LENS WITH A SPHERICAL POLEPIECE

3.4.1 REASONS FOR USING A SPHERICAL POLEPIECE

In this section the possible advantages of a spherical polepiece are discussed. In the model lens, in Figure 3.3, the rectangular polepiece was replaced by a spherical one leaving the overall geometry otherwise unchanged. The advantage of the redesigned polepiece could be to minimise the maximum flux density in the polepiece so as to produce the highest flux density at the tip, rather than in the middle of the polepiece, as happened with the rectangular polepiece. The resulting spherical polepiece lens is shown in Figure 3.11. Its polepiece consists of an iron hemisphere of radius 25 mm since the behaviour of such a polepiece has previously been investigated analytically (Al-Shwaikh and Mulvey, 1977). The magnetic field distribution of this lens was determined by the finite element method (Munro, 1975), as before, setting the relative permeability μ_r of the polepiece as 5000.

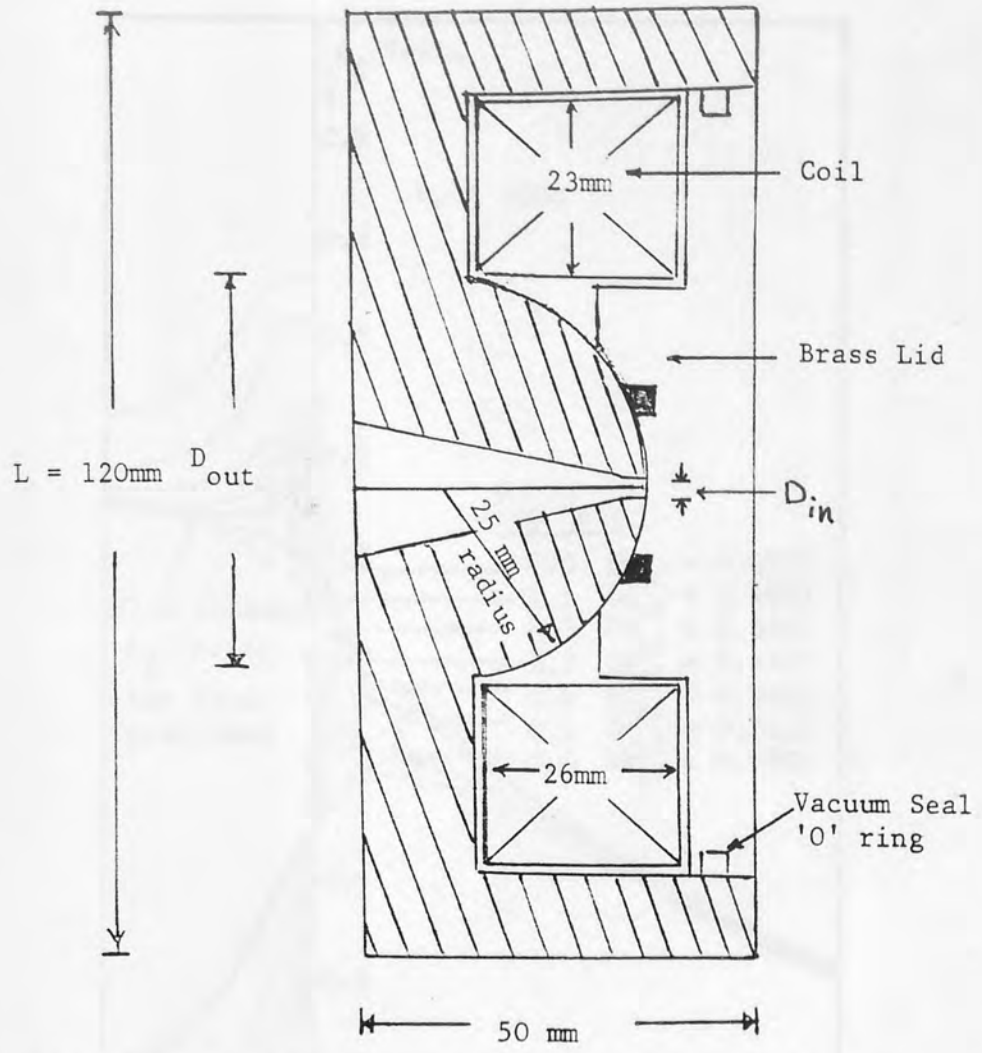

Fig 3.11 Spherical polepiece lens (SPHER-ORIG) of variable bore for the investigation of focal properities and aberration coefficients of single-polepiece lenses with spherical section polepiece (coil area = 23 x 26 mm^2)

The resulting axial flux density distribution of the spherical polepiece is shown in Figure 3.12, computed for different bore ratios D_{in}/D_{out}, at a constant excitation value NI_{OR} = 7000 ampere-turns as for the basic calculation of the rectangular polepiece lens. From this figure, it can be seen at once, that when the bore ratio is equal to zero, the maximum flux inside the magnetic circuit does not occur at the tip of the hemisphere polepiece but the distribution is appreciably more favourable than for the rectangular polepiece. As the bore ratio increases, the maximum flux density inside the iron also increases and moves towards the pole-

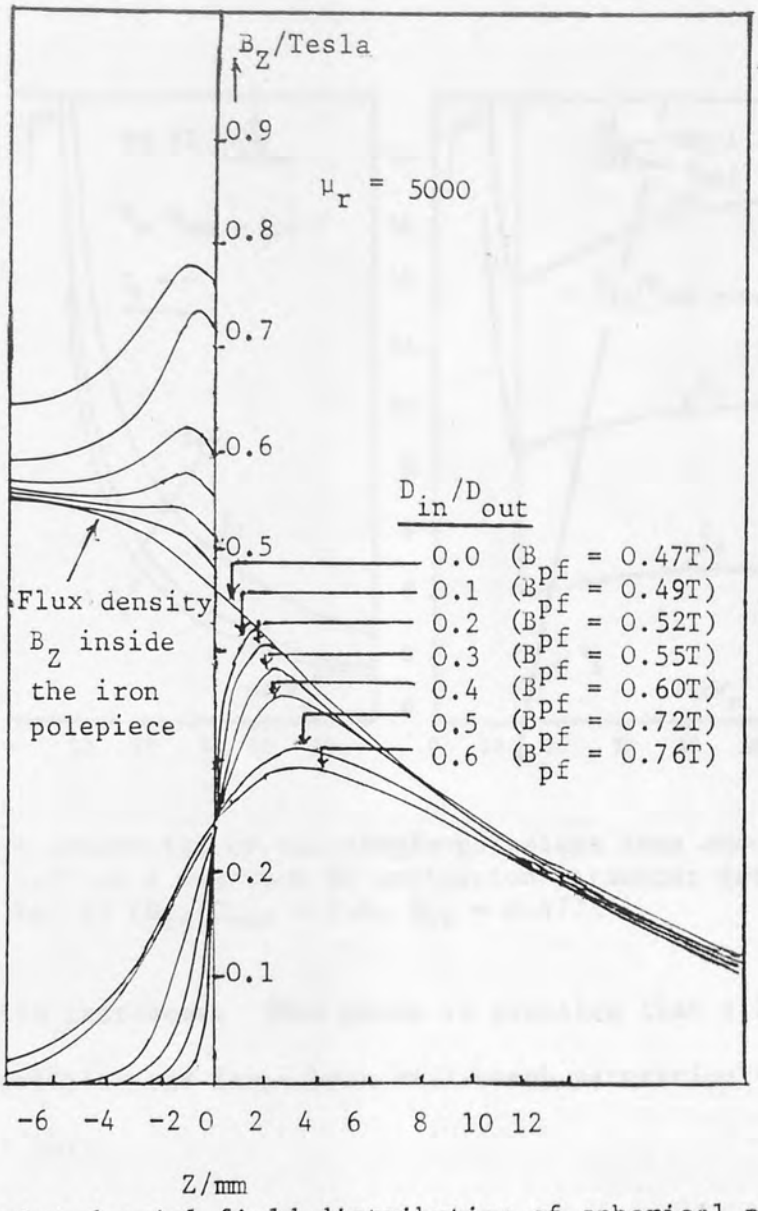

Fig 3.12 Calculated axial field distribution of spherical polepiece lens of Fig 3.11 for different bore ratios D_{in}/D_{out} and for a constant excitation NI_{OR} = 7000 amp-turns. Origin represents poleface.

piece tip. This is due to the reduction in the cross-sectional area of the snout caused by the removal of material in making the bore. The peak of the axial magnetic flux density distribution outside the iron decreases with increasing bore ratio and shifts away from the snout tip. As the bore ratio D_{in}/D_{out} increases, the half-width of the axial flux density distribution increases due to the penetration of the axial magnetic flux density distribution inside the bore. The flux density at the poleface increases

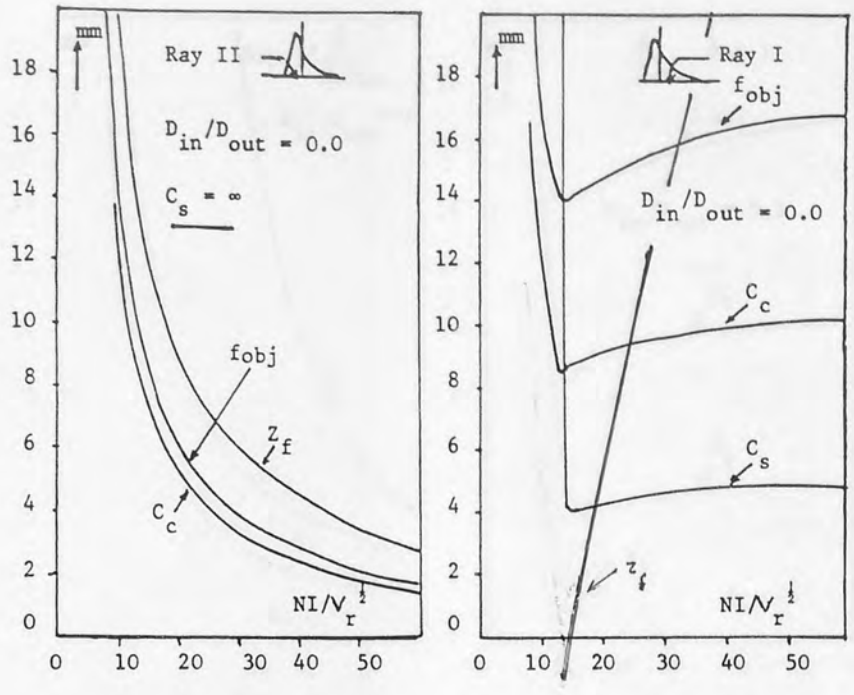

Fig 3.13a Focal properties of the single-polepiece lens shown in Fig 3.11 as a function of excitation parameter for Ray I and Ray II (D_{in}/D_{out} = 0.0, B_{pf} = 0.47T)

as the bore ratio increases. This means in practice that a lens of normal permeability and large bore will reach saturation before a lens of small bore.

Figures 3.13 a-g shows the systematic variation of electron optical properties of this family of lenses as calculated by program M21, for Ray I and Ray II modes of operation. The focal properties for Ray II mode are set out on the left hand side of Figures 3.13 a-g. These focal properties are similar to those for rectangular polepiece lenses. For example, at high excitation ($NI/V_r^{\frac{1}{2}} > 40$) the objective focal length can be very small. It should be noted that for the lens of zero bore ratio the spherical aberration coefficient (C_s) is infinite. This arises from the fact that at the poleface (Z = 0) the flux gradient dB/dZ becomes infinite.

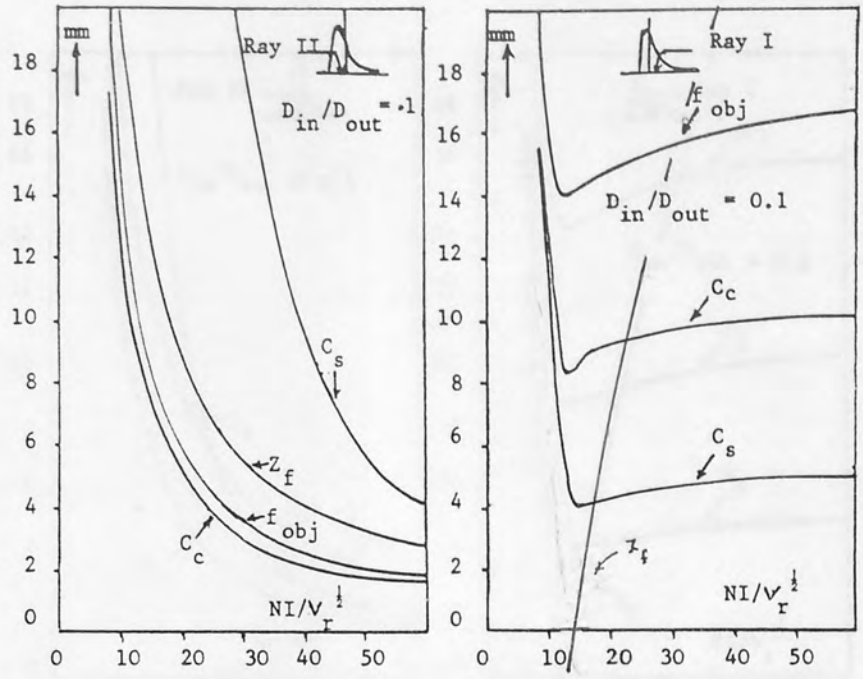

Fig 3.13b Focal properties of the single-polepiece lens shown in Fig 3.11 as a function of excitation parameter for Ray I and Ray II (D_{in}/D_{out} = 0.1, B_{pf} = 0.49T)

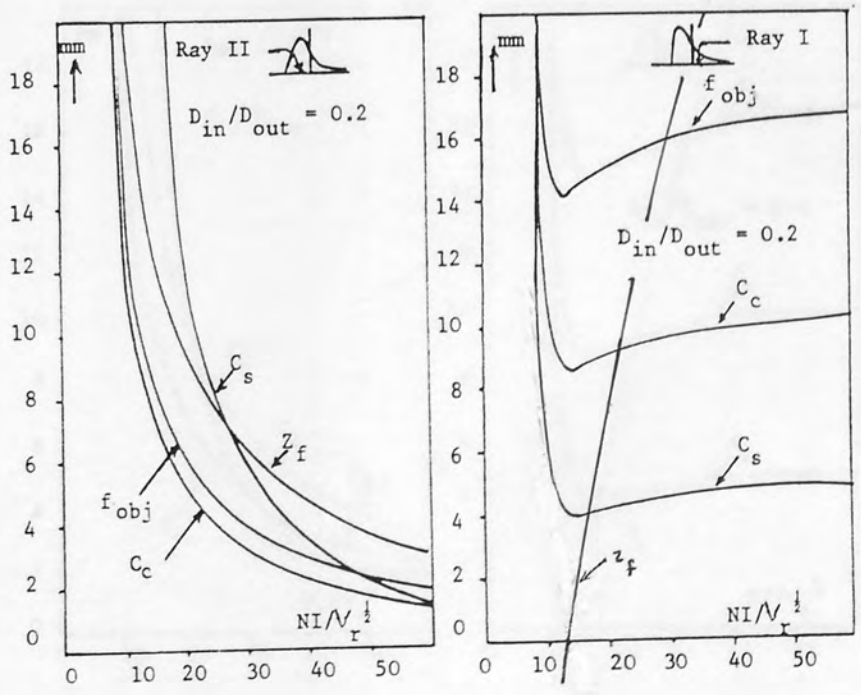

Fig 3.13c Focal properties of the single-polepiece lens shown in Fig 3.11 as a function of excitation parameter for Ray I and Ray II (D_{in}/D_{out} = 0.2, B_{pf} = 0.52T)

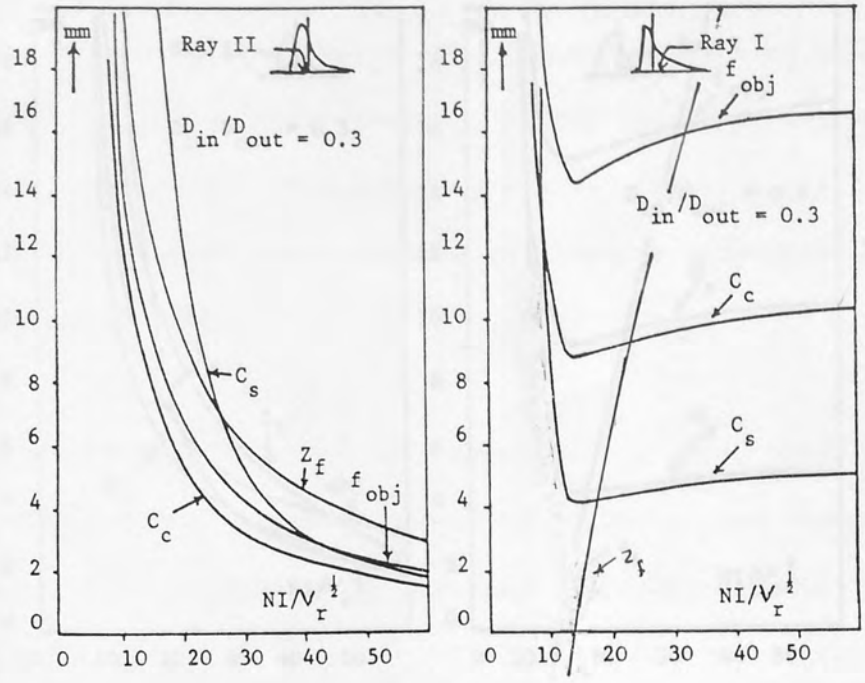

Fig 3.13d Focal properties of the single-polepiece lens shown in Fig 3.11 as a function of excitation parameter for Ray I and Ray II (D_{in}/D_{out} = 0.3, B_{pf} = 0.55T)

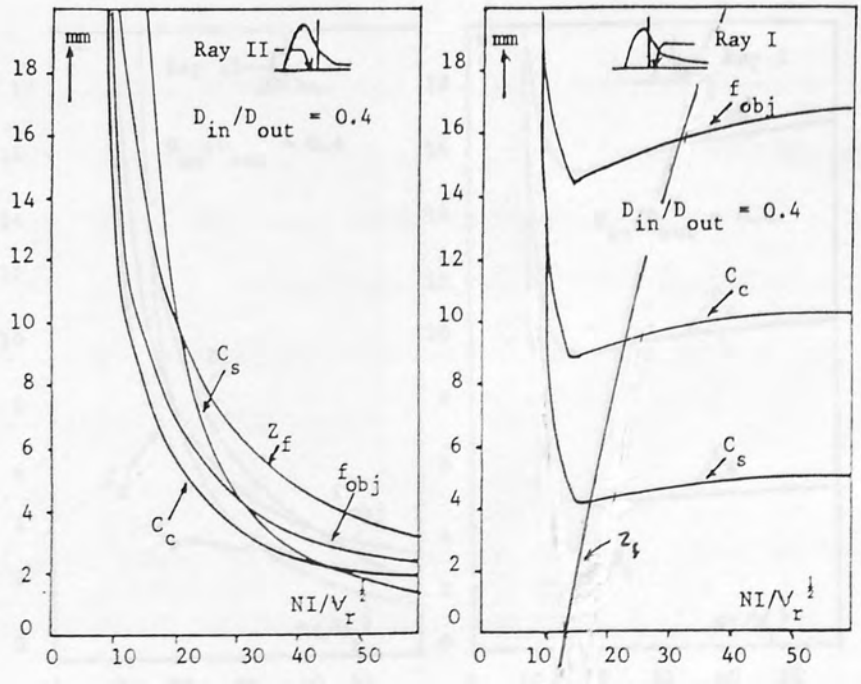

Fig 3.13e Focal properties of the single-polepiece lens shown in Fig 3.11 as a function of excitation parameter for Ray I and Ray II (D_{in}/D_{out} = 0.4, B_{pf} = 0.6T)

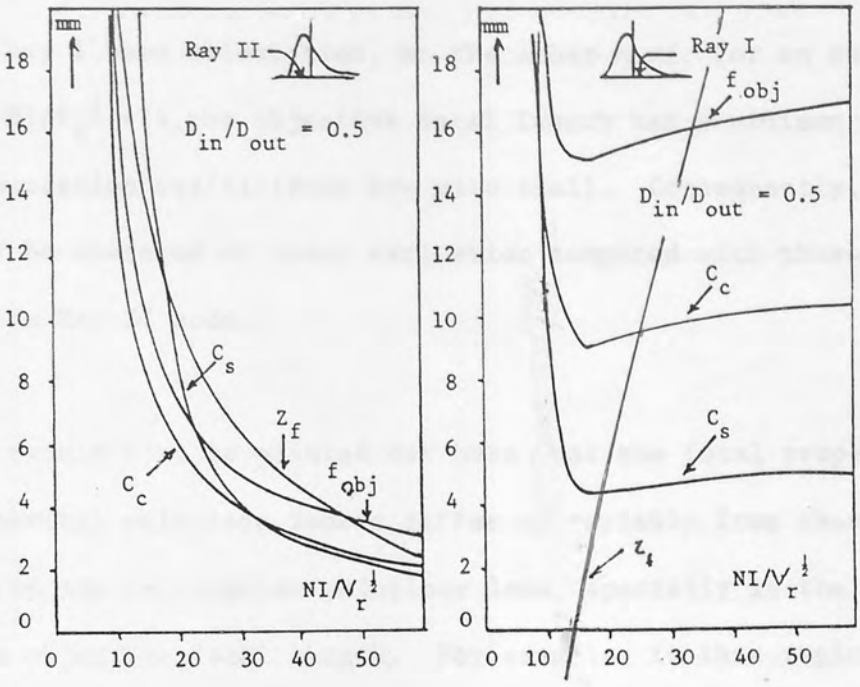

Fig 3.13f Focal properties of the single-polepiece lens shown in Fig 3.11 as a function of excitation parameter for Ray I and Ray II (D_{in}/D_{out} = 0.5, B_{pf} = 0.72T)

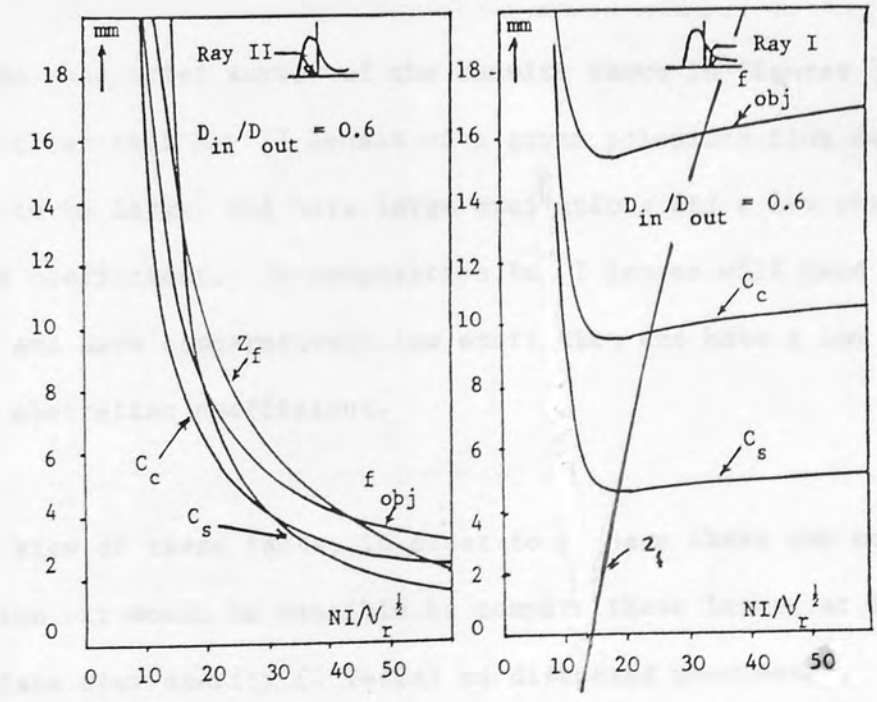

Fig 3.13g Focal properties of the single-polepiece lens shown in Fig 3.11 as a function of excitation parameter for Ray I and Ray II (D_{in}/D_{out} = 0.6, B_{pf} = 0.76T)

Nevertheless, such a lens has an extremely low chromatic aberration coefficient.

In Ray I beam orientation, on the other hand, for an excitation parameter $NI/V_r^{\frac{1}{2}} \simeq 14$, the objective focal length has a minimum value and the aberration coefficients are also small. Consequently, such lenses may be operated at lower excitation compared with those operating in Ray II mode.

It should also be pointed out here that the focal properties of the spherical polepiece lenses differ appreciably from those predicted by the rectangular polepiece lens especially in the region of minimum objective focal length. For example, in this region the aberration coefficients and the objective focal length increase sharply compared with those of the rectangular polepiece lens where the aberration coefficients and the objective focal length increases more smoothly with increasing excitation parameter.

From this brief survey of the results shown in Figures 3.13 a-g it is clear that Ray II lenses of a given polepiece flux density will tend to be large, and have large excitations and a low chromatic aberration coefficient. In composition Ray I lenses will tend to be small, and have comparatively low excitation and have a low spherical aberration coefficient.

In view of these facts, in order to compare these two modes of operation, it would be sensible to compare these lenses at the same poleface flux density (2 Tesla) as discussed previously.

3.4.2 COMPARISON OF THE ELECTRON OPTICAL PROPERTIES OF RAY I AND RAY II BEAM ORIENTATION OF THE SPHERICAL POLEPIECE LENSES

As was the case for rectangular polepiece lenses for comparison purposes all the lenses have been suitably scaled so as to make the poleface flux density B_{pf} equal to 2 Tesla. The resulting normalised focal properties Z_f^*, f_{obj}^*, C_c^*, C_s^*, can then be compared with those for the rectangular polepiece lens.

The variation of the objective focal distance, $Z_f^*(10^5/V_r)^{\frac{1}{2}}$ of the spherical polepiece objective lens with the excitation parameter $NI/V_r^{\frac{1}{2}}$, for different bore ratios is shown in Figure 3.14. This focal distance $Z_f^* (10^5/V_r)^{\frac{1}{2}}$ is the distance between the apex of the polepiece taken as origin ($Z = 0$), and a specimen position Z. It can be seen that for Ray II beam orientation, the objective focal distance is always positive and increases with increasing bore ratio. The lens with a zero bore ratio gives the shortest objective focal distance. For Ray I beam orientation, the objective focal distance starts decreasing with increasing lens excitation, until it reaches a zero value in the region of lens excitation parameter $NI/V_r^{\frac{1}{2}} \simeq 13$, and then decreases with increasing excitation parameter. The lens with the bore ratio equal to zero, gives the shortest working distance.

Figure 3.15 shows the variation of the objective focal length $f_{obj}^*(10^5/V_r)^{\frac{1}{2}}$ as a function of the excitation parameter $NI/V_r^{\frac{1}{2}}$, for different bore ratios. The objective focal length increases with increasing bore ratio. The shortest focal length occurs at a bore ratio equal to zero for both modes of operation.

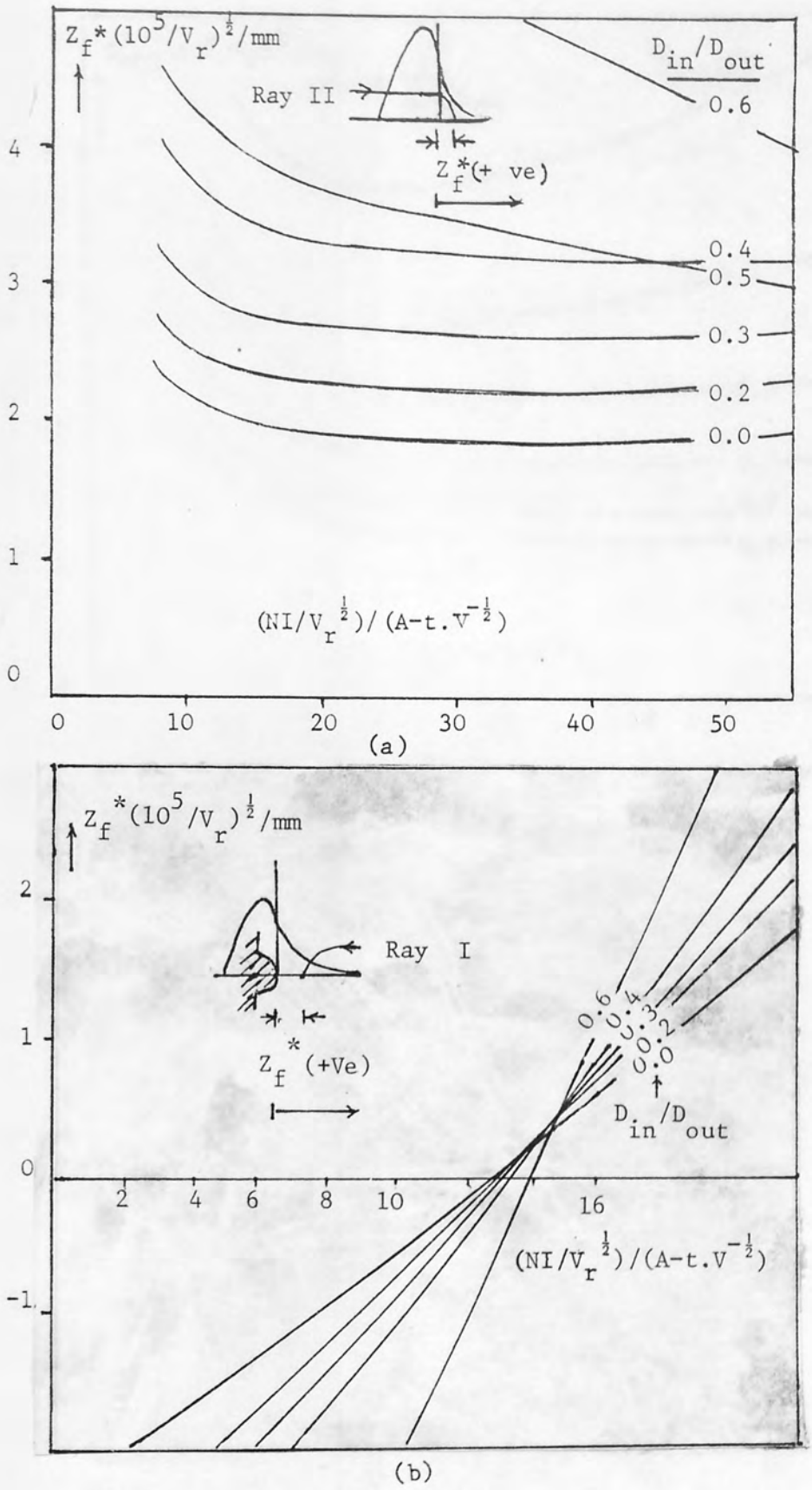

Fig 3.14 Variation of normalised objective focal distance $Z_f^*(10^5/V_r)^{\frac{1}{2}}$ for different bore ratios D_{in}/D_{out} of the lens (SPHER-ORIG) as a function of excitation parameter $NI/V_r^{\frac{1}{2}}$ (a) Ray II, (b) Ray I, (B_{pf} = 2T)

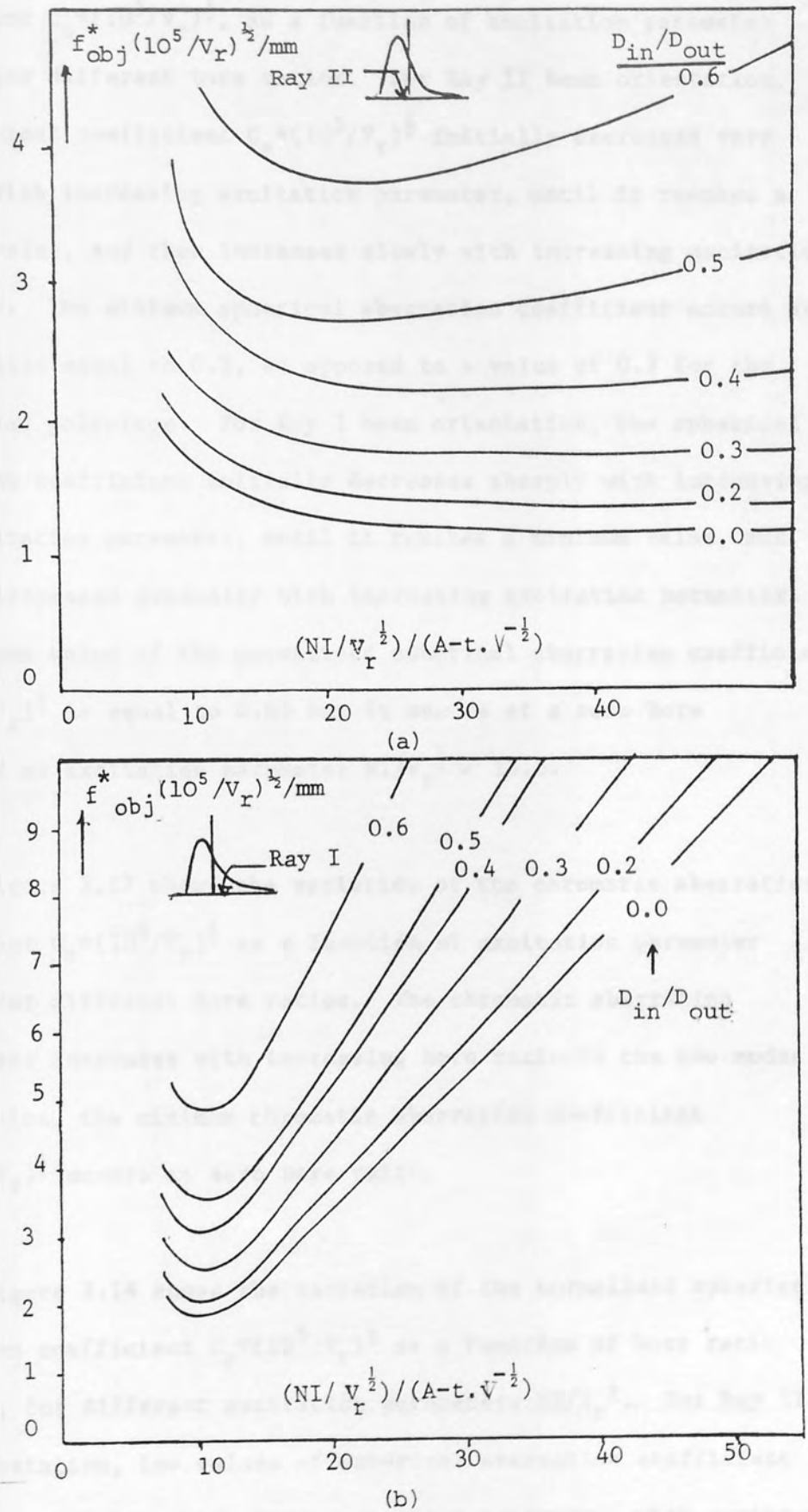

Fig 3.15 Variation of normalised objective focal length $f^*_{obj}(10^5/V_r)^{\frac{1}{2}}$ for different bore ratios D_{in}/D_{out} of the lens (SPHER-ORIG) as a function of excitation parameter $NI/V_r^{\frac{1}{2}}$ (a) Ray II, (b) Ray I. (B_{pf} = 2T)

Figure 3.16 shows the variation of the spherical aberration coefficient $C_s*(10^5/V_r)^{\frac{1}{2}}$, as a function of excitation parameter $NI/V_r^{\frac{1}{2}}$, for different bore ratios. For Ray II beam orientation, the spherical coefficient $C_s*(10^5/V_r)^{\frac{1}{2}}$ initially decreases very steeply with increasing excitation parameter, until it reaches a minimum value, and then increases slowly with increasing excitation parameter. The minimum spherical aberration coefficient occurs at a bore ratio equal to 0.2, as opposed to a value of 0.3 for the rectangular polepiece. For Ray I beam orientation, the spherical aberration coefficient initially decreases sharply with increasing lens excitation parameter, until it reaches a minimum value, and then it increases gradually with increasing excitation parameter. The minimum value of the normalised spherical aberration coefficient $C_s*(10^5/V_r)^{\frac{1}{2}}$ is equal to 0.65 mm; it occurs at a zero bore ratio and an excitation parameter $NI/V_r^{\frac{1}{2}} \simeq 13.5$.

Figure 3.17 shows the variation of the chromatic aberration coefficient $C_c*(10^5/V_r)^{\frac{1}{2}}$ as a function of excitation parameter $NI/V_r^{\frac{1}{2}}$, for different bore ratios. The chromatic aberration coefficient increases with increasing bore ratio in the two modes of operation, the minimum chromatic aberration coefficient $C_c*(10^5/V_r)^{\frac{1}{2}}$ occurs at zero bore ratio.

Figure 3.18 shows the variation of the normalised spherical aberration coefficient $C_s*(10^5/V_r)^{\frac{1}{2}}$ as a function of bore ratio D_{in}/D_{out}, for different excitation parameters $NI/V_r^{\frac{1}{2}}$. For Ray II beam orientation, low values of spherical aberration coefficient can be obtained at a high lens excitation parameter, with a minimum spherical aberration coefficient value in the region of D_{in}/D_{out} equal to 0.22. For Ray I beam orientation, the spherical aberration

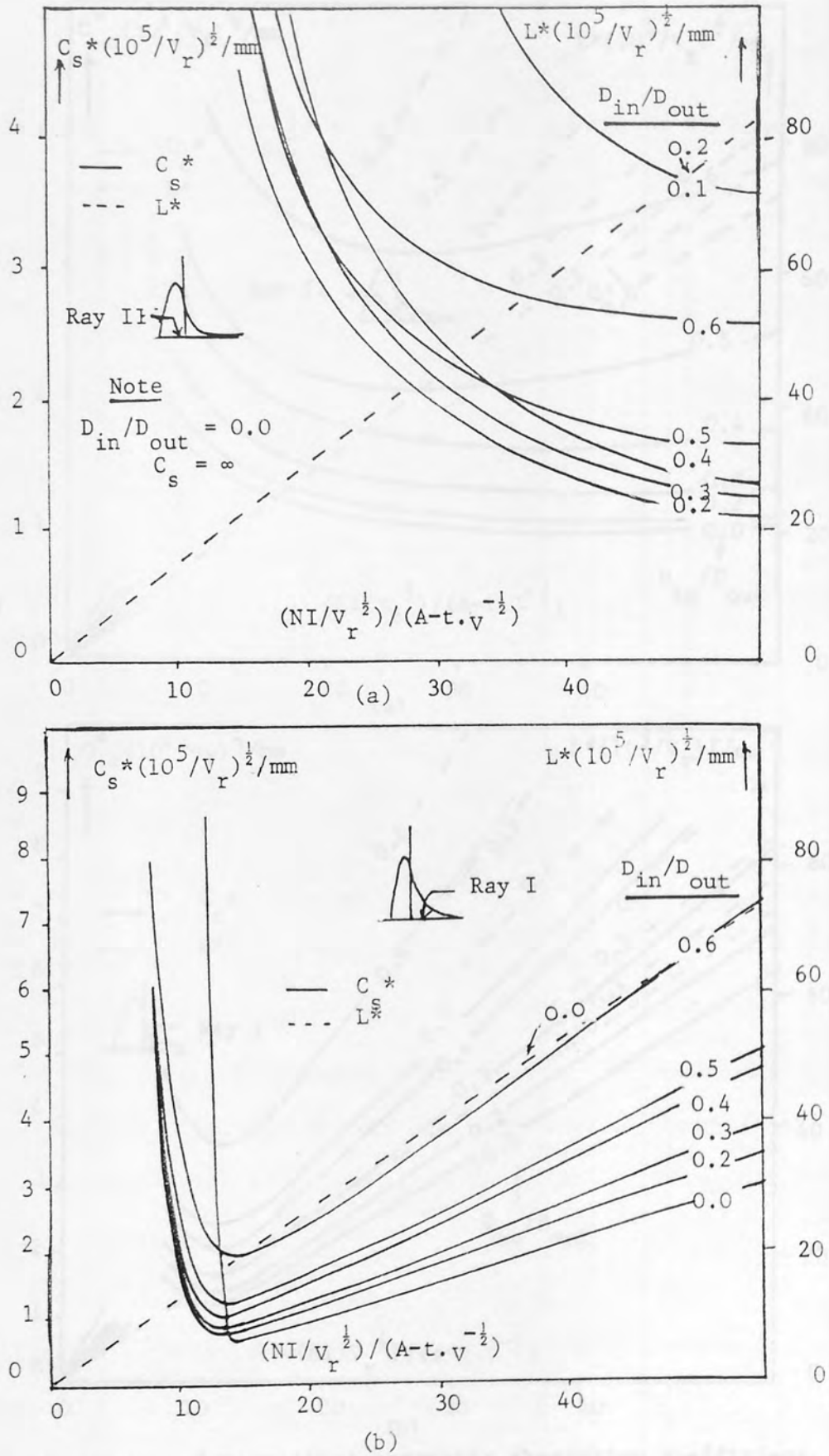

Fig 3.16 Variation of normalised spherical aberration coefficient $C_s*(10^5/V_r)^{\frac{1}{2}}$ for different bore ratios D_{in}/D_{out} of the lens (SPHER-ORIG) as a function of excitation parameter $NI/V_r^{\frac{1}{2}}$ (a) Ray II, (b) Ray I. (B_{pf} = 2T). The dashed line indicates lens size.

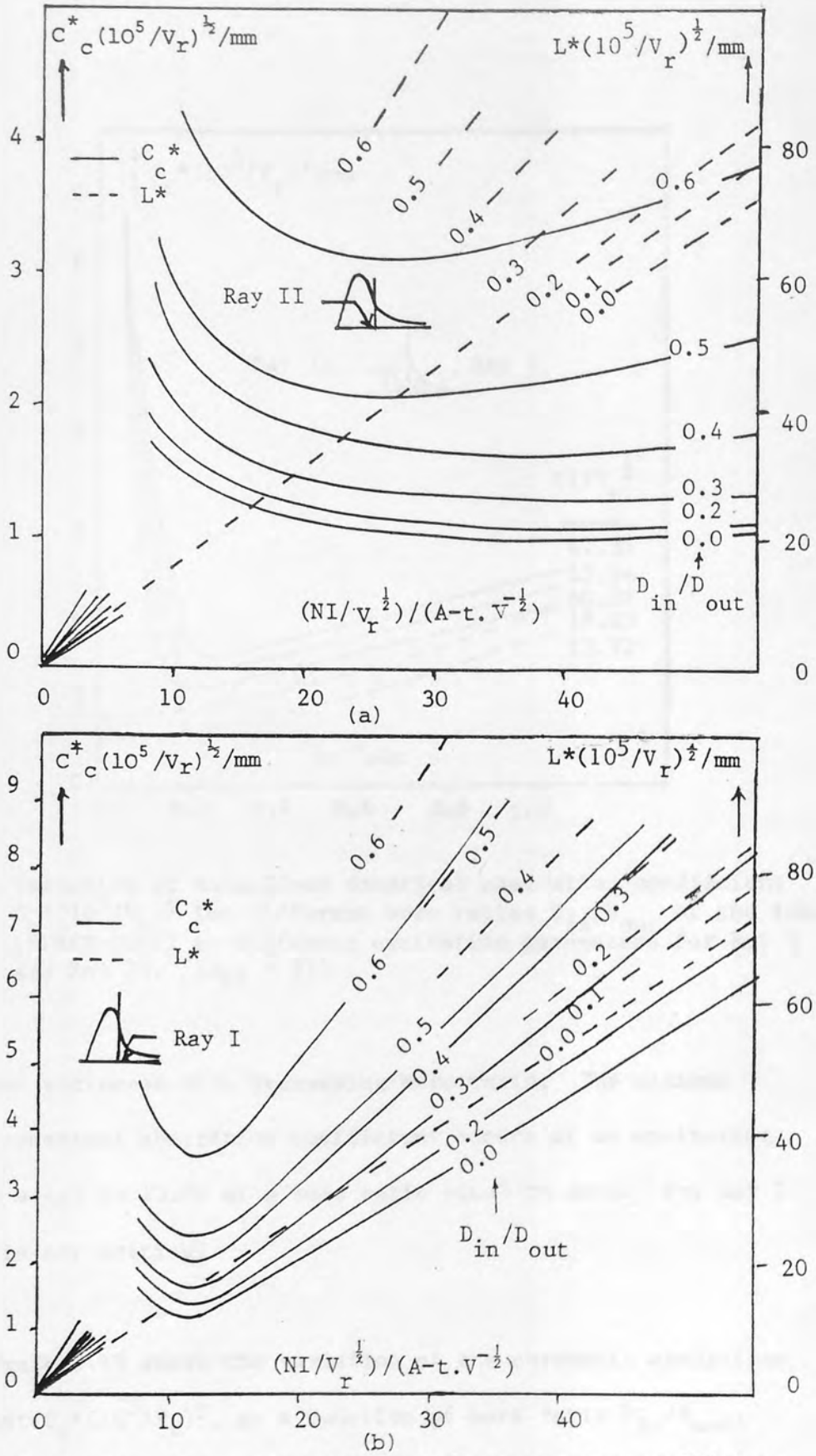

Fig 3.17 Variation of normalised chromatic aberration coefficient $C_c^*(10^5/V_r)^{\frac{1}{2}}$ for different bore ratios D_{in}/D_{out} of the lens (SPHER-ORIG) as a function of excitation parameter $NI/V_r^{\frac{1}{2}}$ (a) Ray II, (b) Ray I. (B_{pf} = 2T). The dashed line indicates lens size.

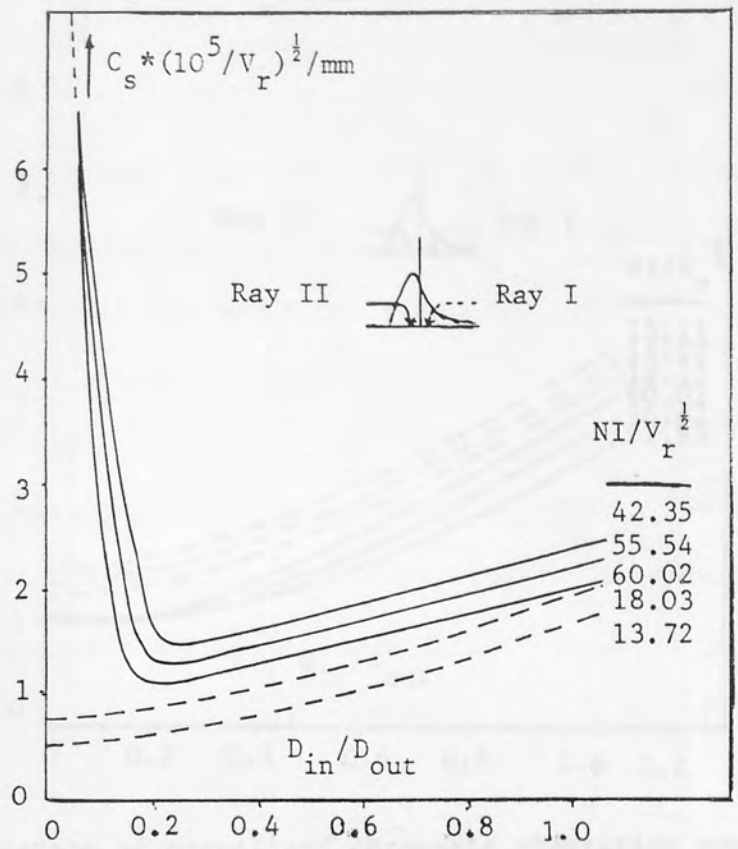

Fig 3.18 Variation of normalised spherical aberration coefficient $C_s*(10^5/V_r)^{\frac{1}{2}}$ for different bore ratios D_{in}/D_{out} of the lens (SPHER-ORIG) at different excitation parameters for Ray I and Ray II. (B_{pf} = 2T)

coefficient increases with increasing bore ratio. The minimum value of spherical aberration coefficient occurs at an excitation parameter equal to 13.72 at a bore ratio equal to zero. For Ray I the bore is not critical.

Figure 3.19 shows the variation of the chromatic aberration coefficient $C_c*(10^5/V_r)^{\frac{1}{2}}$, as a function of bore ratio D_{in}/D_{out}, for different excitation parameters $NI/V_r^{\frac{1}{2}}$. The chromatic aberration coefficient increases gradually with increasing bore ratio.

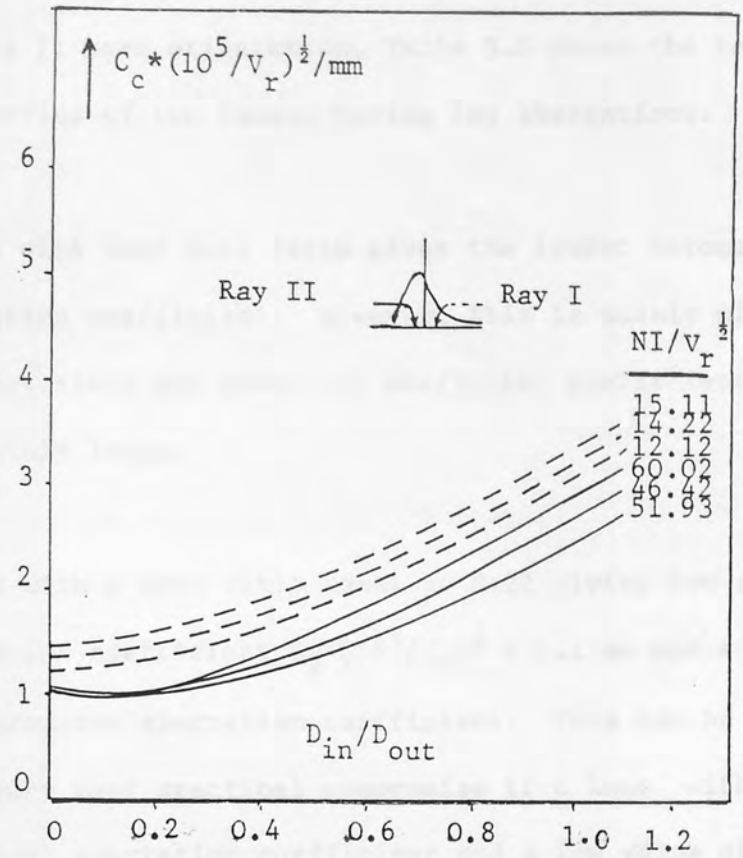

Fig 3.19 Variation of normalised chromatic aberration coefficient $C_c*(10^5/V_r)^{\frac{1}{2}}$ for different bore ratios D_{in}/D_{out} of the lens (SPHER-ORIG) at different excitation parameters for Ray I and Ray II. (B_{pf} = 2T)

For Ray II beam orientation, the minimum value of chromatic aberration coefficient occurs at a high value of excitation parameter and a bore ratio equal to zero. For Ray I beam orientation, the minimum value of chromatic aberration coefficient occurs at low values of excitation parameter and a bore ratio equal to zero. The optical properties of these lenses are given in Figures 3.14, 3.15, 3.16 and 3.17 respectively.

The design of this lens is not very different from the one used by Al-Shwaikh and Mulvey (1977), and the results obtained show a similar variation with lens excitation.

3.4.3 OPTIMUM LENS PROPERTIES FOR RAY I AND RAY II

For Ray II beam orientation, Table 3.6 shows the best electron optical properties of two lenses having low aberrations.

(a) A lens with zero bore ratio gives the lowest chromatic aberration coefficient. However, this is mainly of academic interest since the spherical aberration coefficient is infinitely large.

(b) A lens with a bore ratio equal to 0.22 giving low spherical aberration coefficient $C_s*(10^5/V_r)^{\frac{1}{2}}$ = 1.1 mm and a relatively low chromatic aberration coefficient. This can be regarded as a very good practical compromise if a lens with a low spherical aberration coefficient and a low value of chromatic aberration coefficient is required.

Table 3.6 Normalised focal lengths, lens size and aberration coefficient of lens (SPHER-ORIG) a, (C_s* minimised) and lens b (C_c* minimised) with zero and 0.22 bore ratios for Ray II. (B_{pf} = 2T)

Lens	$\frac{NI}{V_r^{\frac{1}{2}}}$	$C_s*[\frac{10^5}{V_r}]^{\frac{1}{2}}$ mm	$C_c*[\frac{10^5}{V_r}]^{\frac{1}{2}}$ mm	$L*[\frac{10^5}{V_r}]^{\frac{1}{2}}$ mm	D_{in}/D_{out}
(b)	60	∞	1.0	80.0	0.0
(a)	60	1.1	1.1	91.6	0.22

For Ray I beam orientation, Table 3.7 shows two extreme cases of the electron optical properties of the best lens with zero bore ratio; lens (a) with very low spherical aberration coefficient, and lens (b) with very low chromatic aberration coefficient.

Table 3.7 Normalised focal lengths, lens size and aberration coefficients of lens (SPHER-ORIG) a, (C_s* minimised) and lens b (C_c* minimised) with a zero bore ratio for Ray I. (B_{pf} = 2T)

Lens	$\frac{NI}{V_r^{\frac{1}{2}}}$	$C_s^*[\frac{10^5}{V_r}]^{\frac{1}{2}}$ mm	$C_c^*[\frac{10^5}{V_r}]^{\frac{1}{2}}$ mm	$f_{obj}^*[\frac{10^5}{V_r}]^{\frac{1}{2}}$ mm	$Z_f^*[\frac{10^5}{V_r}]^{\frac{1}{2}}$ mm	$L^*[\frac{10^5}{V_r}]^{\frac{1}{2}}$ mm
(a)	13.72	0.62	1.29	2.14	0.0	18.29
(b)	12.12	40.23	1.21	1.94	0.24	16.15

The lens with a low spherical aberration coefficient also has a relatively low chromatic aberration coefficient and it can be regarded as a very good compromise, for both low spherical and chromatic aberrations.

3.5 COMPARISION BETWEEN THE OPTIMUM LENSES FOR RAY I AND RAY II BEAM ORIENTATION

From the previous results, the optimum bore ratio for Ray I and Ray II beam orientation was found for different polepiece shapes. These were compared with Juma and Mulvey's (1980a) experimental results, and with Christofides (1982) results as shown in the Universal curve,Figure 3.20. This shows the variation of normalised spherical aberration coefficient as a function of bore ratio. The minimum spherical aberration obtained by the above authors occurs at the same lens excitation as in the present work. Thus for conditions corresponding to Ray I, the minimum spherical aberration coefficient occurs at zero bore ratio for an excitation parameter in the range

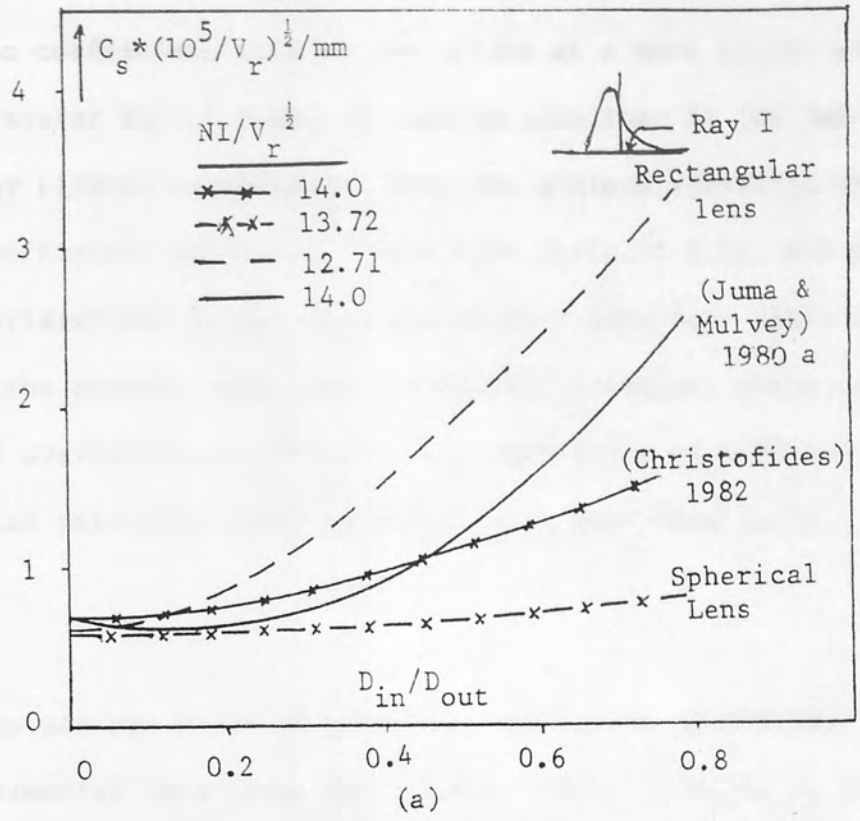

(a)

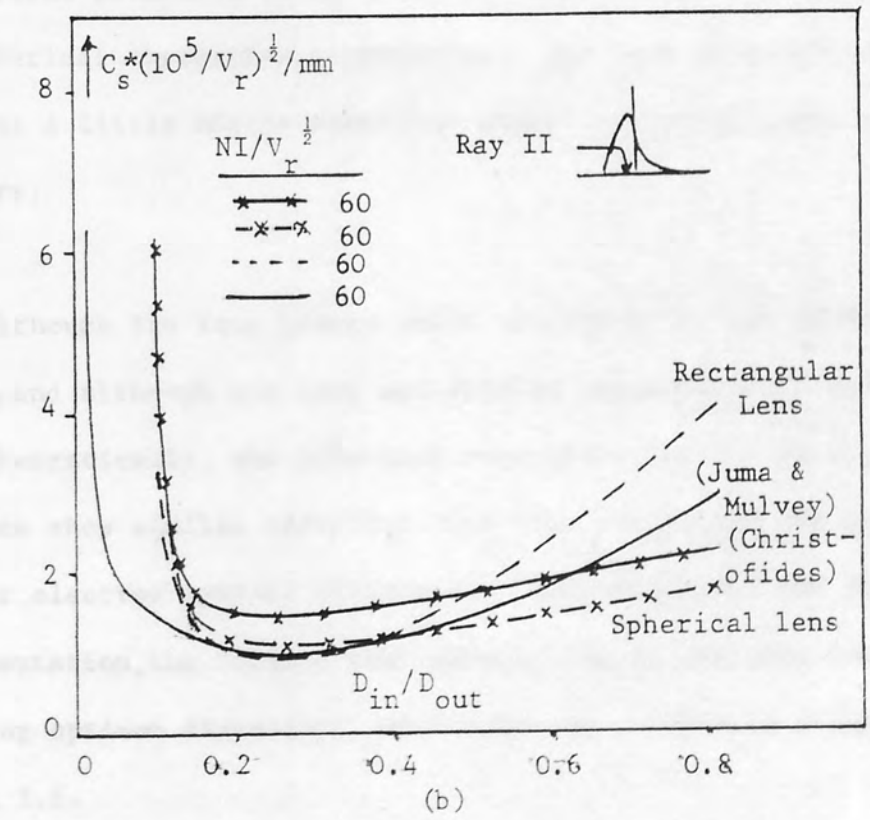

(b)

Fig 3.20 Comparison of the normalised spherical aberration coefficient $C_s*(10^5/V_r)^{\frac{1}{2}}$ as a function of bore ratio D_{in}/D_{out} of the present author with the experimental results of Juma and Mulvey and theoretical results of Christofides for (a) Ray I (b) Ray II. (B_{pf} = 2T)

between 13 to 14. For Ray II beam orientation, the spherical aberration coefficient attains low values at a much higher excitation parameter $NI/V_r^{\frac{1}{2}} = 60$. It can be seen that in the Juma and Mulvey (1980a) experimental lens, the minimum spherical aberration coefficient occurs at a lens bore ratio of 0.25, and that of the Christofides (1982) lens occurs at a lens bore ratio of 0.2. In the present work, for a spherical polepiece shape, minimum spherical aberration occurs at a lens bore ratio of 0.22 and for a rectangular polepiece shape it occurs at a lens bore ratio of 0.3.

The minimum value of spherical aberration coefficient of the experimental lens (Juma and Mulvey, 1980a) is equal to that of the spherical polepiece lens, while the rectangular one has slightly lower spherical aberration coefficient. The lens of Christofides (1982) has a little higher spherical aberration coefficient than the others.

Although the four lenses under consideration are different in shape, and although one lens was studied experimentally and the others theoretically, the spherical aberration coefficients of all the lenses show similar variation with lens excitation and with all other electron optical properties. For both Ray I and Ray II beam orientation, the results lead essentially to the same conclusion concerning optimum dimensions and excitations. This is illustrated in Table 3.8.

Table 3.8 Normalised focal lengths, lens size, and aberration coefficient of different polepiece shapes for Ray I and Ray II, (B_{pf} = 2T). Note for Ray I, D_{in}/D_{out} = 0.0 .

Ray I	$NI[\frac{10^5}{V_r}]^{\frac{1}{2}}$	$C_s*[\frac{10^5}{V_r}]^{\frac{1}{2}}$	$C_c*[\frac{10^5}{V_r}]^{\frac{1}{2}}$	$f_{obj}*[\frac{10^5}{V_r}]^{\frac{1}{2}}$	$L*[\frac{10^5}{V_r}]^{\frac{1}{2}}$	$Z_f*[\frac{10^5}{V_r}]^{\frac{1}{2}}$
	A-t	mm	mm	mm	mm	mm
Spherical lens	4339	0.62	1.30	2.14	18.29	0.0
Rectangular lens	3899	0.60	1.0	1.50	9.96	0.0
Christofides 1982	4300	0.60	1.25	2.10	18.0	0.0
Juma & Mulvey 1980a	4743	0.64	1.25	-	-	-

Ray II	$NI[\frac{10^5}{V_r}]^{\frac{1}{2}}$	$C_s*[\frac{10^5}{V_r}]^{\frac{1}{2}}$	$C_c*[\frac{10^5}{V_r}]^{\frac{1}{2}}$	D_{in}/D_{out}	$L*[\frac{10^5}{V_r}]^{\frac{1}{2}}$
	A-t	mm	mm		mm
Spherical lens	19005	1.1	1.1	0.22	91.56
Rectangular lens	19005	1.0	1.8	0.3	72.24
Christofides 1982	16000	1.3	2.25	0.2	81.7
Juma & Mulvey 1980a	18970	1.1	1.3	0.25	-

Further, the lens size in Ray I beam orientation is always smaller than that of Ray II beam orientation. It should be noted that the actual size of the lens will depend on the accelerating voltage. Thus for low accelerating voltages a Ray I design may be inconveniently small, but quite practical at high voltages. However, the technological difficulties involved with a lens operated

in Ray II orientation are substantially less than those involved with a lens operated in Ray I orientation.

3.6 THE EFFECT OF THE COIL POSITION ON THE AXIAL FLUX DENSITY DISTRIBUTION IN SINGLE-POLEPIECE LENSES

Up to date, attention has been concentrated on single-polepiece lenses in which the coil is conveniently located immediately around the polepiece. However, a careful study of the axial field distributions (see for example Figures 3.4 and 3.12) shows that the maximum flux density occurs somewhere in the centre of the polepiece and not at the pole tip. When the permeability is high, this is not very important. However, such a lens cannot be expected to perform well at high excitations where it is important that saturation effects should be restricted entirely to the polepiece tip. A systematic search revealed that a considerable re-arrangement of the exciting coil is necessary to achieve this condition.

This is illustrated in Figure 3.21. The distance between the centre of the coil and the polepiece tip is denoted by Δ.

The peak flux density (0.6T) occurs in the middle of the polepiece. However, when a narrow coil (Coil E) of small bore is fitted close to the poleface, the flux density in the polepiece drops dramatically and the peak flux density occurs at the polepiece tip as desired. The peak flux density also increases slightly. This effect is even more marked for the spherical polepiece lens (Figure 3.21b) where the increase in peak flux density is even more marked. However, at low excitations and hence high iron permeability,

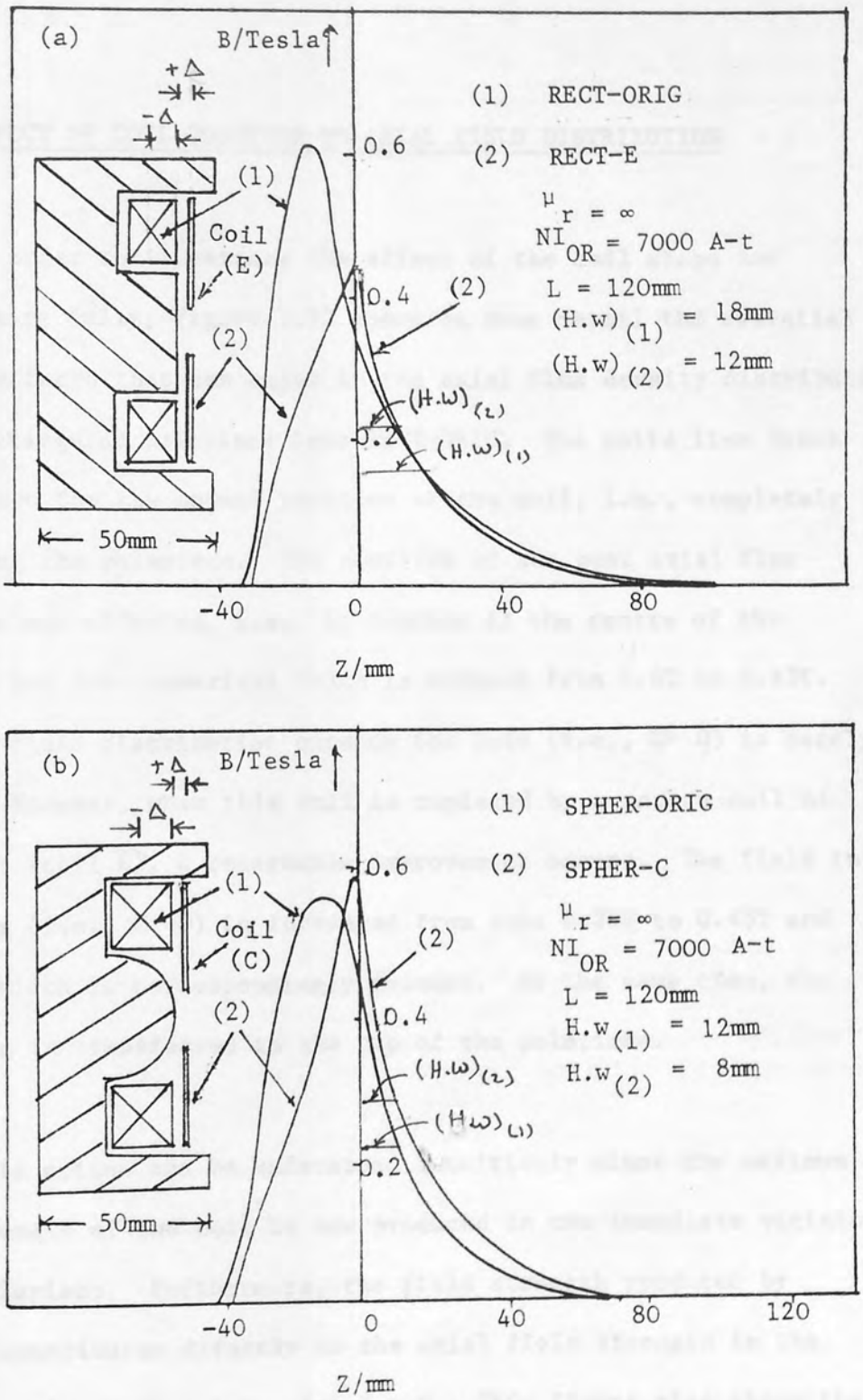

Fig 3.21 Axial flux density distribution of single-polepiece lenses (a) RECT-ORIG and (b) SPHER-ORIG showing the effect of replacing the original coil with a narrower coil (Coils E and C) of small bore placed in close proximity to the poleface

the electron optical properties would not be greatly affected. However, at higher flux densities, one would expect the spherical polepiece design to prove superior.

3.6.1 EFFECT OF COIL POSITION ON AXIAL FIELD DISTRIBUTION

In order to illustrate the effect of the coil shape and position more fully, Figure 3.22 shows in some detail the essential physical effects that can occur in the axial flux density distribution of the rectangular polepiece lens RECT-ORIG. The solid line shows the B_Z curve for the normal position of the coil, i.e., completely surrounding the polepiece. The position of the peak axial flux density is not affected, i.e., it remains at the centre of the polepiece but its numerical value is reduced from 0.6T to 0.43T. The axial field distribution outside the lens (i.e., $Z > 0$) is hardly changed. However, when this coil is replaced by a narrow coil of small bore (coil E), a remarkable improvement occurs. The field in free space (i.e., $Z > 0$) is increased from some 0.29T to 0.45T and the half width is correspondingly reduced. At the same time, the peak field is transferred to the tip of the polepiece.

This action can be understood intuitively since the maximum field strength of the coil is now produced in the immediate vicinity of the polepiece. Furthermore, the field strength produced by the coil contributes directly to the axial field strength in the actual focusing region i.e., for $Z \approx 0$. This figure also shows that although the rectangular section polepiece has an unpromising shape, by careful positioning of the exciting coil it should be capable of operating under saturation conditions.

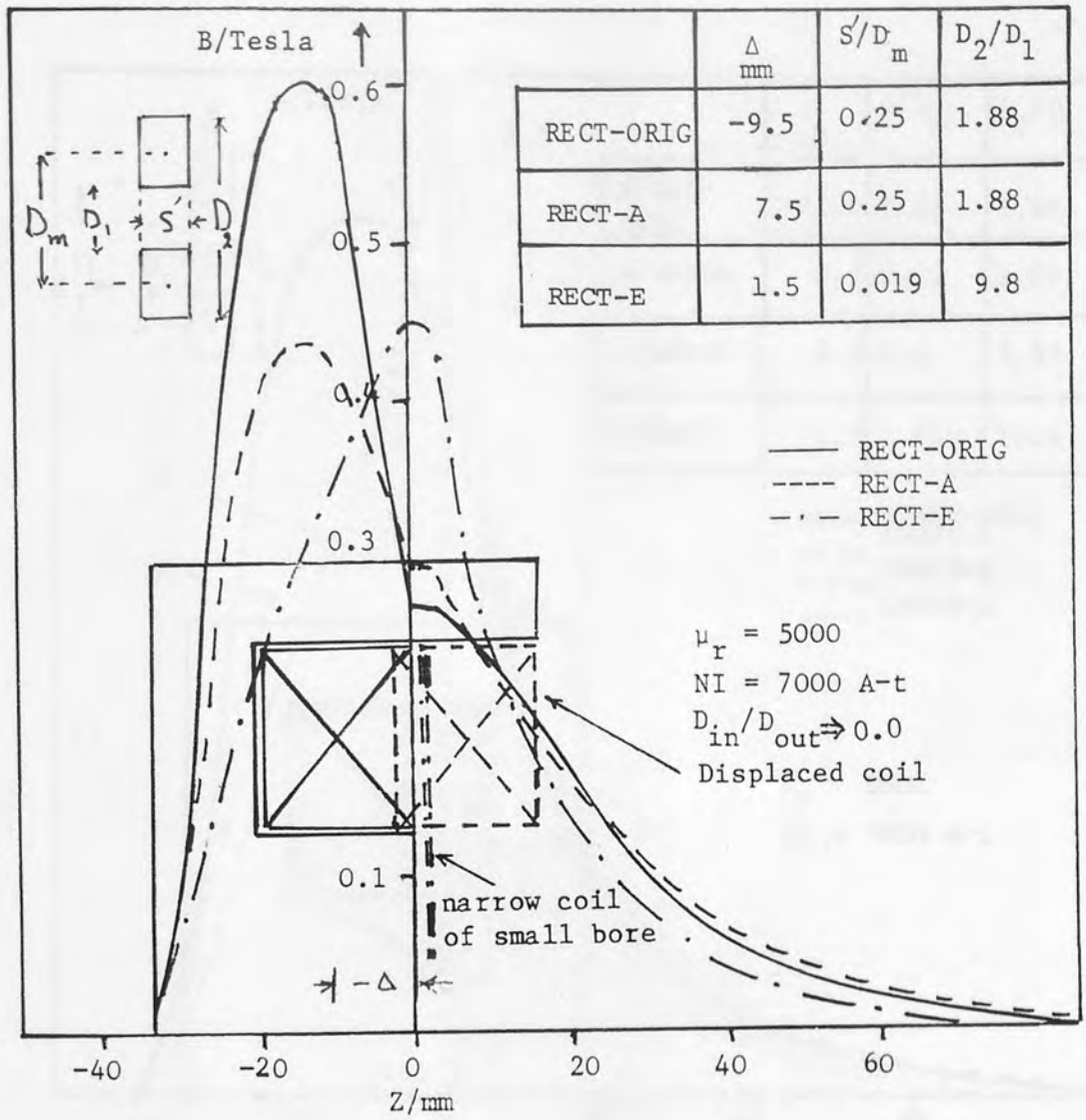

	Δ mm	S'/D_m	D_2/D_1
RECT-ORIG	-9.5	0.25	1.88
RECT-A	7.5	0.25	1.88
RECT-E	1.5	0.019	9.8

Fig 3.22 Effect of coil position and coil shape on the axial flux density distribution in lens RECT-ORIG for D_{in}/D_{out} = 0.0. Solid line —— original coil position. Dashed line ---- field distribution with original coil displaced by 15mm (Coil A). Chain dotted line -.-.- original coil replaced by narrow, small bore coil (Coil E)

Figure 3.23 shows that an even better result is obtained in a similar manner with the spherical polepiece lens SPHER-ORIG. Here, the original coil produced a peak flux density of 0.56T in the centre of the polepiece. The position of this peak is moved slightly in the positive direction of Z by replacing the coil by coil A, of similar inner diameter but reduced width (9.3 mm). The peak axial flux is thereby noticeably reduced to 0.42T. It should

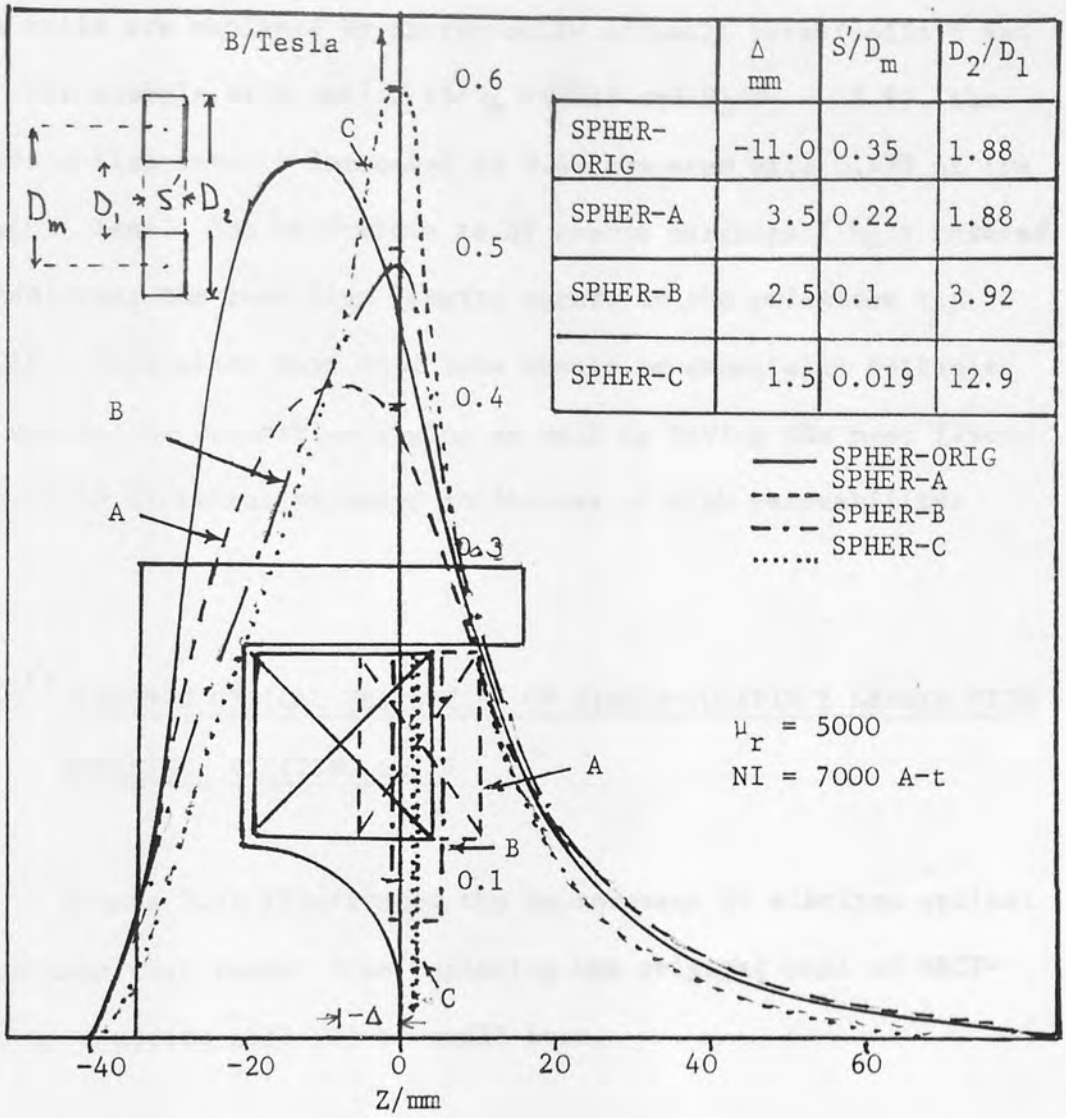

	Δ mm	S'/D_m	D_2/D_1
SPHER-ORIG	-11.0	0.35	1.88
SPHER-A	3.5	0.22	1.88
SPHER-B	2.5	0.1	3.92
SPHER-C	1.5	0.019	12.9

Fig 3.23 Effect of coil position and coil shape on the axial flux density distribution in lens SPHER-ORIG for D_{in}/D_{out} = 0.0. Solid line —— original coil position. Dashed line ---- field distribution with a narrower coil (A) of similar inner diameter but displaced by 15mm. Chain dotted line -.-.original coil replaced by narrow, small bore coil (B). Dotted line .... very narrow, small bore coil (C)

be noted that the poleface flux density is reduced from 0.48T to 0.4T. This is not too serious since it means that at high excitations the poleface can attain flux densities at some 90% of the saturation value of the iron before becoming limited by saturation effects.

However, the saturation changes dramatically when these large bore coils are replaced by narrow coils of small bore (coils B and C). For example with coil C (S'/D_m =0.019 and D_2/D_1 = 12.9), the poleface flux density increases to 0.6T compared with 0.47T of the original lens. The half-width is of course correspondingly reduced. In addition, the peak flux density occurs at the polepiece tip itself. This means that this lens should be especially suitable for use in the saturation region as well as having the most favourable field distribution under conditions of high permeability.

3.6.2 ELECTRON OPTICAL PROPERTIES OF SINGLE-POLEPIECE LENSES WITH OPTIMISED EXCITING COILS

Figure 3.24 illustrates the improvement in electron optical properties that result from replacing the original coil of RECT-ORIG by a narrow coil (E) of small bore.

Figure 3.24 shows the focal properties f_{obj}, Z_f and aberration coefficients C_c, C_s of the lens RECT-ORIG with the original coil and a narrow small bore coil (Coil E), as a function of the excitation parameter $NI/V_r^{\frac{1}{2}}$ for the Ray I condition. From the figure, it may be seen that the effect of the narrow coil is to make the minimum focal length, and hence the aberration coefficients, more pronounced. Thus the minimum chromatic aberration coefficient is reduced from 11.0 mm to 7.0 mm and the minimum spherical aberration coefficient reduced from 5.0 mm to 2.8 mm. At the same time, these reduced values occur at a greatly reduced value of the excitation parameter i.e., from $NI/V_r^{\frac{1}{2}} \simeq 30$ to $NI/V_r^{\frac{1}{2}} = 14$.

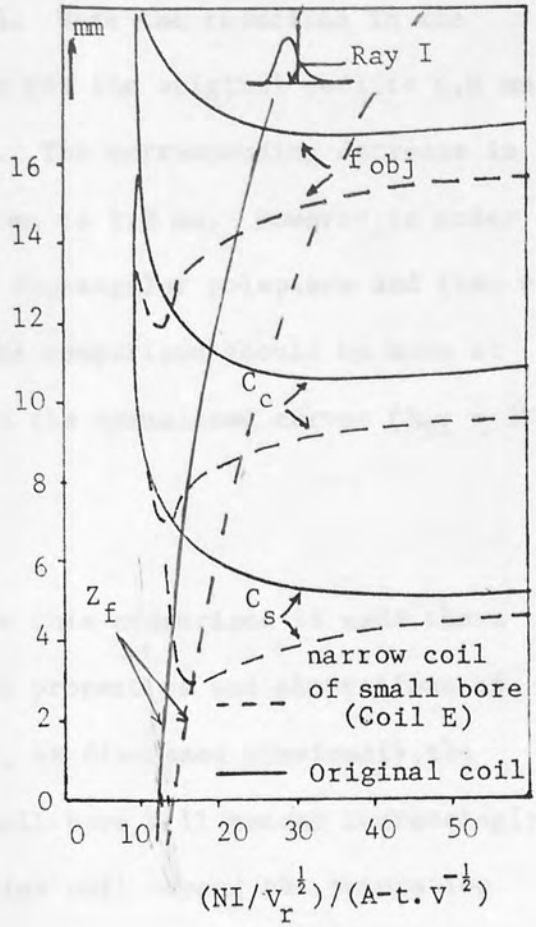

Fig 3.24 Focal properties f_{obj}, Z_f and aberration coefficient C_c and C_s of lens RECT-ORIG as a function of excitation parameter $(NI/V_r^{\frac{1}{2}})$ for the original coil (solid line) and narrow coil of small bore (Coil E) $D_{in}/D_{out} = 0$, L = 120 mm and $\mu_r = 5000$

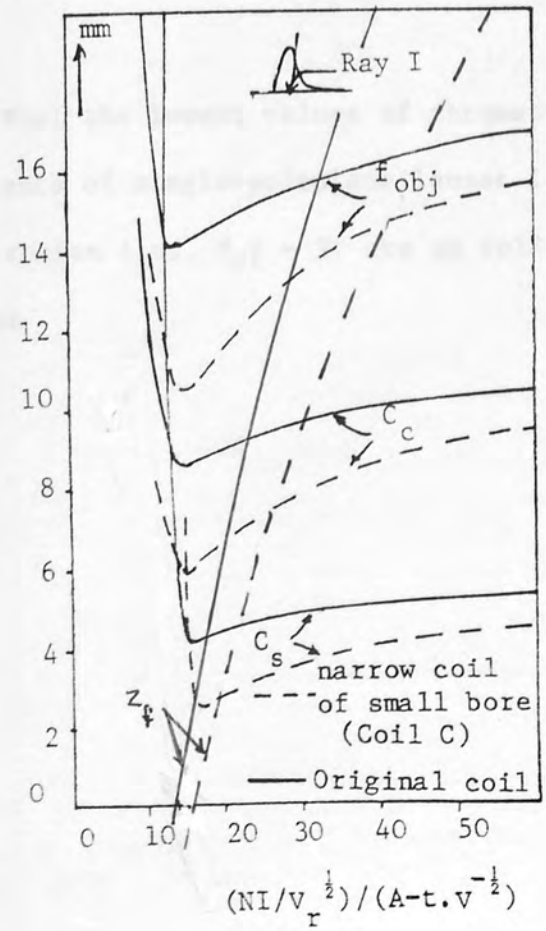

Fig 3.25 Focal properties f_{obj}, Z_f and aberration coefficient C_c and C_s of lens SPHER-ORIG as a function of excitation parameter $(NI/V_r^{\frac{1}{2}})$ for the original coil (solid line) and narrow coil of small bore (Coil C) $D_{in}/D_{out} = 0$, L = 120 mm and $\mu_r = 5000$

Similar results for the lens SPHER-ORIG with a spherical polepiece are shown in Figure 3.25. Here the reduction in the minimum value of C_c is from 8.5 mm for the original coil, to 6.0 mm for the narrow coil of small bore. The corresponding decrease in the minimum value of C_s is from 4 mm to 2.8 mm. However, in order to compare the performance of the rectangular polepiece and that of the spherical polepiece lenses, the comparison should be made at the same flux density, as shown in the normalised curves (B_{pf} = 2T) of Figures 3.26(a) and (b).

Figure 3.26 shows that when this comparison is made there is little to choose between the focal properties and aberrations of two types of polepieces. However, as discussed previously, the advantages of a narrow coil of small bore will become increasingly important at poleface flux densities well beyond the saturation magnetisation of the polepiece material.

We may conclude therefore that the lowest values of chromatic and spherical aberration coefficients of single-polepiece lenses in Ray I mode in the non-saturation region i.e., B_{pf} = 2T are as follows.

For the rectangular polepiece lens

$$C_c^* \, (10^5/V_r)^{\frac{1}{2}} \simeq 1.0 \text{ mm}$$

$$C_s^* \, (10^5/V_r)^{\frac{1}{2}} \simeq 0.5 \text{ mm}$$

$$L^* \, (10^5/V_r)^{\frac{1}{2}} \simeq 19.0 \text{ mm}$$

For the spherical polepiece lens

$$C_c^* \, (10^5/V_r)^{\frac{1}{2}} \simeq 1.1 \text{ mm}$$

$$C_s^* \, (10^5/V_r)^{\frac{1}{2}} \simeq 0.56 \text{ mm}$$

$$L^* \, (10^5/V_r)^{\frac{1}{2}} \simeq 29.2 \text{ mm}$$

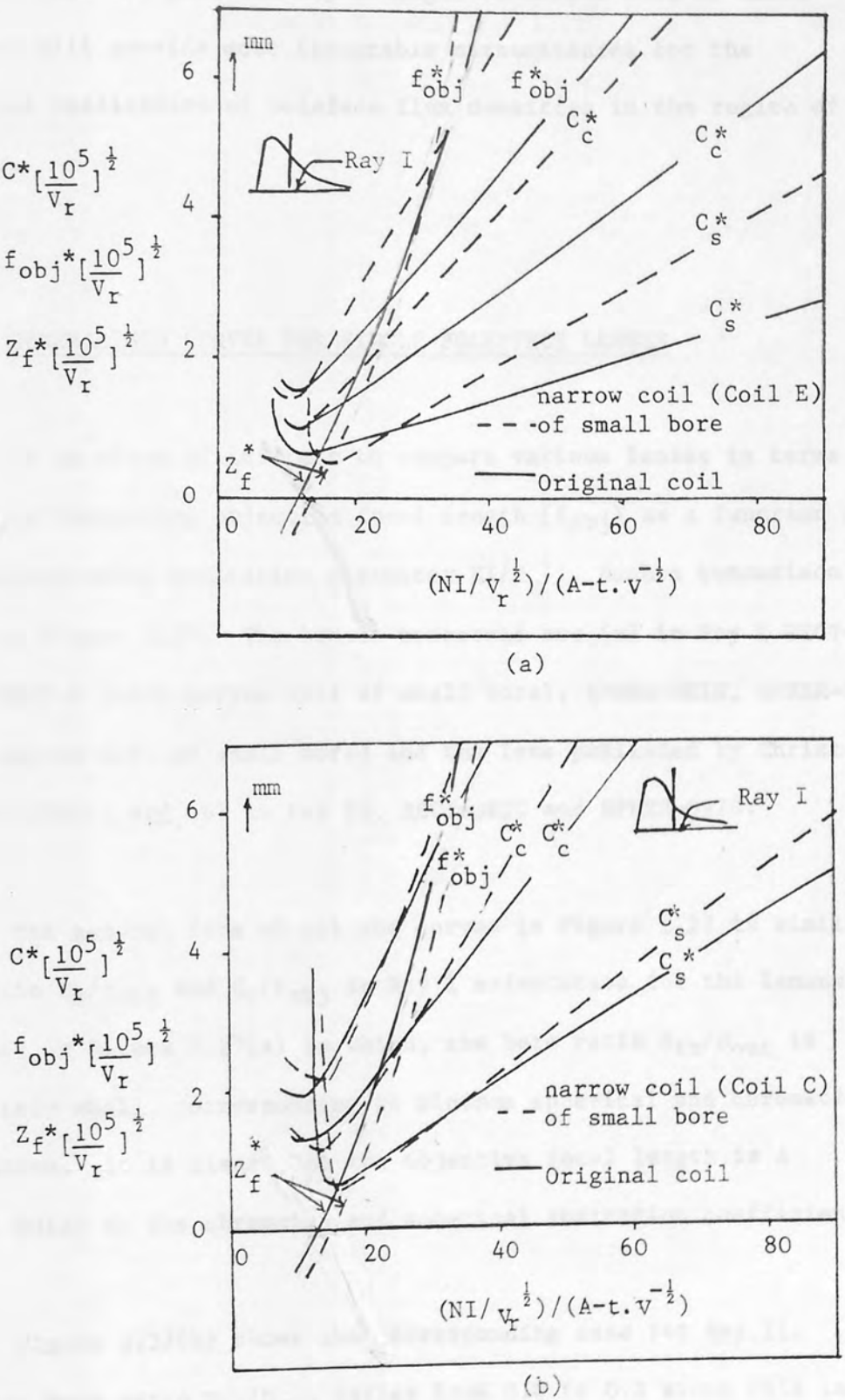

Fig 3.26 Normalised curve showing the focal properties and aberration coefficients as a function of excitation parameter $NI/V_r^{\frac{1}{2}}$ for (a) rectangular polepiece and (b) spherical polepiece lenses of zero bore ratio in Ray I beam orientation. (B_{pf} = 2T)

These calculations have shown that the electron optical properties are not affected by polepiece shapes or coil position, provided that the permeability is high. A narrow coil of small diameter will provide most favourable circumstances for the practical realisation of poleface flux densities in the region of 2 Tesla.

3.6.3 GENERALISED CURVES FOR SINGLE-POLEPIECE LENSES

It is often of interest to compare various lenses in terms of the corresponding objective focal length (f_{obj}) as a function of the corresponding excitation parameter $NI/V_r^{\frac{1}{2}}$. Such a comparison is shown in Figure 3.27. The lenses concerned are (a) in Ray I RECT-ORIG, RECT-E (with narrow coil of small bore), SPHER-ORIG, SPHER-C (with narrow coil of small bore) and the lens published by Christofides (1982), and (b) in Ray II, RECT-ORIG and SPHER-ORIG.

The general form of all the curves in Figure 3.27 is similar. The ratio C_s/f_{obj} and C_c/f_{obj} in Ray I orientation for the lenses is shown in Figure 3.27(a) in which, the bore ratio D_{in}/D_{out} is negligibly small, corresponding to minimum spherical and chromatic aberration. It is clear that the objective focal length is a useful guide to the chromatic and spherical aberration coefficients.

Figure 3.27(b) shows the corresponding case for Ray II. Here the bore ratio D_{in}/D_{out} varies from 0.0 to 0.3 since this is a significant parameter for the ratio C_s/f_{obj}. A comparison of curves of Figure 3.27 shows that there is little to choose for a

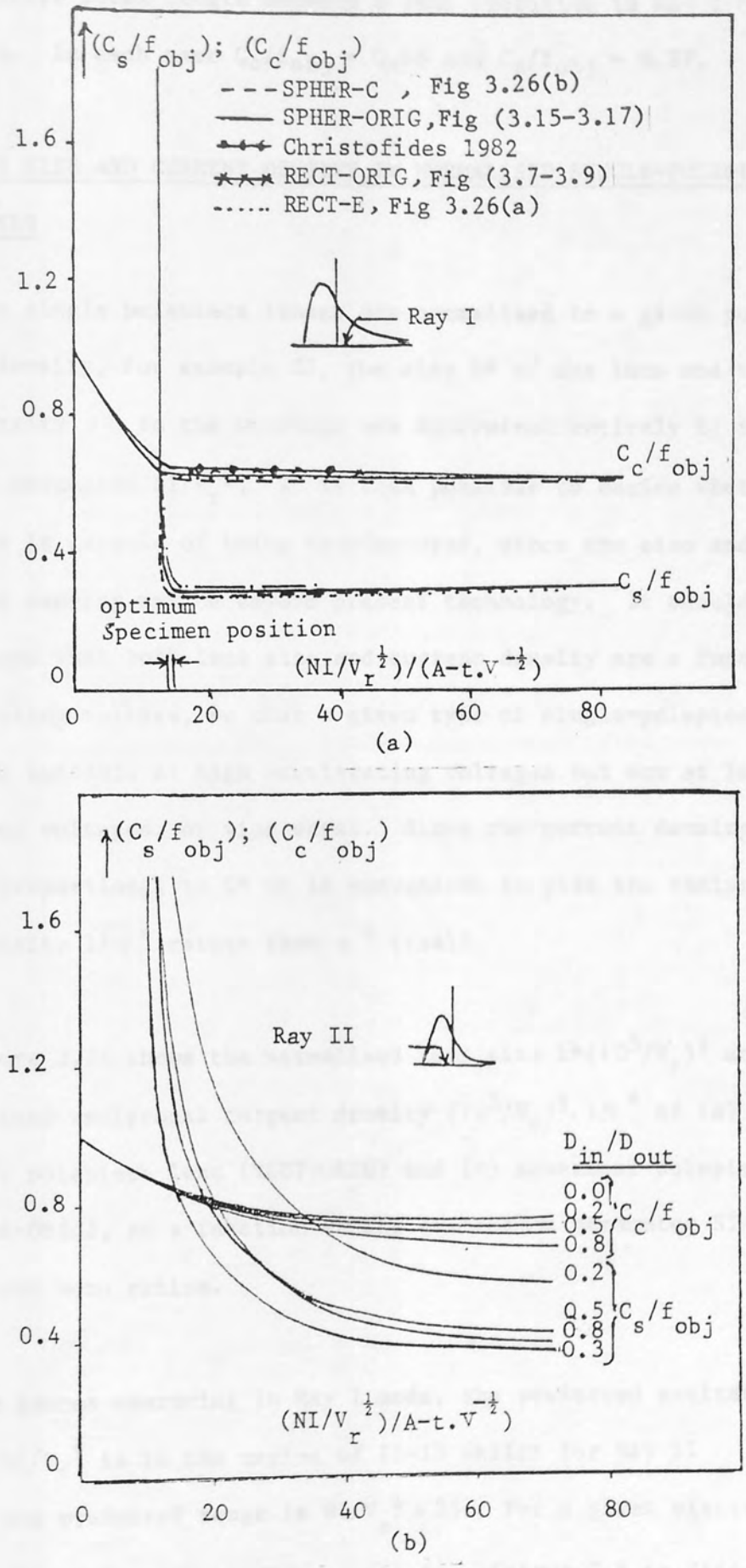

Fig 3.27 The ratios C_s/f_{obj} and C_c/f_{obj} as a function of excitation parameter $NI/V_r^{\frac{1}{2}}$ for (a) Ray I and (b) Ray II

given objective focal length between a lens operating in Ray I or Ray II mode. In each case $C_c/f_{obj} = 0.66$ and $C_s/f_{obj} = 0.37$.

3.7 LENS SIZE AND CURRENT DENSITY IN NORMALISED SINGLE-POLEPIECE LENSES

When single polepiece lenses are normalised to a given pole-face flux density, for example 2T, the size L* of the lens and the current density σ^* in the windings are determined entirely by the excitation parameter $NI/V_r^{\frac{1}{2}}$. It is then possible to decide whether such a lens is capable of being manufactured, since the size and/or the current density may be beyond present technology. It should be remembered that both lens size and current density are a function of accelerating voltage, so that a given type of single-polepiece lens may be suitable at high accelerating voltages but not at low accelerating voltages, or vice versa. Since the current density is inversely proportional to L* it is convenient to plot the reciprocal current density $1/\sigma^*$ rather than σ^* itself.

Figure 3.28 shows the normalised lens size $L^*(10^5/V_r)^{\frac{1}{2}}$ and the normalised reciprocal current density $(10^5/V_r)^{\frac{1}{2}}.1/\sigma^*$ of (a) rectangular polepiece lens (RECT-ORIG) and (b) spherical polepiece lens (SPHER-ORIG), as a function of the excitation parameter $NI/V_r^{\frac{1}{2}}$, for different bore ratios.

For lenses operating in Ray I mode, the preferred excitation parameter $NI/V_r^{\frac{1}{2}}$ is in the region of 12-13 whilst for Ray II operation the preferred range is $NI/V_r^{\frac{1}{2}} > 35$. For a given electron accelerating voltage V_r, the bore ratio for minimum C_s^* is different for Ray I ($D_{in}/D_{out} \simeq 0$) and Ray II ($D_{in}/D_{out} \simeq 0.3$) and therefore

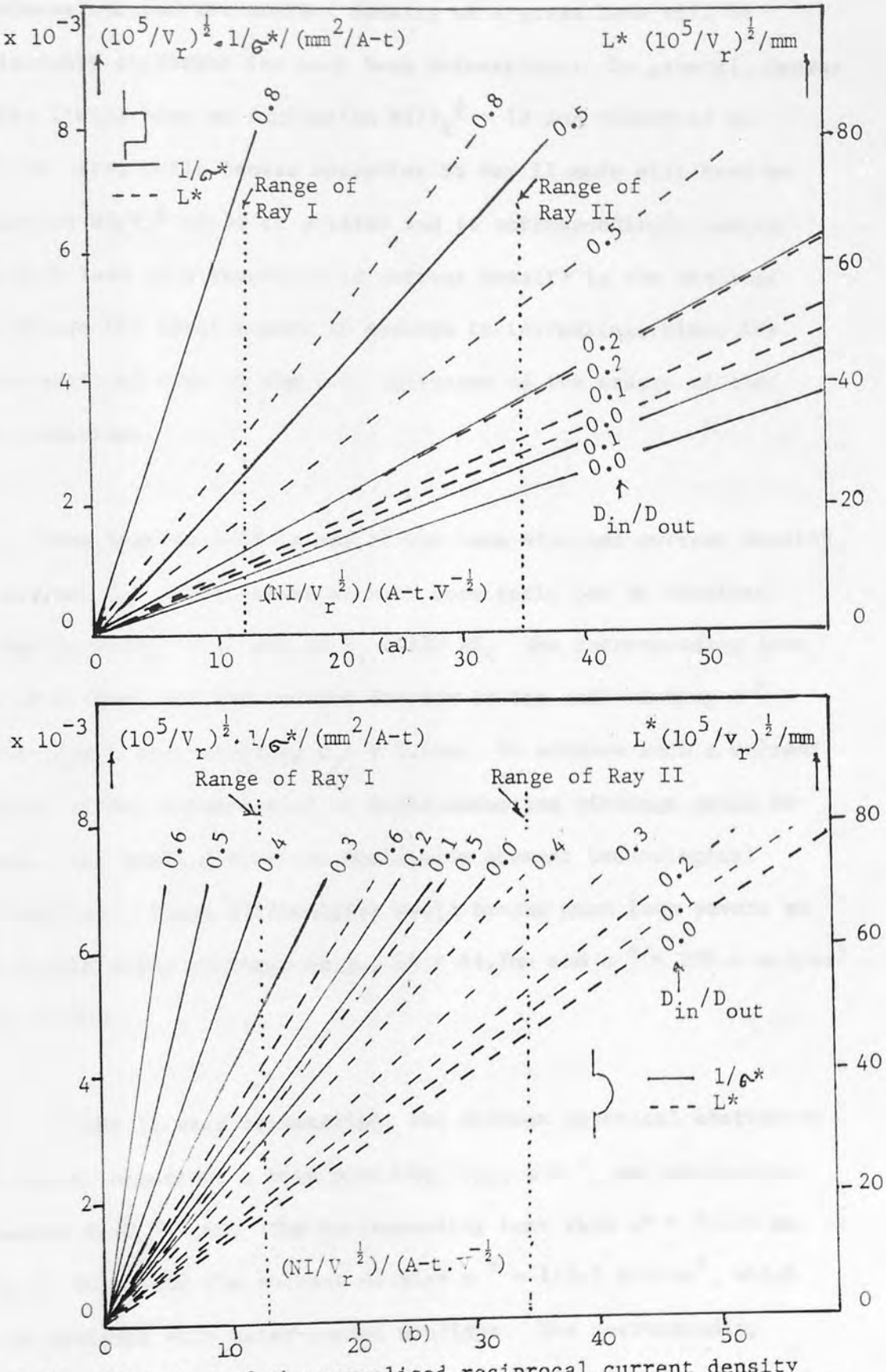

Fig 3.28 Variation of the normalised reciprocal current density $1/\sigma^*$ and size L^* of (a) rectangular polepiece lens (RECT-ORIG) and (b) spherical polepiece lens (SPHER-ORIG), as a function of excitation parameter $NI/V_r^{\frac{1}{2}}$ for different bore ratios D_{in}/D_{out}. (B_{pf} = 2T). Solid line indicates reciprocal current density, dashed line indicates lens size. The normal ranges for the excitation parameter $NI/V_r^{\frac{1}{2}}$ for Ray I and Ray II are also indicated on the figure.

the dimensions and the current density of a given lens will be considerably different for each beam orientation. In general, lenses for Ray I will have an excitation $NI/V_r^{\frac{1}{2}} \simeq 13$ and therefore be small in size, while lenses operating in Ray II mode will have an excitation $NI/V_r^{\frac{1}{2}}$ of 30 or greater and be correspondingly larger. This will lead to a reduction in current density in the windings even though the total number of amperes is increasing, since the cross-sectional area of the coil increases as the square of the lens dimensions.

From Figures 3.28 (a and b) the lens size and current density for minimum C_s^* which occurs at zero bore ratio can be obtained. For Ray I, $NI/V_r^{\frac{1}{2}} \simeq 12$ and at $V_r = 100$ kV, the corresponding lens size $L^* \simeq 10$mm, and the current density in the coil winding $\sigma^* = 1295$ A-t/mm^2; the resulting $C_s^* = 0.6$mm. To achieve such a current density, either steam-cooled or superconducting windings would be needed. Its small dimensions would also present technological difficulties. These difficulties would become much less severe at high accelerating voltages (e.g., $L^* = 44.7$mm and $\sigma^* = 289.6$ A-t/mm^2 at $V_r = 2000$).

In Ray II beam orientation, the minimum spherical aberration coefficient occurs at a bore ratio $D_{in}/D_{out} \simeq 0.3$, and excitation parameter $NI/V_r^{\frac{1}{2}} \simeq 60$. The corresponding lens size $L^* = 72.24$ mm at $V_r = 100$ kV and the current density $\sigma^* = 115.2$ A-t/mm^2, which can be achieved with water-cooled windings. The corresponding $C_s^* = 1.0$ mm which is almost identical to that achievable in Ray I orientation. Although under conditions of high permeability, the spherical polepiece lens would not be expected to lead to much lower values of aberration coefficients, it could possibly have some

practical advantages over the rectangular polepiece lens. To investigate this point, Figure 3.28(b) shows the normalised current density and lens size for the lens SPHER-ORIG. As with lens RECT-ORIG for Ray I, the minimum spherical aberration coefficient will occur at zero bore ratio, but the corresponding excitation parameter $NI/V_r^{\frac{1}{2}} \simeq 13.7$, slightly larger than that for minimum focal length ($NI/V_r^{\frac{1}{2}} \simeq 13.0$). The corresponding lens size $L^* = 18.3$ mm at $V_r = 100$ kV and the current density $\sigma^* = 314.03$ A-t/mm^2, which can easily be achieved with superconducting windings and possibly by steam-cooled windings. The corresponding value of $C_s^* = 0.62$ mm, comparable with that for the best rectangular polepiece lens.

For Ray II, the minimum spherical aberration coefficient C_s^* occurs at $D_{in}/D_{out} = 0.22$ and at $NI/V_r^{\frac{1}{2}}$ in the region of 60; the corresponding lens size = 91.57 mm at $V_r = 100$ kV and the current density $\sigma^* = 54.51$ A-t/mm^2. Such a lens size and current density would cause no constructional problems.

Table 3.9 summarises these results; the normalised current density σ^* and the size L^* of lenses RECT-ORIG and SPHER-ORIG is given at bore ratios and excitation for minimum C_s^* in Ray I and Ray II orientation.

Table 3.9 Normalised current density σ^* and the size L^* of lenses RECT-ORIG and SPHER-ORIG at bore ratios and excitation, for minimum C_s^* in Ray I and in Ray II. (B_{pf} = 2T)

LENSES	Ray I (D_{in}/D_{out} = 0.0)				Ray II (D_{in}/D_{out} = 0.3)			
	C_s^* mm	$NI/V_r^{\frac{1}{2}}$	L^* mm	σ^* A-t/mm^2	C_s^* mm	$NI/V_r^{\frac{1}{2}}$	L^* mm	σ^* A-t/mm^2
RECT-ORIG	0.60	12.0	10.0	1295	1.0	60†	72.24	115
SPHER-ORIG	0.62	13.7	18.3	314	1.1	60	91.57	55

† See figures 3.9(a) and 3.10

It may be concluded therefore that, at high permeability, the spherical polepiece lens does not lead to any appreciable improvement in electron optical properties compared with a rectangular polepiece lens. However for a given C_s^* value it is larger in size and hence operates at a lower current density. Up to now the poleface flux density of 2T has been considered. In the next chapter much higher poleface flux densities will be under consideration. For a given lens excitation this implies that the lens size will be smaller and the current density correspondingly higher. Thus, one may expect that under these conditions the spherical polepiece lens would have a considerable advantage, especially under Ray I orientation.

However, this will only occur if care is taken in the design and positioning of the coil. It seems inevitable that a narrow, flat coil of small internal bore must be employed if poleface flux densities greatly in excess of 2 Tesla are to be achieved.

CHAPTER FOUR

4. DESIGN OF SATURATED SINGLE-POLEPIECE LENSES

4.1 SATURATED LENSES

This chapter is concerned with the optical properties of single-polepiece lenses under the conditions of iron saturation. As before, the finite element method was used to investigate numerically the flux density distribution in the set lens previously investigated under conditions of high iron permeability. Because of the considerable amount of calculation involved, the study was restricted to lenses with zero bore, operating in Ray I condition, since these lenses are conceptually simpler than those of Ray II, in which the lens bore and polepiece profile complicate the issue under saturation conditions.

The axial magnetic flux density distributions were computed by the Munro (1975) program M13, which uses an iterative method to take into account the B/H characteristic of the iron circuit.

The calculations were made for a wide range of excitations (NI). The electron optical properties of these distributions were then determined as a function of electron beam accelerating voltage. From these characteristics, it was possible to determine the optimum properties of saturated single-polepiece lenses .

4.1.1 CALCULATIONS INVOLVING VARIABLE PERMEABILITY (μ_r = VARIABLE)

The magnetic circuit of a magnetic lens usually consists of soft iron. The polepieces can either be made of soft iron or of an

alloy such as 'Permendur'. In this work the polepieces are made of soft iron, but it is not difficult to extrapolate the results to those with Permendur. The magnetic behaviour of a typical soft iron is given by the B/H curve shown in Figure 4.1. The relative permeability μ_r may be deduced from this curve since:

$$\mu_r = \frac{B}{\mu_o H} \quad \ldots\ldots\ldots\ldots\ldots\ldots\ldots\ldots\ldots\ldots\ldots\ldots \quad 4.1$$

where μ_o represents the absolute permeability of vacuum ($4\pi \times 10^{-7}$ henry/m), H and B the field strength and the magnetic flux density respectively. μ_r is dependent on the material concerned (Kamminga W. 1976), (Cleaver J.R.A. 1980b).

Figure 4.1 shows that up to a flux density of some 1.7 Tesla the B/H curve is linear and has a high permeability. This region is called the unsaturated region (see chapter three).

For flux density B greater than 2 Tesla, the magnetisation curve increases less steeply as the magnetic material of the lens starts to saturate. When saturation is complete the flux density in the iron still increases with increasing values of H, but this increase is due to the energising coil and not to the iron itself. Figure 4.1 illustrates how the flux B_{Fe} due to the iron combines with the flux density B_{coil} due to the coil producing the total flux B. Similar effects are to be expected in the polepiece of a single polepiece lens at poleface flux densities greater than 2 Tesla.

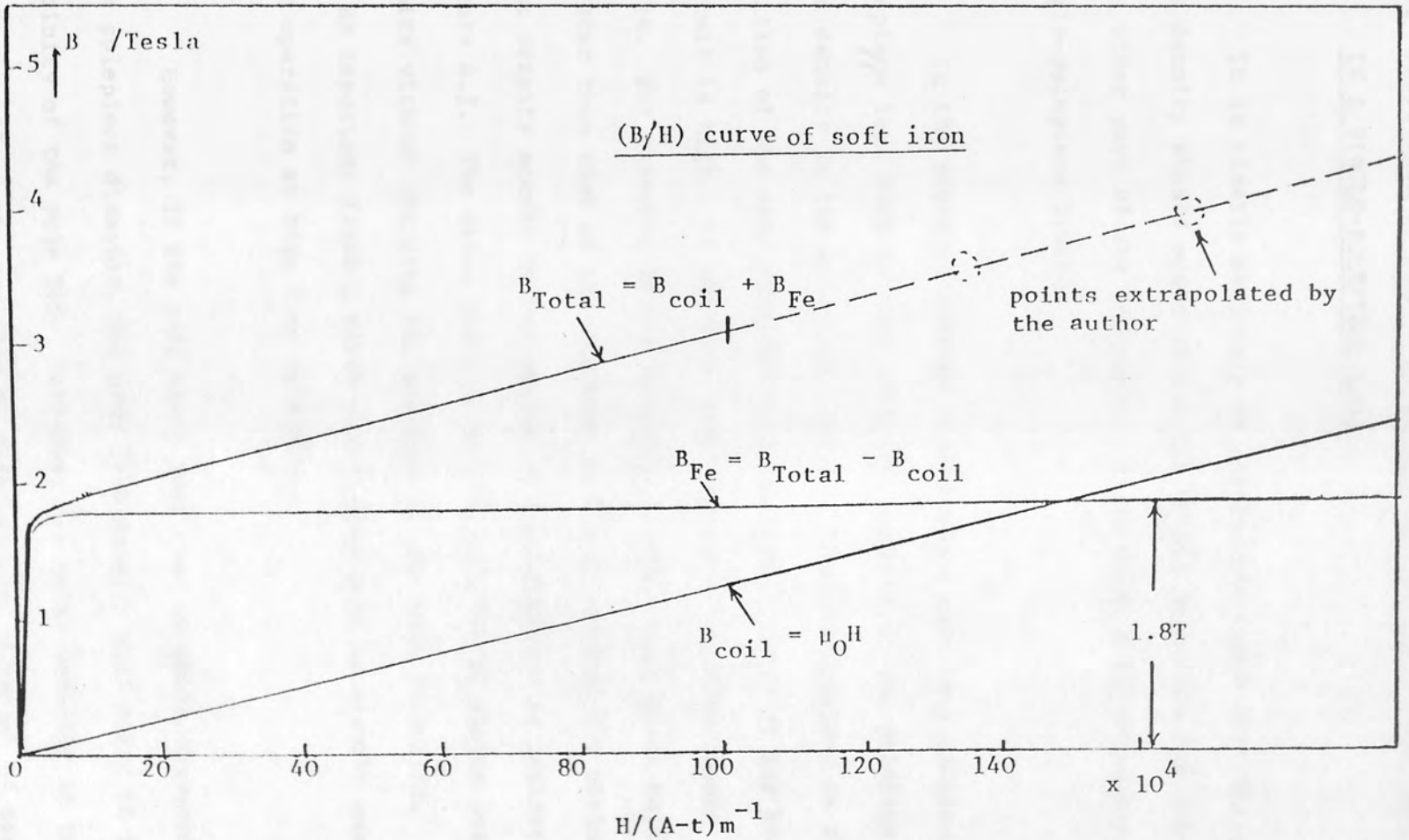

Fig 4.1 Typical non-linear magnetisation B/H curve (taken from Christofides, 1982) of soft iron, together with the individual contribution from the coil (B_{coil}) and from the magnetisation of the iron B_{Fe}. $B_{Total} = B_{coil} + B_{Fe}$

4.2 POSITION OF THE PEAK AXIAL FIELD IN SINGLE-POLEPIECE LENSES

4.2.1 PRODUCTION OF PEAK FLUX DENSITY AT THE TIP OF THE POLEPIECE IN A SINGLE-POLEPIECE LENS

It is clearly desirable in any magnetic lens that the peak flux density should occur at the tip of the polepiece and not in some other part of the polepiece. It is especially important in single-polepiece lenses.

In the previous chapter it was shown that in a single-polepiece lens such as that shown in Figure 4.2, the poleface flux density in the polepiece does not, in general, depend on the position of the coil, provided that the permeability of the iron circuit is high. It was also shown that two important cases arise. For example, if the coil has an inner bore equal to, or greater than that of the diameter of the polepiece, the maximum flux density occurs at the centre of the polepiece as indicated in Figure 4.2. The axial position of the coil can be varied over wide limits without changing the position of the peak intensity. This is an important finding since such a lens will be clearly unsuitable for operation at high flux densities.

However, if the coil has a bore that is small compared with the polepiece diameter, the peak flux density will occur in the vicinity of the pole tip. Likewise, the axial position of the coil will not affect the position of this maximum, although of course it may affect the magnitude of the peak flux density. One would therefore expect that this arrangement would be the most beneficial for lenses operating at high flux density.

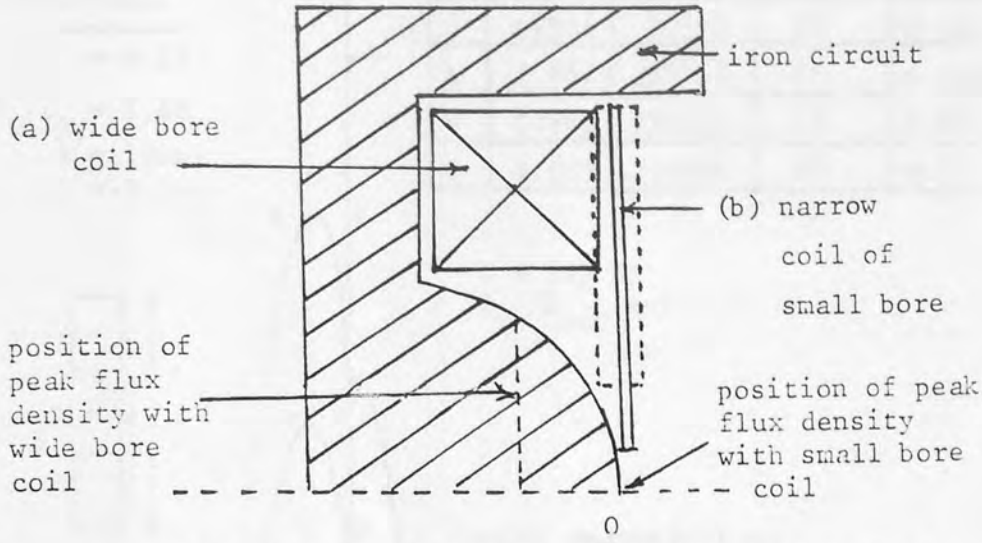

Fig 4.2 Schematic diagram of single-polepiece magnetic lens showing the position of the peak flux density for (a) wide-bore coil (b) narrow bore coil.

Under conditions of extreme saturation, and hence low iron permeability, the axial magnetic field produced by the coil itself may be a dominant factor. Under these conditions the peak axial flux density will tend to occur at the mean axial position of the coil. This is a further advantage of a narrow coil placed near the poletip, since the half-width of its field will be correspondingly small.

4.3 THE DESIGN OF SATURATED RECTANGULAR POLEPIECE LENSES

In order to test these hypotheses,the first calculations were made on the lenses already investigated in Chapter 3, but at much higher excitations. The axial magnetic flux density distributions of the lenses were computed by the Munro program M13, which takes into account the actual B/H curve of the iron circuit. Under saturation conditions the axial field distribution is uniquely determined by the lens ampere turns. This means that the calculations have to be made for a large number of excitations. In order to obtain an insight into the field distribution, the saturation

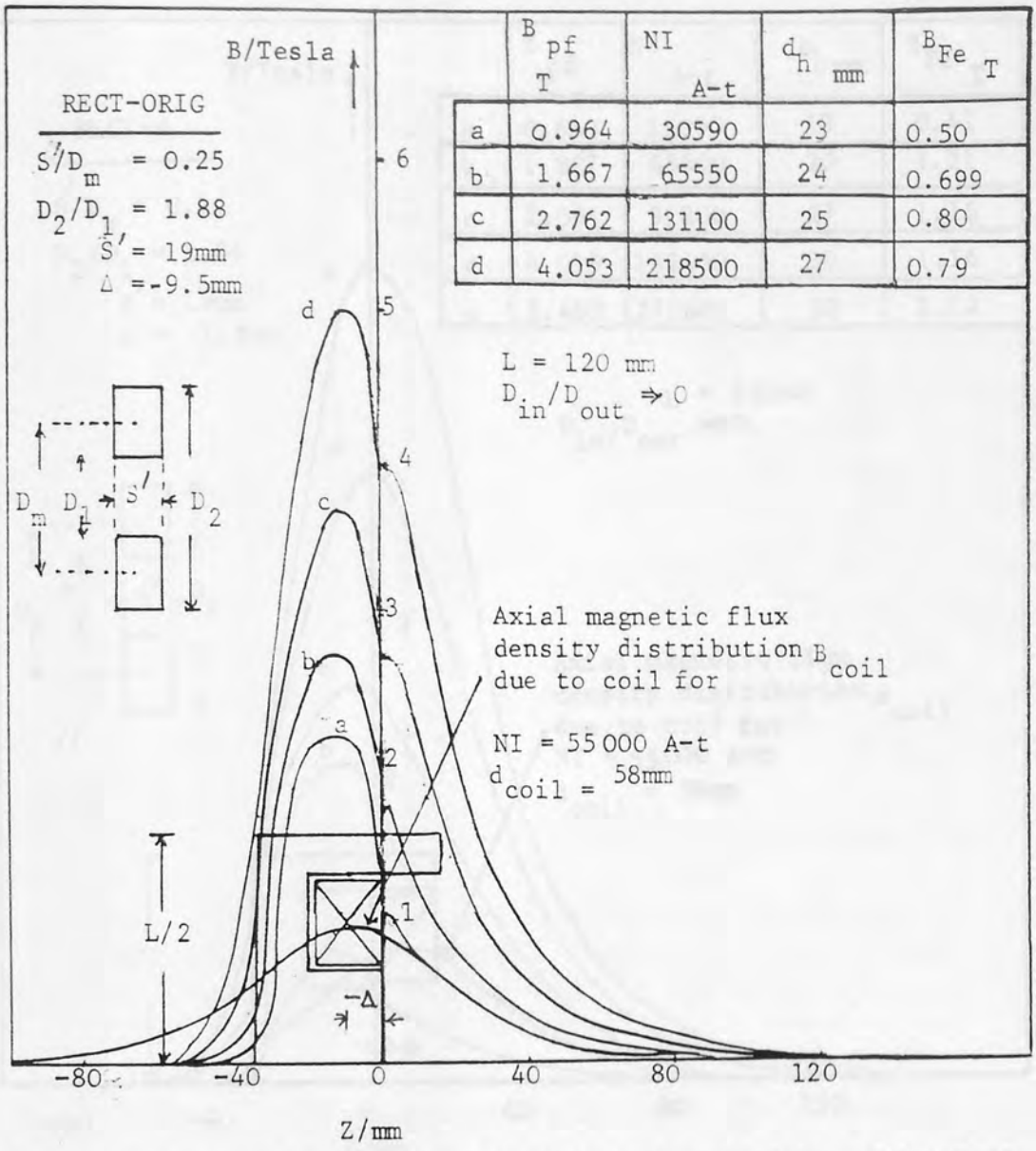

	B_{pf} T	NI A-t	d_h mm	B_{Fe} T
a	0.964	30590	23	0.50
b	1.667	65550	24	0.699
c	2.762	131100	25	0.80
d	4.053	218500	27	0.79

Fig 4.3 Axial magnetic flux density distributions of lens RECT-ORIG at different lens excitations. Coil area = 23 x 19 mm^2. Axial magnetic flux density B_{coil} of NI = 55000 A-t shown for reference.

behaviour of the rectangular polepiece lens was therefore calculated for zero bore and different coil dimensions and positions.

The original rectangular lens with no bore, will still be referred to as RECT-ORIG for identification purposes.

Typical axial magnetic flux density distributions at high excitation are shown in Figure 4.3. The coil completely surrounds the polepiece. The ratio of coil thickness S' to the mean diameter D_m is given by ($S'/D_m = 0.25$). It can be seen that the maximum flux

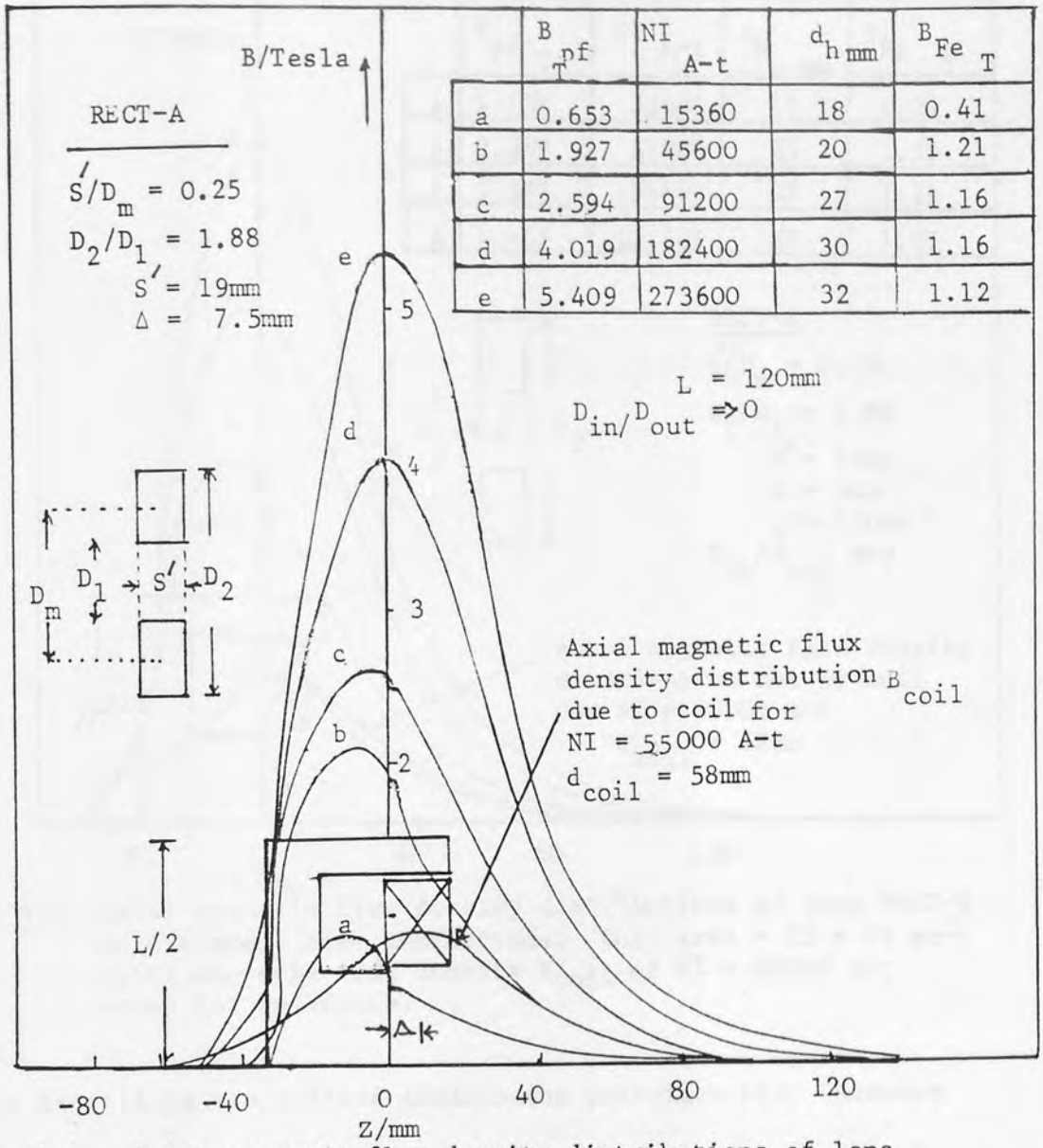

	$B_{T_{pf}}$	NI A-t	d_h mm	B_{Fe_T} T
a	0.653	15360	18	0.41
b	1.927	45600	20	1.21
c	2.594	91200	27	1.16
d	4.019	182400	30	1.16
e	5.409	273600	32	1.12

Fig 4.4 Axial magnetic flux density distributions of lens RECT-A at different lens excitations. Coil area = 23 x 19 mm^2. Axial magnetic flux density B_{coil} of NI = 55000 A-t shown for reference.

density occurs at the centre of the polepiece as previously predicted by the results of Chapter 3. At the polepiece tip itself, the magnetic flux density is considerably lower than this maximum value. This is a waste of ampere turns.

In order to move the saturation point to the tip of the snout (see Appendix A), the coil was moved along the core by an amount equal to the thickness of the coil as shown in Figure 4.4. This figure shows an apparent improvement in as much as the corresponding peak axial

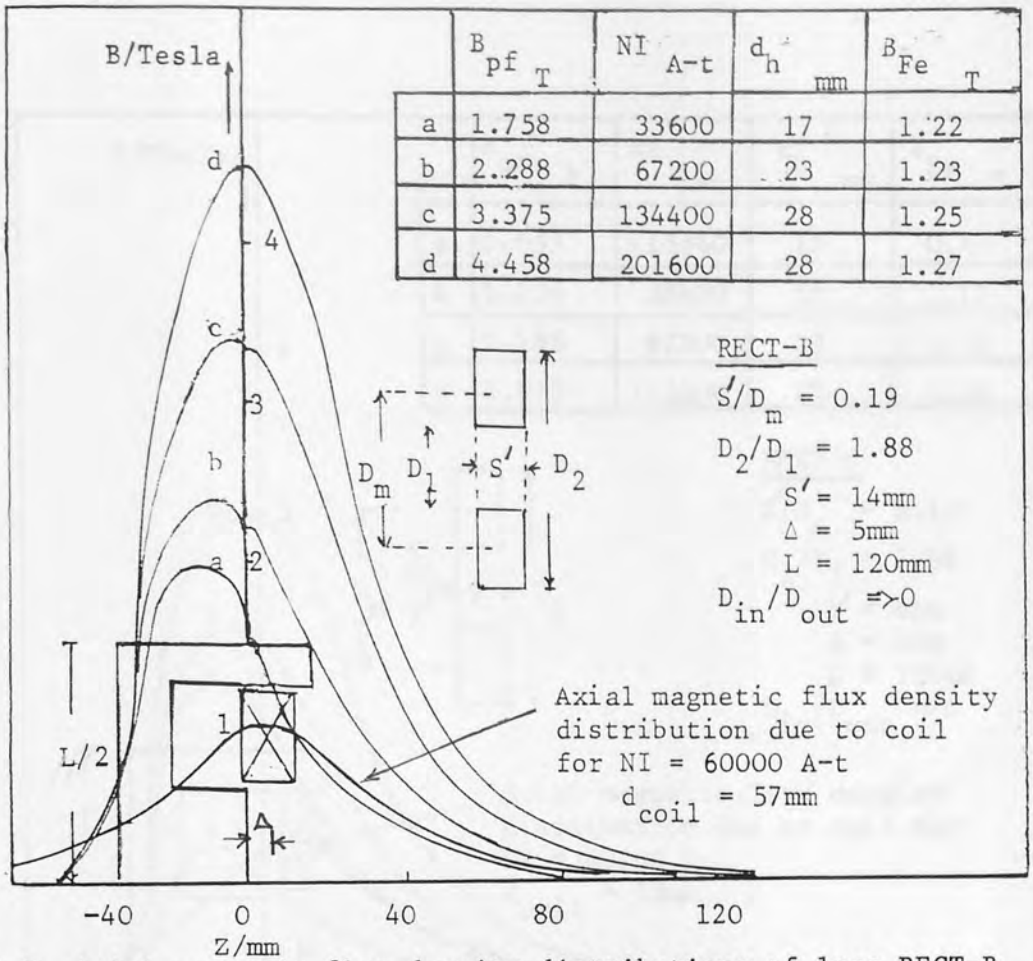

	B_{pf} T	NI A-t	d_h mm	B_{Fe} T
a	1.758	33600	17	1.22
b	2.288	67200	23	1.23
c	3.375	134400	28	1.25
d	4.458	201600	28	1.27

Fig 4.5 Axial magnetic flux density distributions of lens RECT-B at different lens excitations. Coil area = 23 x 14 mm^2. Axial magnetic flux density B_{coil} of NI = 60000 A-t shown for reference.

flux densitites are shifted towards the polepiece tip. However, this is mainly caused by the movement of the field component B_{coil}. In fact the peak flux density B_{Fe} due to the iron remains at the centre of the polepiece. The poleface flux density due to the iron increases from 0.8T to 1.21T. In addition, the half-width of the distribution has increased considerably as shown in the Tables of Figures 4.3 and 4.4. Thus, neither lens is operating under even moderately optimum conditions.

Nevertheless, high total poleface flux densities (in the region of 4T) can be achieved.

Putting a slightly narrower coil in this lens as shown in Figure 4.5 appears to have made a small improvement, but the poleface flux

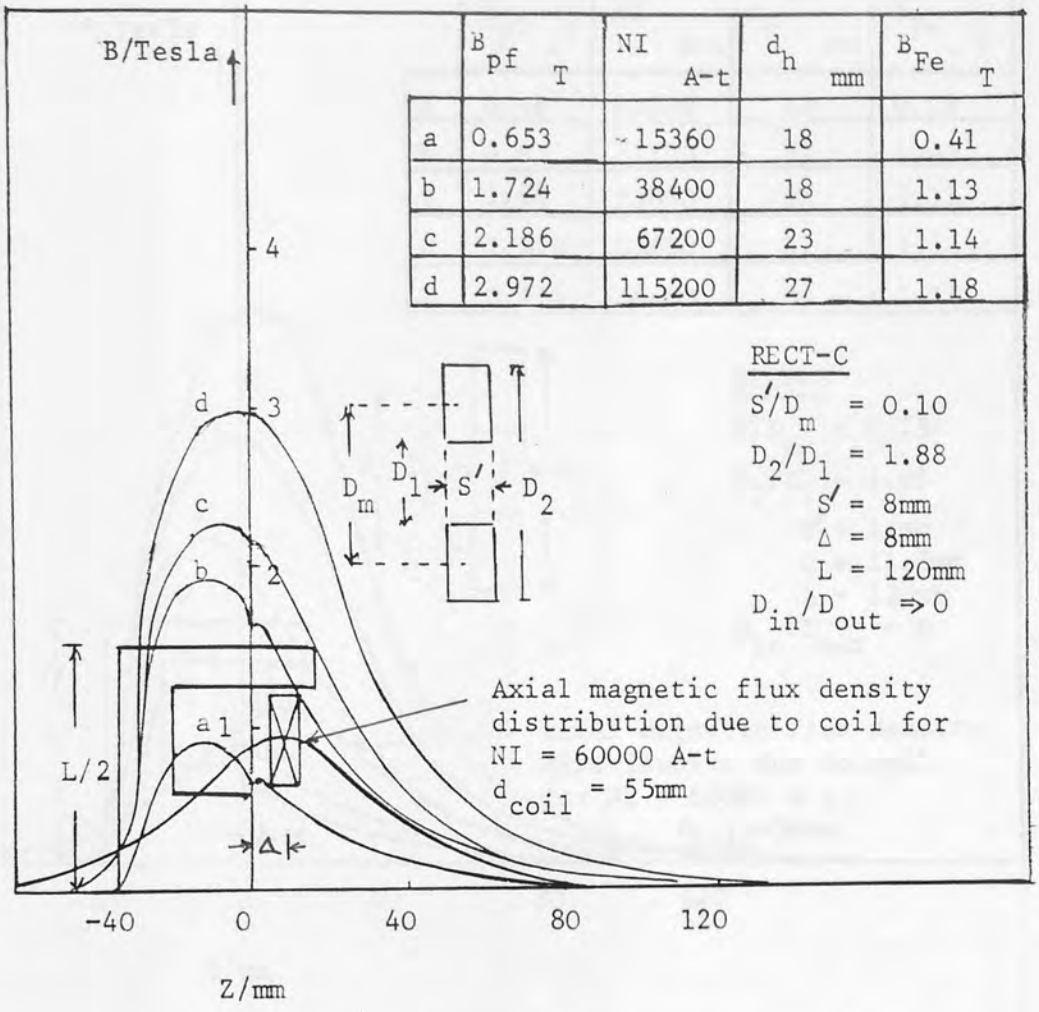

	B_{pf} T	NI A-t	d_h mm	B_{Fe} T
a	0.653	15360	18	0.41
b	1.724	38400	18	1.13
c	2.186	67200	23	1.14
d	2.972	115200	27	1.18

Fig 4.6 Axial magnetic flux density distributions of lens RECT-C at different lens excitations. Coil area = 23 x 8 mm^2. Axial magnetic flux density B_{coil} of NI = 60000 A-t shown for reference.

density due to the iron itself is still only about 1.3T. Some general improvement is however apparent because the loss of ampere turns in the iron circuit is clearly reduced.

Similar remarks apply to the coil arrangements shown in Figures 4.6 and 4.7. Here, the combination of making the coil narrower and placing it outside the polepiece brings only an apparent improvement in the axial field distribution. In fact most of the field is directly due to the coil and not to the polepiece. This is indicated by the notable increase in field half-width with increasing lens

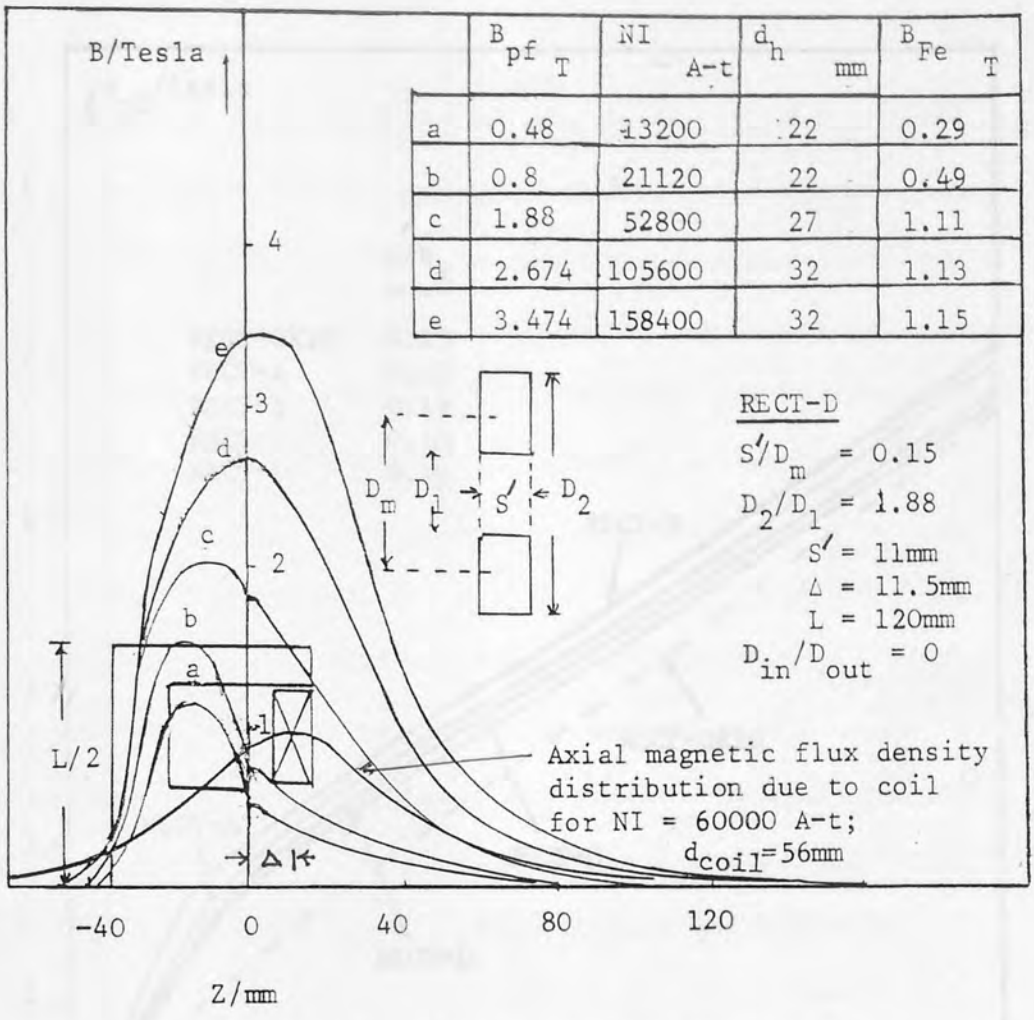

	B_{pf} T	NI A-t	d_h mm	B_{Fe} T
a	0.48	13200	22	0.29
b	0.8	21120	22	0.49
c	1.88	52800	27	1.11
d	2.674	105600	32	1.13
e	3.474	158400	32	1.15

Fig 4.7 Axial magnetic flux density distributions of lens RECT-D at different lens excitations. Coil area = 23 x 11 mm^2. Axial magnetic flux density B_{coil} of NI = 60000 A-t shown for reference.

current and the displacement of the peak towards the centre of the coil. These ideas may be confirmed by the curves of Figure 4.8 which show the poletip flux density as a function of lens excitation NI for this group of lenses (Figures 4.3 - 4.7). This figure shows that at the poletip non-linear effects arise well before the poletip reaches saturation values. The best lens of this group (lens RECT-A) attains a poletip flux density of some 1.7T before exhibiting marked non-linearity. The original lens RECT-ORIG (dashed line in Figure 4.8) is easily the worst lens of the group at poletip

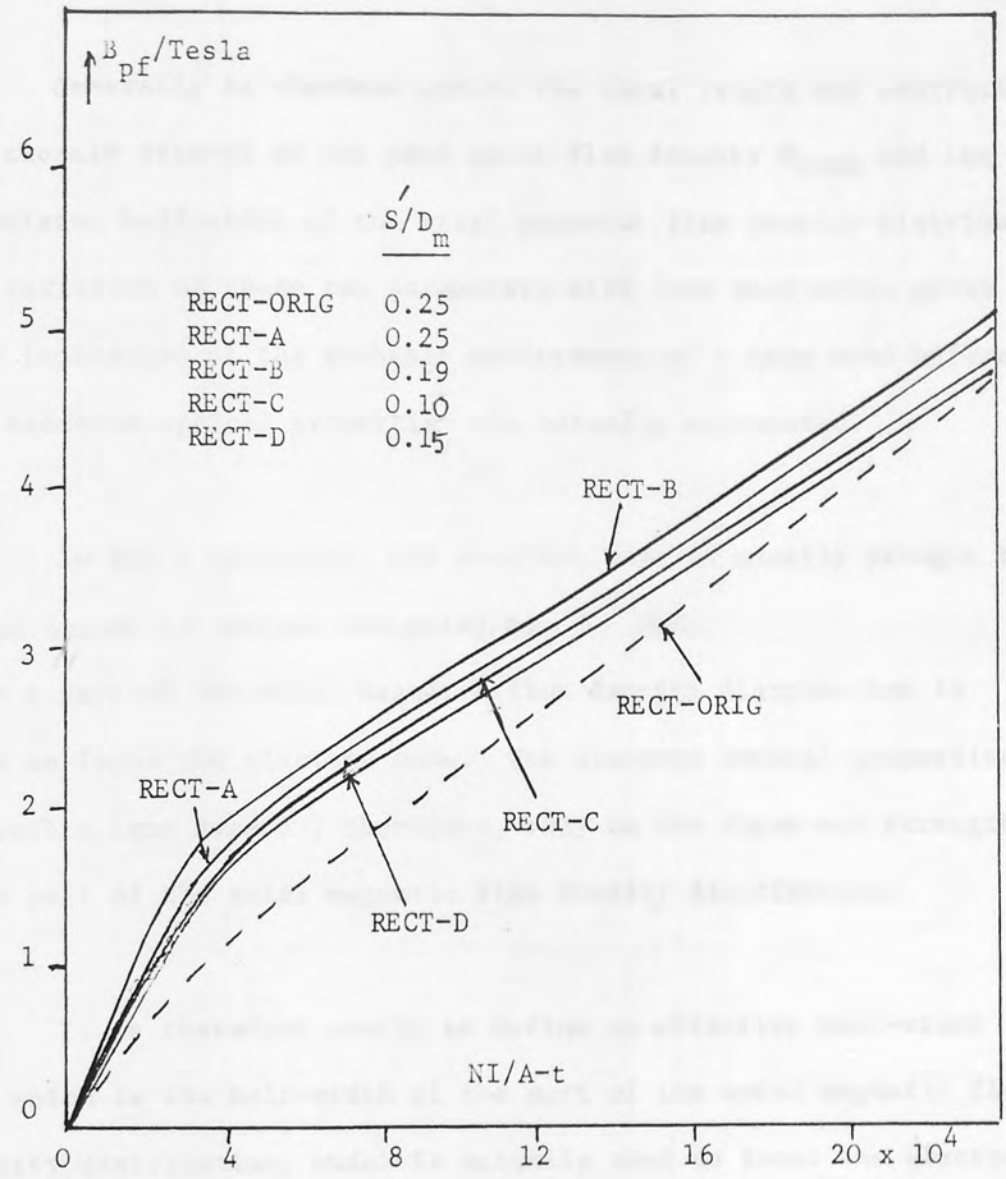

Fig 4.8 Flux density at the poletip of lens RECT-ORIG with zero bore as a function of lens excitaton NI for various coil arrangements A-D as shown in Figures 4.3 - 4.7.

flux densities greater than 1 Tesla.

However, at higher flux densities e.g. around 5T, the differences between these coil arrangements is less noticeable. The reason for this is that at very high lens excitation, the contribution from the poleface itself to the axial field distribution actually decreases for reasons explained in Chapter 3.

4.3.1 THE EFFECTIVE HALF-WIDTH

Generally in electron optics the focal length and aberrations are closely related to the peak axial flux density B_{peak} and the associated half-width of the axial magnetic flux density distribution. The variation of these two parameters with lens excitation gives a good indication of the probable performance of a lens even before its electron optical properties are actually calculated.

In Ray I operation, the electron beam is usually brought to focus before it reaches the polepiece . Thus only a part of the axial magnetic flux density distribution is used to focus the electron beam. The electron optical properties of such a lens depend , therefore, only on the shape and strength of this part of the axial magnetic flux density distribution.

It is therefore useful to define an effective half-width d_h, which is the half-width of the part of the axial magnetic flux density distribution, which is actually used to focus the electron beam. This effective half-width d_h of the axial field distribution will be different for Ray I operation and Ray II operation. This chapter is mainly concerned with Ray I operation.

The calculations carried out on lenses RECT-ORIG and SPHER-ORIG, indicate that the best electron optical properties of these lenses in Ray I beam orientation are obtained from electron trajectories which come to a focus very close to the polepiece tip of the lens (Z = 0).

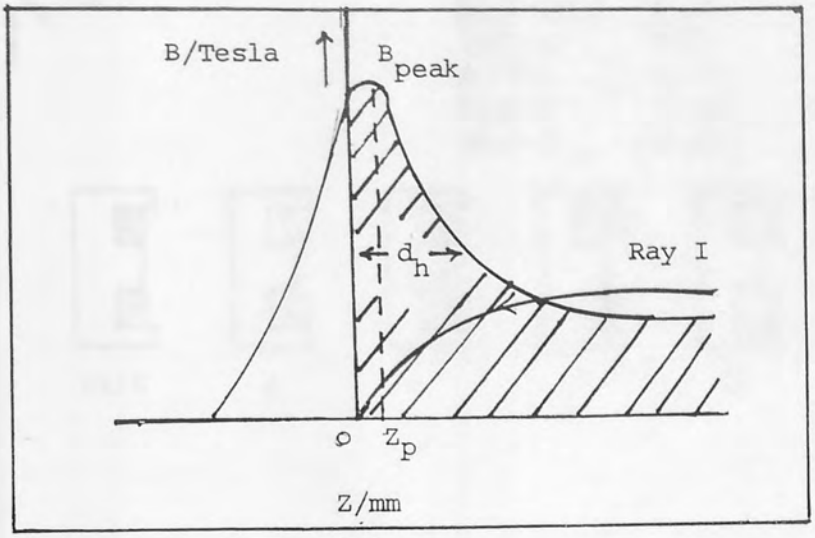

(a)

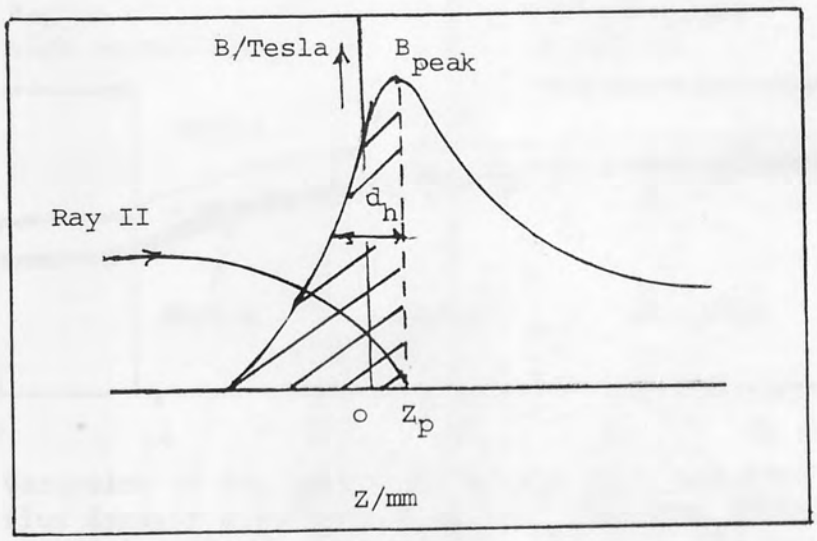

(b)

Fig 4.9 Schematic diagram defining the effective half-width d_h for (a) Ray I, (b) Ray II

In the present work the effective half-width for Ray I beam orientation is defined as the half-width of the axial magnetic flux density distribution in the positive Z region i.e. $Z > 0$, as shown in Figure 4.9a. For Ray II beam orientation the effective half-width d_h, is defined as the effective half-width of the axial magnetic flux density distribution which is in the Z region smaller than Zp (i.e. $Z < Zp$), as shown in Figure 4.9b.

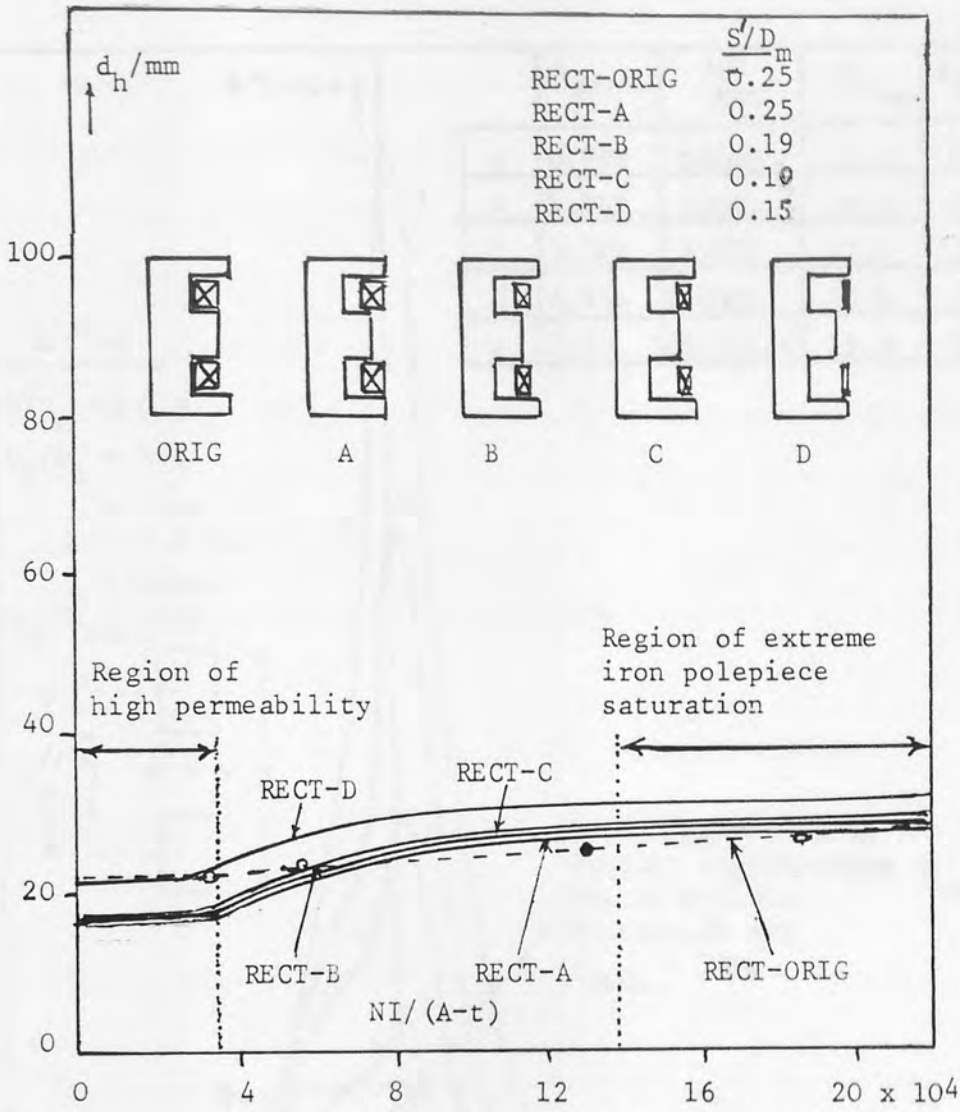

Fig 4.10 Variation of the half-width of the axial magnetic flux density distribution of zero bore lens RECT-ORIG and with coil arrangements (A), (B), (C), (D) as functions of lens excitation NI.

The effect of the coil position on the 'half width' of the axial field distribution in this group of lenses is summarised in Figure 4.10.

At excitations less than 40,000 A-t, the high permeability region, the half width is mainly determined by the magnetisation of the iron polepiece. At high excitations (NI >100,000 A-t) the axial flux density distribution is mainly determined by the coil. Since the half width of the field distribution is measured from the polepiece tip (Z = 0), the axial position of the coil centre will influence the effective half width.

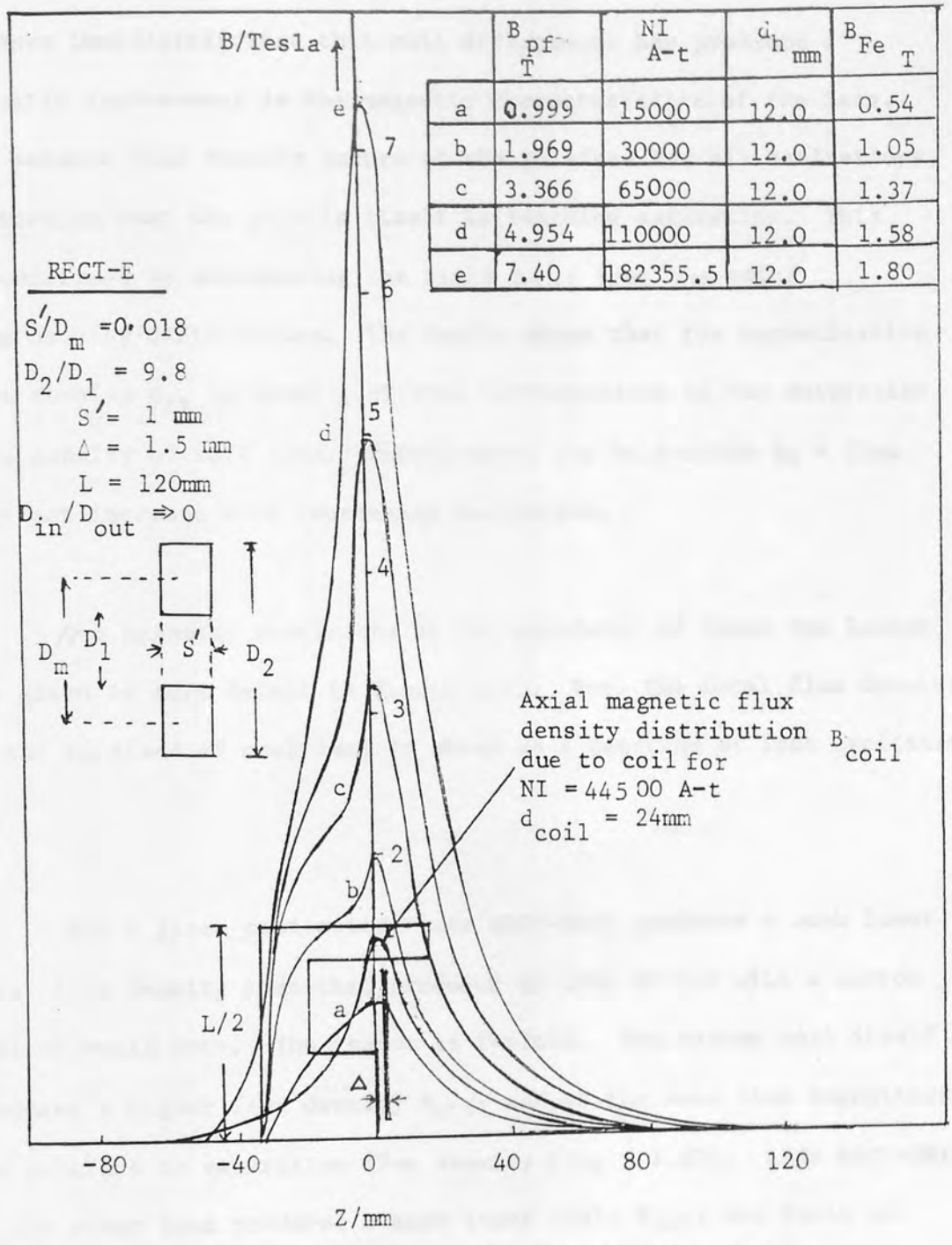

	B_{pf} T	NI A-t	d_h mm	B_{Fe} T
a	0.999	15000	12.0	0.54
b	1.969	30000	12.0	1.05
c	3.366	65000	12.0	1.37
d	4.954	110000	12.0	1.58
e	7.40	182355.5	12.0	1.80

Fig 4.11 Axial magnetic flux density distribution of lens RECT-E with no bore, at different lens excitations. Coil area = 44 x 1mm^2. Axial magnetic flux density B_{coil} of NI = 44500 A-t shown for reference

4.3.2 Flux density distributions under saturation conditions with a narrow-bore coil

Figure 4.11 shows the axial flux density distributions of lens RECT-ORIG but energised by a narrow coil (S'/D_m = 0.018 ,

D_2/D_1 = 9.8) placed in close proximity to the polepiece. It can be seen immediately that this coil arrangement has produced a dramatic improvement in the magnetic characteristics of the lens. The maximum flux density occurs at the poleface for all excitations, indicating that the poletip itself is reaching saturation. This is confirmed by subtracting the field B_{coil} from the total flux density distribution. The result shows that the magnetisation flux density B_{Fe} is about 1.8T thus corresponding to the saturation flux density of soft iron. Furthermore, the half-width d_h = 12mm does not increase with increasing excitation.

The magnetic conditions at the polefaces of these two lenses are given in more detail in Figure 4.12. Here the total flux density at the poleface of each lens is shown as a function of lens excitation NI.

For a given excitation, lens RECT-ORIG produces a much lower axial flux density than that produced by LENS RECT-E with a narrow coil of small bore. The reason is twofold. The narrow coil itself produces a higher flux density B_{coil} and at the same time magnetises the poleface to saturation flux density ($B_{Fe} \simeq 1.8T$). LENS RECT-ORIG on the other hand produces a much lower field B_{coil} and fails to achieve saturation in the iron poleface.

It can be seen intuitively that this type of lens arrangement relies on the coil itself for the production of a favourable axial field distribution. The saturated iron of the poleface then produces a further axial field distribution which is added to that of the coil. There would clearly be some practical difficulties in

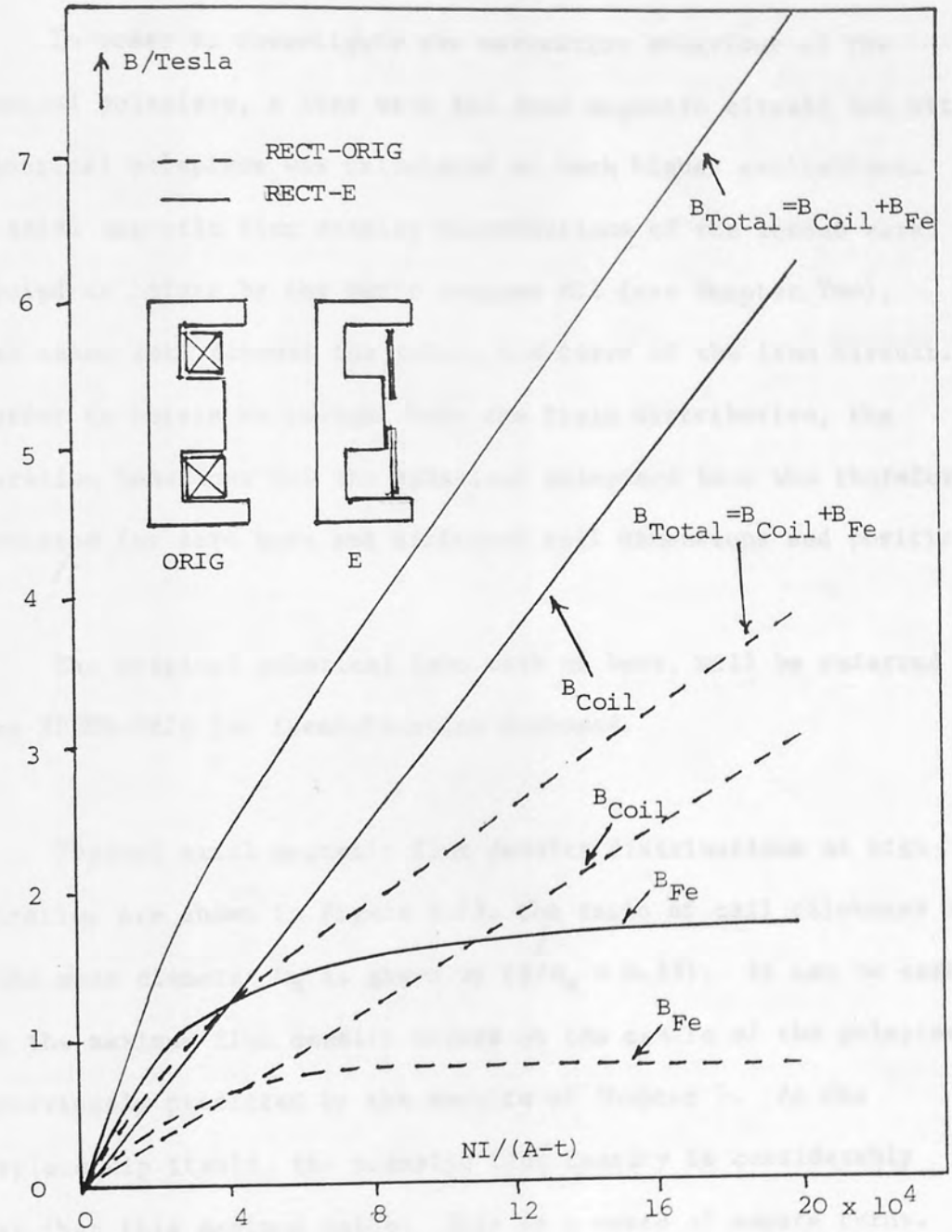

Fig 4.12 Comparison of the total poleface flux density B_{pf} of lens RECT-ORIG and RECT-E with narrow bore coil as a function of lens excitation. The corresponding values of B_{Fe} (due to the iron) are also shown

manufacturing such a lens. A discussion of these will however be postponed for the time being, since it is necessary first to enquire whether a similar, or even better, mode of operation can be obtained with a spherical polepiece.

4.4 THE DESIGN OF SATURATED SPHERICAL POLEPIECE LENSES

In order to investigate the saturation behaviour of the spherical polepiece, a lens with the same magnetic circuit but with a spherical polepiece was calculated at much higher excitations. The axial magnetic flux density distributions of the lenses were computed as before by the Munro program M13 (see Chapter Two), which takes into account the actual B/H curve of the iron circuit. In order to obtain an insight into the field distribution, the saturation behaviour for the spherical polepiece lens was therefore calculated for zero bore and different coil dimensions and positions.

The original spherical lens with no bore, will be referred to as SPHER-ORIG for identification purposes.

Typical axial magnetic flux density distributions at high excitation are shown in Figure 4.13, the ratio of coil thickness S to the mean diameter D_m is given by ($S/D_m = 0.35$). It can be seen that the maximum flux density occurs at the centre of the polepiece as previously predicted by the results of Chapter 3. At the polepiece tip itself, the magnetic flux density is considerably lower than this maximum value. This is a waste of ampere turns.

In order to move the saturation point to the tip of the polepiece (see Appendix A), the coil was moved along the core by an amount less than the thickness of the coil as shown in Figure 4.14. This figure shows an apparent improvement inasmuch as the corresponding peak axial flux densities are shifted towards the polepiece tip. However,

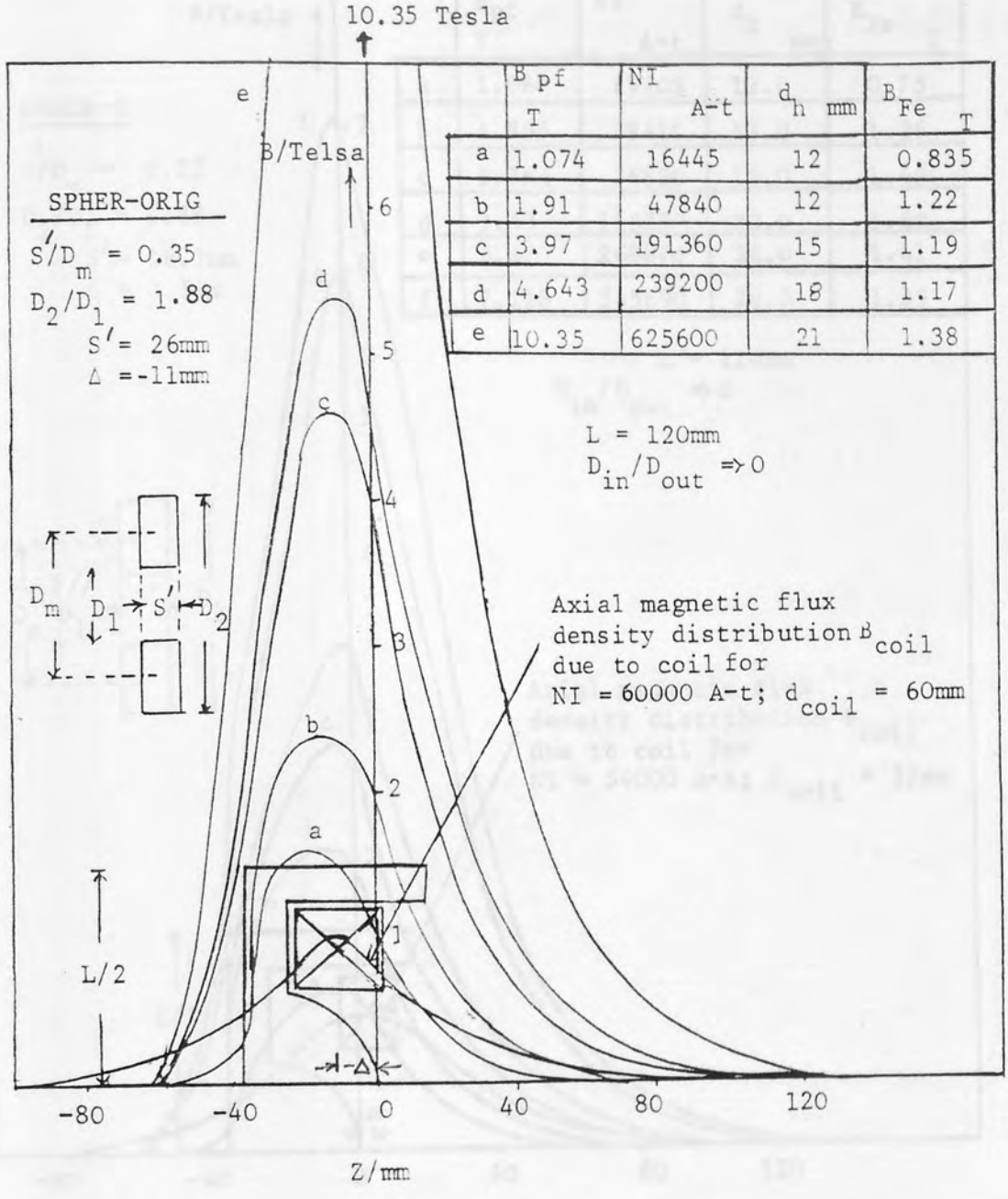

	B_{pf} T	NI A-t	d_h mm	B_{Fe} T
a	1.074	16445	12	0.835
b	1.91	47840	12	1.22
c	3.97	191360	15	1.19
d	4.643	239200	18	1.17
e	10.35	625600	21	1.38

Fig 4.13 Axial magnetic flux density distribution of lens SPHER-ORIG at different lens excitations. Coil area = 26 x 23 mm^2. Axial magnetic flux density B_{coil} of NI = 60000 A-t shown for reference.

this is mainly caused by the movement of the field component B_{coil}. In fact the peak flux density B_{Fe} due to the iron remains at the centre of the polepiece. The poleface flux density due to

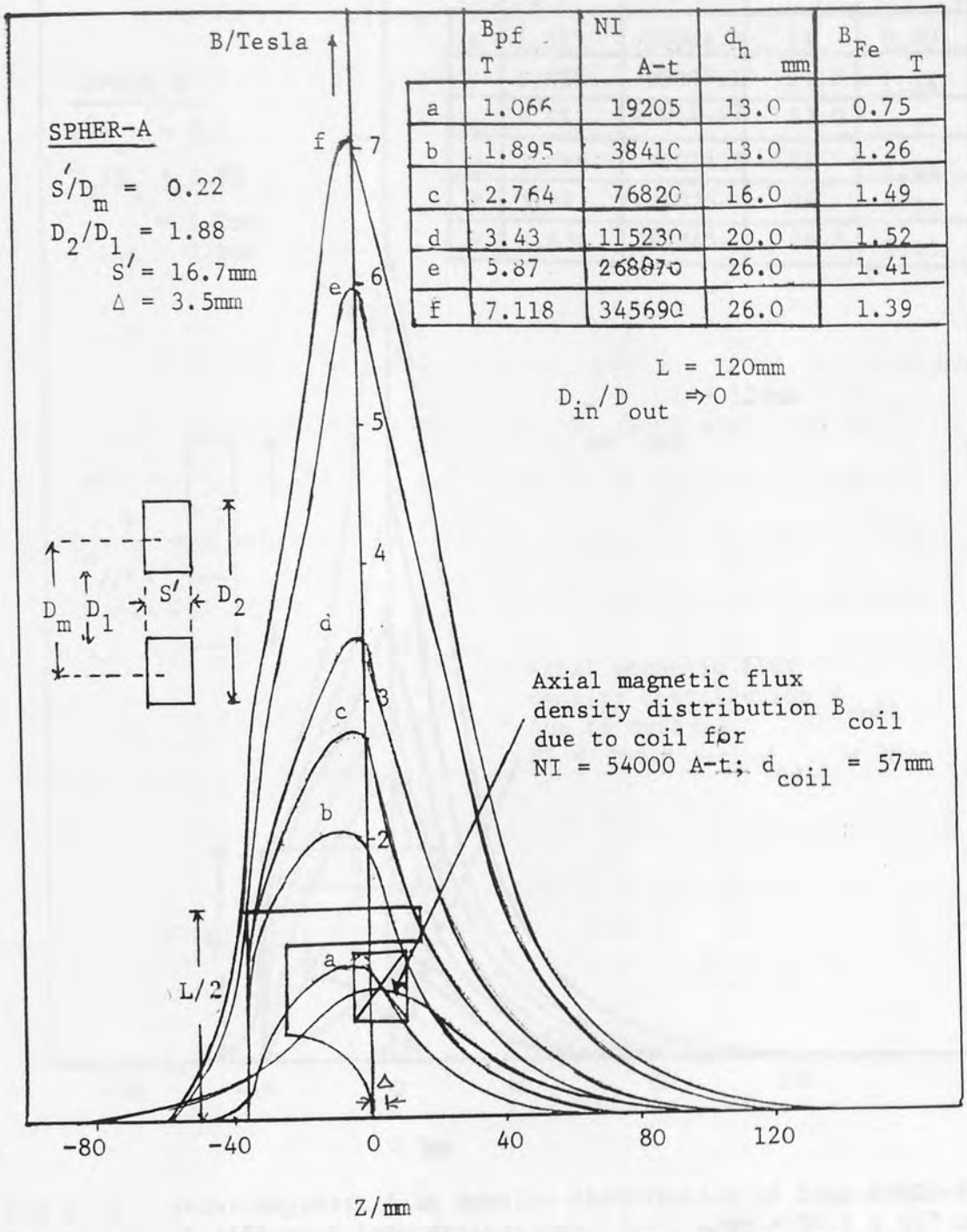

	B_{pf} T	NI A-t	d_h mm	B_{Fe} T
a	1.066	19205	13.0	0.75
b	1.895	38410	13.0	1.26
c	2.764	76820	16.0	1.49
d	3.43	115230	20.0	1.52
e	5.87	268870	26.0	1.41
f	7.118	345690	26.0	1.39

Fig 4.14 Axial magnetic flux density distribution of lens SPHER-A at different lens excitations. Coil area = 23 x 16.7 mm^2. Axial magnetic flux density B_{coil} of NI = 60000 A-t shown for reference.

the iron increases from 1.38T to 1.52T. In addition the half-width of the distribution has increased considerably as shown in the tables of Figures 4.13 and 4.14. Thus, neither lens is operating under even moderately optimum conditions.

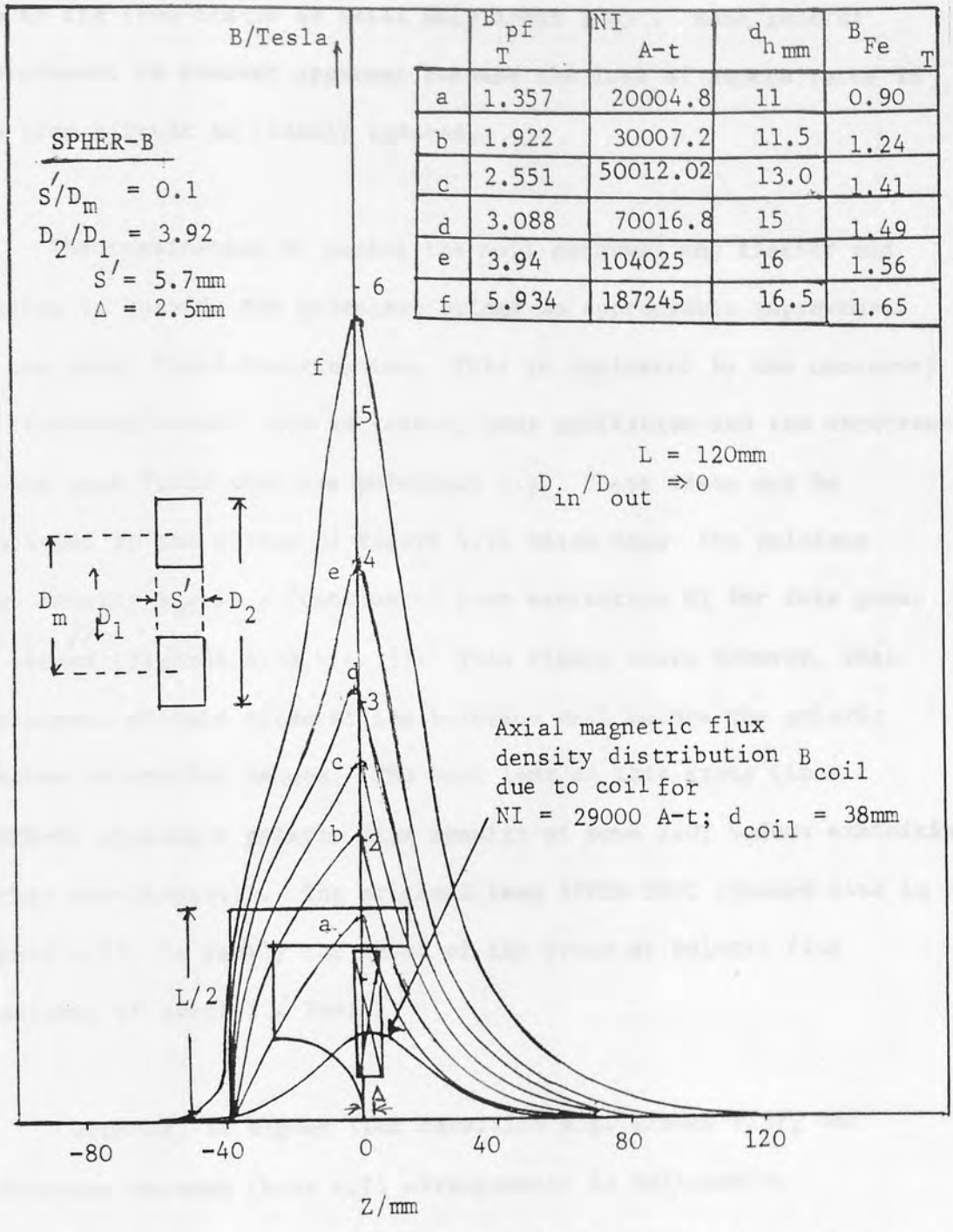

	B_{pf} T	NI A-t	d_h mm	B_{Fe} T
a	1.357	20004.8	11	0.90
b	1.922	30007.2	11.5	1.24
c	2.551	50012.02	13.0	1.41
d	3.088	70016.8	15	1.49
e	3.94	104025	16	1.56
f	5.934	187245	16.5	1.65

Fig 4.15 Axial magnetic flux density distribution of lens SPHER-B at different lens excitations. Coil area = 36.5 x 5.7 mm^2. Axial magnetic flux density B_{coil} of NI = 60000 A-t shown for reference.

Nevertheless, high total poleface flux densities (in the region of 5T) can be achieved. Putting a narrower coil having a large outside diameter D_2 in this lens, as shown in Figure 4.15, appears to have made more improvement, but the poleface flux density

due to the iron itself is still only about 1.65T. Some general improvement is however apparent because the loss of ampere turns in the iron circuit is clearly reduced.

The combination of making the coil narrower and flatter and placing it outside the polepiece brings an appreciable improvement in the axial field distribution. This is indicated by the constancy of field half-width with increasing lens excitation and the occurrence of the peak field near the polepiece tip. These ideas may be confirmed by the curves of Figure 4.16 which show the poleface flux density B_{pf} as a function of lens excitation NI for this group of lenses (Figures 4.13 - 4.15). This figure shows however, that non-linear effects arise at the poleface well before the poletip reaches saturation values. The best lens of this group (lens SPHER-B) attains a poletip flux density of some 2.0T before exhibiting marked non-linearity. The original lens SPHER-ORIG (dashed line in Figure 4.16) is easily the worst of the group at poletip flux densities of about 1.4 Tesla.

However, at higher flux densities e.g. around 7.5T, the difference between these coil arrangements is noticeable.

The effect of the coil position on the half-width of the axial field distribution in this group of lenses is summarised in Figure 4.17.

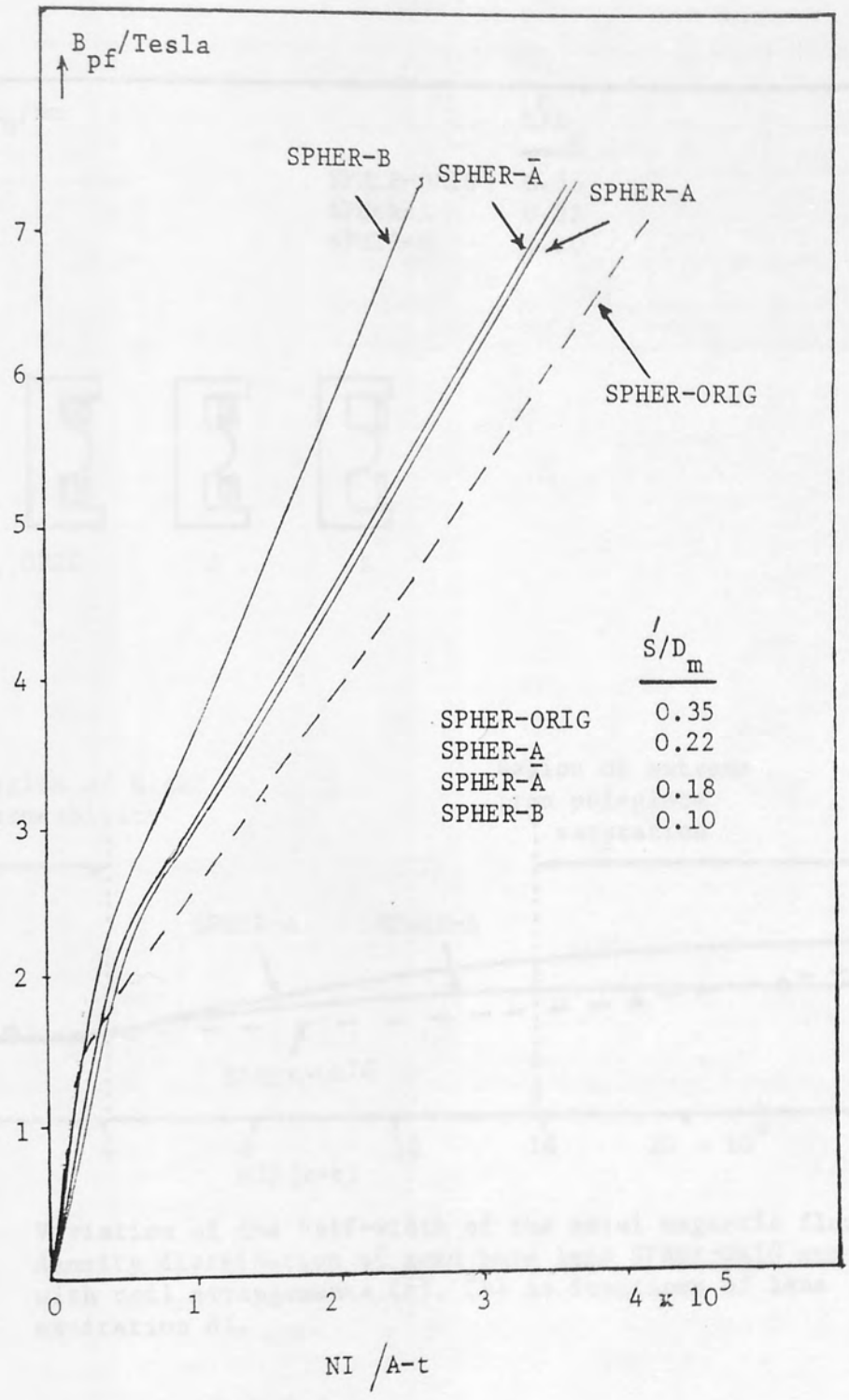

Fig 4.16 Flux density at the poletip of lens SPHER-ORIG with zero bore as a function of lens excitation NI for various coil arrangements A-B as shown in Figures 4.13 - 4.15.

At excitations less than 40000 A-t, the high permeability region, the half-width is mainly determined by the magnetisation of

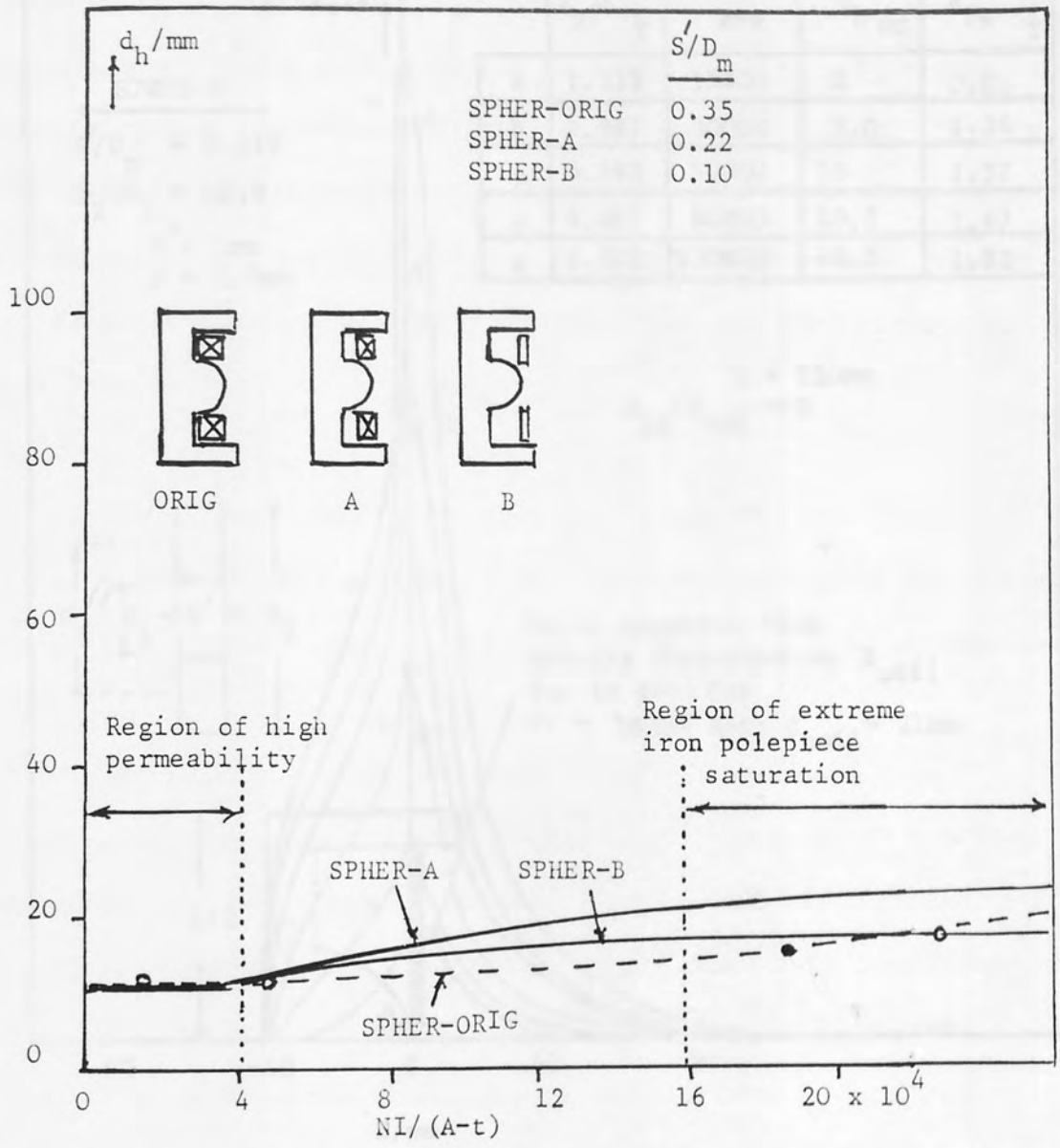

Fig 4.17 Variation of the half-width of the axial magnetic flux density distribution of zero bore lens SPHER-ORIG and with coil arrangements (A), (B) as functions of lens excitation NI.

the iron polepiece. At high excitation (NI $>$ 120000 A-t) the axial flux density distribution is mainly determined by the coil. Since the half-width of the field distribution is measured from the polepiece tip (z = 0), the axial position of the coil centre will influence the effective half-width.

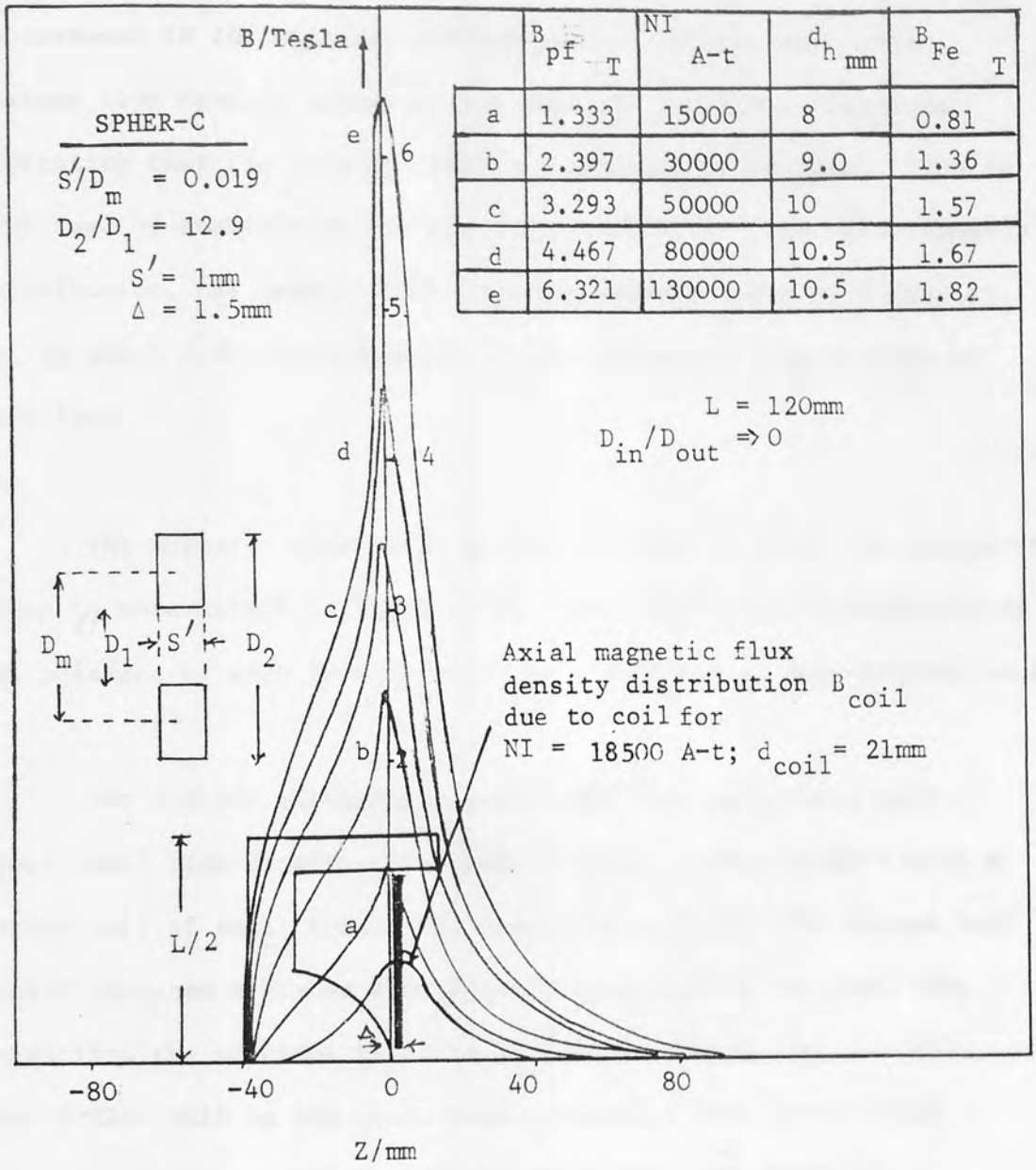

	B_{pf} T	NI A-t	d_h mm	B_{Fe} T
a	1.333	15000	8	0.81
b	2.397	30000	9.0	1.36
c	3.293	50000	10	1.57
d	4.467	80000	10.5	1.67
e	6.321	130000	10.5	1.82

Fig 4.18 Axial magnetic flux density distribution of lens SPHER-C with no bore, at different lens excitations. Coil area = 45.2 x 1 mm^2. Axial magnetic flux density B_{coil} of NI = 18500 A-t shown for reference.

4.4.1 FLUX DENSITY DISTRIBUTIONS UNDER SATURATION CONDITIONS WITH A NARROW-BORE COIL

Figure 4.18 shows the axial flux density distributions of lens SPHER-ORIG but energised by a narrow coil (S'/D_m = 0.019; D_2/D_1 = 12.9)

placed in close proximity to the polepiece. It can be seen immediately that this coil arrangement has produced a dramatic improvement in the magnetic characteristics of the lens. The maximum flux density occurs at the poleface for all excitations, indicating that the poletip itself is reaching saturation. This is confirmed by subtracting the field B_{coil} from the total flux density distribution, the result shows that the magnetisation flux density B_{Fe} is about 1.8T, corresponding to the saturation flux density of soft iron.

The magnetic conditions at the poleface of these two lenses are given in more detail in Figure 4.19. Here the total flux density at the poleface of each lens is shown as a function of lens excitation NI.

For a given excitation, lens SPHER-ORIG produces a much lower axial flux density than that produced by lens SPHER-C with a narrow coil of small bore. The reason is twofold. The narrow coil itself produces a higher flux density B_{coil} and at the same time magnetises the poleface to saturation flux density ($B_{Fe} \simeq 1.8T$). Lens SPHER- ORIG on the other hand produces a much lower field B_{coil} and fails to achieve saturation in the iron poleface.

It can be seen intuitively that this type of lens arrangement relies on the coil itself for the production of a favourable axial field distribution. The saturated iron of the poleface then produces a further axial field distribution which is added to that of the coil. Also it takes full advantage of the lens properties. This suggests that the saturation of the lens poleface tip is essential for low focal length and aberrations. Before a commitment is made as to which one of the lenses investigated so far is the most suitable

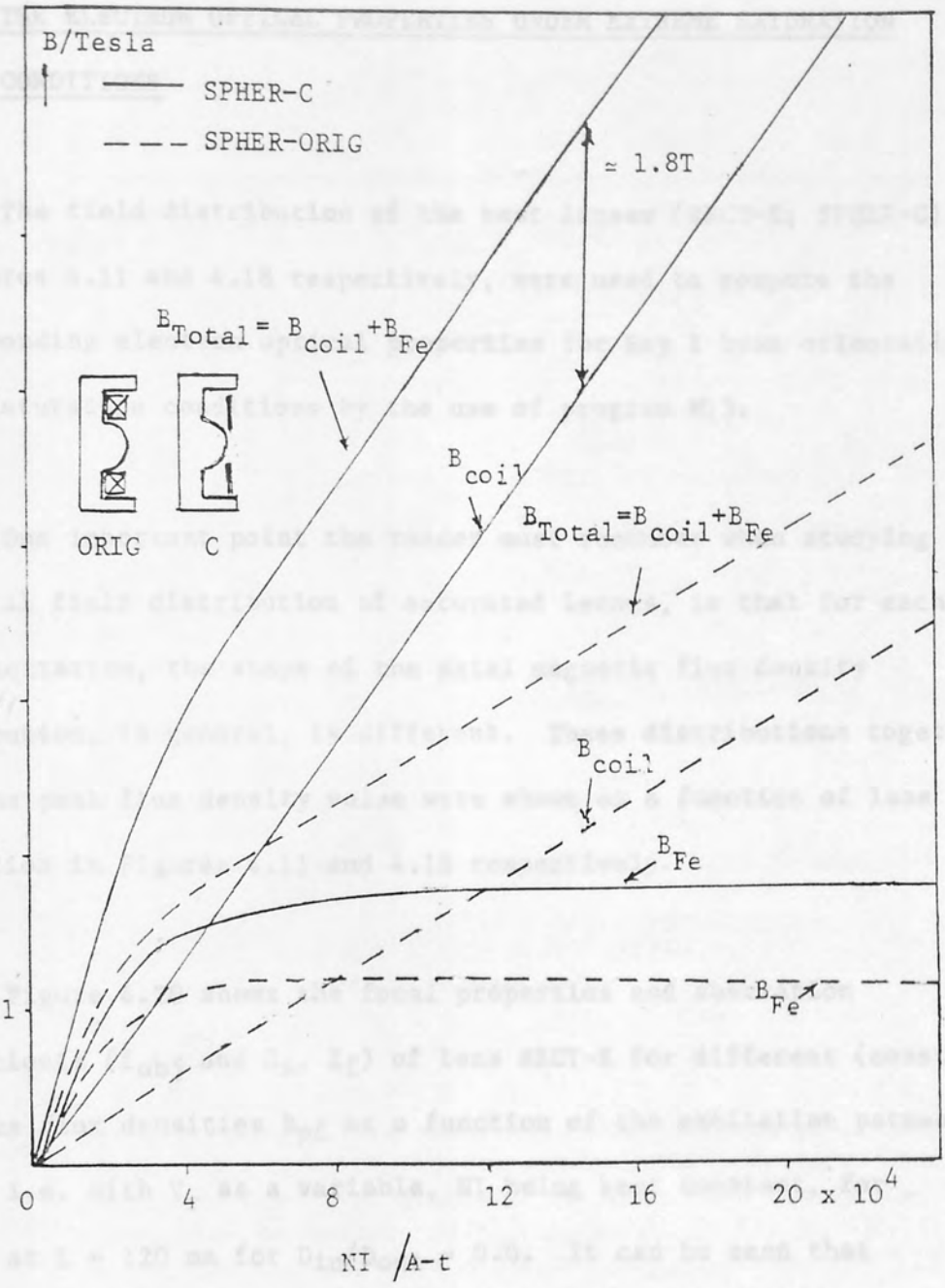

Fig 4.19 Comparison of the total poleface flux density B_{pf} of lens SPHER-ORIG and SPHER-C with narrow bore coil as a function of lens excitation. The corresponding values of B_{Fe} (due to the iron) are also shown.

objective lens, their electron optical properties must be investigated. The electron optical properties are the ultimate criteria for the suitability of a lens for a particular application.

4.5 THE ELECTRON OPTICAL PROPERTIES UNDER EXTREME SATURATION CONDITIONS

The field distribution of the best lenses (RECT-E; SPHER-C) of Figures 4.11 and 4.18 respectively, were used to compute the corresponding electron optical properties for Ray I beam orientation under saturation conditions by the use of program M13.

One important point the reader must remember when studying the axial field distribution of saturated lenses, is that for each lens excitation, the shape of the axial magnetic flux density distribution, in general, is different. These distributions together with the peak flux density value were shown as a function of lens excitation in Figures 4.11 and 4.18 respectively.

Figure 4.20 shows the focal properties and aberration coefficients (f_{obj} and C_s, Z_f) of lens RECT-E for different (constant) poleface flux densities B_{pf} as a function of the excitation parameter, $NI/V_r^{\frac{1}{2}}$ i.e. with V_r as a variable, NI being kept constant, for Ray I, at L = 120 mm for D_{in}/D_{out} = 0.0. It can be seen that under these conditions, the minimum objective focal length and the minimum spherical aberration coefficient do not vary significantly with poleface flux density; minimum f_{obj} = 13.2 mm, and minimum C_s = 3.6 mm. However, this minimum f_{obj} occurs at a different accelerating voltage for each value of lens excitation. A similar situation arises for the minimum values of the spherical aberration coefficient.

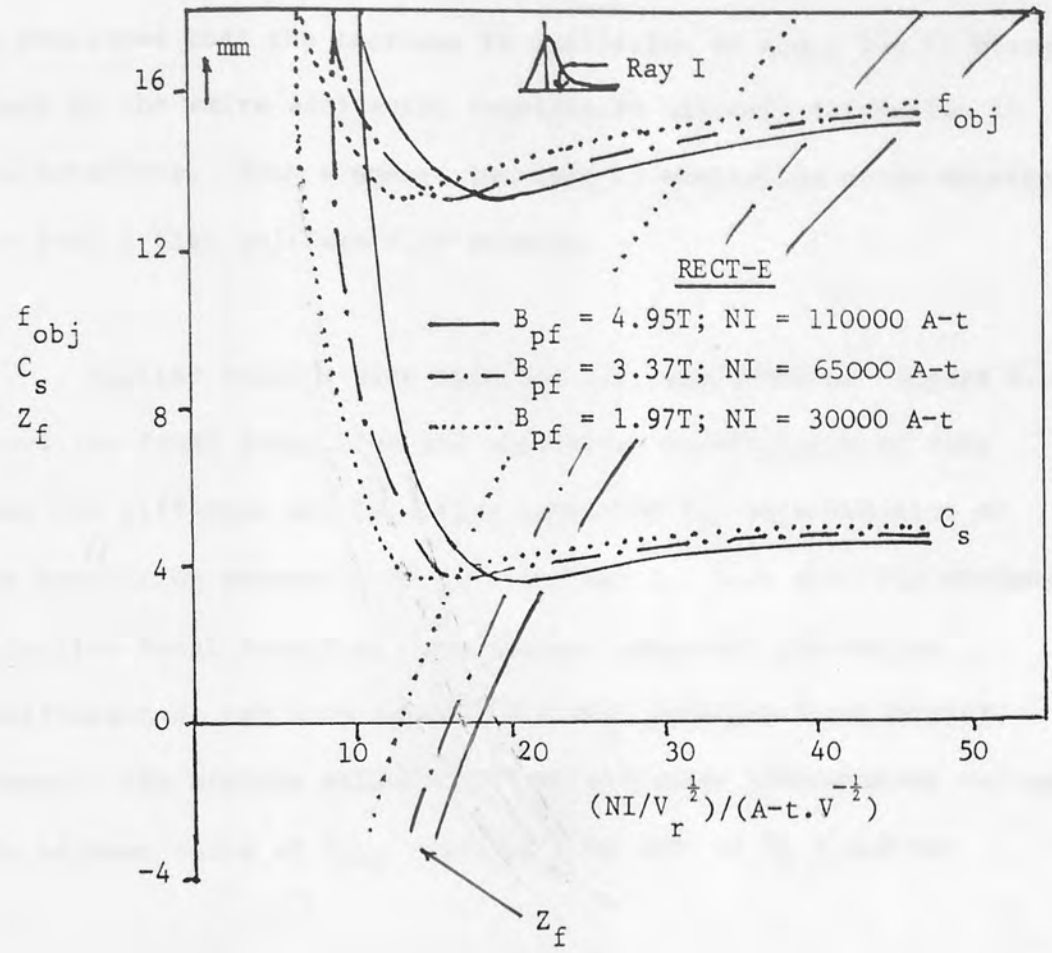

Fig 4.20 Focal properties and aberration coefficients of a lens RECT-E (Fig 4.11) for different constant poleface flux densities B_{pf} (i.e. constant NI) as a function of the excitation parameter, $NI/V_r^{\frac{1}{2}}$ where NI is the total excitation applied to the lens. (D_{in}/D_{out} = 0; L = 120 mm).

Figure 4.20 also shows the values of objective focal distance Z_f with excitation parameter. For a poleface flux density B_{pf} = 1.97T; i.e. at the point where saturation effects are not serious, the excitation parameters $NI/V_r^{\frac{1}{2}}$ = 14 at Z_f = 0. This corresponds to the excitation at which minimum objective focal length is expected to occur. As the lens excitation and hence the poleface flux density increases, minimum objective focal length still occurs at Z_f = 0.

However, the corresponding excitation parameter $NI/V_r^{\frac{1}{2}} = 19.5$. Since the shape of the axial flux density distribution has not changed appreciably as shown by the curves of Figure 4.11, it may be concluded that the increase in excitation by about 30% is brought about by the extra excitation required to maintain saturation in the polepiece. Such a modest increase in excitation seems acceptable for such a high poleface flux density.

Similar results were obtained for lens SPHER-C. Figure 4.21 shows the focal properties and aberration coefficients of this lens for different poleface flux densities B_{pf} as a function of the excitation parameter $NI/V_r^{\frac{1}{2}}$, for Ray I. Once more the minimum objective focal length and the minimum spherical aberration coefficient do not vary appreciably with poleface flux density. However, the minimum values occur at different accelerating voltages. The minimum value of $f_{obj} = 11.4$ mm and that of $C_s = 2.6$ mm.

Figure 4.21 also shows that the minimum objective focal length occurs at zero focal distance i.e. $Z_f = 0$. The 20% increase in excitation at which minimum objective focal length occurs as the poleface flux density is increased from the region of 2 Tesla to some 5T, shows that the design of this lens is superior to that of lens RECT-E.

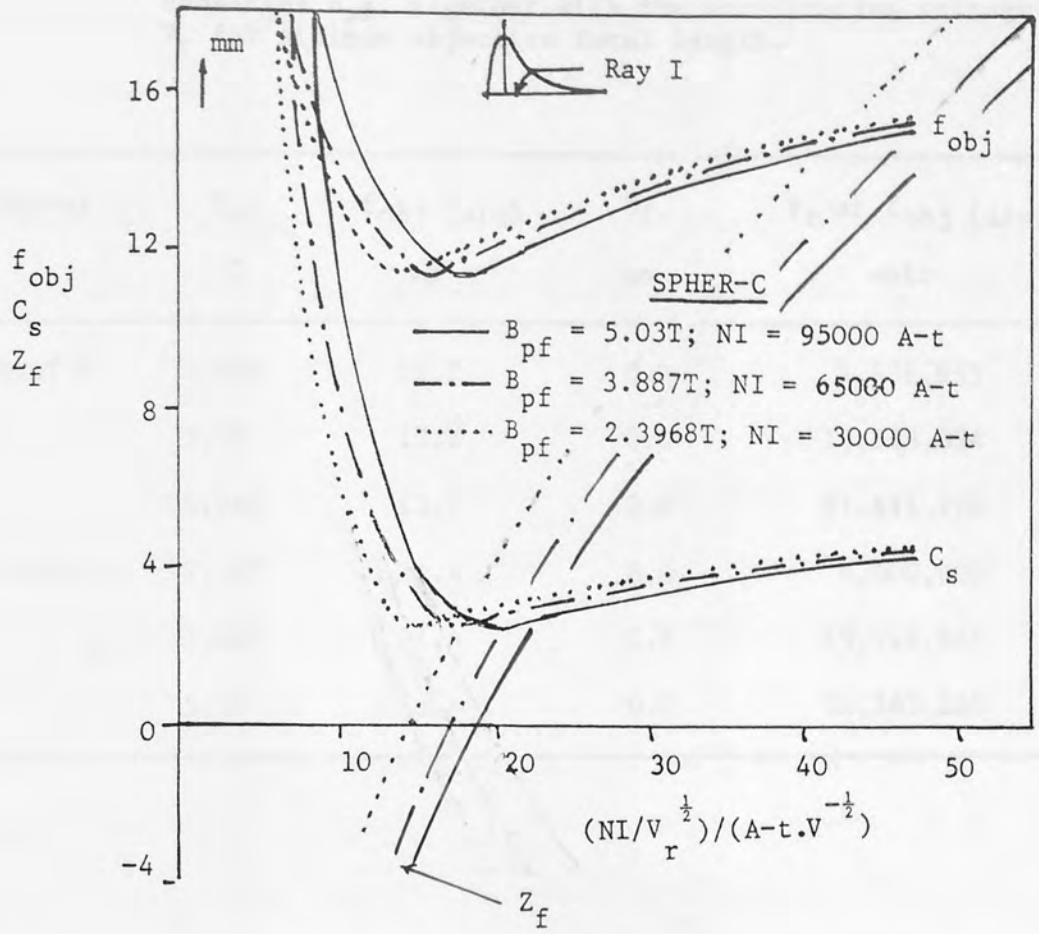

Fig 4.21 Focal properties and aberration coefficients of a lens SPHER-C (Fig 4.18) for different constant poleface flux densities B_{pf} (i.e. constant NI) as a function of the excitation parameter $NI/V_r^{\frac{1}{2}}$, where NI is the total excitation applied to the lens. (D_{in}/D_{out} = 0, L = 120 mm).

On the whole therefore, lens SPHER-C is a better design; especially in view of its shorter focal length and aberration coefficients.

Tables 4.1 and 4.2 summarise the focal properties of lens RECT-E and SPHER-C at different poleface flux densities. The corresponding accelerating voltage V_r for either minimum objective focal length f_{obj} or for minimum spherical aberration coefficient C_s is also shown.

Table 4.1 Summary of electron optical properties f_{obj} and Z_f of lens RECT-E and lens SPHER-C at various poleface flux densities B_{pf}, together with the accelerating voltage V_r for minimum objective focal length.

Lenses	B_{pf} T	f_{obj} (min) mm	Z_f mm	V_r at f_{obj} (min) volt
RECT-E	1.969	13.2	0.0	4,526,935
	3.37	13.2	0.0	15,518,824
	4.954	13.2	0.0	31,831,170
SPHER-C	2.397	11.4	0.0	4,000,000
	3.889	11.4	0.0	15,518,825
	5.03	11.4	0.0	25,265,250

Table 4.2 Summary of electron optical properties C_s and Z_f of lens RECT-E and lens SPHER-C at various poleface flux densities B_{pf}, together with the accelerating voltage V_r for minimum C_s value.

Lenses	B_{pf} T	C_s (min) mm	Z_f mm	V_r at C_s (min) volt
RECT-E	1.969	3.6	0.8	4,500,000
	3.37	3.6	1.0	15,500,000
	4.954	3.6	1.2	31,500,000
SPHER-C	2.397	2.6	0.70	3,882,000
	3.889	2.6	0.75	15,000,000
	5.03	2.6	0.8	25,000,000

The minimum values of spherical aberration coefficients C_s (min) of lens RECT-E and of lens SPHER-C, together with the corresponding values of V_r can now be used in order to predict the properties of similar lenses but of different sizes, in accordance with the scaling lens previously mentioned. The resulting universal curves have been plotted on a double logarithmic plot as a function of the relativistically corrected accelerating voltage V_r, for different values of poleface flux density B_{pf} as shown in Figure 4.22. The resulting curves are, conveniently, straight lines, on a log-log plot, parallel to each other. The spherical aberration coefficient decreases with decreasing relativistically corrected accelerating voltage V_r as the lens is progressively reduced in size. At the same time the current density in the windings will increase. The short vertical lines show the limit of current density for superconducting windings ($\sigma = 10^4$ A-t/mm^2). At a given poleface flux density, the spherical aberration coefficient of lens SPHER-C is systematically lower than that of lens RECT-E. This means that the polepiece shape is indeed important under true saturation conditions. Figure 4.22 shows the spherical aberration coefficient C_s of these two lenses as a function of accelerating voltage for poleface flux densities B_{pf} up to 5T. From all this evidence we can conclude that lens SPHER-C is the best objective lens design of all those considered in the present investigation.

Table 4.3 illustrates the values of the poleface flux density B_{pf} of both lenses (RECT-E; SPHER-C) calculated in terms of the minimum relativistically corrected accelerating voltage allowed for superconducting windings at the limiting current density ($\sigma = 10^4$ A-t/mm2).

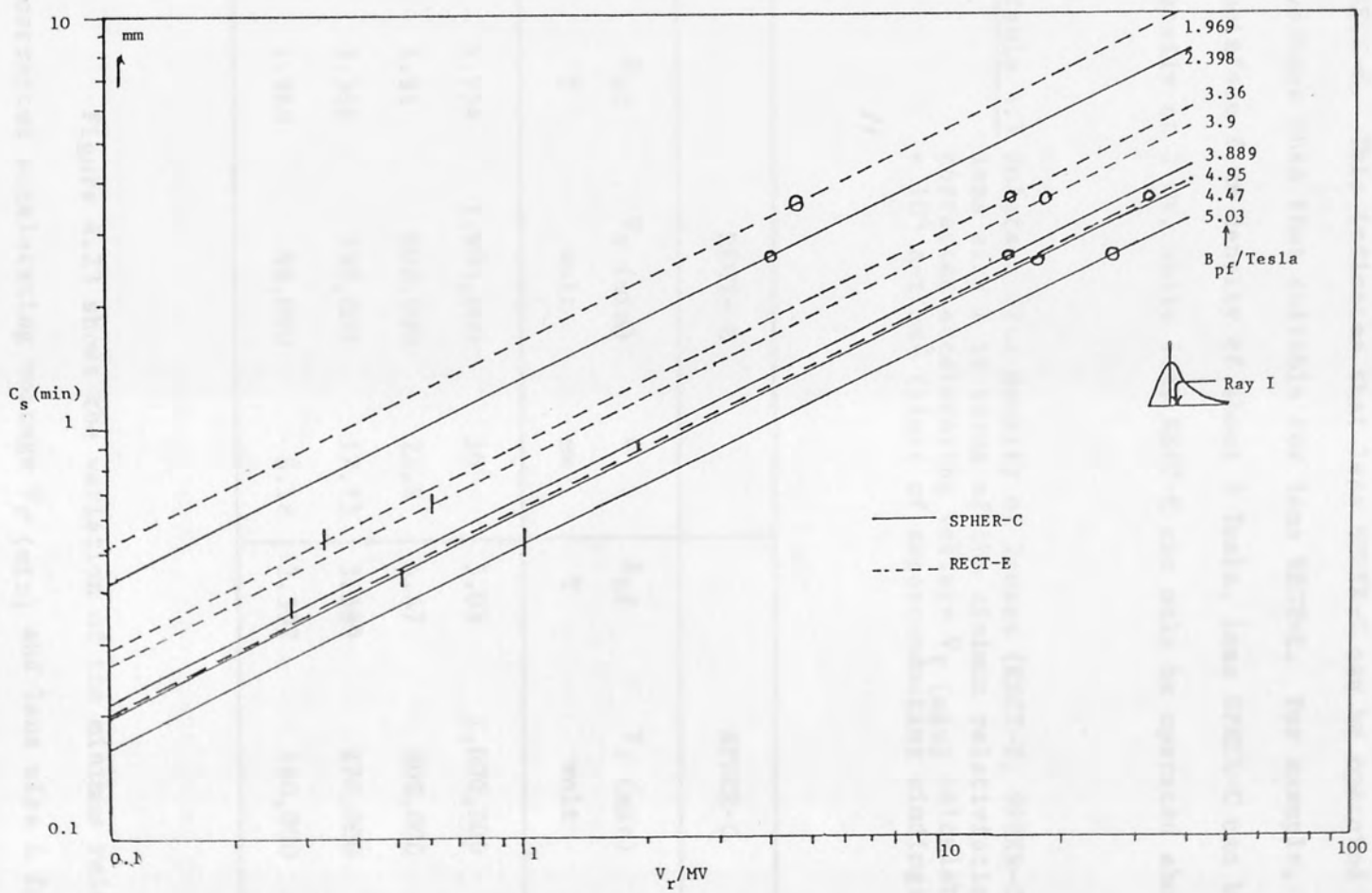

Fig 4.22 Variation of the minimum spherical aberration coefficient C_s (min) of lenses RECT-E and SPHER-C for different poleface flux density as a function of the relativistically corrected accelerating voltage V_r, (D_{in}/D_{out} = 0.0). The short vertical lines indicate the current density limit of superconducting windings ($\sigma = 10^4$ A-t/mm^2). C_s(min) values taken from Figures 4.20 and 4.21.

The limiting lens size is also given in the same table. For a given poleface flux density, the relativistically corrected accelerating voltage of lens SPHER-C is lower than that of lens RECT-E. This indicates that lens SPHER-C can be operated at a lower voltage than that suitable for lens RECT-E. For example, at a poleface flux density of about 5 Tesla, lens SPHER-C can be operated easily at I MV, while lens RECT-E can only be operated above 1.5 MV.

Table 4.3 Poleface flux density of lenses (RECT-E; SPHER-C) and lens size L in terms of the minimum relativistically corrected accelerating voltage $V_{r\ (min)}$ calculated at = 10^4 A-t/mm^2 (limit of superconducting windings)

RECT- E			SPHER-C		
B_{pf} T	$V_{r\ (min)}$ volt	L mm	B_{pf} T	$V_{r\ (min)}$ volt	L mm
4.954	1,900,000	30	5.03	1,000,000	25.2
3.91	600,000	21.8	4.47	500,000	21.24
3.366	330,000	17.73	3.889	270,000	17.26
1.969	98,000	8.18	2.397	160,000	7.96

Figure 4.23 shows the variation of the minimum relativistically corrected accelerating voltage $V_{r\ (min)}$ and lens size L for lens SPHER-C as a function of a poleface flux density B_{pf}. The lens size is adjusted so that $\sigma = 10^4$ A-t/mm^2. The values of $V_{r\ (min)}$ and lens size L increase steadily with increasing poleface flux density.

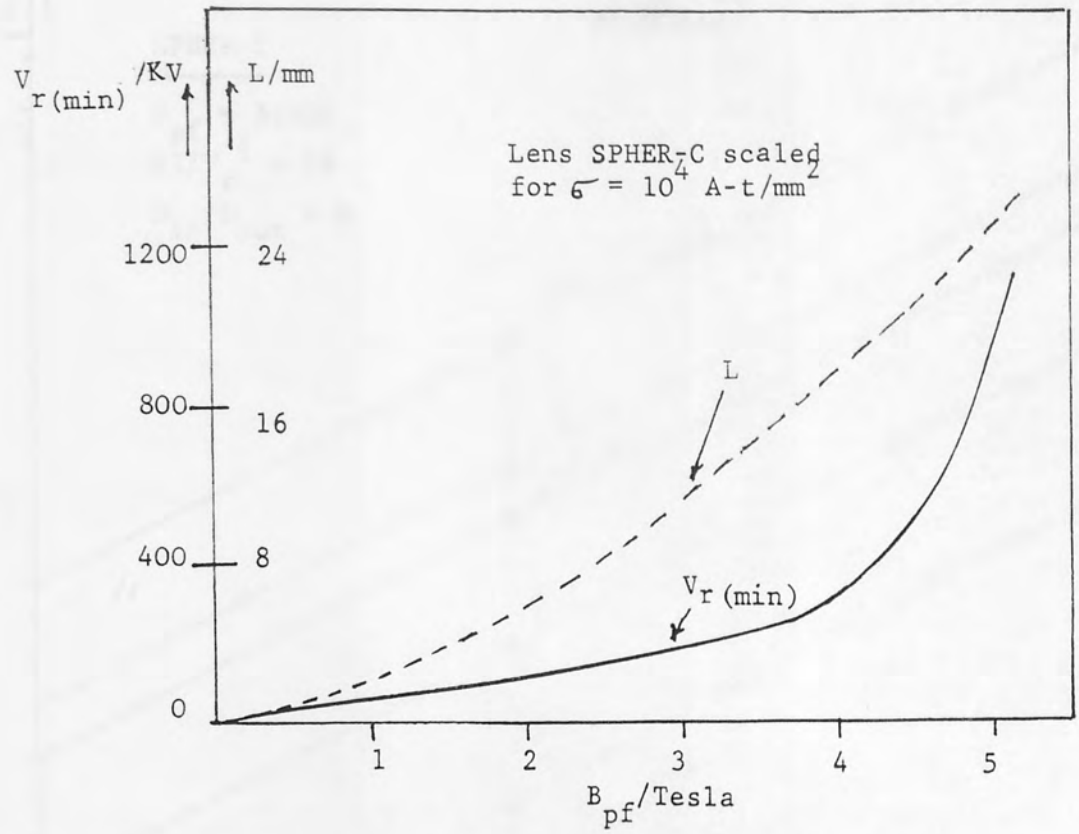

Fig 4.23 Lens size L of the scaled lens SPHER-C operating at a current density of 10^4 A-t/mm^2, together with the minimum permissible operating voltage V_r.

Figure 4.24 shows the variation of the objective properties (C_s, C_c, f_{obj}), lens size L and the reciprocal current density $1/\sigma$ of lens SPHER-C as a function of V_r, when operated at poleface flux density of 5 Tesla.

Figure 4.24 shows that under these conditions the current density in the windings falls below 10^4 A-t/mm^2 for values of V_r greater than 1 MV. This lens therefore can be operated in Ray I mode, at voltages greater than 1 MV with superconducting windings.

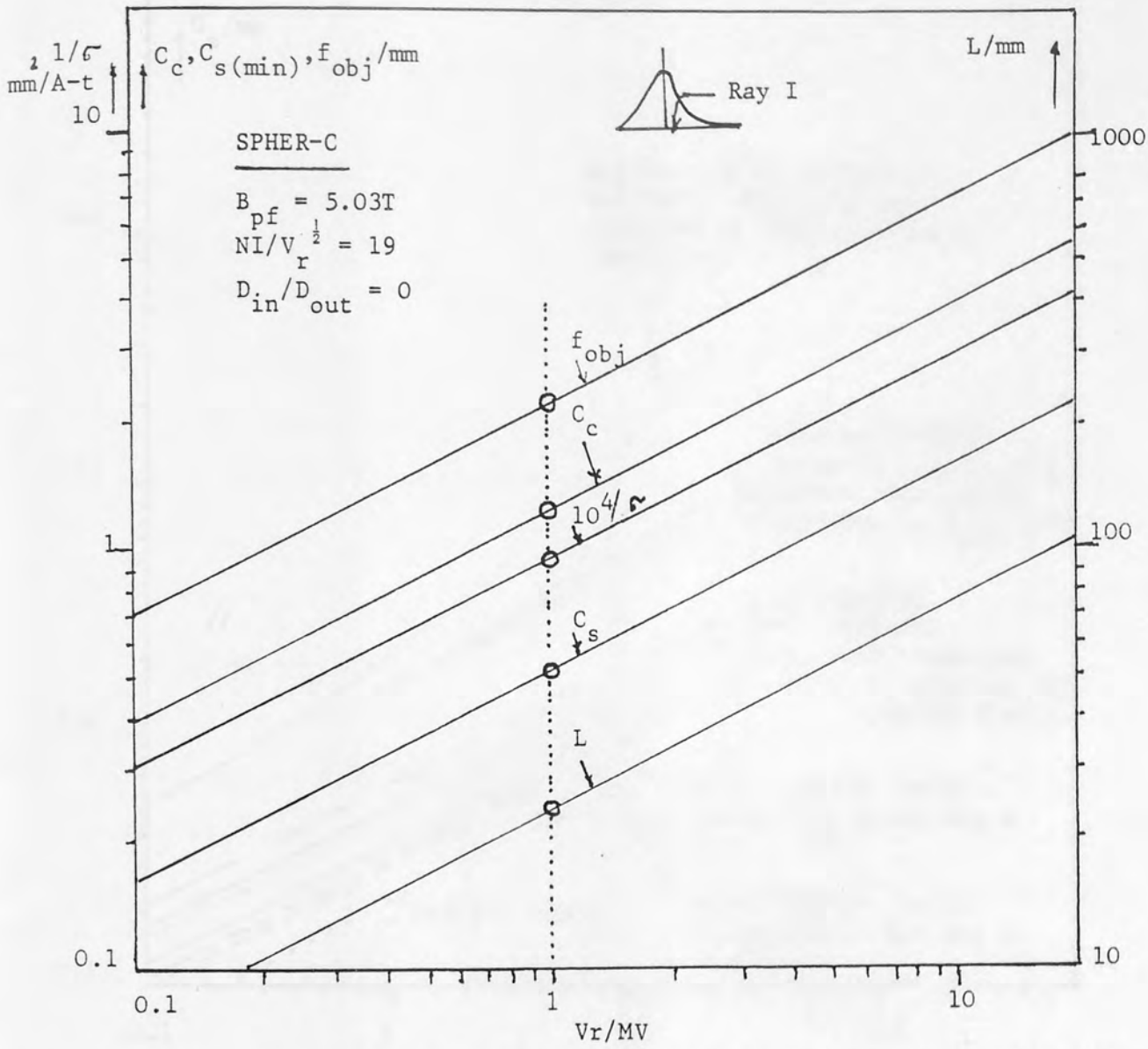

Fig 4.24 Variation of the focal properties and aberration coefficient (f_{obj}, C_s, C_c) with the reciprocal current density $1/\sigma$ and lens size L of a lens SPHER-C as a function of relativistically corrected accelerating voltage V_r. (B_{pf} = 5.03T, $NI/V_r^{\frac{1}{2}}$ = 19, D_{in}/D_{out} = 0.0). The vertical line shows the limit of superconducting windings $\sigma = 10^4$ (A-t/mm^2)

4.6 COMPARISON OF SINGLE-POLEPIECE LENSES WITH CONVENTIONAL LENSES UNDER CONDITIONS OF IRON SATURATION

In order to compare the lens performance generally, and the aberration coefficients in particular, of the optimised single-polepiece

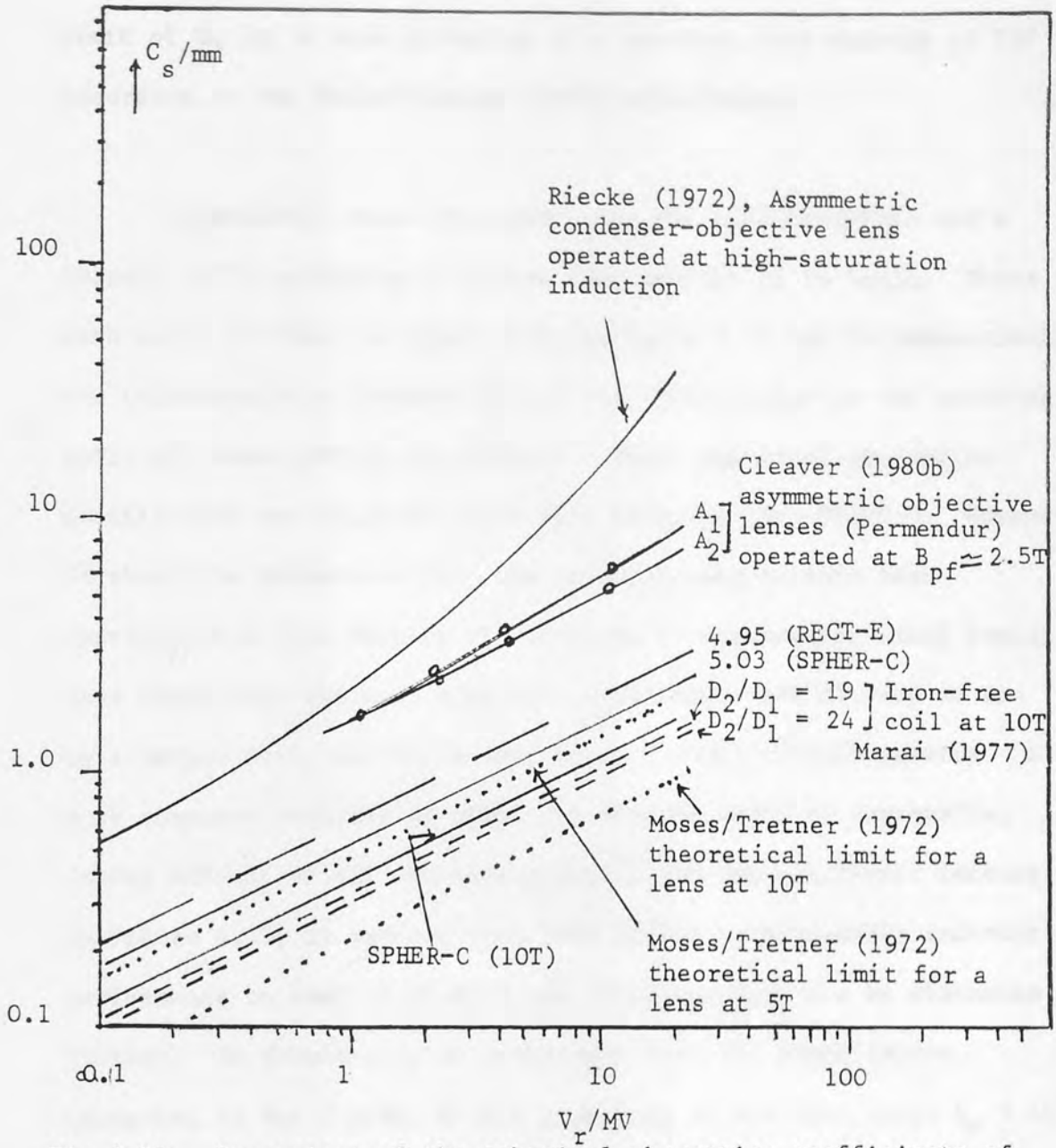

Fig 4.25 Comparison of the spherical aberration coefficients of the single-polepiece lenses SPHER-C and RECT-E, iron-free coil lenses (Marai, 1977), saturated asymmetrical lenses (Cleaver, 1980b) and the saturated single condenser-objective lens (Riecke, 1972). For reference purposes, absolute Moses/Tretner (1972) limit for any lens operating at B_{pf} = 5T and B_{pf} = 10T.

lenses, RECT-E and SPHER-C with previously published designs, Figure 4.25 shows the spherical aberration coefficient C_s as a function of accelerating voltage V_r. As before, a double logarithmic plot has been used since a lens operating at a constant poleface flux density produces a straight line on this plot, as previously shown.

The lowest line on the plot corresponds to the theoretical limit of C_s for a lens operating at a poleface flux density of 10T according to the Moses-Tretner (1972) calculation.

Immediately above this line come the thin iron-free coils (Marai, 1977) operating at a peak flux density of 10 Tesla. These thin coils of outer to inner diameter D_2/D_1 = 19 and 24 respectively and thickness/mean diameter $S/D_m \simeq 0.1$, are similar to the exciting coils of lenses RECT-E and SPHER-C. Their spherical aberration coefficients are slightly lower than those of lens SPHER-C. However, it should be remembered that the iron poleface in this lens contributes a flux density of 2.0 Tesla to the maximum axial field. This means that the coil need only contribute some 8T, and so can be a larger coil, and hence operate at a lower current density. A more complete analysis of these two systems would be worthwhile, taking account of all the technological and constructional factors. In Figure 4.25, it appears that lens RECT-E is noticeably inferior in performance to that of SPHER-C and will therefore not be discussed further. It should also be emphasised that all these lenses, operating in Ray I mode, become practical at voltages above $V_r = 10^6$ volts and with the aid of superconducting windings. They appear therefore, to be primarily suitable for specialised electron microscopes of extremely high resolving power.

Turning to more conventional lenses, Figure 4.25 shows data published by Cleaver (1980b) and also by Riecke (1972). Cleaver's results are not directly experimental results but are based on finite element calculations of lens structures similar to those found in the present best conventional lenses. These results also included a number of asymmetrical lenses, A_1 and A_2, which can be

thought of as loosely related to the present single-polepiece lenses. In these lenses and also in the conventional lenses studied, difficulty was found in producing maximum peak axial field distributions appreciably greater than that of the saturation value 2.2T of the iron used [Permendur]. This is almost certainly due to the design of the coil. Notable field broadening effects took place as the excitation was increased. These results are in accordance with the analysis presented in the previous Chapters. As a result, the spherical aberration coefficient of these lenses is comparatively high. Finally the results of Riecke (1972) are shown for the condenser-objective lens. These results are in fact the spherical aberration coefficients that would be expected by extrapolating measured and calculated results to the point of complete iron saturation. As before, field broadening occurs at high excitation, leading to a more-than-expected fall-off in performance as the accelerating voltage is increased. Once again it seems likely that the cause of this inability to produce high axial field strengths and narrow half-width is likely to be the design of the exciting coil rather than the magnetisation characteristics of the iron.

It should be remembered, of course, that there are many practical reasons of convenience for the present design of exciting coils and that the changes that are needed in coil design could have many implications for the design of the lens as a whole.

In order to illustrate in more detail the production of high poleface flux densities, Figure 4.26 shows the poleface flux density B_{pf} as a function of lens excitation of the original lens SPHER-ORIG with which this investigation began, the improved lens RECT-E and finally the best lens investigated namely SPHER-C. All these

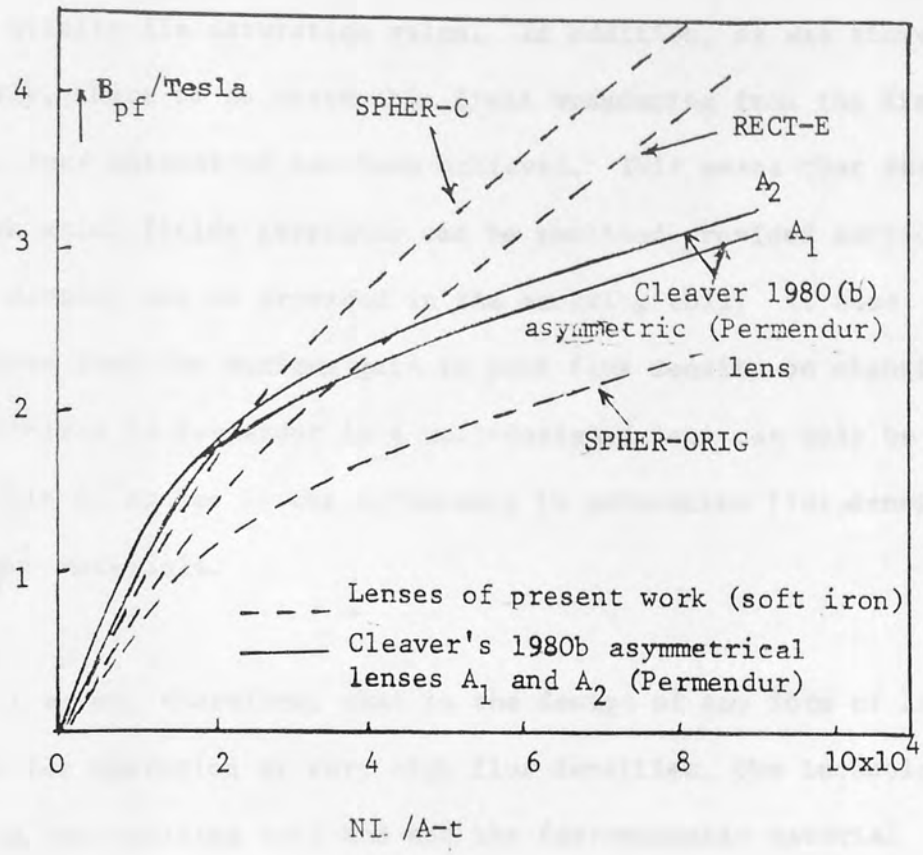

Fig 4.26 Variation of the poleface flux density (B_{pf}) of the optimum lenses (RECT-E, SPHER-C) compared with the lens (SPHER-ORIG) as a function of lens excitation. Note: Cleaver's (1980b) best asymmetric lenses have been added for comparison purposes.

lenses used soft iron (saturation flux density 1.8T). For comparison purposes Cleaver's asymmetrical lenses A_1 and A_2 are added. These lenses used Permendur (saturation flux density 2.2T). Cleaver's lenses exhibit saturation effects in the region of poleface flux densities of about 1.8T, i.e. well below the saturation flux density of Permendur. Similarly lens RECT-E begins to show saturation effects at about 1.2T, considerably below the saturation flux density of soft-iron (1.8T). However, lenses RECT-E and SPHER-C,

especially the latter, remain essentially linear up to flux densities of 2T and continue up indefinitely in flux density as the excitation is increased. The B_{pf}/NI curve changes slope of course, as the poletip attains its saturation value. In addition, as was shown previously, there is no measurable field broadening from the iron circuit, once saturation has been achieved. This means that very high peak axial fields strengths can be realised provided sufficient current density can be provided in the exciting coil. It also illustrates that the maximum gain in peak flux density on changing from soft-iron to Permendur in a well-designed lens can only be 0.4T. This of course is the difference in saturation flux density of the two materials.

It seems, therefore, that in the design of any form of lens intended for operation at very high flux densities, the technological design of the exciting coil and not the ferromagnetic material itself, is the dominant factor.

4.6.1 THEORETICAL LIMITS OF PERFORMANCE OF SINGLE-POLEPIECE LENSES

The previous discussion allows an estimate to be made of the ultimate limits of single-polepiece lenses. For example, a poleface flux density of 10T, which seems technologically possible at an accelerating voltage of 1 MV, of the Moses/Tretner limit, gives a spherical aberration coefficient C_s = 0.23 mm, at V_r = 1 MV. This corresponds to a resolution $\delta \simeq 0.1$ nm (1.0 Å).

The iron-free coil lens with $D_2/D_1 = 24$ calculated by Marai (1977) gave a C_s value of 0.3mm, at V_r = 1 MV, the resolution δ = 0.108 nm (1.08 Å).

Figure 4.25 also shows the C_s values of the single-polepiece lens SPHER-C, for which C_s = 0.37mm, δ = 0.114 nm (1.14 Å) at 10T and 1 MV. This should be compared with C_s = 2mm, δ = 0.174 nm (1.74 Å) for the best conventional double-polepiece lens of Riecke (1972) and C_s = 1.6 mm, δ = 0.165 nm (1.65 Å) for best asymmetrical conventional lens of Cleaver (1980b).

CHAPTER FIVE

5. SINGLE-POLEPIECE PROJECTOR LENSES

5.1 THE OPTICAL PROPERTIES OF SINGLE-POLEPIECE PROJECTOR LENSES

Although the projector lens properties of single-polepiece lenses are not the main concern of this thesis, some systematic calculations were in fact made of projector lens properties. These computed results were not subject to the inevitable experimental errors associated with the measurement of axial field distributions, especially in the presence of small lens bores. They are therefore reported here to provide a possible check on the accuracy of previous experimental determinations of projector lens properties.

The important parameters in a projector lens in an electron microscope are the projector focal length and the radial and spiral distortion coefficients. The computer program "PROJECTOR", described in Chapter Two, was used to calculate the electron optical properties of a projector lens.

The rectangular polepiece lens RECT-ORIG described in Chapter Three, (Fig 3.3) is a typical projector lens design of a type that has been studied experimentally. Its axial magnetic flux density distribution, calculated by Munro's program has already been shown (Fig 3.4). The axial magnetic flux density distribution was used in Marai's program (1977) to compute the radial and spiral distortion coefficients as a function of the excitation parameter $NI/V_r^{\frac{1}{2}}$, together with the corresponding projector focal length. The projector focal length and distortion coefficients of a single-polepiece

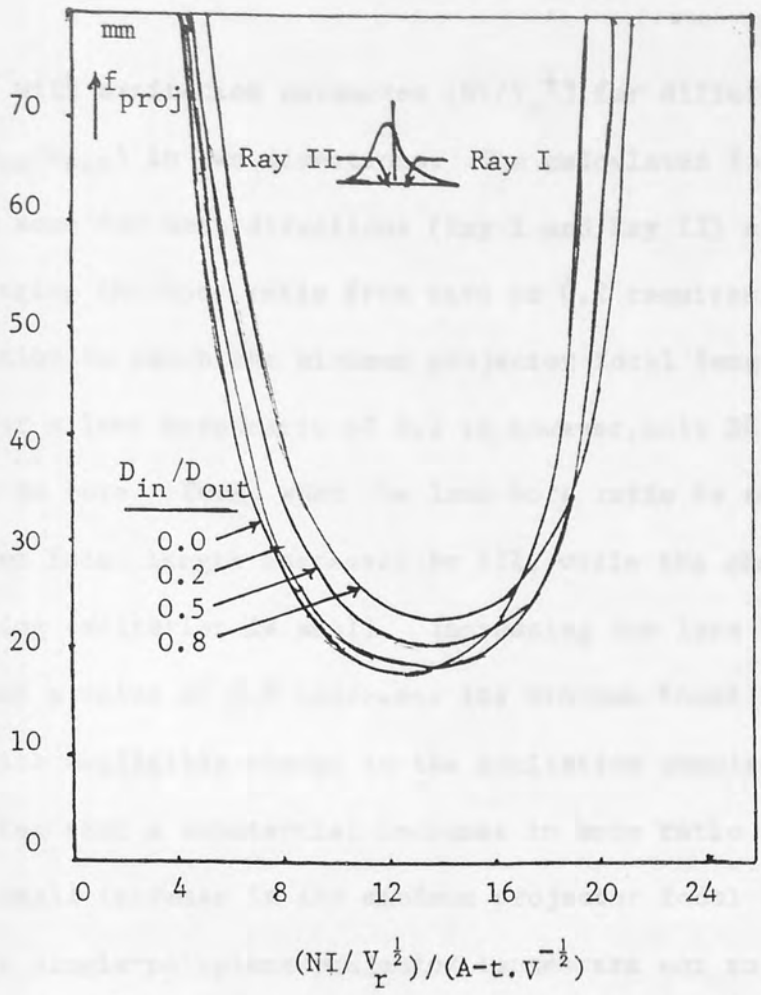

Fig 5.1 Variation of the projector focal length, f_{proj} (identical for Ray I and Ray II) with excitation paramter $NI/V_r^{\frac{1}{2}}$ for different bore ratios D_{in}/D_{out} of lens RECT-ORIG shown in Fig (3.3).

lens is a function of the bore ratio (D_{in}/D_{out}) of the polepiece. It should perhaps be mentioned that although the distortion coefficients are in general different for Ray I and Ray II, the focal length is the same.

5.1.1 FOCAL LENGTH OF THE RECTANGULAR POLEPIECE PROJECTOR LENS

The projector focal length of RECT-ORIG was calculated using the computer program "projector" for different bore diameters and for the two directions of beam entry (Ray I and Ray II) to the lens field. Figure 5.1, shows the variation of the projector focal

length (f_{proj}) with excitation parameter ($NI/V_r^{\frac{1}{2}}$) for different bore ratios (D_{in}/D_{out}) in two directions. The calculated focal length was the same for both directions (Ray I and Ray II) as expected. Changing the bore ratio from zero to 0.2 requires some 7% more excitation to reach the minimum projector focal length. This minimum for a lens bore ratio of 0.2 is, however, only 3% higher than that with no bore. Thus, when the lens bore ratio is equal to 0.5, the minimum focal length increases by 11%, while the change in the corresponding excitation is small. Increasing the lens bore ratio until it reaches a value of 0.8 increases its minimum focal length by about 12%, with negligible change in the excitation required. This demonstrates that a substantial increase in bore ratio causes only a small increase in the minimum projector focal length. This shows that single-polepiece projector lenses are not so sensitive to change in bore size. This fact can be exploited in the design of wide bore projector lenses.

5.2 DISTORTION COEFFICIENTS OF THE RECTANGULAR POLEPIECE PROJECTOR LENS (RECT-ORIG)

5.2.1 RADIAL DISTORTION COEFFICIENT

The variation in projector focal length with distance from the lens axis causes a variation in magnification of the image with distance from the axis, and the image is therefore distorted. Radial

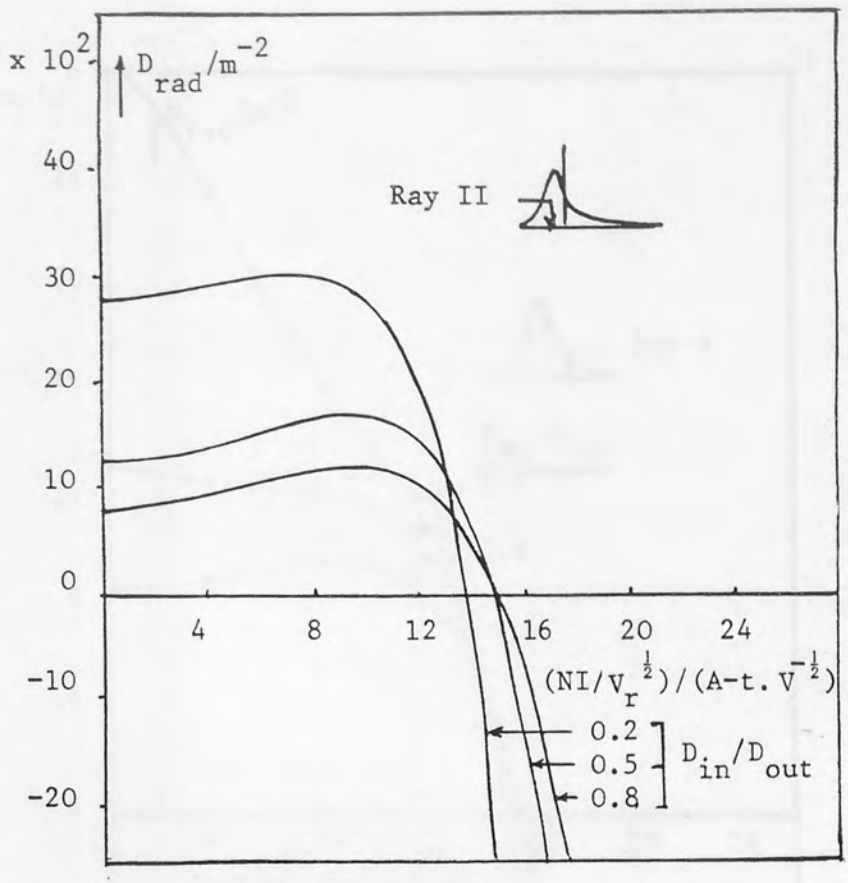

Fig 5.2 Radial distortion coefficient D_{rad} of a lens RECT-ORIG shown in Fig (3.3) for different bore ratios D_{in}/D_{out} as a function of excitation parameter $NI/V_r^{\frac{1}{2}}$ (for Ray II).

distortion changes the shape and the area of the image elements. The radial distortion coefficient depends on the lens geometry and its excitation.

The field distribution data of a lens RECT-ORIG was also used to compute its radial and spiral distortion coefficients. Figures 5.2 and 5.3 show the variation of the radial distortion coefficient, D_{rad}, with excitation parameter for the two opposite directions (Ray I and Ray II) beam orientation. For Ray II beam orientation, Figure 5.2, the D_{rad} curve of 0.8 bore ratio shows that $NI/V_r^{\frac{1}{2}}$ approaches zero, $D_{rad} = 8.3 \times 10^2$ m^{-2}, then goes to the maximum

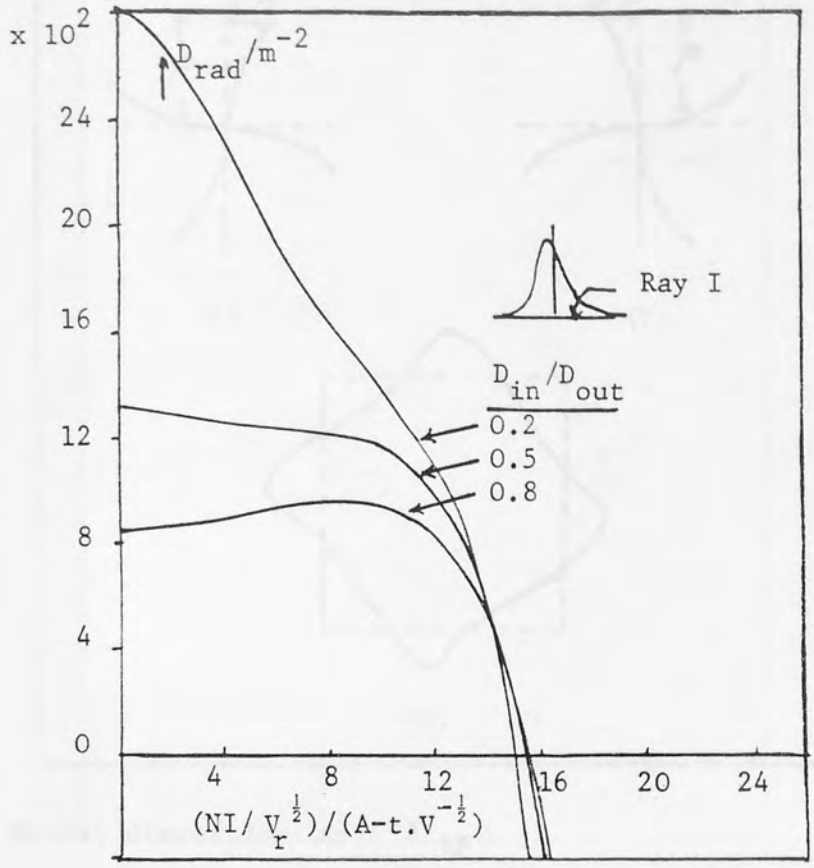

Fig 5.3 Radial distortion coefficient D_{rad} of a lens RECT-ORIG shown in Fig (3.3) for different bore ratios as a function of excitation parameter $NI/V_r^{\frac{1}{2}}$ (for Ray I).

value of 12 x 10^2 m^{-2} at excitation parameter $NI/V_r^{\frac{1}{2}}$ = 9; after this maximum D_{rad} decreases steeply to zero at $NI/V_r^{\frac{1}{2}}$ = 15, whereupon it changes sign. In Figure 5.3 which shows D_{rad} in Ray I orientation, the curve of D_{in}/D_{out} = 0.8 shows that as $NI/V_r^{\frac{1}{2}}$ approaches zero, D_{rad} = 8.3 x 10^2 m^{-2} and goes to the maximum value of 9.4 x 10^2 m^{-2} at $NI/V_r^{\frac{1}{2}}$ = 9.0; after this maximum D_{rad} decreases steeply to zero at $NI/V_r^{\frac{1}{2}}$ = 15.5 whereupon it changes sign. When the bore ratio is equal to 0.5, D_{rad} = 13 x 10^2 m^{-2} as the excitation parameter $NI/V_r^{\frac{1}{2}}$ approaches zero. From both Figures 5.2 and 5.3, the radial distortion of the lens in Ray I is much lower than those with Ray II beam orientation.

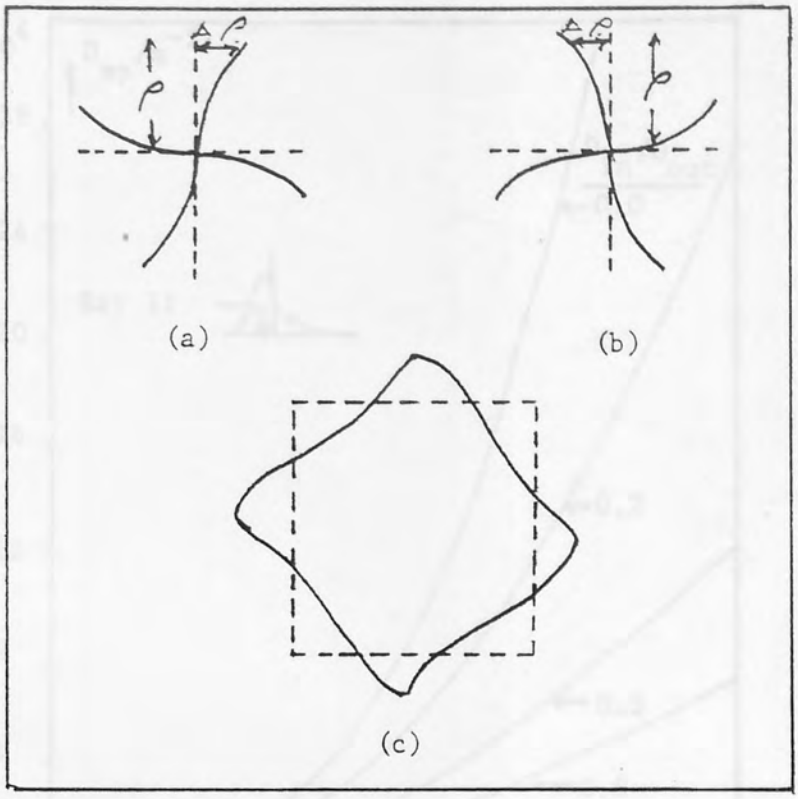

Fig 5.4 Spiral distortion $(\Delta\rho/\rho)_{sp}$.

5.2.2 SPIRAL DISTORTION COEFFICIENT

The anisotropic distortion is often called rotational distortion or spiral distortion. In this case, the angle of rotation is no longer independent of the radial distance of the image point from the axis. It increases by a small amount f_{or} an off-axis ray, giving rise to the spiral distortion. When the current through the lens is reversed, the direction of the field B and the sense of the circulation of the electron is changed. As a consequence, the image of Figure 5.4a changes into the image of Figure 5.4b, the latter being the mirror image (a) by reflection in the axis. The spiral distortion coefficient depends on the lens geometry and the excitation; $\Delta\rho$ represents the lateral displacement in the image

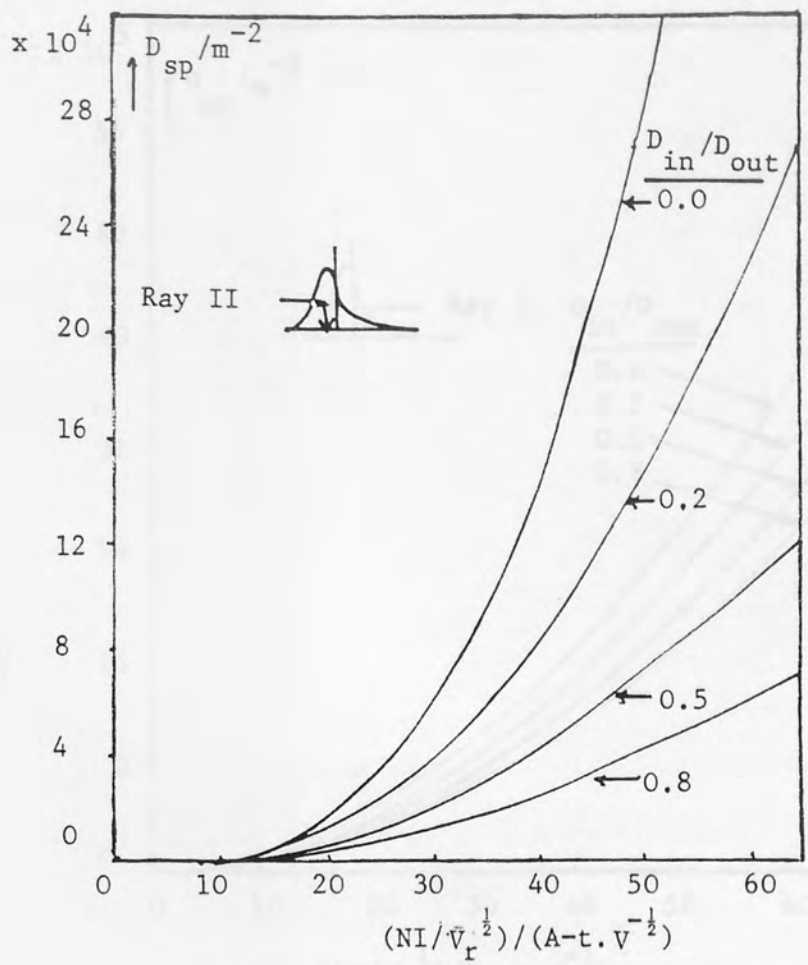

Fig 5.5 Spiral distortion coefficient D_{sp} of a lens RECT-ORIG shown in Fig (3.3) for different bore ratios D_{in}/D_{out} as a function of excitation parameter $NI/V_r^{\frac{1}{2}}$ (for Ray II).

plane. Spiral distortion will be more pronounced than the radial distortion if the lenses are operated near their minimum focal length; however, for decreasing excitation spiral distortion will decrease rapidly compared with radial distortion. Radial distortion changes the shape and the area of an image element, whereas spiral distortion changes its shape only, leaving its area unchanged as shown in Figure 5.4c.

Figures 5.5 and 5.6 show the variation of spiral distortion coefficient D_{sp} as a function of the excitation parameter for Ray

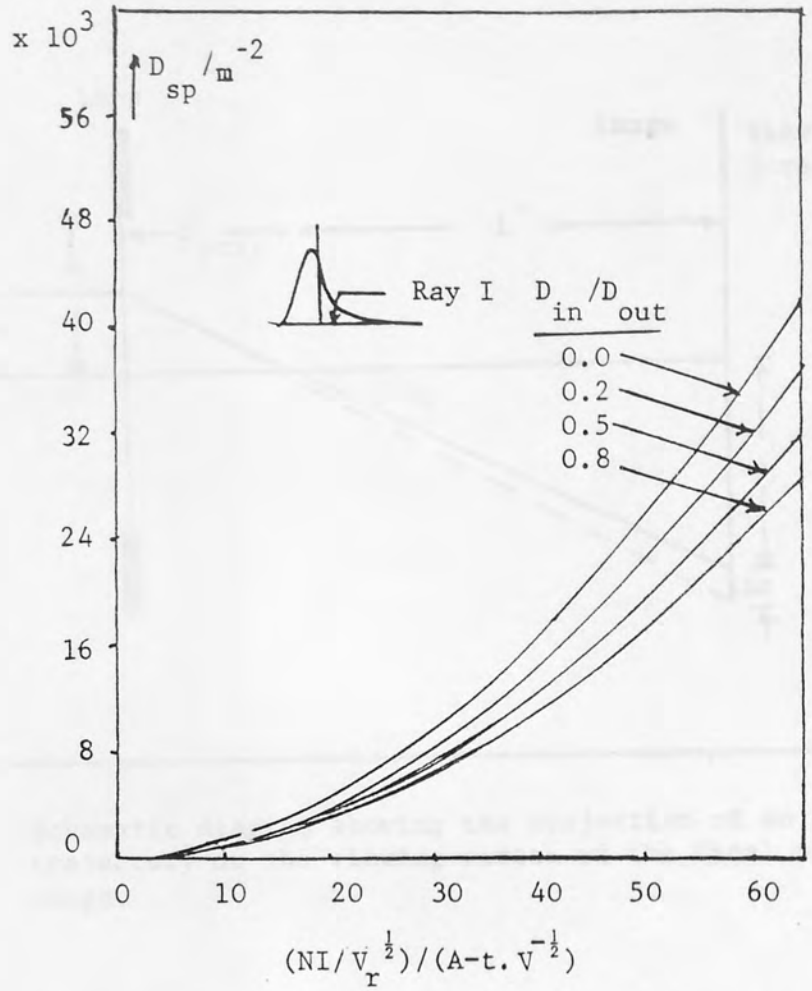

Fig 5.6 Spiral distortion coefficient D_{sp} of a lens RECT-ORIG shown in Fig (3.3) for different bore ratios D_{in}/D_{out} as a function of excitation parameter $NI/V_r^{\frac{1}{2}}$ (for Ray I).

I and Ray II orientation respectively, with different bore ratios (D_{in}/D_{out}). For Ray II, Figure 5.5 shows that for $D_{in}/D_{out} = 0.8$ the spiral distortion coefficient D_{sp} approaches zero, at the excitation parameter $NI/V_r^{\frac{1}{2}} = 10$. When $NI/V_r^{\frac{1}{2}}$ increases, D_{sp} increases gradually, at $NI/V_r^{\frac{1}{2}} = 60$, $D_{sp} = 6 \times 10^4$ m^{-2}. In the case of Ray I, Figure 5.6 shows that for $D_{in}/D_{out} = 0.8$ and at $NI/V_r^{\frac{1}{2}} = 60$; $D_{sp} = 2.5 \times 10^4$ m^{-2}. The distortion of the lens in Ray I operation is smaller than that of Ray II beam orientation by a factor of about two.

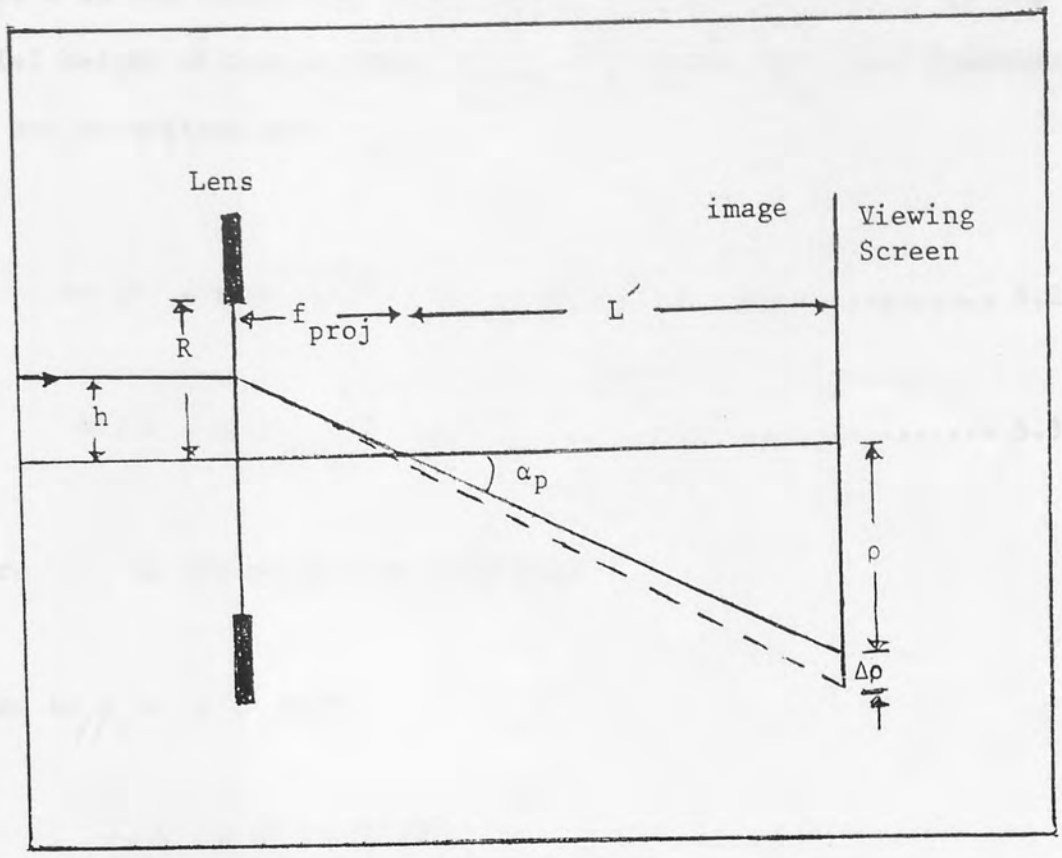

Fig 5.7 Schematic diagram showing the projection of an electron trajectory on the viewing screen of the final projector stage.

5.3 QUALITY FACTORS OF THE RECTANGULAR POLEPIECE PROJECTOR LENS (RECT-ORIG)

The quality of the lens image formed by a projector lens depends not only on the distortion coefficient D, but also the projector focal length f_{proj}. Consider the arrangement shown in Figure 5.7. An incoming ray of height h is magnified by an amount L'/f_{proj} where f_{proj} is the projector focal length and L' is the projection distance. A relevant dimensionless factor Q was found from the relation:

$$\Delta\rho / \rho = D.h^2 \quad \ldots\ldots\ldots\ldots\ldots\ldots\ldots\ldots\ldots\ldots\ldots\ldots\ldots\ldots\ldots\ldots\ldots\ldots\ldots\ldots \quad 5.1$$

where D is the distortion coefficient (radial or spiral); ρ is the radial height of the Ganssian ray in the image. The above Equation 5.1 may be written as:

$$\Delta\rho / \rho = D (\rho / L')^2 \quad (f_{proj})^2 \quad \ldots\ldots\ldots\ldots\ldots\ldots\ldots\ldots \quad 5.2$$

or $$\Delta\rho / \rho = D (f_{proj})^2 \quad \tan^2 \alpha_p \quad \ldots\ldots\ldots\ldots\ldots\ldots\ldots\ldots \quad 5.3$$

where α_p is the projection semi-angle

given by $\alpha_p = \rho / L'$ with

$$\Delta\rho / \rho = Q^2 \ (\rho / L')^2$$

$$Q^2 = D (f_{proj})^2 \quad \ldots\ldots\ldots\ldots\ldots\ldots\ldots\ldots\ldots\ldots \quad 5.4$$

The quality factor Q has been used to compare different projector lenses (Marai and Mulvey, 1977). This factor is used for both spiral and radial distortion corresponding to that of D. A low Q value therefore indicates a projector lens of good quality. Q is close to unity for a double-pole piece lens (Marai, 1977).

The value of the spiral distortion parameter (Q_{sp}) for a single-polepiece lens with different bore ratios (D_{in}/D_{out}) is shown in Figures 5.8 and 5.9 as a function of lens excitation parameter ($NI/V_r^{\frac{1}{2}}$) in both directions (Ray I and Ray II) of beam orientation.

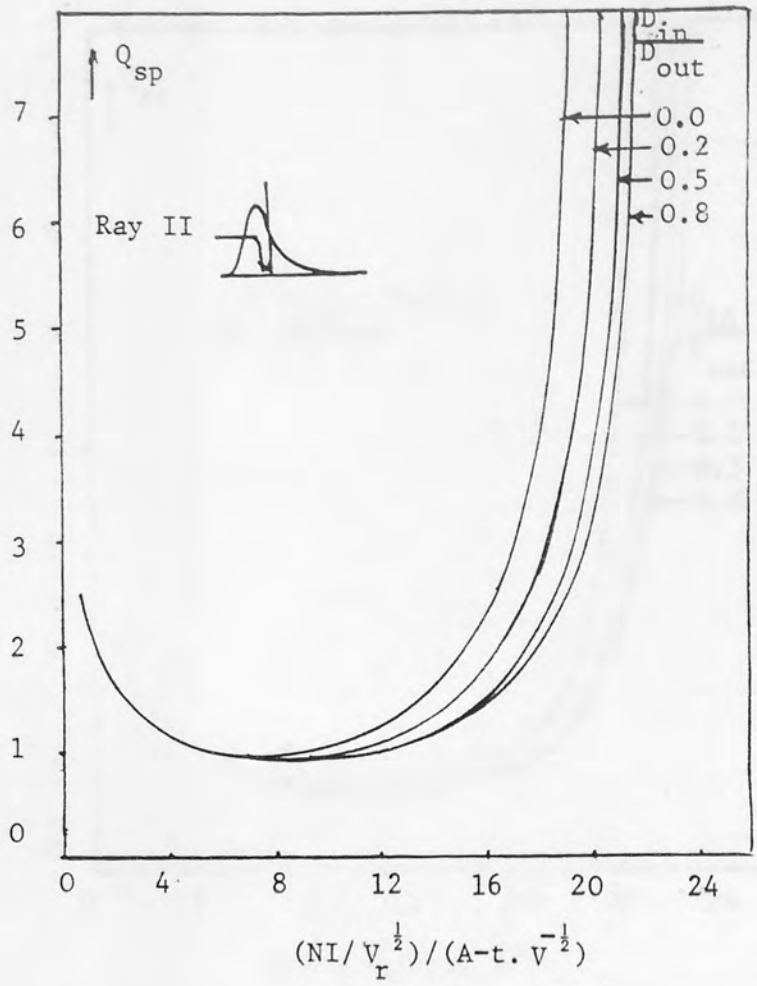

Fig 5.8 Variation of image quality factor Q_{sp} (spiral) of a lens RECT-ORIG shown in Fig (3.3), with excitation parameter $(NI/V_r^{\frac{1}{2}})$ for different bore ratios D_{in}/D_{out} (for Ray II).

From Figure 5.8, it is clear for Ray II beam orientation there is very little difference in the Q_{sp} values over this wide range of bore ratio (D_{in}/D_{out}). Higher (D_{in}/D_{out}) values lead to a slightly lower Q_{sp} value, but from a practical point of view all the lenses have a minimum Q_{sp} value of about unity in the normal range of excitation parameter $NI/V_r^{\frac{1}{2}}$ (6 to 12). At low excitations Q_{sp} is independent of bore ratio. The curve of this behaviour is typical of conventional twin polepiece lenses. Figure 5.9 shows , however, an appreciably lower Q_{sp} value for Ray I beam orientation.

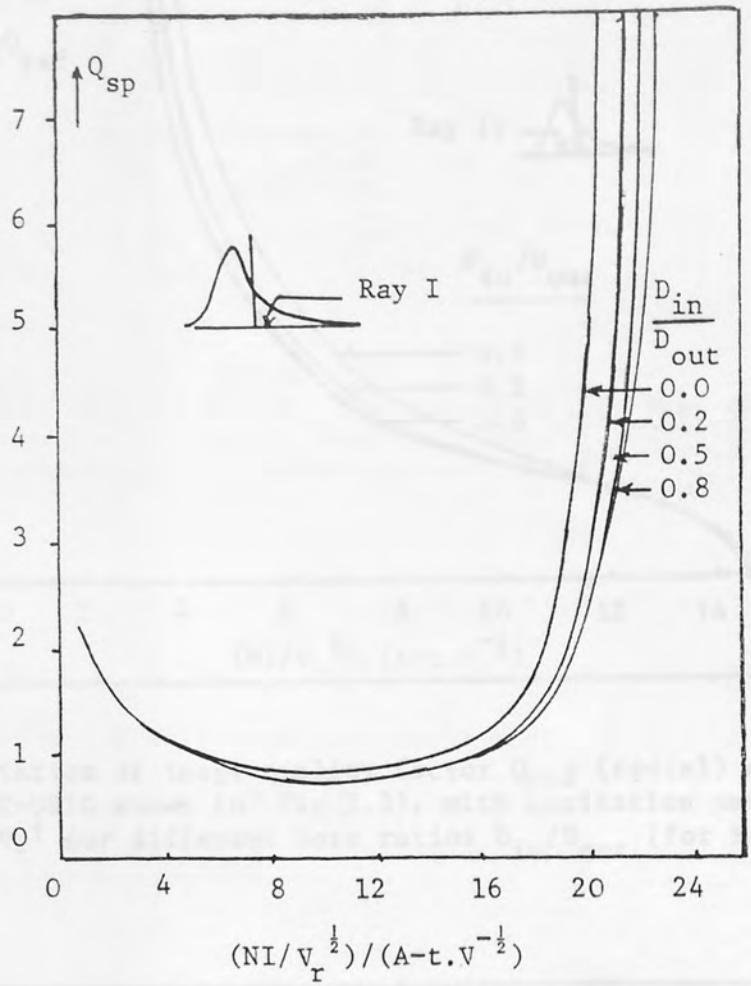

Fig 5.9 Variation of image quality factor Q_{sp} (spiral) of a lens RECT-ORIG shown in Fig (3.3), for different bore ratios D_{in}/D_{out} with excitation parameter $NI/V_r^{\frac{1}{2}}$ (for Ray I).

The minimum value of Q_{sp} is about 0.75, and also it is nearly constant over a range of excitation parameter $NI/V_r^{\frac{1}{2}}$ (8 to 13). From the above figures it can be seen that Ray I is the preferred direction for a low distortion projector lens.

Figures 5.10 and 5.11 show the variation of the radial distortion parameter Q_{rad} as a function of excitation parameter $NI/V_r^{\frac{1}{2}}$, with different bore ratios D_{in}/D_{out}, for the two directions of entry electron beam. It can be seen that Q_{rad} decreases steeply

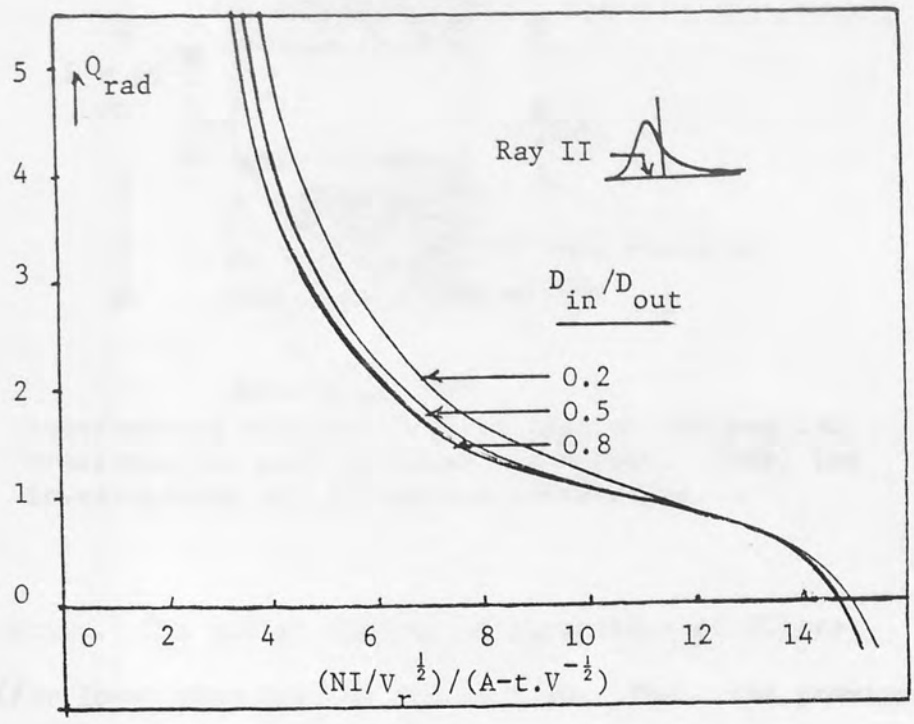

Fig 5.10 Variation of image quality factor Q_{rad} (radial) of a lens RECT-ORIG shown in Fig (3.3), with excitation parameter $NI/V_r^{\frac{1}{2}}$ for different bore ratios D_{in}/D_{out} (for Ray II).

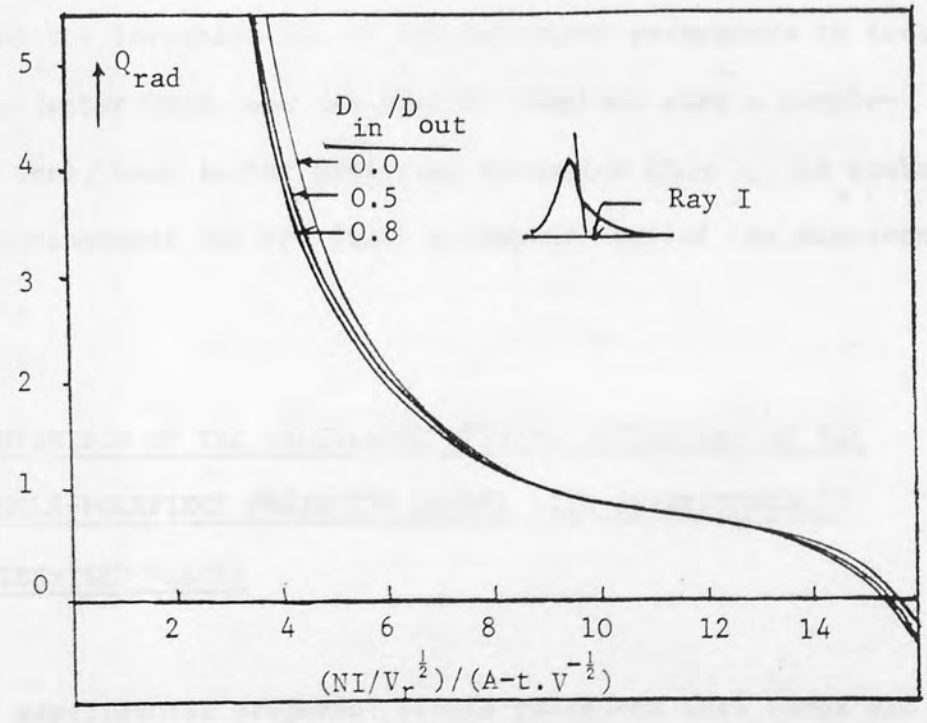

Fig 5.11 Variation of image quality factor Q_{rad} (radial) of a lens RECT-ORIG shown in Fig (3.3), with excitation parameter $NI/V_r^{\frac{1}{2}}$ for different bore ratios D_{in}/D_{out} (for Ray I).

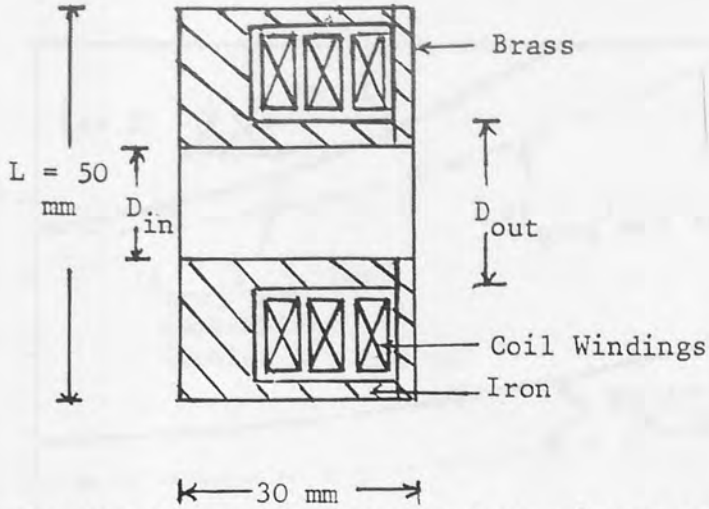

Fig 5.12 Experimental single-polepiece lens of rectangular cross-section used by (Juma and Mulvey, 1980b) for investigating the distortion coefficient.

with excitation. The radial distortion parameters of Figure 5.11 are also lower than that of Figure 5.10. Thus, the previous curves show that the most favourable arrangement for low distortion is for the polepiece tip to face the incoming parallel electron beam (Marai and Mulvey, 1975).

From the investigation of the important parameters in designing the projector lens, one can readily conclude that a single-polepiece lens, used in the preferred direction (Ray I), is probably the best arrangement for the final projector lens of the electron microscope.

5.4 COMPARISON OF THE CALCULATED OPTICAL PROPERTIES OF THE SINGLE-POLEPIECE PROJECTOR LENSES WITH EXPERIMENTALLY DETERMINED VALUES

An experimental projector single-polepiece lens (Juma and Mulvey, 1980b) of simple geometrical rectangular polepiece shape, shown in Figure 5.12, was constructed, in which the outside

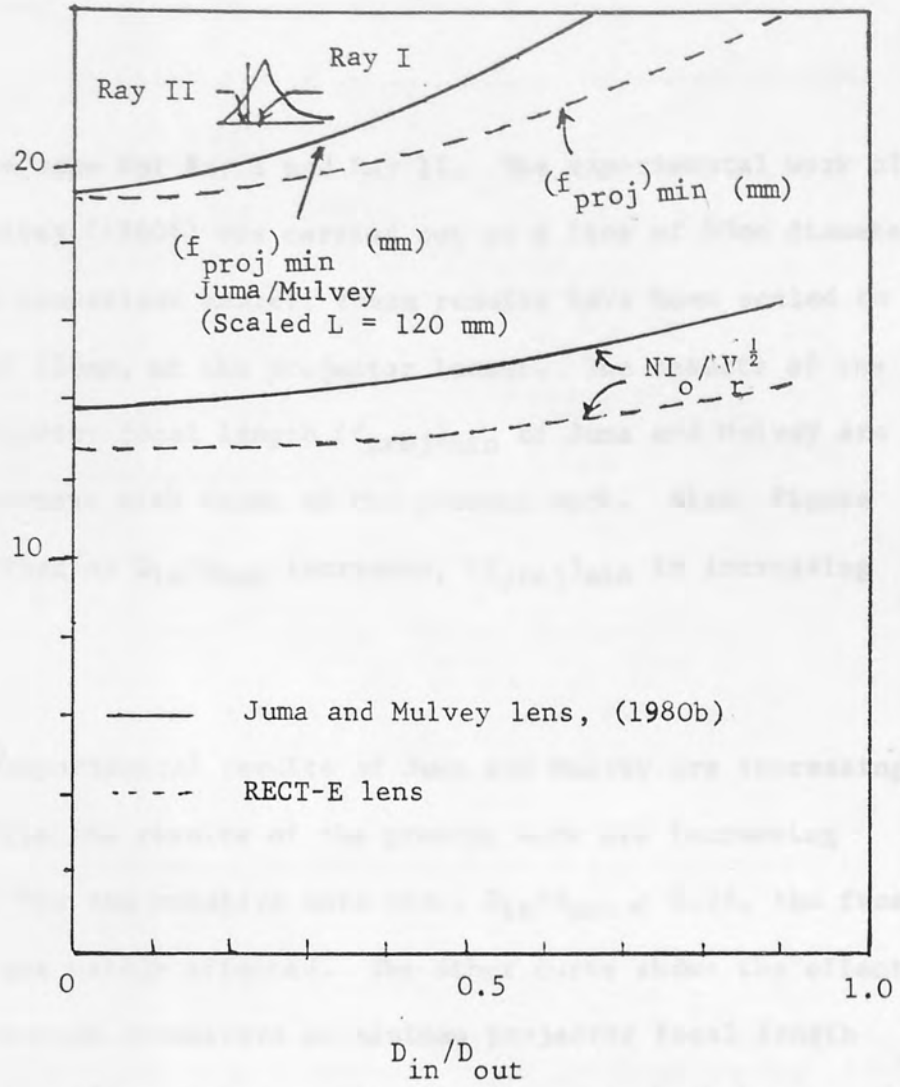

Fig 5.13 Variation of minimum projector focal length $(f_{proj})_{min}$, and the associated excitation parameter $NI_o/V_r^{\frac{1}{2}}$ with bore ratio D_{in}/D_{out} (Juma and Mulvey), shown in Fig 5.12 was added for comparison purposes. (Ray I and Ray II).

diameter D_{out} of the polepiece was fixed at 20mm, but the inner diameter D_{in} was varied. The outer diameter L is equal to 50mm. The lens was excited by coil windings of (NI = 1755 A-t) rectangular cross-section.

Figure 5.13, shows the effect of the relative lens bore D_{in}/D_{out} on the minimum projector focal length $(f_{proj})_{min}$,

which is the same for Ray I and Ray II. The experimental work of Juma and Mulvey (1980b) was carried out on a lens of 50mm diameter. To make the comparison easier, these results have been scaled to a lens size of 120mm, of the projector lenses. The results of the minimum projector focal length $(f_{proj})_{min}$ of Juma and Mulvey are in fair agreement with those of the present work. Also, Figure 5.13 shows that as D_{in}/D_{out} increases, $(f_{proj})_{min}$ is increasing also.

The experimental results of Juma and Mulvey are increasing sharply, while the results of the present work are increasing gradually. For the relative bore size, $D_{in}/D_{out} < 0.25$, the focal properties are hardly affected. The other curve shows the effect of the excitation parameters at minimum projector focal length $NI_o/V_r^{\frac{1}{2}}$, with different bore ratios D_{in}/D_{out}, in both beam orientation also have only one curve line. The work of Juma and Mulvey (1980b) is plotted. The results of $NI_o/V_r^{\frac{1}{2}}$ of the present work are lower than those reported by Juma and Mulvey. With increasing D_{in}/D_{out}, the value of $NI_o/V_r^{\frac{1}{2}}$ of the present work will increase slightly, while, $NI_o/V_r^{\frac{1}{2}}$ of Juma and Mulvey lenses is increasing gradually. The result of the present author encourages one to suggest that a single-polepiece projector lens can have a comparatively large bore without undue sacrifice of magnification or increases in excitation.

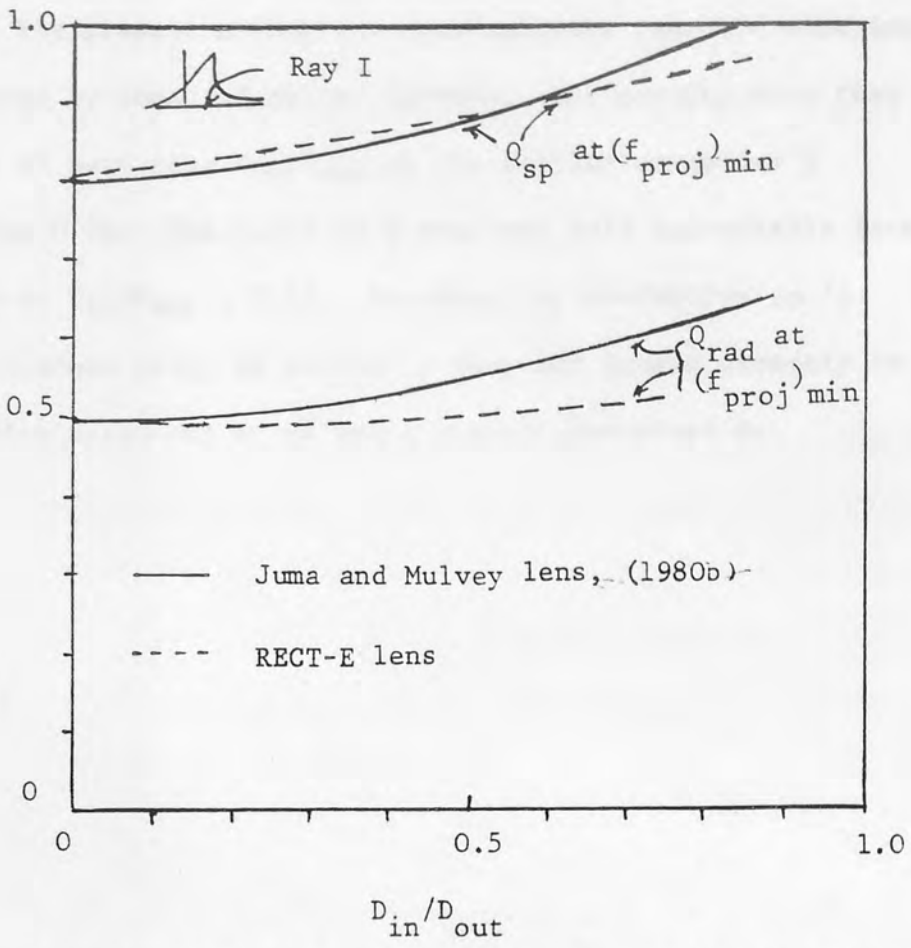

Fig 5.14 Variation of image quality factor Q_{sp} (spiral) and Q_{rad} (radial), with bore ratio D_{in}/D_{out} shown in Fig 5.12 (for Ray I). (Juma and Mulvey) lens added for comparison purposes.

The calculations of the image quality factor (Q_{rad} and Q_{sp}) with different bore ratios D_{in}/D_{out} for the preferable direction are shown in Figure 5.14. The experimental results of Juma and Mulvey (1980b) are added for comparison purposes. The image quality factor (Q_{sp}) of the present work increases slightly as D_{in}/D_{out} is increased until it reaches the value of one, while Q_{sp} of Juma and Mulvey's results is increased gradually with increasing the ratio D_{in}/D_{out}. With a value of $D_{in}/D_{out} < 0.4$, both results are in strong agreement with each other, Q_{rad} of the present work increases slightly, while Q_{rad} of Juma and Mulvey's results is increased gradually

with increasing the ratio of D_{in}/D_{out}. The theoretical results of the present author are more accurate than the experimental ones reported by Juma and Mulvey (1980b). The results show that the effect of bore size D_{in}/D_{out} on the quality parameter Q is less than 0.25. The value of Q does not vary appreciably from that value at $D_{in}/D_{out} < 0.25$. However, the distortion $\Delta\rho/\rho$ in the microscope image of radius ρ does not depend directly on these coefficients, but on an image quality parameter Q.

CHAPTER SIX

6. APPLICATION OF SINGLE-POLEPIECE MAGNETIC ELECTRON LENSES

6.1 ELECTRON FIELD EMISSION SOURCES

Field emission electron guns have an electron optical brightness some ten thousand times higher than that of a thermionic emission electron gun. However, field emission guns are at present limited to the production of fine electron probes (smaller than 100 nm) because of aberrations in the accelerating system. For a recent review of the subject and relevant further references see Venables and Fathers (1982).

A way proposed by Venables to improve the performance of field emission electron guns is to place a single pole-piece lens as close to the field emitting cathode as possible. Two possible designs FE1 and FE2 were suggested as shown in Figures 6.1 and 6.2 respectively. In order to obtain a preliminary estimate of the suitability of these lenses, a study was made of their focal properties and aberrations, for an electron beam of constant energy. In practice the electrons leave the field emitter at energies of a fraction of an electron volt and would be accelerated to the final potential while they are under the influence of the magentic field. Nevertheless it was felt that for a preliminary analysis the assumption of a constant electron energy would still yield useful results.

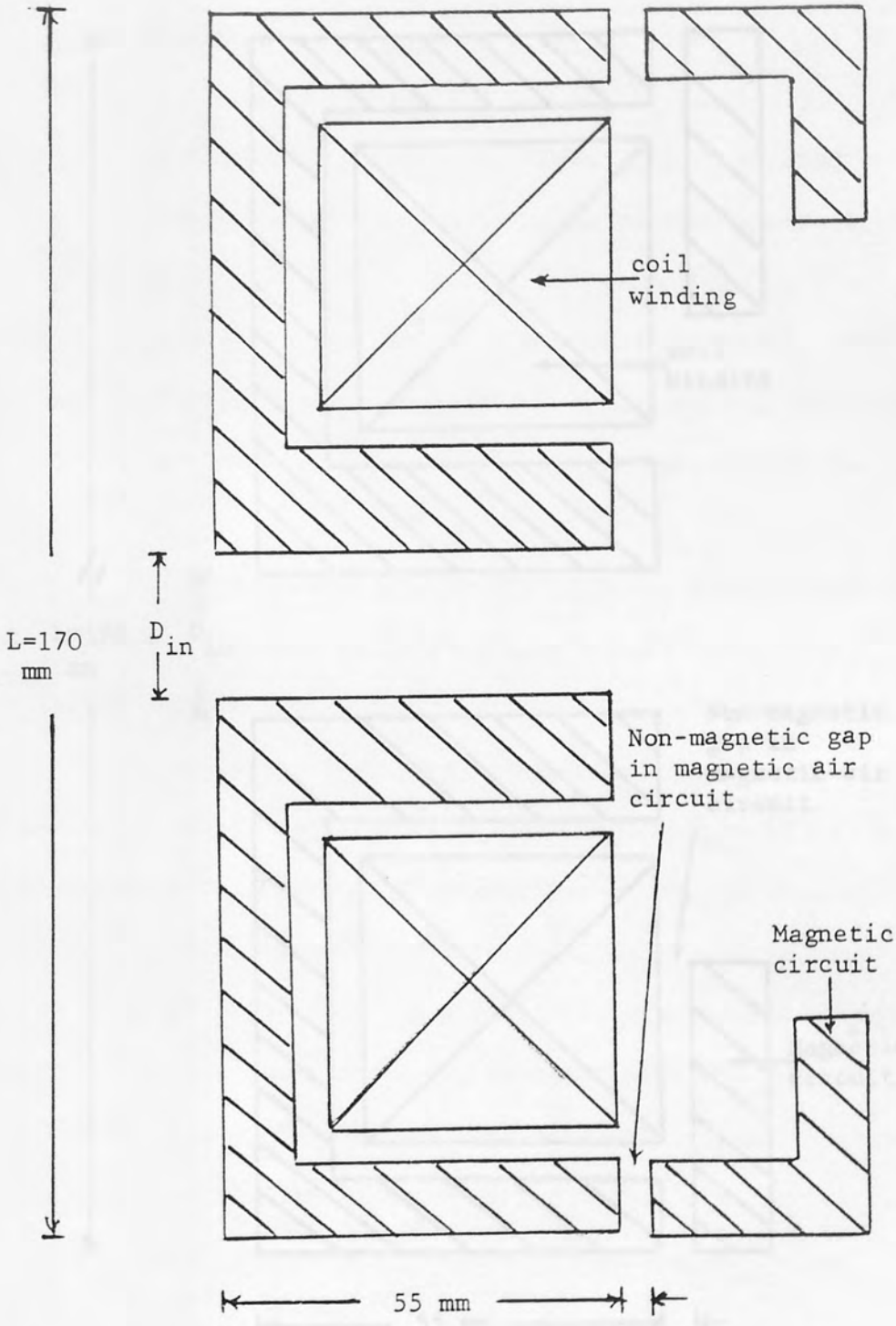

Fig 6.1 Schematic cross-section diagram of a field emission lens (FE1) of 20mm bore diameter for the investigation of focal properties and aberration coefficients. Note The non-magnetic gap is provided for constructional reasons. (L = 170 mm).

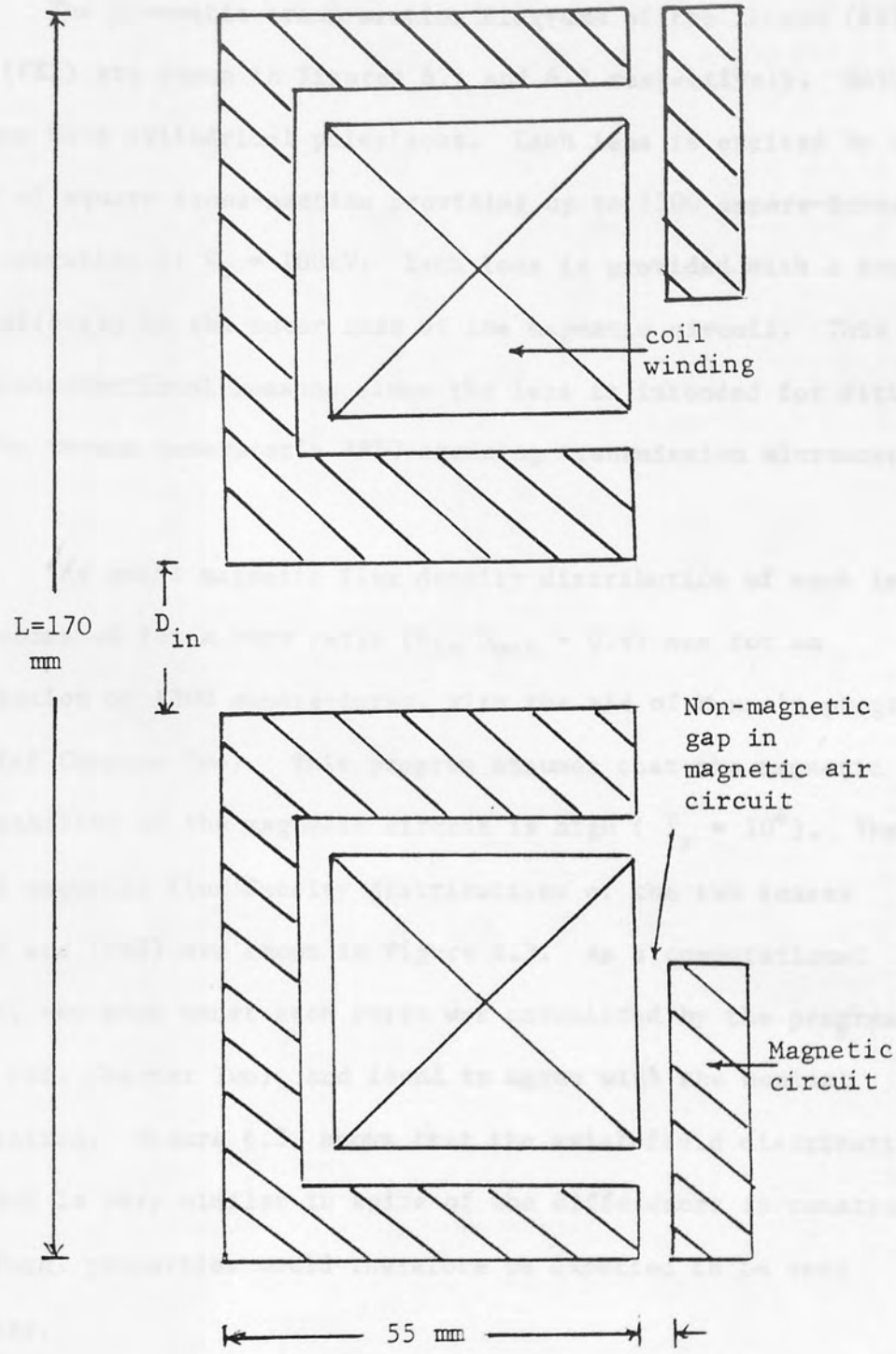

Fig 6.2 Schematic Cross-section diagram of a field emission lens (FE2) of 20mm bore diameter for the investigation of focal properties and aberration coefficients. Note The non-magnetic gap is provided for constructional reasons. (L = 170 mm).

6.2 AXIAL MAGNETIC FLUX DENSITY OF THE FIELD EMISSION LENSES

The schematic cross-section diagrams of the lenses (FE1) and (FE2) are shown in Figures 6.1 and 6.2 respectively. Both lenses have cylindrical polepieces. Each lens is excited by a coil of square cross-section providing up to 1300 ampere-turns for operation at V_r = 100kV. Each lens is provided with a non-magnetic gap in the outer case of the magnetic circuit. This is for constructional reasons since the lens is intended for fitting in the vacuum generator's HB50 scanning transmission microscope.

The axial magnetic flux density distribution of each lens was computed for a bore ratio (D_{in}/D_{out} = 0.4) and for an excitation of 1300 ampere-turns, with the aid of Munro's program M12 (cf Chapter Two). This program assumes that the magnetic permeability of the magnetic circuit is high ($\mu_r = 10^4$). The axial magnetic flux density distributions of the two lenses (FE1) and (FE2) are shown in Figure 6.3. As a computational check, the area under each curve was calculated by the program AREA (cf. Chapter Two), and found to agree with the nominal excitation. Figure 6.3, shows that the axial field distribution of each is very similar in spite of the differences in construction. The focal properties would therefore be expected to be very similar.

The field distribution curves shown in Figure 6.3 were used to calculate the electron optical properties (as objective and projector lenses) by means of the programs M21 and PROJECTOR

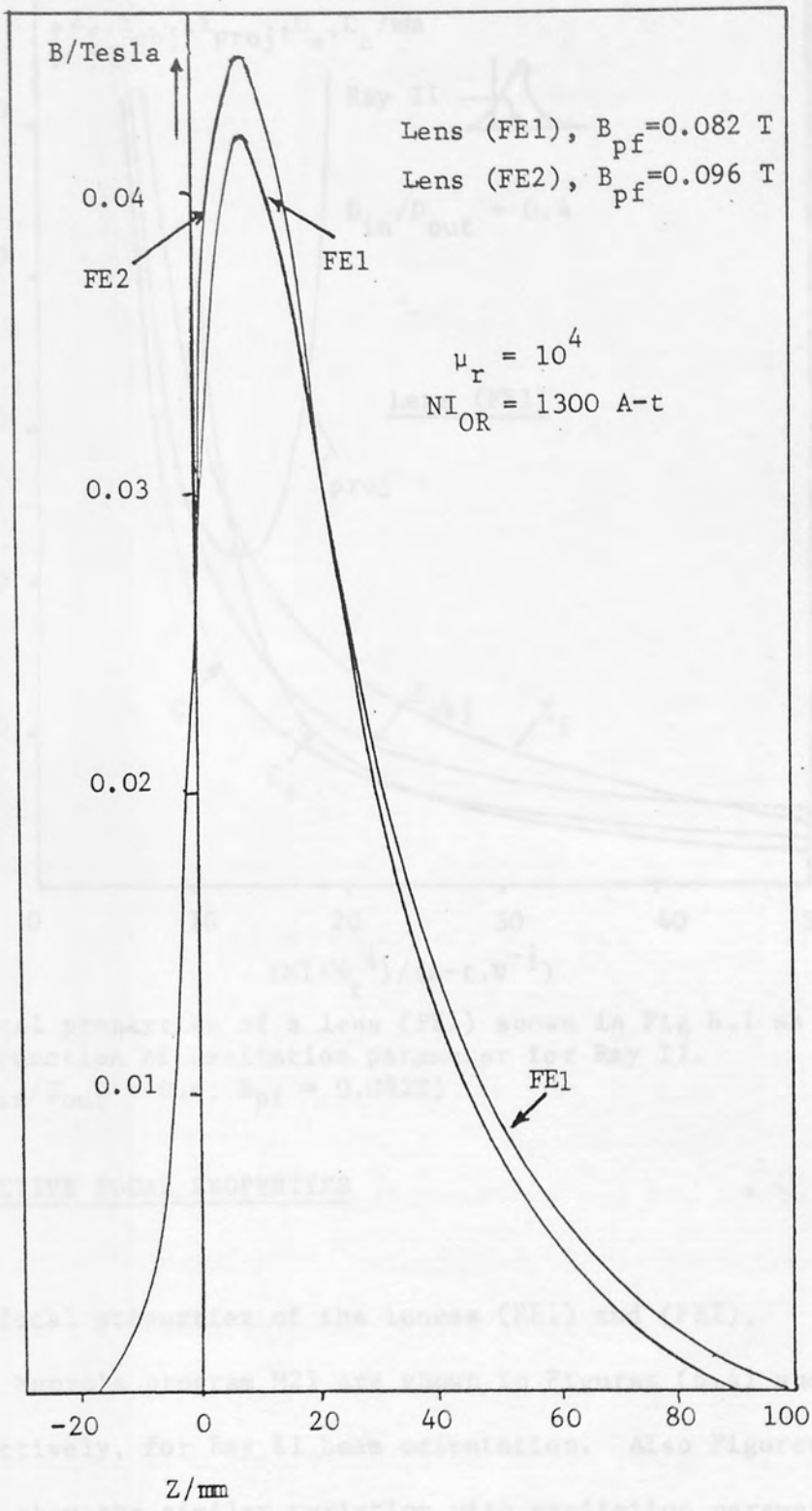

Fig 6.3 The axial magnetic flux density of field emission lenses (FE1) and (FE2) with bore ratio D_{in}/D_{out} = 0.4 (L = 170 mm).

referred to in Chapter Two, for both Ray I and Ray II beam orientation.

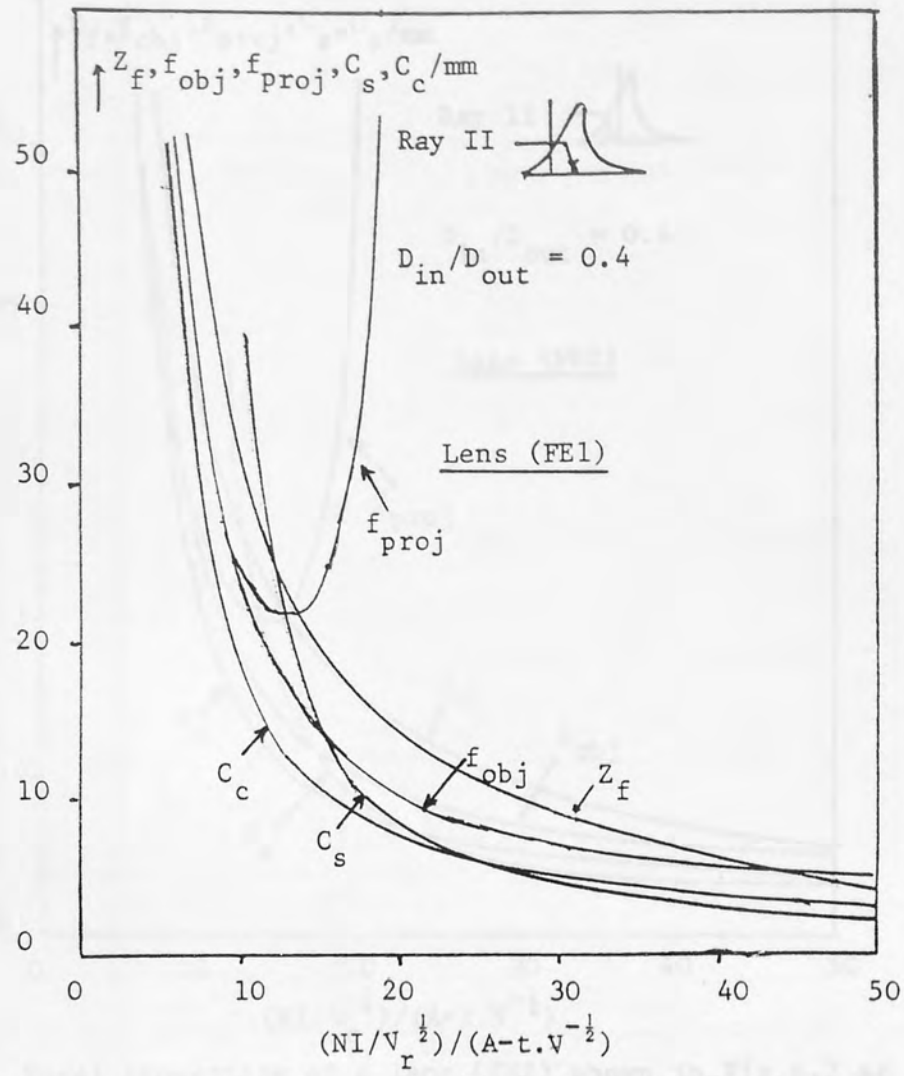

Fig 6.4 Focal properties of a lens (FE1) shown in Fig 6.1 as a function of excitation parameter for Ray II. (D_{in}/D_{out} = 0.4; B_{pf} = 0.082T)

6.2.1 OBJECTIVE FOCAL PROPERTIES

The focal properties of the lenses (FE1) and (FE2), computed by Munro's program M21 are shown in Figures (6.4) and (6.5) respectively, for Ray II beam orientation. Also Figures 6.6 and 6.7 show the similar variation with excitation parameter for Ray I beam orientation. From the previous figures it is clear that Ray II lenses of a given poleface flux density will tend to be large, have large excitations and low aberration, while Ray I lenses will tend to be small, have comparatively low excitations and have low spherical aberration.

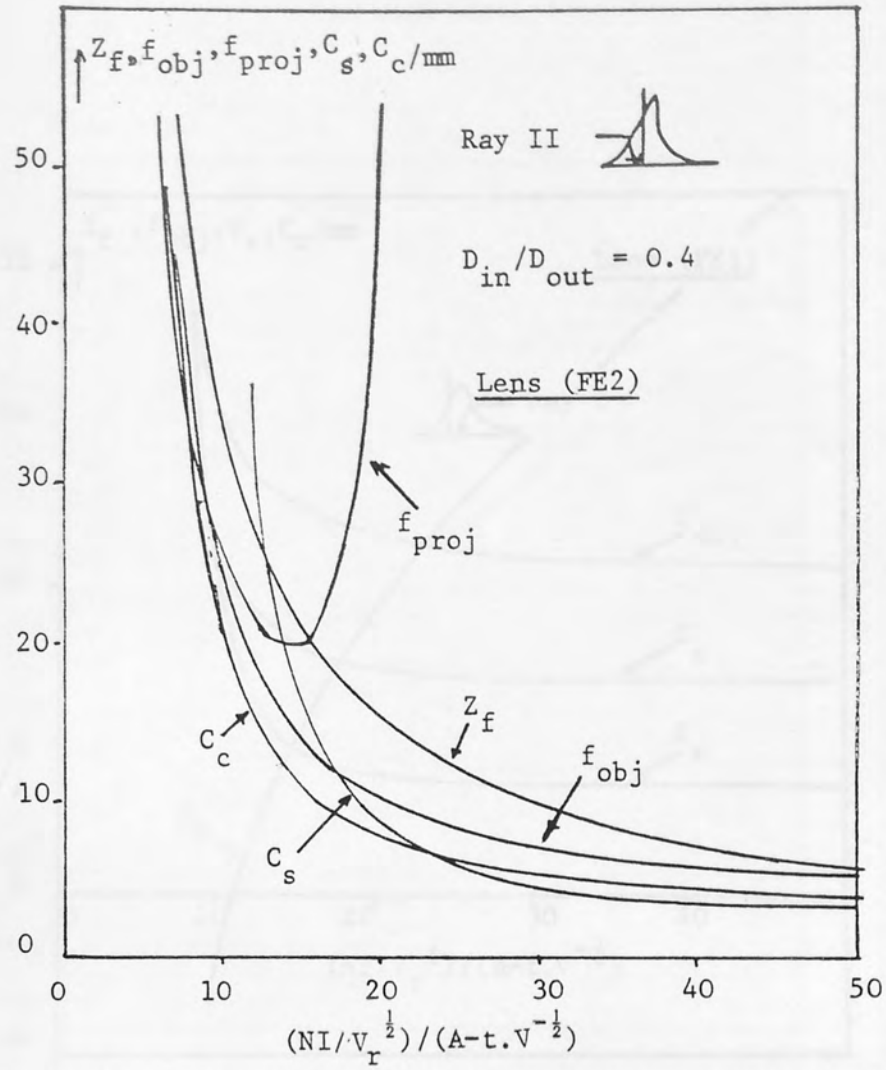

Fig 6.5 Focal properties of a lens (FE2) shown in Fig 6.2 as a function of excitation parameter for Ray II. (D_{in}/D_{out} = 0.4; B_{pf} = 0.096T).

In order to compare the performance of the two lenses, it seems reasonable to compare the performance of the above lenses at a standard poleface flux density of 2 Tesla.

In order to give the results a universal character, the electron optical properties in these curves are expressed in the form of [focal properties $(10^5/V_r)^{\frac{1}{2}}$] with a corresponding excitation parameter $NI/V_r^{\frac{1}{2}}$.

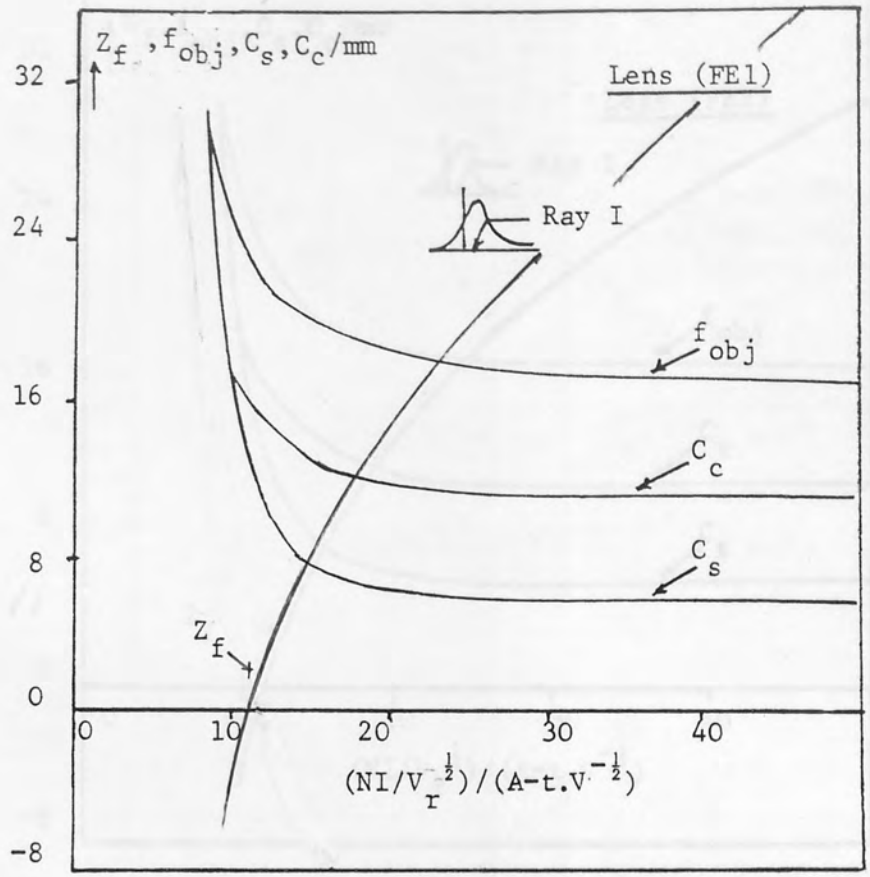

Fig 6.6 Focal properties of a lens (FE1) shown in Fig 6.1 as a function of excitation parameter for Ray I. (D_{in}/D_{out} = 0.4; B_{pf} = 0.082T).

Figure 6.8 shows the scaled focal properties and aberration coefficients of objective lenses (FE1) and (FE2) with excitation parameter $NI/V_r^{\frac{1}{2}}$, for (a) Ray II and (b) Ray I. The curves of Figure 6.8a shows that in Ray II all the focal properties and aberration coefficients of lens (FE1) are only slightly lower than those of lens (FE2). The minimum value of spherical aberration coefficient $C_s*(10^5/V_r)^{\frac{1}{2}}$ of lens (FE1) is 1.3 mm and it is independent of the excitation parameter in the range higher than ($NI/V_r^{\frac{1}{2}}$ = 35). The minimum values of $f_{obj}*(10^5/V_r)^{\frac{1}{2}}$ and

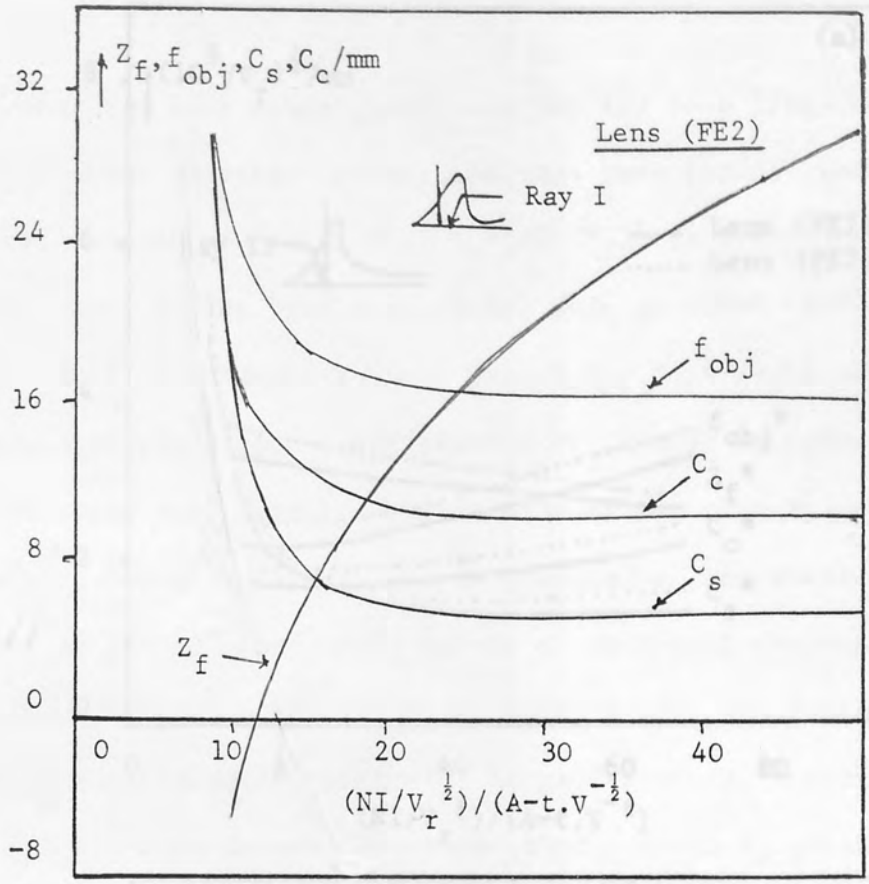

Fig 6.7 Focal properties of a lens (FE2) shown in Fig 6.2 as a function of excitation parameter for Ray I. (D_{in}/D_{out} = 0.4; B_{pf} = 0.096T).

$C_c*(10^5/V_r)^{\frac{1}{2}}$ occur at $NI/V_r^{\frac{1}{2}}$ = 15 and are equal to 2.2 mm and 1.7 mm respectively.

For Ray I beam orientation, Figure 6.8b shows a similar variation with excitation parameter for both lenses (FE1) and (FE2); in addition, the values of the focal properties and aberration coefficients of a lens (FE1) are slightly lower than those of a lens (FE2), for a given flux density, in this case 2 Tesla. At excitation parameter ($NI/V_r^{\frac{1}{2}}$ = 13), the objective focal distance of a lens (FE1) is $Z_f*(10^5/V_r)^{\frac{1}{2}}$ = 0.0, and the minimum values of the chief electron optical properties are given as

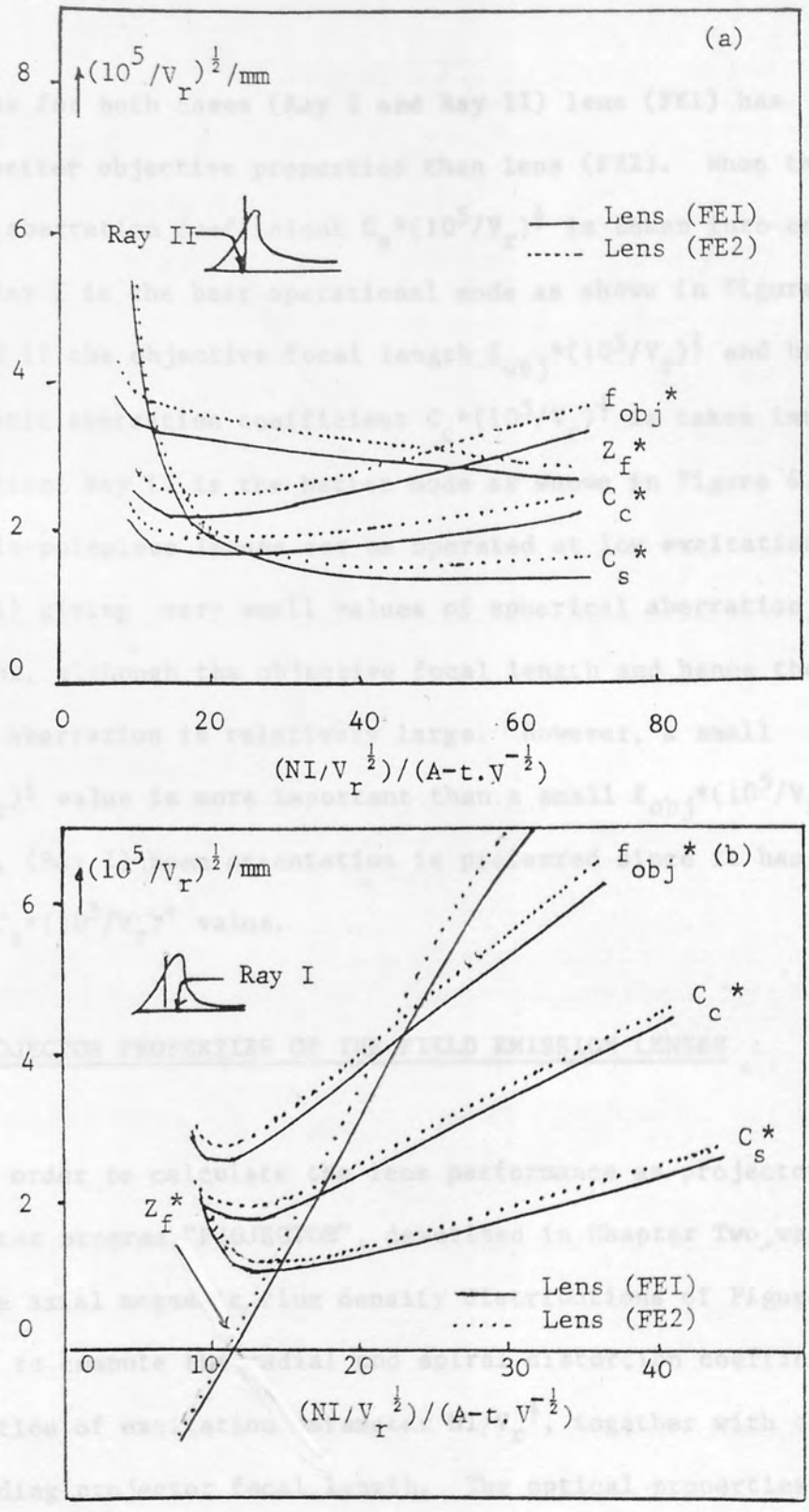

Fig 6.8 Variation of normalised focal properties of the lenses (FE1) and (FE2) as a function of excitation parameter $NI/V_r^{\frac{1}{2}}$, (a) Ray II, (b) Ray I. (B_{pf} = 2T; D_{in}/D_{out} = 0.4).

follows $C_s*(10^5/V_r)^{\frac{1}{2}}$ = 1.0mm, $C_c*(10^5/V_r)^{\frac{1}{2}}$ = 1.75mm, and $f_{obj}*(10^5/V_r)^{\frac{1}{2}}$ = 2.5mm respectively.

Thus for both cases (Ray I and Ray II) lens (FE1) has slightly better objective properties than lens (FE2). When the spherical aberration coefficient $C_s*(10^5/V_r)^{\frac{1}{2}}$ is taken into consideration, Ray I is the best operational mode as shown in Figure 6.8b. And if the objective focal length $f_{obj}*(10^5/V_r)^{\frac{1}{2}}$ and hence the chromatic aberration coefficient $C_c*(10^5/V_r)^{\frac{1}{2}}$ is taken into consideration, Ray II is the better mode as shown in Figure 6.8a. Thus single-polepiece lenses can be operated at low excitations (for Ray I) giving very small values of spherical aberration coefficient, although the objective focal length and hence the chromatic aberration is relatively large. However, a small $C_s*(10^5/V_r)^{\frac{1}{2}}$ value is more important than a small $f_{obj}*(10^5/V_r)^{\frac{1}{2}}$. Therefore, (Ray I) beam orientation is preferred since it has the smallest $C_s*(10^5/V_r)^{\frac{1}{2}}$ value.

6.2.2 PROJECTOR PROPERTIES OF THE FIELD EMISSION LENSES

In order to calculate the lens performance as projectors, the computer program "PROJECTOR", described in Chapter Two, was used. The axial magnetic flux density distributions of Figure 6.3 were used to compute the radial and spiral distortion coefficients as a function of excitation parameter $NI/V_r^{\frac{1}{2}}$, together with the corresponding projector focal length. The optical properties of the lenses were calculated in Ray I and Ray II beam operation. Figure 6.9 shows the variation of the projector focal length (f_{proj}) of lens (FE1) and (FE2) with excitation parameter $NI/V_r^{\frac{1}{2}}$ for

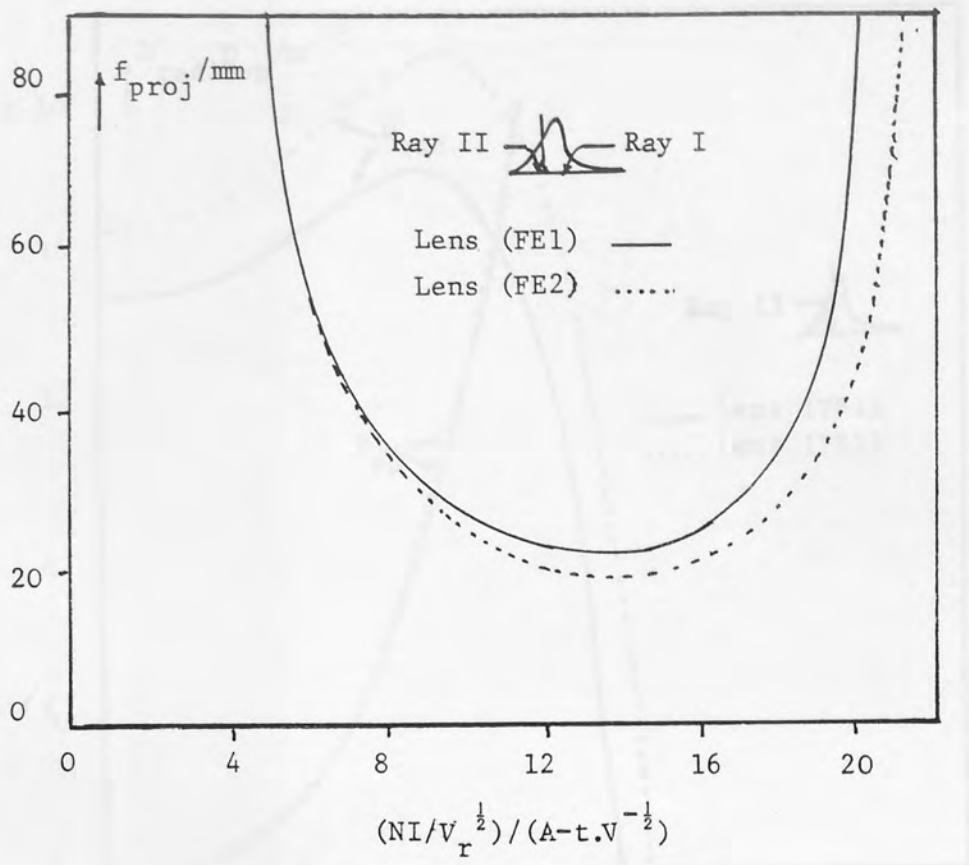

Fig 6.9 Variation of the projector focal length f_{proj} for the lenses (FE1) and (FE2) with excitation parameter $NI/V_r^{\frac{1}{2}}$ for Ray I and Ray II (D_{in}/D_{out} = 0.4).

Ray I and Ray II beam orientation. The projector focal length of field emission lens (FE2) is slightly lower than that of lens (FE1). For lens (FE2) $(f_{proj})_{min}$ = 20mm at $NI/V_r^{\frac{1}{2}}$ = 14, while for lens (FE1) the value of $(f_{proj})_{min}$ = 22mm at $NI/V_r^{\frac{1}{2}}$ = 13. The projector focal length is of course identical in Ray I and Ray II, for a given excitation.

Figure 6.10 shows the variation of the spiral distortion coefficient, D_{sp}, and the radial distortion coefficient D_{rad} for lenses (FE1) and (FE2) in Ray II as a function of excitation parameter. For lens (FE1), D_{rad} = 15 x 10^2 m^{-2} for $NI/V_r^{\frac{1}{2}}$ = 0

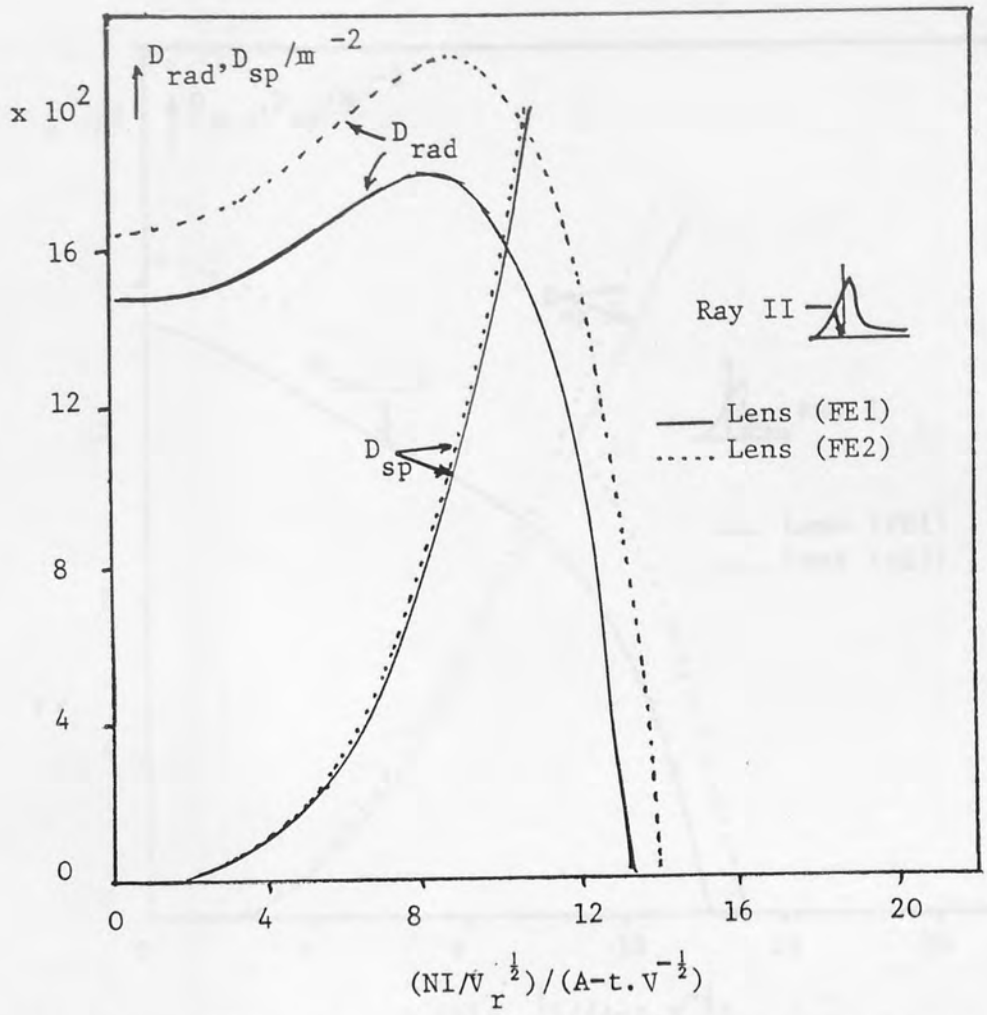

Fig 6.10 Variation of the spiral distortion coefficient D_{sp} and radial distortion coefficient D_{rad} for the lenses (FE1) and (FE2) with excitation parameter $NI/V_r^{\frac{1}{2}}$ for Ray II. (D_{in}/D_{out} = 0.4)

and at D_{rad} = 0, $NI/V_r^{\frac{1}{2}}$ = 13 while for lens (FE2), D_{rad} = 16.7 x 10^2 m^{-2} for zero excitation parameter and at D_{rad} = 0, $NI/V_r^{\frac{1}{2}}$ = 14. The corresponding distortion coefficients D_{rad} and D_{sp} of lens (FE1) are slightly lower than that of lens (FE2). Thus the curves show that lens (FE1) is slightly better than lens (FE2). Figure 6.11 shows the variation of the spiral distortion coefficient (D_{sp}) and radial distortion coefficient (D_{rad}) of lenses (FE1) and (FE2) with excitation parameter for Ray I beam orientation. The corresponding distortion coefficient D_{rad} and D_{sp} of lens (FE1) is slightly lower than that of a lens

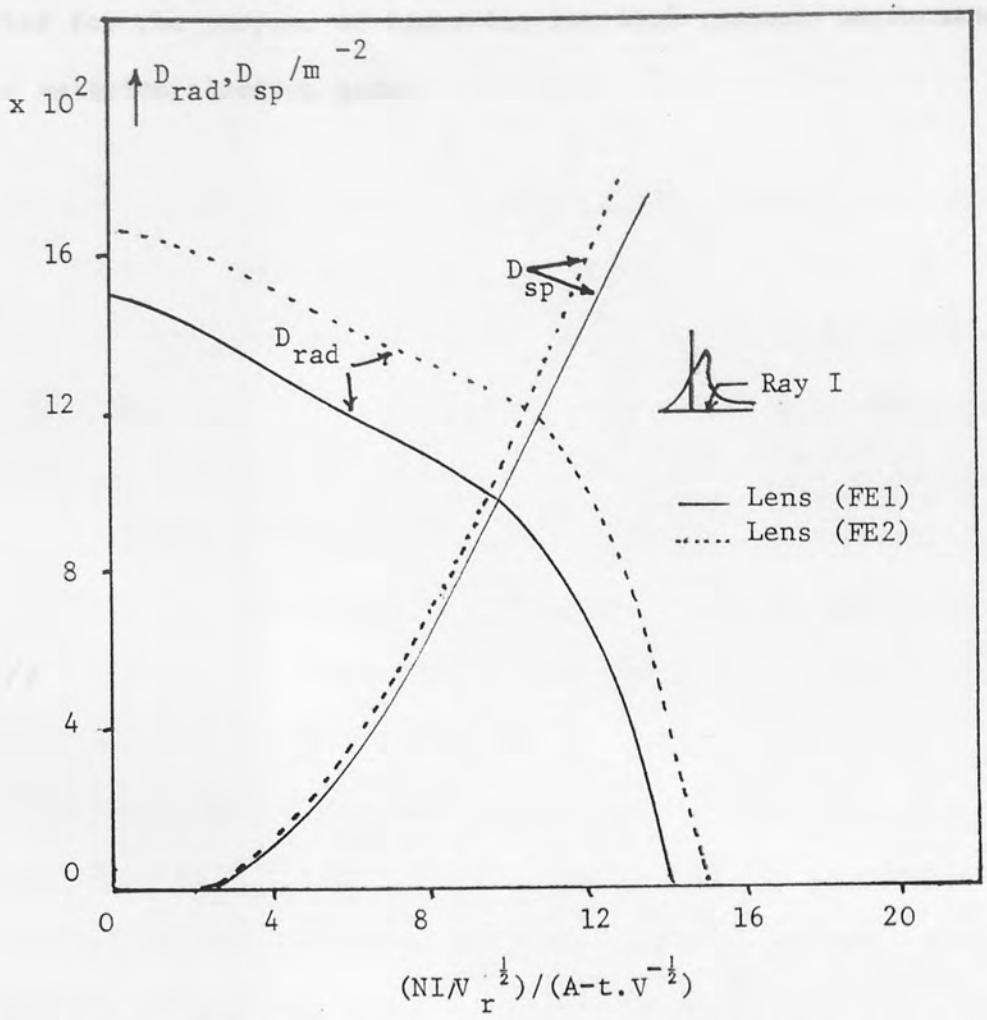

Fig 6.11 Variation of the spiral distortion coefficient D_{sp} and radial distortion coefficient D_{rad} for the lenses (FE1) and (FE2) with excitation parameter $NI/V_r^{\frac{1}{2}}$ for Ray I. (D_{in}/D_{out} = 0.4)

(FE2). From the above Figures 6.10 and 6.11 the most favourable arrangement for low distortion is for Ray I beam orientation. Hence single-polepiece projector lenses (FE1) and (FE2) should ideally be operated for Ray I beam orientation in order to obtain the advantage of their electron optical properties.

These results show that as far as the electron optical properties are concerned, there is little to choose between lens FE1 and FE2. However lens FE1 is slightly superior.

Both lenses appear to have favourable electron-optical properties for the purpose of improving the high current performance of field emission electron guns.

CHAPTER SEVEN

GENERAL CONCLUSIONS

We recall that the purpose of the present investigation was to try to throw new light on the physical factors that limit the performance of single-polepiece lenses in a wide range of electron optical instruments. In this investigation, current technological and engineering limits were not initially imposed on the calculations, as this might have inhibited the breadth of the investigation. However, the final results have been displayed in a way that makes clear the technological limitations in any practical design.

The chief, and perhaps most surprising, conclusion of the investigation is that the saturation properties of the iron and the detailed shape of the iron circuit are not dominant factors. Wide variations of these parameters are possible in practice. For example, when operating a single-polepiece lens at a flux density of 10T, it makes very little difference whether the iron circuit is made from soft iron or Permendur.

The crucial factor that has been revealed by this investigation is the shape and position of the exciting coil. Since the ideal coil shape is that of a narrow flat helix of large outer to inner diameter, the main problem resides in the high current density that is required in the winding. Paradoxically, the problem is more serious at low, rather than high accelerating voltages. The reason for this is that the lens size for a given poleface flux density decreases as the square root of the accelerating voltage.

It has been shown that in a single-polepiece lens the optimum lens size is very different depending on the direction of entry of the electron beam. For example, at a given accelerating voltage, for Ray I the lenses will be small, whereas for Ray II the lenses will be large. Since the optimum electron properties do not differ appreciably for such lenses, it is clearly a matter of operational convenience which design should be used.

In the present investigation, attention has been concentrated on the Ray I mode, since this has slightly superior properties, although it is technologically more difficult to realise, and probably requires the use of superconducting windings in practice. For very high voltage electron microscopes of high resolution these lenses could be attractive. Saturated lenses operating in Ray II mode are however to be preferred for conventional electron microscopes, since their size is smaller than that of conventional lenses but not inconveniently so.

More work is required in the practical design of these lenses, since in this mode the imaging properties are influenced by the detailed shape and permeability of the iron circuit. The position and shape of the coil is nevertheless also important in Ray II mode. However, because the optimum coil will be bigger, the current density will be much lower and hence conventional lens windings will probably be adequate.

It would appear that previous authors have totally neglected the importance of the coil position in single-polepiece lenses. This must also be of importance in the design of saturated conventional lenses.

This would perhaps explain the widespread belief that field broadening is inevitable under saturation conditions. That this is not so is clearly shown by lens SPHER-C in which field broadening does not occur under saturation conditions.

In conclusion then, it appears possible to design single-polepiece objective lenses operating at 10T, at an accelerating voltage V_r = 1000kV, with a resolution factor close to 0.1 nm (1 Å).

REFERENCES

Al-Shwaikh, A. A. (1979), Ph.D. Thesis, The University of Aston in Birmingham.

Al-Shwaikh, A. A. and Mulvey, T. (1977), Development in Electron Microscopy and Analysis, Ed. D. L. Misell, Institute of Physics London Conference Series, No: 36, Chapter 1. pp. 25-28.

Bassett, R. and Mulvey, T. (1969), Zeitschrift fur angewandte Physik, 27, pp. 142-145.

Boersch, H. Bostanjoglo, O. and Niedrig, H. (1964), Z. Phys., 180, pp. 407.

Busch, H. (1926), Ann. Phys. 81, pp. 974.

Christofides, S. (1982), Ph.D. Thesis, The University of Aston in Birmingham.

Christofides, S. and Mulvey, T. (1980), Electron Microscopy, eds. Brederoo, P. and Boom, G. (7th European Congress on Electron Microscopy Foundation, Leiden), Vol. 1, pp. 70-71.

Cleaver, J. R. A. (1977), Optik, 48, pp. 98-99.

Cleaver, J. R. A. (1978), Optik, 49, pp. 413-431.

Cleaver, J. R. A. (1980a), Inst. Phys. Conf. Series No. 52, Chapter 1. pp. 55-57.

Cleaver, J. R. A. (1980b), Optik, 57, pp. 9-34.

Cosslett, V. E. (1946), Introduction to electron optics, Oxford University Press.

Crewe, A. V. Wall, J. (1970), Journal of Molecular Biology 48, pp. 375.

Dietrich, I. (1976), Superconducting Electron Optics Devices, Plenum Press, New York.

Durandeau, P. and Fert, C. (1957), Rev. Opt. Theor. Instrum. 36, pp. 205-234.

Elkamali, H. H. (1981), Ph.D. Thesis, The University of Aston in Birmingham.

Fert, C. and Durandeau, P. (1967), Focusing of Charged Particles, Vol. 1, Ed. A. Septier, Academic Press.

Glaser, W. (1941), Z. Physik 117, pp. 285.

Glaser, W. (1952), Grundlagen der Elektronen Optik Springer, pp. 306-307.

Juma, S. M. (1975), Ph.D. Thesis, The University of Aston in Birmingham.

Juma, S. M. and Faisal, A. D. (1981), J. Phys. E: Sci, Instrum, Vol. 14, pp. 1389-1393.

Juma, S. M. and Mulvey, T. (1974), 8th International Congress on Electron Microscopy, Canberra, Vol. 1, pp. 134-135.

Juma, S. M. and Mulvey, T. (1975), "A new experimental electron microscope with a rotation-free projector system" in "Developments in electron microscopy and analysis", (Venables, ed.), Academic Press, pp. 45-48.

Juma, S. and Mulvey, T. (1980a), "The axial field distribution of single-polepiece lenses", Inst. Phys. Conf. Series No. 52, Chapter 1, 1980, pp. 59-60.

Juma, S. M. and Mulvey, T. (1980b), Electron Microscopy, eds. Brederoo, P. and Boom, G. (7th European Congress on Electron Microscopy Foundation, Leiden, 1980), Vol. 1, 1980, pp. 78-79.

Kamminga, W. (1976), Optik, 45, pp. 39-54.

Kamminga, W., Verster, J. L., and Francken, J. C. (1968/9), Optik, 28, pp. 442-451.

Kelvin (Thomson, W.) (1872), in "Reprints of papers on electricity and Magnetism", 2nd Ed. (London, Macmillan, 1884), pp. 489-491.

Laberrigue, A., and Levinson, L., (1964), C. R. Acad. Sci. 259, pp. 530.

Liebmann, G. (1951), Proc. Phys. Soc. B64, pp. 972-977.

Liebmann, G. (1955), Proc. Phys. Soc. B68, pp. 679-681.

Liebmann, G. and Grad, E. M. (1951), Proc. Phys. Soc. B64, pp. 956-971.

Marai, F. Z. (1977), Ph.D. Thesis, The University of Aston in Birmingham.

Marai, F. Z. and Mulvey, T. (1974), 8th Int. Cong. on Electron Microscopy, Canberra, Vol. 1, pp. 130-131.

Marai, F. Z. and Mulvey, T. (1976), Developments in Electron Microscopy and Analysis, ed. J. A. Venables, (London; Academic Press), pp. 43-44.

Marai, F. Z. and Mulvey, T. (1977), Ultramicroscopy, 2, pp. 187-192.

Moses, R. W. (1972), Electron Microscopy 1972, ed. W. C. Nixon, Inst. Phys. Conf. Series 14, (1972), (Proc. 5th European Congress in Electron Microscopy), pp. 86-87.

Mulvey, T. (1972a), U.K. Patent, 1395201.

Mulvey, T. (1972b), Proc. 5th European Congress on Electron Microscopy, pp. 64-69.

Mulvey, T. (1974), 8th Int. Conf. on Electron Microscopy, Canberra, Vol. 1, pp. 16-17.

Mulvey, T. (1976), Design trends in TEM, STEM and SEM Electron Microscopy, Vol. 1. ed. D. G. Brandon (Jerusalem Tal), pp. 59-64.

Mulvey, T. and Nasr, H., (1981), Proc. 1st Conf. on charged particle optics, Giessen, Germany, Sept., 1980, ed. Wollnik, H., North Holland publishing Co., Amsterdam, 1981, pp. 201-208.

Mulvey, T. and Newman, C. D. (1972), Proc. 5th European Conference Electron Microscopy, London, Institute of Physics, pp. 116-117.

Mulvey, T. and Newman, C. D. (1974), Proc. 3rd Int. Conf. H. V. Microscopy, Oxford, pp. 98-102.

Mulvey, T. and Wallington, M. J. (1969), Journal of Physics E: Sci. Instrum. 2, pp. 466-472.

Mulvey, T. and Wallington, M. J. (1973), Rep. Prog. Phys. 36, pp. 375-403.

Munro, E. (1971), Ph.D. Thesis, Cambridge University.

Munro, E. (1975), "A set of computer programs for calculating the properties of electron lenses". Engineering Department, Cambridge University.

Nasr, H. (1981), Ph.D. Thesis, The University of Aston in Birmingham.

Riecke, W. D. (1962), 5th Int. Congr. for Electron Microscopy 1, kk5.

Riecke, W. D. (1972), Proc. of the 5th European Congress on "Electron Microscopy", The Institute of Physics London and Bristol, pp. 98-103.

Tretner, W. (1959), Optik, 16, pp. 155.

Venables, J. A. (1982), Electron Microscopy. Vol 1. Symposia and Physical Sciences. Ed. Congress Organising Committee pp. 181-188. Deutsche Gesellschaft für Elektronen Mikroskopie. Hamburg, 1982.

Von Ardenne, M. (1938), Z. Physik, 109, pp. 553-572.

APPENDIX A

THE EFFECT OF THE POLEPIECE SHAPE AND COIL POSITION ON THE AXIAL MAGNETIC FLUX DENSITY DISTRIBUTION OF A SINGLE-POLEPIECE LENS

When the lens is operated under the saturation condition, the polepiece shape and the design and position of the coil is of the utmost importance if full advantage is to be taken of the saturation magnetisation of the poletip. In particular,the coil should be placed in such a way that the saturation flux density is always localised at the tip of the snout as the excitation is increased.

To imagine a suitable shape for the polepiece of a lens under saturation conditions, one may start by considering the uniform magnetic field produced by a uniformly-magnetised iron sphere, for which Thomoson (see Kelvin 1872) and (Al-Shwaikh and Mulvey, 1977) have calculated its magnetic potential. The iron sphere in a uniform magnetic field and the axial magnetic flux density distribution are shown in Figure (A1) along the axial direction of the sphere. The magnetic flux density inside the sphere is constant in this case.

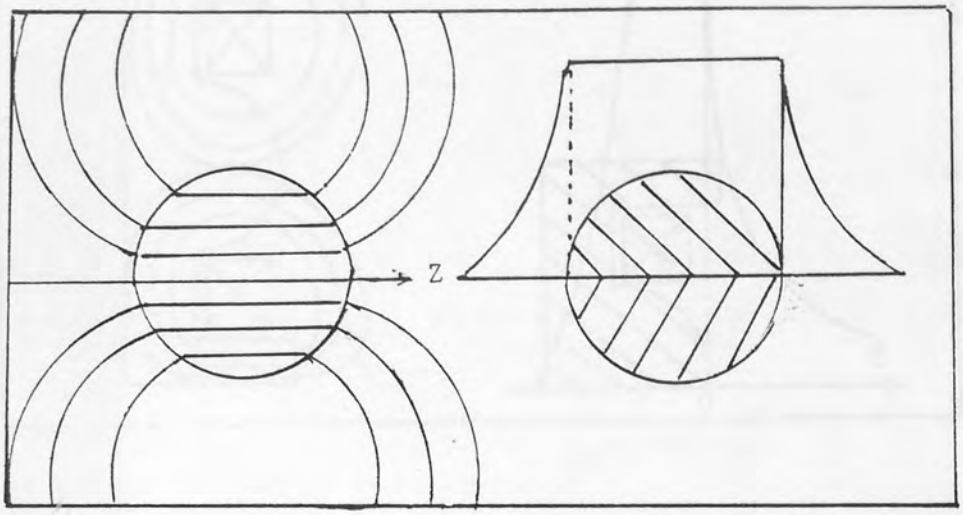

Fig A1 Schematic representation of an iron sphere located in a uniform magnetic field and its axial magnetic flux density distribution.

Taking this idea as a basis for understanding the spherical single-polepiece lens, the axial magnetic flux density distribution can be expected to be similar to that shown in Figure A2. The flux density inside the iron polepiece can be expected to be constant within the thickness of the coil and after that drop sharply outside the iron sphere. This can only be so provided that the thickness and position of the coil is such that it will magnetise the spherical polepiece uniformly.

The energising coil has the effect of raising the flux density at the polepiece tip, if a coil is shifted from the arm of the lens towards its tip, as shown in Figure A3. The flux density inside the polepiece will not then be constant. Initially it

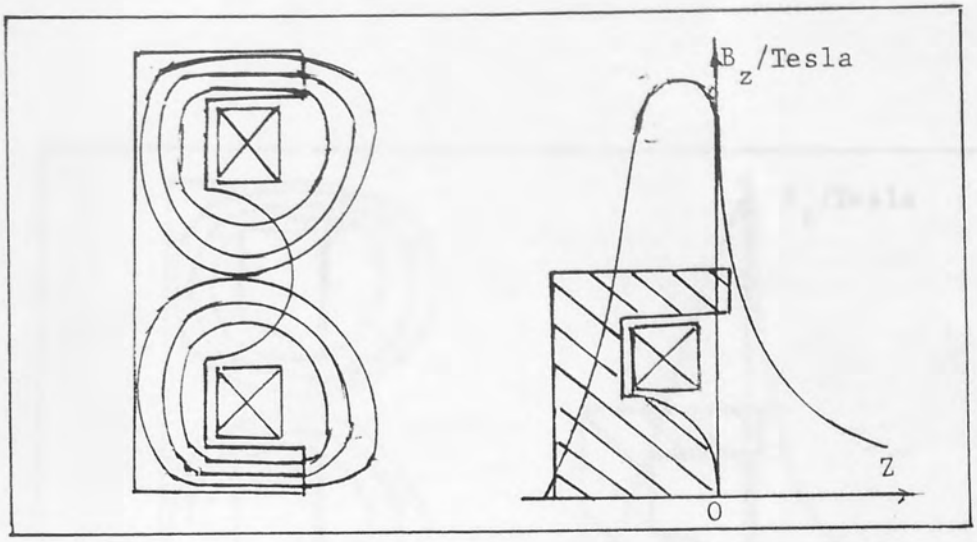

Fig A2 Schematic representation of a spherical single-polepiece lens and its axial magnetic flux density distribution.

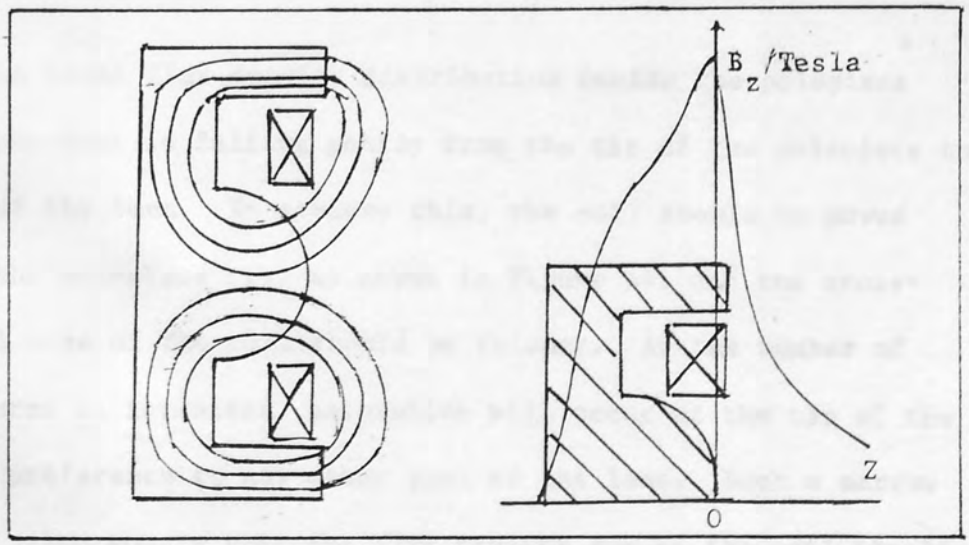

Fig A3 Schematic representation of a spherical single-polepiece lens and the effect of axial magnetic flux density distribution.

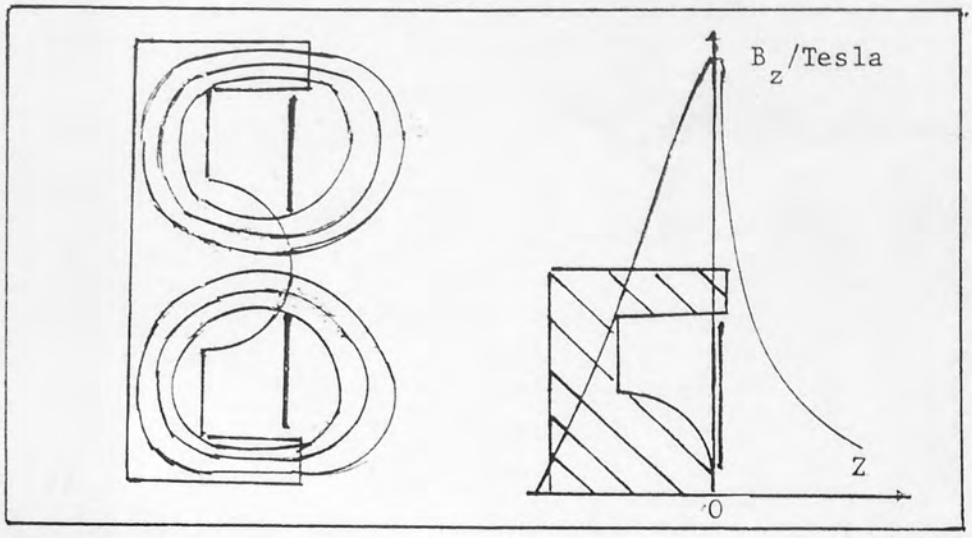

Fig A4 Schematic representation of a spherical single-polepiece lens and the effect of coil geometry on the axial flux density distribution

will drop gradually from the tip to the end of the polepiece and then it will fall sharply to zero at the end of the lens.

The ideal flux density distribution inside the polepiece will be one that is falling gently from the tip of the polepiece to the end of the lens. To achieve this, the coil should be moved towards the polepiece tip, as shown in Figure A4, and the cross-sectional area of the coil should be thinner. As the number of ampere-turns is increased, saturation will occur at the tip of the snout in preference to any other part of the lens. Such a narrow coil will also ensure that the flux density due to the coil itself will have a suitably narrow half-width.